THE UNIVERSITY
of EDINBURGH

Mms6 Expression in Adipose-derived Mesenchymal Stem Cells: Development of Biogenic Magnetic Nanoparticles and Its Therapeutic Potential

Fransiscus Fiano Anthony Kerans

THE UNIVERSITY *of* EDINBURGH

A thesis submitted for the degree of
Doctor of Philosophy

The University of Edinburgh
2019

DECLARATION

I declared that this thesis was composed by myself and that the work presented within is my own except where explicitly stated otherwise in the text, and that this work has not been submitted for any other degree or professional qualification except as specified.

Fransiscus Fiano Anthony Kerans

September 2019

I dedicate this thesis to my beloved parents, Dominikus Kerans and Lenny Sogen, and my little sister, Noni Kerans, who encouraged me to pursue my dreams.

I also dedicate this thesis to my little family, Vivin and Vecia, who have supported me throughout the process. Both of you have been my best cheerleaders.

I love you all to the moon and back.

ABSTRACT

Magnetic nanoparticles (MNP) are attracting interest for a range of biomedical applications being used either alone or as part of cell-based therapies. An area of particular interest is magnetic nanoparticle-mediated hyperthermia (MNHT), when MNP absorb energy from alternating magnetic fields (AMF) and transform this energy into heat which results in cancer cell death. While promising, the use of MNP for diagnosis and therapy has been limited by their rapid removal from the blood and biological barriers at the tissue and cellular levels. Moreover, MNP may have adverse side effects when used clinically.

To overcome these problems there is increasing interest in the development of cell-based strategies to deliver MNP. Current strategies include combining commercially available MNP with mesenchymal stem cells (MSC), as these cells can migrate to sites of tissue injury and tumor growth. However, problems with MNP cytotoxicity have hindered progress in this area and need to be overcome. Therefore, the ultimate aim of this PhD project was to find an alternative way to develop MSC that contain MNP using a genetic engineering approach by which the cells can be induced to stably produce biogenic MNP and to establish whether such an approach could be of value for MNHT for cancer treatment.

To achieve this goal, the experiments conducted in this PhD project involved transfection of adipose-derived mesenchymal stem cells (AD-MSC) to introduce a synthetic magnetic gene, *mms6,* into the cells. The gene is originally derived from *Magnetospirillum magneticum* AMB-1, a genus of magnetotactic bacteria (MTB), which has unique intracellular structures called magnetosomes. The magnetosomes contain iron-rich magnetic nanoparticles that are enclosed within a lipid bilayer membrane. During the formation of magnetosome, *mms6* has been known for its key role in the formation of uniform isomorphic magnetite nano-crystals and helps regulate the crystal morphology of magnetite. Due to the unique feature of this gene, therefore

the novelty of this study was in introducing codon-optimised *mms6* into AD-MSC, enabling the cells to produce biogenic nanoparticles.

In this study, *mms6* mRNA expression in AD-MSC, following transfection, was demonstrated by reverse transcription polymerase chain reaction (RT-PCR). The His-GFP tag Mms6 protein expression was demonstrated by Flow cytometry, Western blot and GFP imaging analysis revealing the expression of Mms6 protein in AD-MSC. Furthermore, for stable *mms6* expression, a lentiviral transduction approach was used. AD-MSC stably expressing *mms6* were then used in *in vitro* MNHT studies.

The effect of *mms6* stable expression on MSC markers of stemness and differentiation ability of AD-MSC were also investigated. The cellular ultrastructure of AD-MSC expressing *mms6* was demonstrated by transmission electron microscopy (TEM), revealing the presence of nanoparticles. The magnetism of AD-MSC expressing *mms6* was proved by superconducting quantum interference device (SQUID). Furthermore, as a comparison study, Ferucarbotran, chemically synthesized superparamagnetic nanoparticles, were also used to magnetize AD-MSC. Both AD-MSC expressing *mms6* and Ferucarbotran-loaded AD-MSC were used in *in vitro* MH and magnetic resonance (MR) imaging studies.

In vitro studies of MNHT were undertaken to investigate whether AD-MSC expressing *mms6* and Ferucarbotran-loaded AD-MSC could have a MNHT effect when exposed to an AMF. Cell viability, cell apoptosis and HSP70 expression were assessed to investigate the MNHT effect. The results did not indicate that the AMF application on AD-MSC expressing *mms6* have a MNHT effect, showing no observable difference in cell viability, cell apoptosis and HSP70 expression. *In vitro* MRI experiments were conducted to test whether *mms6* can function as a MR reporter gene for molecular imaging. The result revealed AD-MSC expressing *mms6* produced a detectable magnetic signal, revealing a promising potential of *mms6* as a reporter gene for MR imaging.

Overall, the results indicate that an MTB gene, *mms6,* can be expressed in AD-MSC without an adverse effect on important cell functions. Moreover, these results also

indicate that no appreciable cell necrosis or cell apoptosis was found when AD-MSC expressing *mms6* were exposed under AMF. However, this study has helped our knowledge on the biosynthesis of MNP in AD-MSC which also has potential use in MR imaging.

LAY SUMMARY

Magnetic nanoparticles are at the core of today's nanomedicine: they serve as diagnostic imaging agents, thermal anti-cancer agents, drug targeting agents, and tissue engineering agents. These tiny structures have shown promise for cancer therapy as they can be injected directly into the cancerous growth and activated by an external alternating magnetic field (AMF) to produce local increases in which causes the cancer cells to die, without affecting the healthy tissue surround the tumours. This approach is called magnetic hyperthermia (MNHT).

The challenge for delivering MNHT to the clinic application is identifying optimal nanoparticles which are biocompatible, less toxic and when administered systemically in clinically appropriate doses, accumulate in the tumour well enough to allow the AMF to heat and kill cancer cells. To overcome this challenge, a cellular approach using mesenchymal stem cells (MSC) as carriers of MNP has been proposed as these cells can home to sites of tissue injury and tumor growth. However, progress in this field has been hindered by variable toxicity of available magnetic nanoparticles. As such it has been proposed that inducing adiposed-derived mesenchymal stem cells (AD-MSC) to synthesize MNP directly may overcome at least some of these problems.

A genetic engineering approach has been developed by introducing a ‘magnetic gene’ derived from magnetotactic bacteria (MTB) into MSC with the aim to induce production of biogenic MNP. MTB have tiny nanoscale organelles called magnetosomes which consist of a chain of membrane-enclosed nanoparticles that act like a compass needle helping the bacteria navigate to nutrient-rich locations in aquatic environments, their natural habitats, by using the Earth's magnetic field. Magnetosomes contain magnetite nanocrystals (Fe_3O_4), uniform nanoparticles that have desirable magnetic properties. MTB use proteins to form crystalline particles about 50 nanometres in size, and one protein, Mms6, has been known to bind iron to initiate and regulate the nanoparticle formation. Therefore, a major goal of this study was to investigate whether it was possible to modify MSC with the *mms6* gene so they

would be able to self-produce MNP, thus allowing their use for MNHT applications and cancer treatment.

In this study, I was able to perform *mms6* gene transfection and demonstrate that *mms6* can be expressed in AD-MSC, allowing them to self-produce MNP, something that would not be achieved without the gene. Importantly, experiments revealed that the expression of *mms6* on AD-MSC did not have adverse effects on the function of these cells.

Overall, experiments conducted in this study demonstrated that AD-MSC expressing *mms6* produce a detectable magnetic signal, suggesting a promising potential of *mms6* as a reporter gene for magnetic resonance imaging (MRI). However, the *in vitro* MNHT experiments conducted in this study did not indicate that the AMF application on AD-MSC expressing *mms6* have a MNHT effect, showing no cell killing effect detected after the AMF exposure. Therefore, the MNP produced by AD-MSC expressing *mms6* does not appear to be adequate to generate heat in order to trigger hyperthermia effect.

ACKNOWLEDGEMENTS

First and most importantly, I would like to express my sincere gratitude to my primary supervisor Professor Donald Salter. His support, both on a scientific and a personal level, has been invaluable to me. I can only give him a huge thank you for all his effort to guide me from the beginning to the end of my PhD with his precious advice, patience and immense knowledge. I would also like to thank my second supervisor Dr. Christopher Boyd for his great ideas and his kind support to help me through my depression and anxiety during my PhD. A huge thanks also to Indonesia Endowment Fund for Education for providing me with the funding to complete this PhD project.

I would like to give my special thanks to Dr Asim Azfer, who has been more than a friend. He has been a great teacher, a lovely mentor, and a kind friend who always brings me joy in doing experiments. I thank him for always encouraging me to have passion in science.

Extra special thanks must go to Lisa Lungaro and Harisson Worrell, who guided me through all experiments. Without their precious suggestion and technical support, it would not be possible to conduct this research. It was nice to have them as my senior in the lab who understood how tough it could be as PhD student.

Thanks too to Helen Caldwell and Elein McClay for their assistance making sure I got all the reagents I needed for my experiments. I would like to thank them for their non-stop outstanding support over the past four years.

I would like to express my special appreciation to all members of the Bone group CGEM for helpful discussion and input in lab meetings. Massive thank you to all of you: Mica, Beatrice, Nerea, Sachin, Kathryn, Erika and Rosa. I've really enjoyed working with you. Thanks a lot for making the workplace a fun place to be.

On a personal level, I would like to thank my officemate Maheva Vallet for always being a lovely coworker, and for her encouragement and friendship. Thank you for all the laughter that kept me going through the tough times and all of your kind help with experiments. You're the most amazing coworker.

Last but not least, this thesis would have not been possible without my parents, my wife Vivin and my little daughter Luh Vecia, whose love and support over the course of my education has enabled me to succeed to this level. I am forever grateful for your love and faith in me during my education. I’m so lucky to have all of you in my life.

ABBREVIATIONS

AAV	Adeno-associated virus
AD-MSC	Adipose-derived mesenchymal stem cells
AMF	Alternating Magnetic Field
ATCC	American Type Culture Collection
BBB	Blood - brain barrier
BLAST	Basic Local Alignment Search Tool
BM	Bone marrow
CCW	Counter clockwise
CRISPR	Clustered regularly interspaced short palindromic repeats
CT	Computed tomography
CTD	C-terminal domain
CW	Clockwise
ddH_20	Distilled water
DMEM	Dulbecco's Modified Eagle's medium
DNA	Deoxyribonucleic Acid
DOX	Doxorubicin
FACS	Fluorescence-activated cell sorting
FBS	Fetal Bovine Serum
FC	Field-cooled
GFP	Green Fluorescent Protein
HCELL	Haematopoietic cell E-/L-selectin ligand
HEK293T	Human Embryonic Kidney 293T
HGF	Hepatocyte growing factor
HSPs	Heat shock proteins
HT	Hyperthermia therapy
IF	Immunofluorescence
IGF-1	Insulin-like growing factor 1 (IGF-1)
ILP	Intrinsic loss power
MAG	MAGISTER gene
MAI	Magnetosome island

MHC	Major histocompatability complex
MM	Magnetosome membrane
MNHT	Magnetic nanoparticle-mediated hyperthermia
MNP	Magnetic Nanoparticle
MRI	Magnetic Resonance Imaging
MSC	Mesenchymal stem cells
MTB	Magnetotactic bacteria
NH	northern hemispheres
NK	Natural killer
NP	Nanoparticles
OATZ	Oxic-anoxic transition zone
PBS	Phosphate buffered saline
PTX	Paclitaxel
P/S	Penicillin/Streptomycin
RES	Reticuloendothelial system
RNA	Ribonucleic Acid
ROS	Reactive oxygen species
RT-PCR	Reverse transcription polymerase chain reaction
SAR	Specific absorption rate
SH	Southern hemispheres
SLP	Specific loss power
SPION	superparamagnetic iron oxide nanoparticles
SQUID	Superconducting quantum interference device
TALENS	transcription activator-like effector nucleases
TEM	Transmission Electron Microscopy
TNF	Tumour necrosis factor
TRAIL	TNF-related apoptosis-inducing ligand
TUNEL	Terminal deoxynucleotidyl transferase (TdT) dUTP Nick-End Labeling
UC	Umbilical cord
ZFC	Zero-field-cooled
ZFN	Zinc finger nuclease

CONTENTS

LIST OF FIGURES

LIST OF TABLES

1 LITERATURE REVIEW

1.1 INTRODUCTION

Due to their small size and high surface-to-volume ratio, magnetic nanoparticles (MNP) have attracted great interest for their potential biomedical applications either alone or through cell-based therapies (Cole *et al.*, 2011). One of the most promising approaches is magnetic nanoparticle-mediated hyperthermia (MNHT) for cancer treatment, where magnetic nanoparticles (MNP) absorb energy from alternating magnetic fields (AMF) and transform this energy into heat. While they are promising, the major drawback has been the difficulty of delivering MNP to the tumour site due to their rapid removal from blood and biological barriers at tissue and cellular level (Gao *et al.*, 2013; Huang and Hainfeld, 2013).

To overcome these problems, the use of MNP-labelled mesenchymal stem cells (MSC) has been proposed due to their inherent tumour-tropic and migratory properties, thus enabling cell-based MNP vehicle for the targeted delivery into tumour (Roger *et al.*, 2010; Duchi *et al.*, 2013; Gao *et al.*, 2013; Huang and Hainfeld, 2013). However, problems with MNP cytotoxicity have hindered progress in this area and need to be overcome. Therefore, the main goal of this project was to develop MSC able to self-express MNP by genetically modifying them with the *mms6* gene, a specific magnetosome gene derived from magnetotatic bacteria (MTB)

1.2 MAGNETIC NANOPARTICLE

1.2.1 Overview

Nanotechnology is an emerging and promising field for research and development in the 21st century. The growing interest in nanotechnology and materials at nanoscale, including magnetic nanoparticles (MNP), has provided invaluable sources for healthcare and biomedical application. Considerable efforts have been made in engineering the MNP, leading to significant advances in medical areas such as

hyperthermia, drug delivery, tissue engineering, and theranostics (Shubayev *et al.*, 2009; Mohammed *et al.*, 2017)

MNP, which are amorphous or semi-crystalline structures, have gained great popularity because of their important properties such as non-toxicity, biocompatibility, size uniformity, and the ability to control their accumulation in the target tissue or organ (Corchero and Villaverde, 2009). Their increasing use includes a range applications include magnetic-based separation or selection, magnetic relaxometry, magnetic resonance imaging (MRI) and therapeutic applications such as drug delivery and magnetic hyperthermia (Hedayatnasab *et al.*, 2017).

1.2.2 Biomedical application of magnetic nanoparticles

Due to their nanoscale size with at least one dimension up to 100 nm and their ability to be functionalized, MNP exhibit the ability to operate on cellular and molecular levels to attain specific performance based on required biomedical applications. In general, the use of MNP depend on the physicochemical properties of MNP, which are mainly affected by the particle structure, particle size, synthesis methods, and interaction among MNP. Therefore, precise control over the method of MNP synthesis is required in order to effectively tune the magnetic properties which are suitable for its biomedical purposes (Reddy *et al.*, 2012; Hedayatnasab *et al.*, 2017)

MNP can be classified as metal, alloys or oxides, and commonly consist of magnetic elements of iron, nickel and cobalt or manganese. However, iron based-nanoparticles are the most widely studied due to their biocompatibility (Conde *et al.*, 2014). An iron oxide core material, such as superparamagnetic iron oxide nanoparticle (SPIONs) are the most widely used MNP for biomedical application. SPIONs are composed of either magnetite or maghemite nanocrystals, and mainly coated with organic materials such as fatty acids, polysaccharides or polymers. These coating materials are specifically designed to improve biocompatibility, colloidal stability and to prevent separation into particles and carrier medium (Tietze *et al.*, 2015). Due to those advantages, these MNP have already been tested in clinical trials for various cancer types, such as brain and

prostate cancers (Johannsen *et al.*, 2010; Mazur *et al.*, 2018). MNP have also been used as contrast agents for MRI to detect liver metastases, metastatic lymph nodes, inflammatory and degenerative diseases at early stages (Gobbo *et al.*, 2015). Moreover, the magnetic properties of MNP also allow the remote control of their accumulation into specific tissue which are directed by an external magnetic field. This application provides an improved strategy for magnetic targeting of drugs as well as magnetic hyperthermia therapy which is the main focus of this study (Silva *et al.*, 2011).

1.2.3 The potential use of magnetic nanoparticle in cancer therapy

Cancer management remains one of the major challenges facing health services around the world. Indeed cancer is now the second major cause of death in developing countries (Jemal *et al.*, 2016). The fact that the available cancer treatment options are limited and, in many situations, the timely diagnosis and prognosis are difficult makes the effort more challenging. Facing this, much effort has been set on finding state of the art approaches for its diagnosis and therapy, which can be combined in cancer theranostics (Lima-Tenório *et al.*, 2015)

Theranostics can be defined as the fusion of therapeutic and diagnostic approaches with the main aims to personalize and advance medicine (Shubayev *et al.*, 2009). In cancer theranostic, the main objective is not merely improving the diagnosis and increasing the efficacy of the treatment of cancers but also minimizing the systemic toxicity associated with this treatment. Thus, the critical feature of this approach is directing therapeutic agents that can be precisely concentrated on the target sites in the body. In this scenario, MNP are promising as theranostic agents, in which, they represent a particularly appropriate tool based on their ability to be simultaneously functionalized and controlled by an external magnetic field. With this ability, the MNP can be directed toward certain area of the body allowing MRI detection and releasing a therapeutic drugs with limited side effects as shown in

Figure **1-1** (Gobbo *et al.*, 2015)

The fundamental aspect behind this theranostic capability of MNP is the surface design of MNP which consist of multi-layered structure as shown in Figure 1-2. Through this multi-layered functionalization, MNP could have various properties with multifunctional purposes. For this, SPIONs formed by three main functional layer: (1) an iron oxide core functioning as MRI contrast agent, (2) a biocompatible coating and (3) a therapeutic coating targeted with a pharmacogenomics biomarker (Gobbo *et al.*, 2015).

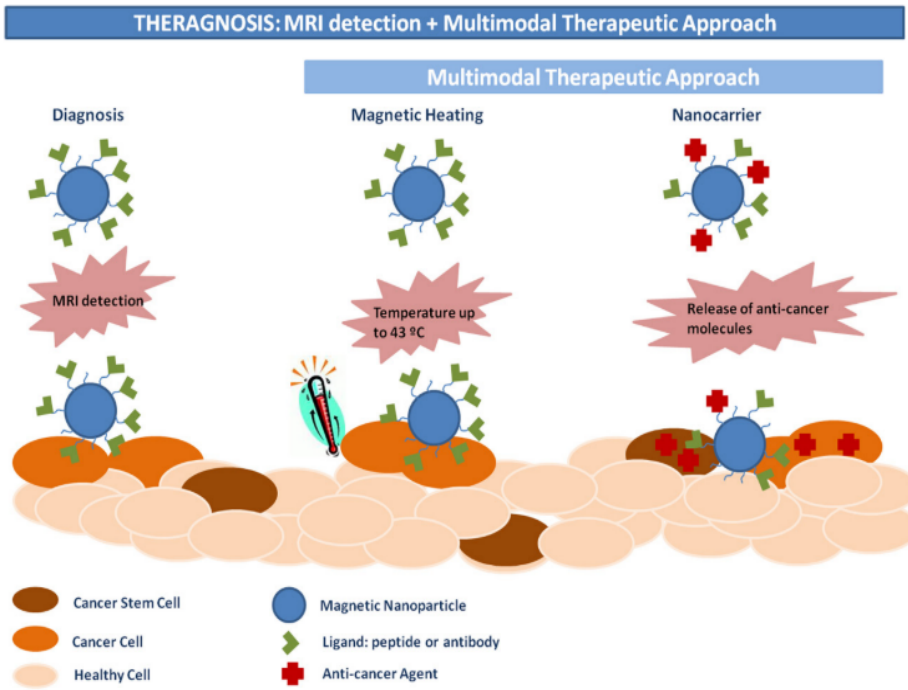

Figure 1-1: Example of magnetic nanoparticle for theranostic applications. *Image taken from Gobbo et al (2015).*

In cancer diagnostic, the high magnetic susceptibility of MNP cores provides strong enhancement of transverse (T2 and T2*) relaxivity in tissue regions where nanoparticles have localized. Strong relaxivity is manifested on T2-weighted MR images as pronounced negative contrast (Cole *et al.*, 2011). For example, the approved drugs Feridex IV and Resovist have been used as contrast agents for hepatic imaging. These polymer-coated MNP agents were polydisperse (size heterogeneous) superparamagnetic iron oxides that were rapidly cleared from the blood by

macrophages of the reticuloendothelial system (RES), thus leading to significant deposition in the liver and spleen. Consequently, these MNP darken normal liver tissue preferentially over cancerous lesions in T2 weighted images, allowing detection of primary or metastatic hepatic tumours (Abraham Lee, 2006).

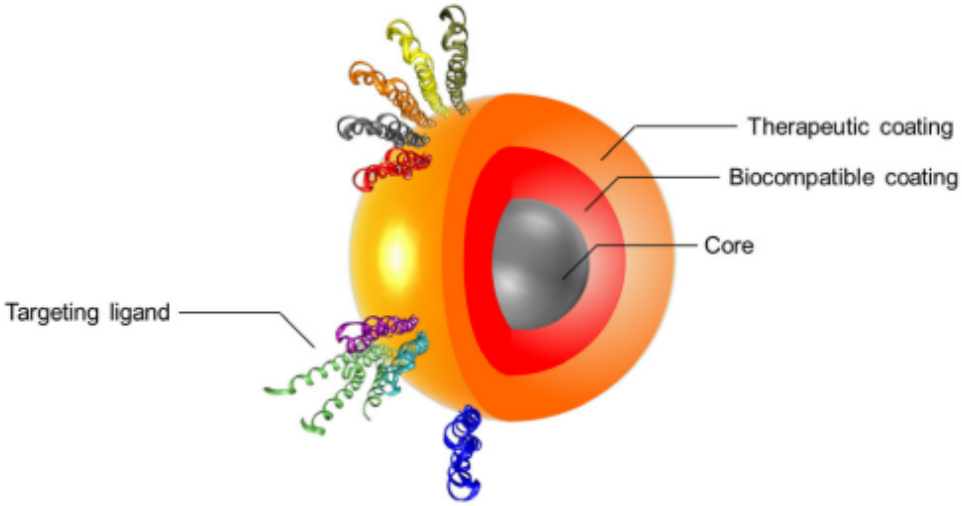

Figure 1-2: Schematic of a multilayered SPION with personalized medicine application. *The figure represents the three main components formed by "layering" an iron oxide nanoparticle: (1) MNP core, (2) biocompatible coating and (3) therapeutic coating/targeting ligand. Image taken from Gobbo et al (2015).*

In 2010, Liu *et al* reported a study developing a theranostic system combining MRI and therapeutic MNP conjugated with the anticancer drug epirubicin for delivery and image tracking functions in a C6 tumour-bearing rat model (Liu *et al.*, 2010). The study was also focused on using ultrasound to disrupt the blood - brain barrier (BBB) at the tumour site to improve nanoparticle accumulation. The result showed MNP distribution and enhancement of drug delivery then can be monitored by MRI in real time in vivo. A 2.6 fold increase in relaxation rate with MRI was observed in animals injected with the nanoparticles following the focused ultrasound/magnetic targeting treatment compared to the non-treated groups. This study provides a promising potential of multifunctional MNP to deliver therapeutic doses locally and simultaneously reduce the problem of systemic toxicity common to i.v.-administered therapeutic agents. Furthermore, the study also provides an integrated nanoplatform to monitor and quantify the drug delivery in real time *in vivo*.

Another area of interest in cancer theranostics is synergistic cancer diagnostic and treatment by combining three important elements: the improved ability of the magnetic nanoparticles as contrast agents for MRI, the unique drug delivery targeting cancer cell, and the unique heat generation property of magnetic nanoparticles in an alternating magnetic field (AMF) to induce hyperthermia. In 2016, Ramachandra Kurup Sasikala *et al.* reported a study developing a multifunctional nanocomposite consisting of Graphene Oxide–Iron Oxide-Doxorubicin (GO-IO-DOX) as a theranostic cancer platform which acts both as a hyperthermic agent that delivers heat when an alternating magnetic field is applied and a chemotherapeutic agent in a cancer environment by providing a pH-dependent drug release to administer a synergistic anticancer treatment with an enhanced T2 contrast for MRI (Ramachandra Kurup Sasikala *et al.*, 2016). The study showed that periodic hyperthermia for three cycles resulted in a moderate cell cytotoxicity of 26% due to the mild hyperthermia at a temperature of ~40 °C in the GO-IO-MH group, whereas GO-IO-DOX-MH group exhibited an enhanced cell cytotoxicity of 82% due to both hyperthermia and drug activity. Therefore, the synergistic enhancement in the combined scenario can be explained to be a result of an increase in drug cytotoxicity due to the mild hyperthermia that was concurrently delivered.

1.3 MAGNETOTACTIC BACTERIA

1.3.1 The discovery of magnetotactic bacteria

Magnetotactic Bacteria (MTB) are a diverse group of Gram-negative microorganisms that passively align and actively swim along the geomagnetic field and other fields (Lower and Bazylinski, 2013). This unique ability is dependent on its specific intracellular organelles, the magnetosomes, which are composed of a nanometer size magnetic crystal, either magnetite (Fe_3O_4) or greigite (Fe_3S_4) surrounded by a lipid bilayer membrane known as the magnetosome membrane as shown in Figure 1-3 (Balkwill *et al.*, 1980; Bazylinski and Frankel, 2004).

The discovery of MTB was first reported by Salvatore Bellini in 1963 when he microscopically observed a certain group of bacteria that moved toward the Earth's North Pole, thus these group of bacteria named "magnetosensitive bacteria" (Jogler and Schuler, 2009). However, eleven years later, it was Blakemore who independently used the terms "magnetotaxis" for the phenomenon and MTB for the bacteria after he discovered aquatic bacteria from Woods Hole, Massachusetts. He noticed that the swimming direction of these bacteria was always the same, independently from the external stimulus given, as they migrated northward in water drops along magnetic field lines. In his landmark paper, he also discovered that the cells were roughly coccoid with two bundles of seven flagella each on one side of the cell by using Transmission Electron Microscope (Blakemore, 1975). The study also demonstrated that MTB cells contained chains of elongated, electron-dense, iron-rich crystals, comprise of magnetite. These chains of nanocrystal were enclosed within intracytoplasmic vesicles arranged next to the cytoplasmic membrane in the cell. It was speculated that magnetotaxis movement of MTB recovered from aquatic sediments in Woods Hole probably has correlation to the chains of crystals within MTB (Richard B. Frankel *et al.*, 2006).

Phylogenetically, MTB belong to the domain Bacteria and are associated with different subgroups of the Proteobacteria and the Nitrospira phylum. They represent a diverse group of microorganisms with respect to morphology and physiology (Bazylinski and Frankel, 2004). Based on its morphology, MTB have a cell wall structure which is a distinctive feature of Gram-negative bacteria (Bazylinski and Frankel, 2004). Structurally, they also have flagella as their motility organelle which varies between species/strains and can be either polarly monotrichous, bipolar, or in tufts (lophotrichous). This structure allows MTB to propel through the water actively by rotating their helical flagella, but passively orient along the geomagnetic field (Blakemore, 1975; Rodgers *et al.*, 1990; Richard B. Frankel *et al.*, 2006).

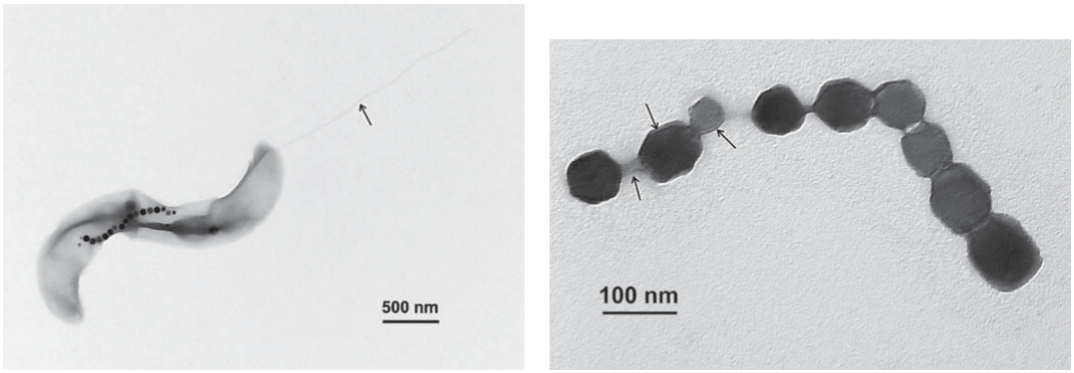

Figure 1-3: Transmission electron microscopy image of a cell of a magnetotactic bacterium. *(Left) Transmission electron microscopy image of a cell MTB collected from the Olentangy River, Columbus, Ohio, USA. The MTB contains chain of electron-dense magnetosomes containing cuboctahedral crystals of magnetite running along the long axis of the cell and the single polar long flagellum (at arrow). (Right). Transmission electron microscopy image of a chain of purified magnetosomes from M. marinus. Arrows denote magnetosome membrane. Image taken from Lower and Bazylinski (2013).*

1.3.2 The ecology and behavior of MTB

MTB are generally distributed in water columns or sediments with vertical chemical stratification (Bazylinski and Williams, 2006). MTB are a great example of gradient-loving organisms due to their preference to live in the oxic-anoxic transition zone (OATZ) which is a particular zone created by two opposite gradients, one formed by the oxygen coming from the surface and another created by the sulphide produced by the sediments of the bottom. OATZ provides low level of oxygen, which is a preferable environment for MTB. In general, MTB located in environments with higher than optimal oxygen concentration will move toward the OATZ by rotating their flagella counter clockwise, whereas bacteria located in environments having lower than optimal oxygen concentration will rotate their flagella clockwise and move toward the OATZ. This typical MTB orientation of moving toward OATZ, exploiting magnetic field through their magnetosomes, is called "magneto-aerotaxis" and can be seen in Figure 1-4 (Frankel *et al.*, 1997; Bazylinski and Frankel, 2004). However, despite their major preference towards OATZ, several different species of MTB are dependent on

specific chemical/redox conditions, hence can be found at different positions within the gradients. A greigite-producing MTB, for example, are found below the OATZ when the anoxic zone is sulfidic (Moskowitz *et al.*, 2008).

In 1997, Frankel *et al* hypothesized MTB has two forms of magneto-aerotaxis, which are polar magneto-aerotaxis and axial-aerotaxis (Frankel *et al.*, 1997). In polar magneto-aerotaxis, MTB have a polar preference in their swimming direction under oxic conditions. Some MTB strains, mainly the magnetotactic cocci, are polar magneto-aerotactic that swim persistently in one direction along the magnetic field. For example, north-seeking MTB in the northern hemisphere have north polarity, which means that they swim toward geomagnetic north into anoxic sediments or waters in a vertical chemical gradient when they exposed to higher than optimal oxygen levels. For the same reason, south-seeking MTB swim toward geomagnetic south. In contrast to polar-aerotaxis MTB, axial magneto-aerotaxis MTB use the magnetic field as an axis while swimming under oxic conditions in both directions along magnetic field lines without polar preference. The earth geomagnetic field provides both an axis and a direction of motility for polar magneto-aerotactic bacteria, whereas it only provides an axis of motility for axial types of bacteria (Frankel *et al.*, 1997; Frankel *et al.*, 2006; Lower and Bazylinski, 2013).

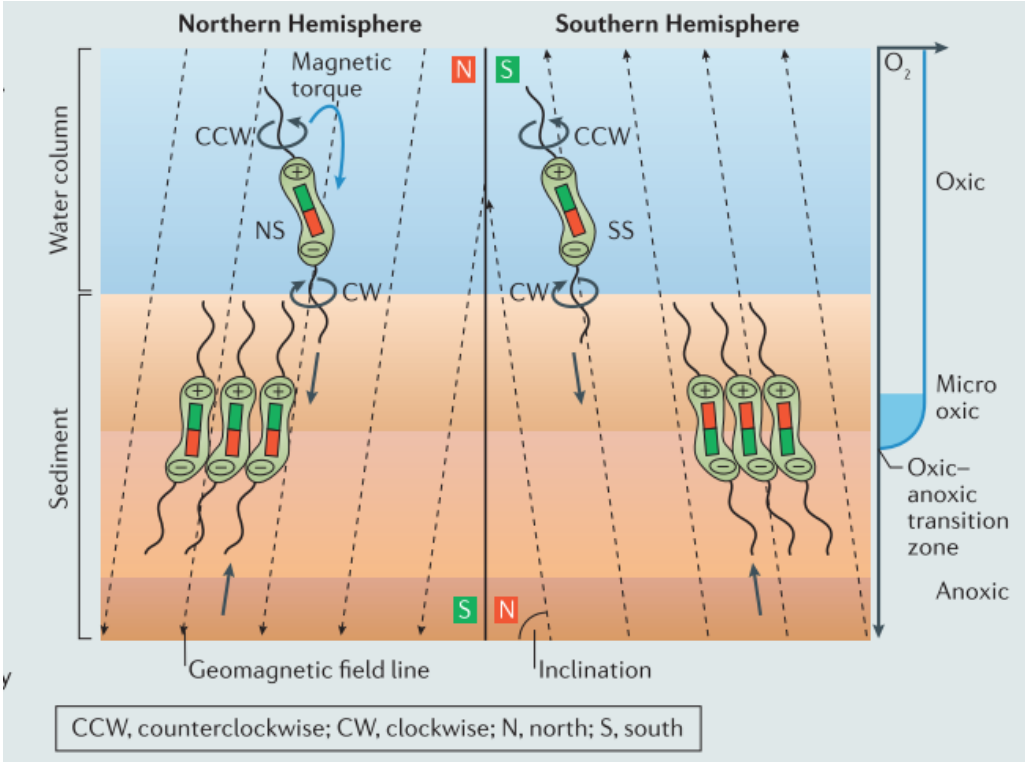

Figure 1-4: Schematic representation of Magneto-aerotaxis in the northern (NH) and southern (SH) hemispheres. *MTB exploit magnetic field to find their optimal oxygen concentration at the microaerobic oxic–anoxic transition zone (OATZ). To move across different stratifications, in both the hemispheres, MTB on the oxic side of OATZ swim down geomagnetic field lines, whereas those on the anoxic side swim up along the magnetic lines. The MTB on oxic side of OATZ rotate their flagella counterclockwise (CCW), whereas the ones on the anoxic side rotate their flagella clockwise (CW). MTB showing north or south-seeking behaviour show also different magnetic polarity, indicated by arrows. Image taken from Uebe and Schüler (2016).*

Conflicting reports to the polar magneto-aerotaxis, however, were reported by Simmons and his coworkers (2006). They found that populations of polar MTB in the northern hemisphere respond to high oxygen levels by swimming toward geomagnetic south, in contrast to all previous studies on MTB magneto-aerotaxis. It may be possible that MTB respond by other routes in order to find optimal condition outside from OATZ (Simmons *et al.*, 2006). Moreover, the first study of phototaxis in MTB *Magnetospirillum magneticum* strain AMB-1 was reported by Chen *et al.* in 2011.

They found out that Magnetotactic AMB-1 cells migrated toward light, and migration increased with higher light intensity. The study demonstrated that the phototaxis response proved to be independent of the geomagnetic field and affected the formation of magnetosome (Chen *et al.*, 2011).

1.3.3 Magnetosome formation

The fundamental organelle of MTB is the magnetosome, which is defined as an intracellular, membrane-bounded magnetic iron-bearing inorganic crystal (Bazylinski and Frankel, 2004; Lefèvre *et al.*, 2011). Many studies have been done using *Magnetospirillum magneticum* AMB-1 (AMB) and *Magnetospirillum gryphiswaldense* MSR-1 (MSR) as model strains of MTB in the laboratory. These Alphaproteobacteria class MTB are known for their magnetosomes containing single chains of cuboctahedral magnetite (Fe_3O_4) crystals. It was observed in this strain that magnetosomes biosynthesis comprises of four important steps (Uebe and Schüler, 2016):

1) the magnetosome membrane is invaginated from the cytoplasmic membrane, which then developing either vesicle-like permanent invaginations or detached vesicles.
2) magnetosome proteins are sorted to the magnetosome membrane, either before, simultaneously or following invagination,
3) iron is transported into the magnetosome membrane invagination before initiating biomineralization to form magnetite crystals,
4) a highly ordered magnetosome chain is then assembled and positioned for segregation during cell division

The formation of bacterial magnetosomes is a tightly-regulated process involving genetic control over the biomineralization of perfectly shaped and sized magnetic crystals as well as highly ordered crystal chains arrangement to function as magnetic field sensor (Schüler, 2008). The molecular mechanism of magnetosome formation remained poorly understood for some time, however it was observed that genetic

controls of magnetosome biosynthesis are associated with a set of magnetosome membrane (mam) and magnetic particle-membrane specific (*mms*) genes as can be seen in Figure 1-5 (Arakaki *et al.*, 2003; Grunberg *et al.*, 2004). These specific genes are clustered in a single chromosomal region, named genomic magnetosome island (MAI) (Ullrich *et al.*, 2005; Fukuda *et al.*, 2006).

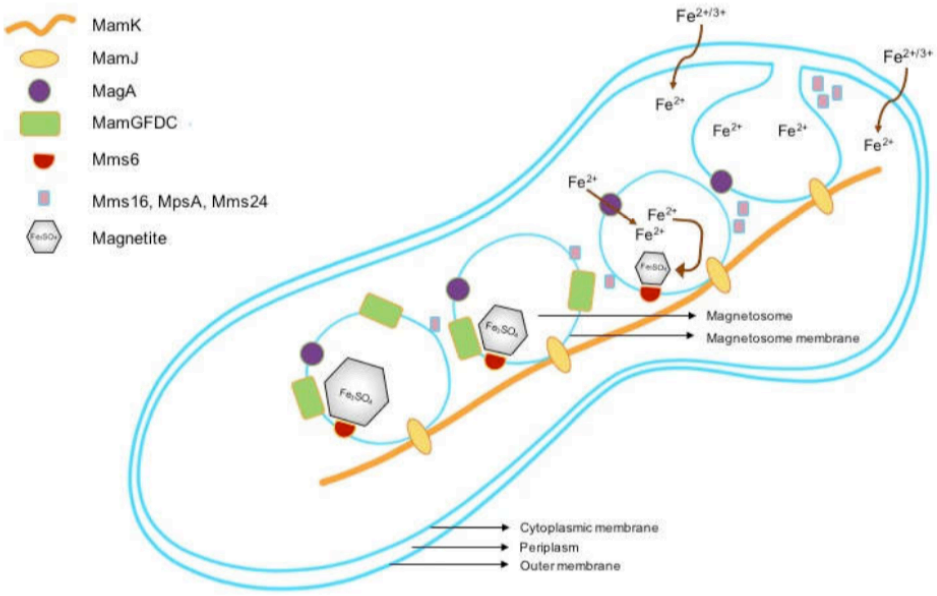

Figure 1-5: Sequential steps of the hypothesized mechanism of magnetosomes formation and magnetite biomineralization in magnetotactic bacteria. *Image taken from (Kerans et al., 2018).*

The MAI extends across about 100 kb and are organized into five polycistronic operons: one large (16–17kb) mamAB operon and the small *feoAB1*, *mamGFDC*, *mms6* and *mamXY* operons as can be seen in Figure 1-6. The *mamAB* operon contains several genes that are involved in important steps in the synthesis of magnetosome. The *mamAB* operon is also fundamental in maintaining some process of biomineralization. It was found that without *mamAB* operon, there is no magnetic phenotype. In contrast, the four small operons encode non-essential proteins that have accessory roles in, specifically in regulating the biomineralization of crystals as well as controlling size and shape of the crystal. This role involves the putative iron transporters FeoAB1 and MamZ; the tubulin-like protein FtsZm; and the magnetotactic bacteria-specific proteins MamC (also known as Mms13), MamD (also

known as Mms7), MamF, MamG, MamX, MamY, Mms6, MmsF, Mms36 and Mms48 (Scheffel *et al.*, 2008; Lohße *et al.*, 2011; Rong *et al.*, 2012; Raschdorf *et al.*, 2013).

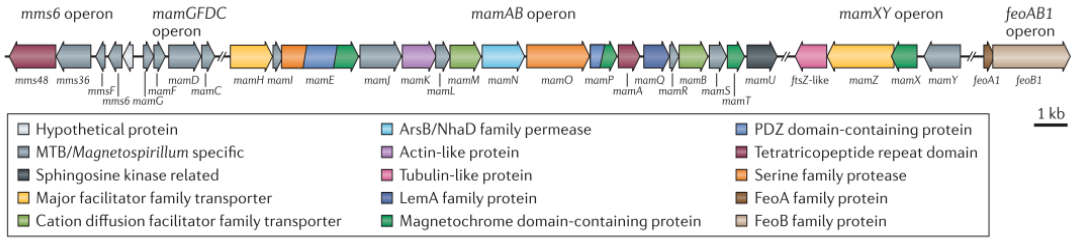

Figure 1-6: Schematic representation of the genomic magnetosome island (MAI). *Schematic picture of MAI genes consists of the five operons regulating genes involved in the magnetosome biogenesis. The genes are coloured according to the features of their encoded proteins. Image taken from Uebe and Schüler (2016).*

Since the MAI is critical in encoding factor for multi-steps process of magnetosome formation, Kolinko and coworkers (2014) attempted to produce sustainable magnetic nanostructures in *Rhodospirillum rubrum*, photosynthetic model organism, by introducing expression cassettes comprising of 30 genes of MAI (Kolinko *et al.*, 2014). The study validated the proof of principle that magnetic crystal nanostructure can be produced in non-magnetic bacteria or biotechnologically relevant hosts by genetic engineering using genes from MTB. Therefore, this finding is important in developing nanomagnetic material biomedical application, such MNHT or for endogenous expression of magnetic reporters for bioimaging.

1.3.4 Magnetosome membrane formation.

The growing of magnetic crystal within magnetosome required a specialized 'nano-reactor' compartmentalization, where factors such pH environments, iron and redox are finely controlled. For this reason, magnetosome membrane (MM) plays a major role in creating this compartmentalization allowing strictly regulated magnetosome biomineralization and cell protection from toxic products. The magnetosome membrane was demonstrated to comprise a 5–6 nm proteinaceous phospholipid

bilayer which is invaginated from the cytoplasmic membrane (Balkwill *et al.*, 1980; Gorby *et al.*, 1988; Komeili *et al.*, 2006; Katzmann *et al.*, 2010).

Studies conducted on both MSR and AMB have shown that the invagination process occur simultaneously from several nonspecific cellular locations, as was confirmed by tracking *de novo* magnetosome biogenesis by time-lapse fluorescence microscopy and cryoelectron tomography, using inducible gene expression systems (Raschdorf *et al.*, 2013; Cornejo *et al.*, 2016). In MSR, it was found that the invagination of magnetosome membranes is likely to proceed immediately since the initial stages of membrane deformation was not detected (Raschdorf *et al.*, 2016). Interestingly, magnetosome vesicles can be empty or filled with iron, which confirms the invagination mechanism is independent to biomineralization process (Komeili *et al.*, 2004; Katzmann *et al.*, 2010; Cornejo *et al.*, 2016).

The invagination ability of MTB is generally thought to depend on specific proteins that provide the energy required to generate the magnetosome membrane. MamB seems to have a function in magnetosome membrane invagination and iron transportation; whereas MamI and MamL are integral membrane proteins associated with the MM. MamB is believed to play a major role in guiding the formation of multiprotein complexes to induce invagination in the later steps of magnetosome biogenesis (Uebe and Schüler, 2016). Another protein associated with membrane invagination is MamY, which has been found to be involved in constriction of the cell membrane to create the magnetosome cell membrane (Tanaka *et al.*, 2011).

1.3.5 Biomineralization

Following the magnetosome compartments are formed and positioned, the final step in magnetosome biogenesis is the biomineralization of magnetite. The biomineralization process involves iron transport, initiation of crystallization, crystal maturation, and control over size and morphology (Komeili, 2012). The first important step is the transport of iron from the extracellular environment into the cell. MTB are capable of accumulating significant amounts of intracellular iron that are at least 100

times higher than non-MTB species such as *E. coli.* For most MTB, the iron uptake process is regulated in response to environmental oxygen levels which mainly occurs in anaerobic conditions (Blakemore *et al.*, 1985; Schüler and Baeuerlein, 1996, 1998; Heyen and Schüler, 2003).

A genetic study investigating the ferric uptake regulator (Fur) transcription factor in MSR-1 indicate that the overall balance of cellular iron must play an important role in the biomineralization process. The study showed that deletion of the fur homolog in MSR-1 resulted in the production of fewer magnetite crystals. (Uebe *et al.*, 2010). In agreement with this finding, Yijun and coworkers (2017) also found that iron uptake and magnetosome formation were dramatically inhibited by disruption of fur-like proteins, suggesting some transport of iron from a cytoplasmic pool into magnetosomes may be required for magnetite formation (Yijun *et al.*, 2007).

After the iron uptake process, the next step is the initiation of crystallization which is likely a process where the chemical environment of the magnetosome needs to be modified to allow for transformation of concentrated iron into nuclei of magnetite (Komeili, 2012). In 2007, Faivre and coworkers found iron-containing Ferritin-like protein in the cellular membrane fraction. They suggested that the iron within this protein is co-precipitated, along with soluble ferrous iron, to form magnetite crystallites at the cell membrane, which are then matured into magnetite within the magnetosome. In addition, they also believed that the steps involved in magnetite formation and biochemical iron uptake are distinct, suggesting magnetite formation occurs via membrane-associated crystallites, while the final step of magnetite crystal growth possibly is spatially separated from the cytoplasmic membrane (Faivre *et al.*, 2007). A genetic analysis study has showed that the deletion of *mamM, mamN*, *mamE* and *mamO* in AMB-1 results in magnetosome membranes with a full complement of magnetosome proteins, yet without mineral formation, suggesting the important role of these genes in the biomineralization process (Murat *et al.*, 2010). Moreover, the study also tested the hypothesis that the absence of crystal formation could also be a consequence of the inability of the mutant to properly localize magnetosome proteins. It was found that the absence of MamE protein resulted in mislocalized of MamA and

MamJ, which are not essential for biomineralization, suggesting that MamE may act as precursor or enzyme to control the localization of other magnetosome proteins. The empty magnetosome could be a consequence of the mislocalization of at least a subset of magnetosome proteins (Murat *et al.*, 2010).

Crystal maturation process occurs to form a stable crystal state, enabling the magnetosome chain's ability to reorient cells in magnetic field. In the initial crystal form, the magnetites are composed of a single magnetic domain in a superparamagnetic state, meaning that the direction of their dipole moment is unstable. Once the maturation process started, they reach a size > 35 nm, and become a stable single domain magnetic crystal (Komeili, 2012). A genetic study has demonstrated that the deletion of *mamS*, *mamT*,or *mamR* results in a reduction in size of the crystal and defects in their morphology (Murat *et al.*, 2010).

FtsZ-like proteins are a copy of FtsZ, defined as bacterial tubulin-like cell division proteins found in three Magnetospirillum species (Richter *et al.*, 2007; Ding *et al.*, 2010). FtsZ-like proteins genes are localised into the MAI region, in MamXY operon, a feature that suggests a possible involvement of these proteins in magnetosome chains assembly or in Magnetospirillum cells division (Jogler and Schuler, 2009; Müller *et al.*, 2014).

1.4 MMS6 PROTEIN

1.4.1 Mms6 protein and its function

In 2003, Arakaki and his coworkers found Mms6 protein may be directly involved in biological magnetite crystal formation in MTB. The protein was isolated from magnetosomes of *M. magneticum* AMB-1 together with the other magnetosomes associated proteins, after lipid membrane stripping and treatments based on detergent and heat (Arakaki *et al.*, 2003). The group found four proteins which showed common features in their amino acid sequences which contain hydrophobic N-terminal and hydrophilic C-terminal regions: magnetosome membrane specific5 (Mms5), magnetosome membrane specific7 (Mms7), magnetosome membrane specific13

(Mms13) and Mms6. These proteins were called “Mms”, which stands for their magnetosome membrane specific (Mms) localization and were numbered according to their molecular mass (Arakaki *et al.*, 2003).

Mms6 has a negative charge at neutral pH, being different from all the other Mms proteins that are positively charged (Arakaki *et al.*, 2003). In 2006, a proteomic study identified magnetosome membrane proteins also to be prevalent in the cytoplasmic membrane, several of which are related to magnetosome biosynthesis, such as Mms13. Mms6, however, was not found in other membrane fractions of the cell, suggesting this protein is specifically targeted to the magnetosome membrane (Tanaka *et al.*, 2011).

Mms6 gene sequence shows a high consensus among different MTB species, especially in the C-terminal region. The sequence codes for a protein of approximately 12–15 kDa, which is larger than the 6 kDa species identified in magnetosomes by SDS/PAGE. This finding suggests Mms6 protein undergoes *in vivo* protease cleavage to form 6 kDa truncated protein (Arakaki *et al.*, 2003; Grunberg *et al.*, 2004).

In 2014, Nudelman and Zarivach demonstrated structure prediction of magnetosome-associated proteins which indicates Mms6 has secondary structure. It was predicted that this structure is formed by an unstructured N-terminal domain followed by one transmembrane helix and a C-terminal, suggesting it may form α-helix structure. It was believed that the C-terminal domain (CTD) can act as an iron binding site which was predicted by the 3D model protein structure on its (Nudelman and Zarivach, 2014).

In 2010, Tanaka and his coworkers discovered that the Mms6 protein is tightly associated with magnetite crystals. They performed *in vitro mms6* gene deletion experiments to understand the role of Mms6 in *Magnetospirillum magneticum* AMB-1. The study found smaller magnetite crystals with uncommon crystal faces in Δ*mms6* mutant strain, while the wild-type and complementation strains synthesized highly ordered cubo-octahedral crystals. In addition, Δ*mms6* mutant strain also displayed drastic changes in the profiles of the proteins tightly bound to magnetite crystals. It

was observed that Mms6 plays a role in the regulation of a nano-sized crystallographic structure in *in vivo* biomineralization in MTB. Moreover, by analyzing the protein profiles in gel images, Δ*mms6* mutant strain also showed the drastic decrease of the Mms5, Mms7, and Mms13 protein expressions in the protein fraction obtained from the magnetite crystal surface, suggesting Mms6 protein may also be involved in other Mms protein interactions and as it co-locates on the magnetite crystal surface (Tanaka *et al.*, 2010).

Arakaki *et al.* (2014) demonstrated that all *mms* genes were involved in different ways in the promotion of crystal growth and defining the surface structure of the magnetic nanocrystals in *M. magneticum* strain AMB-1. In their study, various *mms* gene deletion mutants were designed and the magnetite crystals formed by the mutant strains were characterized. Deletion of *mms6* or *mms7* resulted in decreased of the amount of proteins in the outside region of the magnetosome chain. Furthermore, based on the phenotypic characterization, formation of elongated nanocrystal was shown in Δ*mms6* and Δ*mms7* mutant strains (Arakaki *et al.*, 2014).

Using high-resolution transmission electron micrograph, the functions of Mms proteins can be estimated from the magnetosome crystal faces modeled for each Δ*mms* strain mutants (Arakaki *et al.*, 2014). Using this predictive model, it was observed Mms proteins have different dimensional effects on the crystal growth of magnetite due to their preferences of proteins for binding to specific sites during crystal growth, which determine their specific surface structures on magnetite crystals (Arakaki *et al.*, 2014). This was in agreement with previous *in vitro* study which showed the active site for Mms6 is most likely present in its C-terminal region, which contains acidic amino acids (Arakaki *et al.*, 2010).

1.4.2 Synthesizing MNP with Mms6 *in vitro*

Despite the nature of the magnetite precipitation and biomineralization process within the magnetosome not yet being clearly understood, purified Mms6 has been investigated in synthetic magnetite formation reactions to look for effects on the MNP

products (Arakaki *et al.*, 2003, 2010; Amemiya *et al.*, 2007; Prozorov *et al.*, 2007; Galloway *et al.*, 2011, 2012; Bird *et al.*, 2016). Magnetite (Fe_3O_4), is formed by ferric (Fe^{3+}), and ferrous iron (Fe^{2+}), at the 2:1 stoichiometric ratio. Most of methods to produce magnetite synthetically involve *in vitro* precipitation and series of pH titration of mixtures of iron. By adding purified Mms6 to these *in vitro* methods, the size, shape and material purity of the resulting nanoparticles can be compared with protein-free nanoparticles prepared under identical conditions (Arakaki *et al.*, 2003, 2010; Amemiya *et al.*, 2007; Prozorov *et al.*, 2007; Bird *et al.*, 2016).

In 2003, Arakaki and his coworkers reported that addition of Mms6 at 20 μg/ml to a room-temperature co-precipitation reaction resulted in a product which was mainly magnetite and few alternative iron oxide precipitates, suggesting the ability of Mms6 to promote a reaction towards magnetite (Arakaki *et al.*, 2003). Furthermore, the magnetite also displayed a cuboidal shape, and a narrow size distribution, similar to the ones observed in the magnetosomes. In a good agreement with this, recent findings also demonstrated similar result despite using lower concentration of Mms6 protein (Amemiya *et al.*, 2007) and different ratios of iron in the mixture (Galloway *et al.*, 2011), and using a surface system as a mimic of the interior of magnetosome membrane (Bird *et al.*, 2016).

Amemiya *et al.* (2007) showed Mms6-mediated synthesis of magnetite nanocrystal by partial oxidation of ferrous hydroxide generated nanocrystal of a uniform size and narrow size distribution with a cubo-octahedral morphology, similar to bacterial magnetite observed in *M. magneticum* AMB-1. In the absence of Mms6, the crystal produced were octahedral, larger with an increased size distribution. In the presence of Mms6, iron ions bind to the iron binding site of Mms6, concentrating them about the protein aggregate. It was suggested that the self-assembled aggregate mediated by Mms6 acting as a template and regulating the crystal size to approximately 20 nm. Therefore, the study also proposed that Mms6 has important roles in controlling the size and the shape of the crystal to be specifically cubo-octahedral (Amemiya *et al.*, 2007).

Recently, Shipunova *et al.* (2019) reported surface modification of nanoparticles mediated by Mms6 protein. The study developed a novel method of magnetite nanoparticles stabilization using recombinant protein for the targeted delivery to HER2/neu oncomarker for cancer diagnostic purposes. The study found that a biocompatible Bs-C-Mms6 fusion protein containing the C-terminal part of the Mms6 (magnetite-binding protein of magnetotactic bacteria) and Barstar (an inhibitor of bacterial ribonuclease Barnase) was able stabilize magnetic nanoparticles formed by co-precipitation, allowing stable protein-coated of nanoparticle in physiological condition (Shipunova *et al.*, 2019)

1.4.3 Mms6 in vitro: self-assembly and iron binding

Mms6 alone is not responsible for the formation of magnetite nanocrystals *in vivo* (Tanaka *et al.*, 2011), however Mms6 *in vitro* activity may provide understanding of how magnetosome-related proteins are involved in biomineralization. Mms6 protein has been shown to have two phases of iron binding: one high affinity and stoichiometric and the other low affinity, high capacity, and cooperative with respect to iron. Mms6 protein is amphipathic with a hydrophobic N-terminal domain and hydrophilic C-terminal (Wang *et al.*, 2012) This structure was first reported by Wang and his coworkers (2012) who found that in aqueous solution the amphiphilic nature of Mms6 tends to form micelle-like structures with the C-terminal hydrophilic regions exposed, protecting the hydrophobic N-terminal regions within the core. Using size-exclusion chromatography, the study also identified that self-assemblies of Mms6 protein form the 200-400 kDA, micelles with most particles consisting of 20−40 monomers (Wang *et al.*, 2012).

In 2014, the direct evidence of the localization of the bound iron to the C-terminal region of the Mms6 micelles was firstly reported by Kashyap and coworkers. Using *in situ* liquid cell scanning transmission electron microscopy they demonstrated a direct visualization of biomimetic iron oxide nanoparticle nucleation mediated by an acidic bacterial recombinant protein, Mms6, during an *in situ* reaction induced by the controlled addition of sodium hydroxide to solution-phase Mms6 protein micelles

incubated with ferric chloride as can be seen in Figure 1-7. The result of the study indicated that slow addition of NaOH to the micelles *in situ* leads to a contrast change at the surface of the micelles, suggesting the formation of an amorphous precursor phase. Whereas further addition of NaOH led to nucleation of iron oxide on the Mms6 protein micelles (Kashyap *et al.*, 2014). Moreover, other study also found that the addition of ferric and ferrous iron ions to the Mms6 protein solution promotes morphological changes in the micellar structure by transforming the micelle structure into 3D-mass fractal-like structure or, alternatively, 2D platelet-like structures (Zhang *et al.*, 2015).

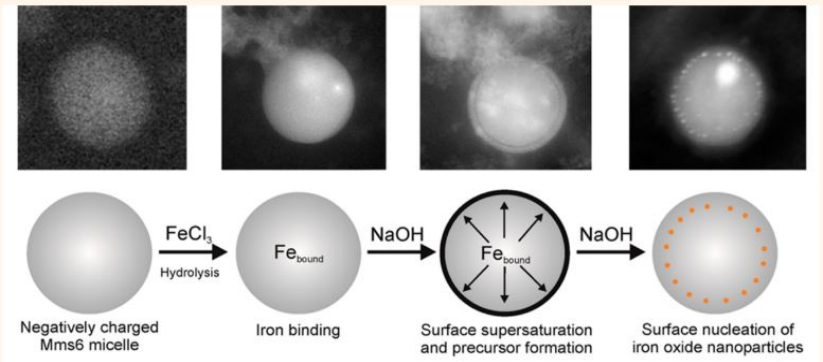

Figure 1-7: Schematic of Mms6-mediated iron oxide nucleation of micelle-bound iron species. *Image taken from* Kashyap *et al.* (2014).

Staniland and Rawlings (2016) hypothesized that Mms6 self-assembles to generate protein rafts on the interior of magnetosome membrane, showing a C-terminal surface, as seen in the surface of *in vitro* micelles. To test this, they assessed the ability of biomimetic Mms6 to self-assemble on a surface to model self-assembly in the magnetosome membrane environment. They found that the biomimetic Mms6 surface nucleated and controlled magnetite formation. On the other hand, biomimetic Mms6 without the N-terminal (named C20Mms6) could self-assembly on the surface, but no nucleated surface and magnetite formation was observed indicating the importance of the N-terminal region of Mms6 in controlling magnetite formation. Furthermore, a glycine–leucine repeating sequence is present in the conserved 6 kDa protein but absent in the C20Mms6. This sequence is an important feature of self-assembly proteins and is suggested to form a regularly packed structure generated by arrangement of hydrophobic residues which could interlock with adjacent Mm6

molecules. It is believed that without this structure the magnetite nucleation ability is lost (Staniland and Rawlings, 2016).

Rawlings *et al.* (2016) suggested that Mms6 is acting as a 'mineral/ferrous ion buffer' being able to direct mineralization towards magnetite synthesis. They have studied magnetite formation *in vitro* with or without Mms6 at different pH titrations. They found that the activity of Mms6 below pH4 is negligible for a range of different ferric:ferrous ratios, reducing Mms6 iron binding ability. However as pH increases to 7, deprotonation occurs forming negatively charged micelles that bind iron, suggesting Mms6 is active under these conditions (Rawlings *et al.*, 2016). Although pH inside magnetosomes has not been determined, it must be high enough to enable magnetite to precipitate, enabling Mms6 for nucleating or shape controlling the magnetite (Staniland and Rawlings, 2016). NMR spectroscopy analysis on Mms6 protein suggested that DEEVE acidic residue cluster within the C-terminal region of Mms6 acts as ferrous binding site. Mms6 is found to be active in ferrous-rich conditions *in vitro*, thus it is thought that *in vivo* conditions in the magnetosome are likely to be similar with respect to pH, the ability of Mms6 to form a self-assembled charged surface and the availability of ferric precursors in a ferrous-ion-rich solution in order to promote the crystallization of magnetite, as illustrated in Figure 1-8. Therefore, it was suggested that Mms6 plays a key role in binding both ferric and specifically ferrous iron to initiate the process of templating the magnetite crystal (Rawlings *et al.*, 2016).

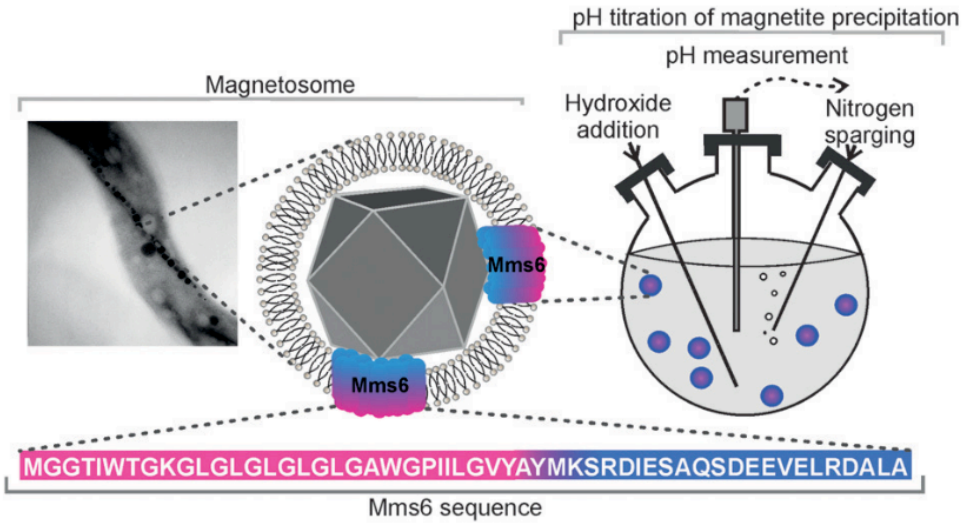

Figure 1-8: Mms6 protein with its sequence in magnetotactic bacterial magnetosome. *The hydrophilic acid-rich region is shown in blue color, whereas the hydrophobic membrane region is shown in pink color. Experimental schematic showing pH recording during addition of base to ferric/ferrous solution with or without Mms6 micelles is also illustrated. Mms6 is found to be active in ferrous-rich conditions* in vitro. *Image taken from Rawlings et al.* (2016).

1.5 MESENCHYMAL STEM CELLS

1.5.1 Mesenchymal stem cells distinctive characteristic

In 1974, mesenchymal stem cells (MSC) were identified by Friedenstein as proliferating fibroblastic cells from bone marrow capable of differentiating into osteoblasts, chondrocytes and adipocytes (Friedenstein *et al.*, 1974). Afterwards, the term 'MSC' was adopted by the Caplan group to define a population of stem cells with capability of self-renewal and differentiation into multiple lineages including cartilage, adipose, and bone (Caplan and Dennis, 2006).

Self-renewal refers to the ability to proliferate whilst maintaining the undifferentiated state: the cell divides symmetrically creating two identical copies of itself for long periods of time. Depending on the stem cell, self-renewal is a well-modulated process,

involving complex signaling networks (He *et al.*, 2009). Multipotency is defined as the ability of a progenitor cell to differentiate into a limited number of cell types with specific functions. MSC' plasticity to differentiate in different cell lineages (osteogenic, adipogenic, and chondrogenic), together with their immunomodulatory and anti-inflammatory properties, and their ability to migrate to sites of tissue injury/inflammation make these cells attractive in regenerative medicine and drug delivery (Figure 1-9) (Chapel *et al.*, 2003; Mouiseddine *et al.*, 2007; Nixon *et al.*, 2012; J. R. Park *et al.*, 2015; J. S. Park *et al.*, 2015).

In 2006, the International Society for Cell Therapy produced the minimal criteria to define human MSC. They must adhere to plastic in culture and differentiate into osteocytes, chondrocytes and adipocytes. In addition, they also must express CD105, CD90 and CD73 and lack expression of CD45, CD34, CD14 or CD11b, CD79alpha or CD19, and HLA-DR surface molecules (Dominici *et al.*, 2006). Moreover, MSC should escape immune recognition. Although MSC do not express MHC class II antigens, the expression of these molecules can be upregulated following exposure to inflammatory cytokines or during MSC differentiation (Le Blanc and Ringdén, 2005). Due to these distinctive characteristics the clinical application of these cells has been extensively studied, especially in regenerative medicine such as Orthopaedics where MSC are used to repair large bone defects (Bashir *et al.*, 2014), in haematology, where they have been used to support the engraftment of hematopoietic stem cells (Fouillard *et al.*, 2007; De Becker and Van Riet, 2015), and as a cell based technology for delivery of anticancer treatments (Ďuriniková *et al.*, 2014; Hammer *et al.*, 2015; J. S. Park *et al.*, 2015; Qiao *et al.*, 2015).

MSC have been isolated from a wide range of sources including bone marrow (BM) (Gnecchi and Melo, 2009), adipose tissue, umbilical cord (UC) (Bieback and Kluter, 2008; Hermantara *et al.*, 2016; Rizal *et al.*, 2018), liver (Lu *et al.*, 2014), and multiple dental tissues (G. T.-J. Huang *et al.*, 2009). Each of these sources has its own advantages and disadvantages. BM is the most characterized and documented source of MSC. However, the collection of MSC from BM is painful, invasive, and characterized by a low yield (Gnecchi and Melo, 2009). Adipose tissue is another

popular source, mainly because a large number of MSC can be obtained through minimally invasive methods (Bieback and Kluter, 2008). Although there are many sources for MSC, the quality of the MSC is highly variable from donor to donor and is significantly affected by age and aging disorders. To overcome this problem, MSC can also be derived from induced pluripotent stem cells (iPSC) (Lian *et al.*, 2010). MSC derived from iPSC show similar distinctive characteristics of MSC, such as the potential for adipogenesis, osteogenesis, and chondrogenesis, and display higher capacity for proliferation and stronger telomerase activity, leading to better engraftment and survival after transplantation (Lian *et al.*, 2010).

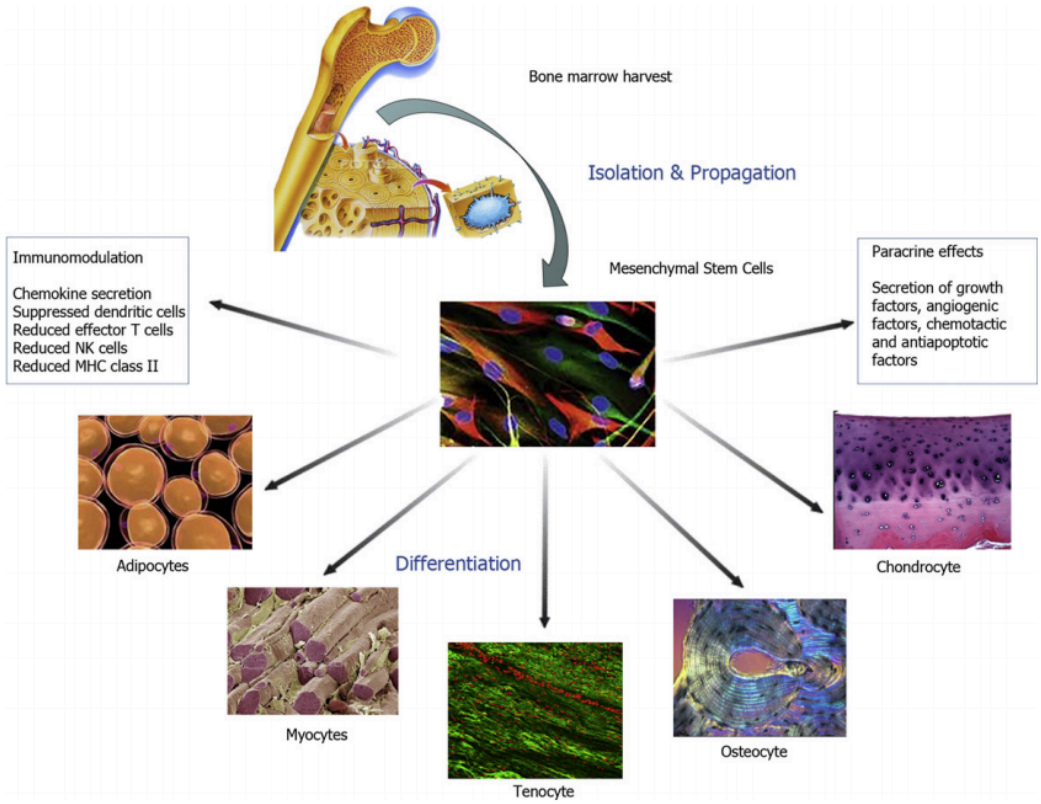

Figure 1-9:Mesenchymal stem cells distinctive characteristic. *Isolation of MSC can be from numerous connective tissues but is most common from bone marrow. The MSC plasticity to differentiate into osteogenic, adipogenic, and chondrogenic different cell lineages, together with their ability to migrate to sites of tissue injury/inflammation; secretion major histocompatability complex (MHC) of angiogenic, chemoattractant, and antiapoptotic factors; immunomodulatory and anti-inflammatory properties through reduced T-cell activity and MHC suppression. NK, Natural killer. Image taken from* Nixon *et al.* (2012).

1.5.2 Mesenchymal stem cells homing and migration

The exact mechanisms used by MSC to migrate and home to tissues have are not fully understood. However, it is generally suggested that MSC follow a similar process to that described for leukocyte homing. Firstly, the cells come into contact with the endothelium by tethering and rolling, resulting in a deceleration of the cells in the blood flow. In the second step, G-protein-coupled receptors activate the MSC cells, followed by integrin-mediated activation-dependent arrest in the third step. Finally, in the last step, the cells transmigrate between endothelial cells and through the underlying basement membrane (Butcher and Picker, 1996). Different molecules play a distinctive role in MSC migration and engraftment to the site of injury. Selectins on the endothelium are primarily involved in the first step. For bone marrow homing in particular, the expression of haematopoietic cell E-/L-selectin ligand (HCELL), a specialized glycoform of CD44 on the migrating cell, is very important (Sackstein, 2004). Although MSC express CD44, they do not express HCELL (Sackstein *et al.*, 2008). The G-protein coupled receptors that are involved in the activation step are typically chemokine receptors. It has been extensively demonstrated that the CXCR4-stromal derived factor-1 (SDF-1) axis is critical for bone marrow homing (Moll *et al.*, 2012). Both molecules are very physiologically important, as knock-outs are lethal due to bone marrow failure and abnormal heart and brain development (Nagasawa *et al.*, 1996; Zou *et al.*, 1998). CXCR4 expression has been enhanced both directly by designed transfection or transduction studies to improve the MSC homing efficiency by introducing plasmid into the cells by viral (Bobis-Wozowicz *et al.*, 2011) or non-viral means (Otani *et al.*, 2009; Wiehe *et al.*, 2013) or indirectly, by using molecules or processes that favour CXCR4 expression. To improve MSC CXCR4 expression a number of strategies have been proposed, such as treating the MSC culture before of the injection with a cocktails of cytokines (Shi *et al.*, 2007) like flt3 ligand stem cell factor (SCF), IL3, IL6 and hepatocyte growing factor (HGF), insulin-like growing factor 1 (IGF-1), tumour necrosis factor α (TNF α), IL 1β, interferon γ (IFN γ).

Integrins are important players in the stable activation-dependent arrest in the third step of homing. Inhibition of integrin β1 can block MSC homing (Ip *et al.*, 2007).

Integrins form dimers that bind to adhesion molecules on the endothelial cells. Integrin α4 and β1 combine to form very late antigen 4 (VLA-4), which interacts with vascular cell adhesion molecule 1 (VCAM-1). VCAM-1-VLA4 interaction is functionally involved in MSC homing (Rüster *et al.*, 2006; Segers *et al.*, 2006).

1.5.3 Engineering mesenchymal stem cells for therapy

The clinical application of MSC is often hindered by poor *in vivo* performance with respect to survival, retention, and engraftment. To overcome this problem, genetic engineering is one approach to improve the *in vivo* performance of MSC. In general, engineering MSC by genetic modification is achieved via viral vector transduction. However, non-viral vectors are becoming attractive as alternative techniques recently (J. S. Park *et al.*, 2015).

Engineering MSC by genetic modification using viral transduction has been promising. Standard protocols can lead to 90% transduced cells without detrimental effect on cell self-renewal or differentiation (Nolta *et al.*, 1994; Mosca *et al.*, 2000). In principle, the use of viral transduction allows transgene integrate into host genome, thus it can also offer a long-term and stable expression of the gene of interest. The most common vectors include retrovirus, lentivirus, baculovirus, and adeno-associated virus (AAV) (Airenne *et al.*, 2013). Retrovirus offers highly stable expression of gene of interest in the host genome, allowing long-term protein production which is ideal for treatment of genetic diseases. However, it could also lead to insertional mutagenesis and activation of oncogenes (Hacein-Bey-Abina *et al.*, 2008; Wu and Dunbar, 2011). Lentivirus also enables stable transgene expression through integration into the genome. Non-integrating lentiviral vectors have also been designed which can be useful to overcome the problems associated with integration (Banasik and McCray, 2010). Baculovirus, neither replicates nor integrates into the host genome and is capable of transducing with high efficiency. Baculovirus can transduce adipose-derived mesenchymal stem cells (AD-MSC) with 95% efficiency and have shown no toxic effect on the cells (Lu *et al.*, 2012). Finally, AAV is one of the most promising viral vectors due to its non-pathogenic feature to humans and results in long-term gene

expression. However, a large fraction of the human population have neutralizing antibodies against AAV, which significantly reduces their potential use in *in vivo* application (Nayak and Herzog, 2010).

Komarova and coworkers (2010) studied the feasibility of enhancing MSC tumour targeting by expressing an artificial tumour-binding receptor on the MSC surface using viral transduction approach. To test this, genetically modified adenoviral vectors encoding an artificial receptor (MSC-AR) were used to transduce human MSC, generating cells expressing an artificial receptor that binds to erbB2, a tumour cell marker. MSC-AR properties were tested *in vitro* in cell binding assays and *in vivo* using two model systems: transient transgenic mice that express human erbB2 in the lungs and ovarian xenograft tumour model. The levels of luciferase-labeled MSC in erbB2- expressing targeted sites were determined by measuring luciferase activity. The result demonstrated the expression of AR enhanced binding of MSC-AR to erbB2-expressing cells *in vitro*, and showed an increased retention of MSC-AR in lungs expressing erbB2. This result clearly showed targeting abilities of MSC can be enhanced by adenoviral-mediated genetic modification to produce artificial receptors, thus could increase a number of cell carriers in tumours and enhance efficacy of cell-based therapy (Komarova *et al.*, 2010).

The issue related to using viral transduction approaches have been the possibility of oncogene activation and the lack of targeted integration. To overcome this problem, Benabdallah and coworkers used zinc finger nuclease (ZFN) to add erythropoietin gene (Epo) into the chemokine (C-C motif) receptor-5 gene locus of MSC. Adenovirus vectors were utilized to deliver ZFN into MSC, while integrase-defective lentiviral vectors were utilized to deliver Epo. The MSC derived from human BM, adipose tissue, and umbilical cord blood was transduced with Epo by the ZFN-driven targeted gene addition. These cells were injected into the peritoneum of non-obese diabetic severe combined immunodeficient interleukin-2Rc null mice, resulting the hematocrit levels increased from an average of 49% to more than 60% at day. This study clearly demonstrates the potential of site directed insertion compared to the conventional random integration using viral vectors (Benabdallah *et al.*, 2010). Moreover, other

techniques such as transcription activator-like effector nucleases (TALENS), and clustered regularly interspaced short palindromic repeats (CRISPR) can be also used for site-directed integration (J. S. Park *et al.*, 2015).

Despite viral transductions have high efficiency, the major drawback of these vector has been the high production cost and adverse immune reactions. Some viral vectors have limitations in the packaging capacity of exogenous DNA and the possibility of oncogene activation (J. S. Park *et al.*, 2015). Therefore, non-viral vectors have been an alternative option which offer versatility in design choices and scale-up manufacturing. In addition, they are low in immune stimulation and also favorable for short term protein expression in therapy, which requires only a transient expression. However, the main issue with these techniques so far is MSC are difficult to transfect without affecting their viability, resulting in very low efficiencies (J. S. Park *et al.*, 2015; Kaestner *et al.*, 2015).

Current methods used to transfect MSC can be classified into chemical methods and physical methods. Lipid agents, polymeric carriers, dendrimers, and inorganic nanoparticles are common chemical methods used to transfect variety of cell types. However, lipid and polymeric agents typically can transfect 2–35% of MSC (Santos *et al.*, 2011). The conventional cationic liposome method was not effective for MSC transfection as it resulted in very low transfection efficiency even close to 0 % (Mun *et al.*, 2016). In contrast, recent report also indicated 95-100% transfection rate when human AD-MSC transfected using Lipofectamine 2000® transfection reagent (Mirzaei *et al.*, 2018).

Dendrimers have demonstrated great success in transfecting a wide variety of cell types but not MSC, particularly resulting lower transfection efficiency at 10-17% (Gheisari *et al.*, 2008) Inorganic nanoparticles such as gold nanoparticles (AuNPs) have emerged as attractive nonviral gene vectors due to their ease of synthesis, tunable size and shape, flexible surface modification, and tunable optical and electronic properties. Gold nanoparticles designed with Jet-poly(ethylenimine) (PEI) reagent can condense DNA on the surface to achieve a 2.5-fold increase in transfection efficiency over conventional Jet-PEI polyplexes (Uchimura *et al.*, 2007).

Recent report by Peng and coworkers (2016) demonstrated the synthesis of antimicrobial peptide conjugated cationic gold nanoparticle as highly efficient carriers for gene delivery to MSC with antibacterial ability. The gold-peptide complexes combine the advantages of cationic gold and antibacterial peptides: the presence of cationic can effectively condense DNA and the antimicrobial peptides are important for the cellular & nucleus entry enhancement to achieve high transfection efficiency and antibacterial ability. The study showed the gene transfection efficiency in rat MSC was strongly improved by using the gold-peptide complexes, showing highest transfection ability when the peptide content was about 2.5% of the gold nanoparticles. While the gold/pDNA without peptide complexes also showed strong gene transfection ability, lead to about 1/3 luciferase expression of that expressed by gold-peptide/pDNA complexes. This result showed promising nanoparticle-peptide conjugation as non-viral gene vectors for MSC-based therapy and antibacterial abilities in clinic(Peng *et al.*, 2016).

Physical transfection approaches include electroporation and nucleofection (J. S. Park *et al.*, 2015). Although these methods offer high transfection efficiency, the main obstacles have been the significant cell death (~40%) if not handled properly (Aslan *et al.*, 2006). Electroporation uses an electrical pulse to transiently open the pores of the cells, allowing the nucleic acid to enter the cytoplasm. Nucleofection also uses electrical pulse but the nucleic acid is directly introduced into the nucleus of cells. Other physical approach such as sonoporation uses mechanical vibration to increase the transport of nucleic acid into the cells by enhancing the permeability of the cell membrane (J. S. Park *et al.*, 2015).

1.5.4 Mesenchymal stem cells as drug and nanoparticle carrier

MSC have been regarded as a potential approach for drug and gene delivery. These recombinant MSC act as cell vehicles to carry various genes and drugs to divergent organs for therapy, owing to the high affinity of the injury or tumour sites and migration ability. Bonomi and coworkers (2015) investigated MSC isolated from the amniotic membrane of human term placenta (hAMSC) as candidates for drug delivery

in vitro. They primed hAMSC with paclitaxel (PTX) and investigated their ability to resist the cytotoxic effects of PTX, to upload the drug, and to release it for up to 120 hours when co-culturing with human ductal pancreatic adenocarcinoma cell lines. The result showed hAMSC are highly resistant to the cytotoxicity of PTX loading even at highest dosage of 10μg/ml, suggesting potential use of placental MSC as vehicles for delivery of cytotoxic agents (Bonomi *et al.*, 2015).

The idea of using MSC for delivering chemotherapeutics as an alternative option for therapy was also reported by Pessina and coworkers (2013), who demonstrated both *in vitro* and *in vivo* study, where PTX loaded MSC further attract and kill leukemia cells, inhibit angiogenesis and tumour growth (Pessina *et al.*, 2013). In recent report, Coccè and coworkers (2017) studied MSC isolated and expanded from gingival papilla (GinPa-MSC). These cells were studied for their ability to uptake and release three antineoplastic drugs: PTX, Doxorubicin (DOX) and Gemcitabine (GCB). The result indicated that GinPa-MSC efficiently uptake the drugs and then released them in active form and in sufficient amount to promote a dramatic inhibition of squamous cell carcinoma growth *in vitro* (Coccè *et al.*, 2017).

Beside the promising use as a vehicle for anti-tumour drugs, MSC also can uptake drug loaded and diagnostic nanoparticles to specific target sites. Drug-loaded nanoparticles can be uptake through endocytosis pathways by cells as intracellular drug stores and maintain sustained release, thus decreasing anticancer-drug cytotoxicity and chemotherapeutic loss by rapid drug efflux (Wu *et al.*, 2019). Due to the tumour tropism of MSC, drug-conjugated nanoparticles loaded MSC were localized in the tumour tissues like prostate cancer tissue (Levy *et al.*, 2016), lung (Sadhukha *et al.*, 2014; Zhao *et al.*, 2017), and glioma tissue (Pacioni *et al.*, 2015; Wang *et al.*, 2018).

Wang and coworkers (2018) utilized MSC as lung cancer-targeted drug delivery vehicles by loading nanoparticles (NP) with anti-cancer drug. IR-780 dye, a fluorescent probe was used to represent docetaxel (DTX) in NP, delivered via MSC accumulated in the lung. The study demonstrated both *in vitro* MSC/A549 cell experiments and *in vivo* MSC/lung cancer experiments showing the intercellular transportation of NP between MSC and cancer cells, suggesting exocytosis-

endocytosis process between both cells. Moreover, *in vivo* experiments indicated that the MSC/NP/DTX drug delivery system resulted in primary tumour inhibition efficiency similar to that of a NP/DTX drug system, suggesting a promising lung-targeted drug delivery for the treatment of lung cancer.

Duchi and coworkers (2013) investigated the combination of photodynamic therapy, nanoparticles and MSC in killing osteosarcoma *in vitro.* Fluorescent core-shell PMMA nanoparticles (FNPs) were post-loaded with a photosensitizer, namely meso-tetrakis (4-sulfonatophenyl) porphyrin (TPPS) and loaded into MSC. The result showed the incorporation of TPPS@FNPs into MSC is nontoxic until an external photoactivation is applied. The result also indicated TPPS@FNPs were internalized through endocytosis mechanism with no significant motility alteration. It was observed that upon the first light irradiation MSC undergo cell death, while the TPPS@FNPs continue to be available at the diseased site for successive irradiations, suggesting a very promising use of MSC as nanoparticle carrier and therapeutic agent. (Duchi *et al.*, 2013).

Other nanoparticles that have been extensively studied for photothermal cancer therapy is gold nanoparticles (AuNPs) due to their ability to generate heat upon near-infrared irradiation. Kang and coworkers (2015) demonstrated that MSC can aggregate pH-sensitive gold nanoparticles (PSAuNPs) in mildly acidic endosomes of target tumours, and be used for photothermal therapy. These aggregated structures had a higher cellular retention in comparison to pH-insensitive, control AuNPs (cAuNPs). When PSAuNP-laden MSC (MSC-PSAuNPs) injected intravenously to tumour-bearing mice, the tumour-targeting efficiency was improved, resulting a 37-fold higher tumour-targeting efficiency (5.6% of the injected dose). Moreover, when laser radiation was applied, elevated temperature at 8.3 °C higher than control was observed, suggesting a significantly improved anticancer effect (Kang *et al.*, 2015).

MSC can also serve as cellular vehicles for delivery of nanoparticles to brain tumours due to the difficulty of delivering therapeutic agents to tumour and to the infiltrating tumour cells. To test this, Roger and coworkers (2010) investigated two types of NPs loaded with coumarin-6: poly-lactic acid NPs (PLA-NPs) and lipid nanocapsules

(LNCs). Both PLA-NPs and LNCs provide considerable drug encapsulation capacity and also manifest sustained release functions at the site of action. These NPs were loaded into a unique subpopulation of human MSC named "marrow-isolated adult multilineage inducible" (MIAMI) cells. The results of study indicated that these NPs can be efficiently internalized into MSC with no significant effect on cell viability and differentiation. Furthermore, these NP-loaded cells were able to migrate toward an experimental human glioma model, suggesting a potential approach of MSC-based cellular carriers for NPs in brain tumours (Roger *et al.*, 2010).

Magnetic resonance (MR) contrast agents are valuable tools in the diagnostic evaluation and follow-up of managed treatment. Recently, superparamagnetic iron oxide nanoparticles (SPION) are being used as contrast agent for intracellular magnetic labeling of stem cells and variety of cells types in order to monitor cell trafficking by magnetic resonance imaging (MRI) as part of cell-based therapy (Frank *et al.*, 2004). Boutry and coworkers (2008) investigated the influence of MNP incubation concentration on MSC and fibroblasts cells in culture. Cells were incubated for 48h with increasing iron concentrations of SPION (25–1000mg Fe/ml Endorem®). The study demonstrated that intracellular iron content increased as a function of the iron concentration in the incubation medium, suggesting the cells labeling with SPION was found to be dose-dependent uptake. The study also showed higher uptake capacity of the MSC as compared with an established fibroblast cell line. Even more interesting, efficient magnetic labeling with commercially available superparamagnetic MRI contrast agents was simply done by mixing the magnetic nanoparticle to the cell culture medium, resulting no significant effect in cell viability (Boutry *et al.*, 2008).

Other report also investigated the tracking of MSC with SPION-loaded Poly (lactide-co-glycolide) microparticles for MRI. The study demonstrated internalization of SPION (10 nm) loaded biodegradable poly(lactide-co-glycolide) microparticles in MSC increases magnetic resonance parameters such as the r_2 relaxivity (5-fold), residence time inside the cells (3- fold) and R_2 signal (2-fold) compared to SPION alone. Both *in vitro* and *in vivo* experiments also showed no significant effect on cell

properties such as viability, proliferation, migration and their ability to home to sites of inflammation, suggesting a promising opportunity for longitudinal tracking of MSC without compromising cell phenotype including cell migration/homing ability (Kultima *et al.*, 2012).

The SPION-labelled MSC or MNP-labelled MSC can also be used for magnetic targeting as reported by Riegler and coworkers (2012) who investigated MSC labelled with FluidMAG-D SPION for vascular injury therapy. The study indicated that magnetic targeting of MSC gives rise to a 6-fold increase in cell retention following balloon angioplasty, which reduced restenosis three weeks after cell delivery in a rabbit model using a clinically applicable permanent magnet. No negative effects on cell viability, differentiation or secretion patterns was also noticed on FluidMAG-D SPION labelled MSC (Riegler *et al.*, 2013).

More advanced approach was also reported by Yin and coworkers (2016) who proposed dual purpose of delivering and activating a heat-inducible gene vector that encodes TNF-related apoptosis-inducing ligand (TRAIL) in adipose-derived mesenchymal stem cells (AD-MSC), providing an attractive approach to enhance the control over the activation of stem cell-based gene therapies. The study indicated a decrease in ovarian cell viability due to the mild magnetic hyperthermia-activated secretion of TRAIL from the engineered AD-MSC as determined by significant activation of caspases *in vitro.* Whereas, *in vivo* experiments showed when engineered AD-MSC were delivered into a metastatic ovarian cancer mouse model and magnetic hyperthermia was applied, AD-MSC were found to secrete TRAIL, which significantly decrease tumour volume compared to controls over a two-week period (Yin *et al.*, 2016).

1.5.5 MSC as double-edged sword in tumour growth.

Despite promising use of MSC-based therapy to target tumour, the exact role of MSC in tumour progression is still unknown. Studies have shown that MSC are involved in tumour growth and metastasis, while others indicate the inhibitory effect of MSC on

growth of tumours such as hepatoma and leukemia, suggesting MSC migrate towards tumour microenvironment and are involved in both pro-tumourigenic and antitumourigenic functions (Ramasamy *et al.*, 2007; Qiao *et al.*, 2008; Norozi *et al.*, 2016). Norozi and coworkers (2016) explained these dual functions of MSC as double-edge sword since they can be regarded both as friends or enemies in suppression or progression of solid tumour cells. It is believed MSC behavior at tumour sites is dependent upon a variety of factors, including the type and origin of MSC, the cancer cell line under study, *in vivo* or *in vitro* conditions, the factors secreted by MSC and interactions between MSC, host immune cells and cancer cells (Norozi *et al.*, 2016).

In regard to MSC function in tumour, they seem to be capable of immunosuppressive and immunomodulatory (Niess *et al.*, 2016). They are capable of modulating their local tissue environment through direct cell-cell contacts or through secretion of different immune-related molecules in order to repair or regenerate tissue. While suppression of immune response by MSC may facilitate tissue remodeling and repair, however this may be risky in progression of cancer (Kuhn and Tuan, 2010).

Tumour stroma, also known as the tumour microenvironment that surrounds expanding cancer cells with immediate contact is believed to mainly function as a pool of surrounded and recruited "normal" cells that then become manipulated by cancer cells to support the formation of an organ-like macroscopic tumour (Hanahan and Coussens, 2012). These cells can be categorized as infiltrating immune cells, cancer-associated fibroblasts (CAFs), and angiogenic vascular cells (AVCs; endothelial cells and pericytes) (Tlsty and Coussens, 2006). Both experimental and clinical studies have indicated supporting evidence that MSC contribute to the cancer stroma. Expanding tumours persistently alter their surrounding tissue causing an inflammatory response, suggesting tumours behave in the body like wounds (Dvorak, 1986).

Cuiffo and Karnoub classified four categories by which MSC within the tumour stroma may influence tumour growth (Cuiffo and Karnoub, 2012) : 1) through direct actions on tumour cells: 2) through indirect effects; such as the enhancement of angiogenesis; 3) through their immunosuppressive properties; and 4) as progenitors for tumour stromal cells.

In regard to MSC direct action, they seem to be capable of releasing chemokines, cytokines, and growth factors on cancer cells, which aid tumour proliferation, invasion, and metastasis. Studies have shown MSC-derived CXCL1/2 and CXCL12/SDF-1 can enhance cancer cell proliferation through signaling on their respective CXCR2 and CXCR4 receptors expressed by cancer cells (Rhodes *et al.*, 2010; Halpern *et al.*, 2011). Other reports also have shown that IL-6 and IL-8 released by MSC enhance malignancy in breast and colorectal cancer models (Liu *et al.*, 2011; Tsai *et al.*, 2011), and epidermal growth factor (EGF) secreted by MSC enhances tumourigenesis in a breast cancer model (Yan *et al.*, 2012). Whereas, though their indirect effect, MSC within the tumour stroma could promote tumour growth by promoting process of tumour angiogenesis, in particular, by recruitment of endothelial progenitor cells and by enabling the formation and maturation of tumour vasculature (Koike *et al.*, 2004; Au *et al.*, 2008).

MSC could defend tumour cells from both adaptive and innate immune systems, suggesting their immunomodulatory function within tumour stroma. Despite not necessarily based on cancer models, it has been proven that MSC are capable of participating in the major key immune activities involved in the process of tumour formation (Cuiffo and Karnoub, 2012). Furthermore, MSC may also involve in the tumour microenvironment by providing a cell pool and molecules which may result the differentiation of MSC toward a more specialized stromal cells. Studies have shown that the transdifferentiation of MSC to CAFs and myofibroblasts, which aid tumour growth, was indicated after signaling from tumour-conditioned medium (Mishra *et al.*, 2008), tumour-derived exosomes (Cho *et al.*, 2012), and xenografts from breast, pancreatic, and ovarian cancers (Spaeth *et al.*, 2009) as well as prostate cancer (Jung *et al.*, 2013).

On the other hand, the inhibitory effect of MSC on tumour may involve decreased activity of signaling pathway of AKT, Wnt/β-catenin, Bcl-2, c-Myc, proliferating cell nuclear antigen and surviving, which result in decreased proliferation, G1 arrest, suppression of oncogenes, and increased apoptosis (Ramasamy *et al.*, 2007; Gao *et al.*, 2015). Cousin and coworkers (2009) studied the effect of human stromal cells derived

from adipose tissue (ADSC) on pancreatic tumour cell (PDAC) proliferation. The study demonstrated that co-culture of pancreatic tumour cells with ADSC and ADSC-conditioned medium sampled from different donors inhibited cancer cell viability and proliferation. ADSC-mediated inhibitory effect was further conducted to other epithelial cancer-derived cell lines (liver, colon, prostate), resulted in induced cancer cell necrosis following G1-phase arrest *in vitro*. Moreover, a single intra-tumoural injection of ADSC in a model of pancreatic adenocarcinoma also resulted in a significant inhibition of tumour growth. It was believed that the anti-proliferative effect of ADSC on pancreatic cancer cells may be mediated at least in part by a secreted molecules which could alter cell cycle progression, and the capability of ADSC to modify the microenvironment of the tumour and thus inhibit its proliferation (Cousin *et al.*, 2009).

Despite the main reason behind the duality behavior of MSC function against tumours is not well understood, it may be dependent upon several factors, including large variety of cytokines, growth factors produced by MSC, type of cancer cell line tested, and the type and source of MSC (Norozi *et al.*, 2016). Akimoto and coworkers (2013) investigated anticancer therapeutic application of MSC from two different MSC sources: umbilical cord blood-derived MSC (UCB-MSC) and adipose-tissue-derived MSC (AD-MSC). They found that UCB-MSC inhibited primary brain tumour growth and caused apoptosis through secretion of tumour necrosis factor-related apoptosis-inducing ligand (TRAIL), whereas AD-MSC promoted tumour growth. The opposite effects of AD-MSC was believed due to higher CXCL12 expression on AD-MSC which might act as antiapoptotic factor inhibiting the TRAIL pathway. The result of this study clearly demonstrate that differences of MSC source must be evaluated when choosing MSC source for safety in clinical application (Akimoto *et al.*, 2013).

1.6 MAGNETIC HYPERTHERMIA

1.6.1 Magnetic nanoparticle-mediated Hyperthermia

Hyperthermia therapy (HT) is defined as a therapeutic treatment of diseases in which tissues are heated above normal physiological ranges. It has been an established alternative therapy for cancer treatment, in part due to the likelihood that its application could result in fewer side effects than standard chemotherapy or radiotherapy. Depending on the degree of cellular damage induced, hyperthermia treatment can be classified into two different ranges. In conditions of moderate temperature increases (41-46°C), the treatment may alter the functionality of intercellular proteins, leading to cellular degradation and apoptosis (Sellins *et al.*, 1991; Deatsch and Evans, 2014). In thermoablation, hyperthermia treatment at temperatures greater than 46°C results in direct cell death, tissue necrosis, coagulation or carbonization (Kumar and Mohammad, 2011)

In clinical application for cancer therapy HT can be classified into three categories: local, regional and whole-body hyperthermia (van der Zee, 2002). In general, local hyperthermia can be induced with external or internal energy sources which are used to increase tumour temperatures as high as possible, as long as the tolerance limits of the surrounding normal tissues are not exceeded. For larger areas of treatment or for deeper tissues, regional hyperthermia is commonly used by perfusion of organs or limbs with heated blood or heater fluids for a defined duration to obtain therapeutic effects. Whole body hyperthermia is typically used to treat metastatic disease. The use of a flexible infra-red chamber or simply wrapping the patient in heated blankets are the most common examples in whole-body hyperthermia (van der Zee, 2002).

Despite the promise of HT in the clinical setting, a major drawback with conventional HT application is the difficulty of controlling the desired temperature at the local tumour region without damaging adjacent normal tissue. Indeed, although raising the normal physiological temperature can kill a great number of tumour cells normal tissues are also affected under these conventional hyperthermia treatments. To overcome this problem, the development of novel hyperthermia systems such as the use of Magnetic nanoparticle-mediated hyperthermia (MNHT) has advanced and

attracted attention for medical applications (Ito *et al.*, 2005). The concept of MNHT is the conversion of dissipated magnetic energy into thermal energy under an oscillating magnetic field. This approach was first proposed in 1957 by Gilchrist et al. in a study investigating the application of magnetic materials for hyperthermia treatment of cancer (Gilchrist *et al.*, 1957). Since then this concept has advanced into a well-researched field due to the introduction of MNP. Principally, the MNHT approach relies on the ability of MNP to transform electromagnetic energy into heat which results in an increase of temperature in well-defined regions of the human body where tumour cells and exogenous nanoparticles are located. Therefore, MNP can be controlled remotely from outside of the body by applying or removing an oscillating magnetic field. The electromagnetic radiation used in magnetic hyperthermia is in the range of radio-frequency (between several kHz and 1 MHz) which is non-toxic and gives sufficient penetration depth to access inner organs in the body (Bañobre-López *et al.*, 2013).

In a review by Kumar and Mohammad (2011), MNHT treatment was stated as having a number of advantages compared to the conventional HT. These are: 1) MNP can be taken up by tumour cells thus improving the effectiveness of hyperthermia by delivering therapeutic heat directly to them, 2) the use of the frequencies of oscillating magnetic fields to pass through the body are non-invasive and produce heat selectively only in tissues where MNP are located(Rand *et al.*, 1985); MNP can also effectively cross blood-brain barrier (BBB), thus can be used for treating brain tumours (Liu *et al.*, 2010); 4) MNHT treatment may also induce antitumoural immunity (Kobayashi *et al.*, 2014); 5) The heating can be stimulated at cellular levels effectively through alternating magnetic field (AMF), 6) MNP could be administered through a number of drug delivery routes, and importantly 7) MNHT can also be utilized for controlled delivery of drugs which opens up possibilities for the cancer theranostic approaches (Kumar and Mohammad, 2011).

1.6.2 Mechanisms of action of hyperthermia

Despite the exact mechanism of direct HT-induced cell death being not well understood, the thermal energy required for induction of cell death is likely to be close to the energy needed for protein denaturation or inactivation, leading to membrane alteration and cytoskeletal damage. Protein denaturation can also have an effect in the alteration of DNA synthesis and repair (Hervault and Thanh, 2014).

It is known that cancer cells are more susceptible to increases in temperature than the surrounding normal cells, in part explained by the higher sensitivity to heat for cells in the mitosis phase of the cell cycle (Hildebrandt *et al.*, 2002; Lepock, 2003). *In vivo* studies have also shown that temperatures in the range of 40–44°C cause more selective damage to tumour cells (van der Zee, 2002). This may be related to basic physiological differences between cancerous and normal tissue vasculature. Due the fast proliferation of tumour cells, the architecture of the vasculature in growing tumours is disorganised and abnormal compared to normal tissue vasculature. Owing to these structural differences, when hyperthermia is applied at temperatures over 42°C, tumour blood flow is likely to be decreased while in normal tissue it significantly increases. As a consequence, the slower blood flow in tumour leads to a lower heat dissipation rate, thereby further increasing the local intratumoural temperature whereas in normal tissue increased blood flow would act to maintain a lower temperature. Moreover, the abnormal structure of vasculature also results in poor tumour perfusion, resulting in oxygen and nutrient deprivation which are even more favored with the reduction of the blood flow caused by HT (Hildebrandt *et al.*, 2002; Hervault and Thanh, 2014).

In addition to direct cell killing effects, HT also affects cell shape and induces changes in the cellular environment. Cellular membrane becomes more fluidic and less stable, preventing the function of transmembrane transport proteins, cell surface receptor and cell attachment. Elevated fluidity of cell membranes occurs in thermosensitive, but not thermotolerant cells (Calderwood and Hahn, 1983; Konings and Ruifrok, 1985; Majda *et al.*, 1994). Cells exposed to HT treatment also show membrane blebbing, a distinctive feature of apoptosis-mediated programmed cell death. Moreover, although

not directly related to hyperthermia cell death but a reflection of altered cell physiology, several reports have shown changes in membrane potential, elevated intracellular sodium and calcium content, and increasing potassium-efflux under hyperthermia conditions (Hildebrandt *et al.*, 2002).

Disruption of the cell cytoskeleton is also likely to be important in HT induced cell injury (Pawlik *et al.*, 2013). The cytoskeleton orchestrates many cell functions, such as cell division, macromolecules transport, protein synthesis regulation and intracellular organelles distribution and anchoring. HT exposure reduces the number of actin stress fibers, alters microtubule assembly leading to a looser meshwork and collapses vimentin filaments into perinuclear complexes. Subsequent mitotic catastrophe occurs likely leading to apoptosis (Pawlik *et al.*, 2013).

1.6.3 Hyperthermia-induced apoptosis

HT induces cancer cell death through apoptosis, a programmed cellular suicide as a homeostatic mechanism to maintain cell populations in tissues (Hildebrandt *et al.*, 2002). The degree of apoptosis and the apoptotic pathway vary in different cancer cell types. Since apoptosis plays a fundamental role in maintaining a proper balance between cell survival and cell death, dysregulation of this defense mechanism process promotes uncontrolled cellular proliferation and accumulation of genetic defects, which ultimately result in tumourigenesis. Chemotherapy- and radiotherapy-induced killing of cancer cells is mainly mediated through activation of apoptosis, thus impairment of apoptotic pathways can also result in cancer cells developing resistance to conventional anti-cancer agents(Plati *et al.*, 2011).

Apoptosis can be triggered by activation of caspases in two different pathways: the intrinsic or mitochondrial pathway and the extrinsic or death receptor pathway, as can be seen in Figure 1-10 (Ahmed *et al.*, 2015). Most studies report that HT kills cells through activation of the intrinsic apoptotic pathway. Caspase-2 plays an important role in cell death by acting on microtubules organisation in this pathway (Ahmed *et al.*, 2015). Several reports indicate that caspase-2 forms a complex with its adaptor

protein named RAIDD (RIP-associated Ich-1/Ced-3-homologue protein with a death domain) immediately after HT treatment. This complex then activates caspase-2 and cleaves Bid (BH3 interacting-domain death agonist) which then stimulates mitochondrial outer membrane potential (MOMP), cytochrome c release, and formation of an Apaf-1-caspase-9 apoptosome (Bonzon *et al.*, 2006; Tu *et al.*, 2006; Ho *et al.*, 2008; Bouchier-Hayes *et al.*, 2009).

With regards to the extrinsic apoptotic pathway, hyperthermia activates an apoptotic pathway initiated by specific ligands such as antigen 1 or Fas ligand (Reap *et al.*, 1997), the cytokine tumour necrosis factor (TNF)-related apoptosis-inducing ligand (TRAIL) (Yoo and Lee, 2007), and the TNF-α ligand that plays a major role in binding TNFR1 and TNFR2 receptors in the extrinsic apoptotic pathway (Ahmed *et al.*, 2015). In the pathway initiated by Fas ligand, Fas can either directly activate downstream effector caspases or trigger the mitochondrial apoptosis amplification loop. This pathway involves series of activation mechanism orchestrated by caspase-8 result in the release of cytochrome c, which binds to Apaf-1 and caspase-9 apoptosome complex (Tran *et al.*, 2003). Mild hyperthermia has been shown to enhance TRAIL-induced cytotoxicity of CX-1 human colorectal cancer cells through the activation of caspases-8, -9 and -3 and cytochrome c release from mitochondria (Yoo and Lee, 2007). The apoptotic signal of TRAIL is transduced by binding to the death receptors TRAILR1 (DR4) and TRAILR2 (DR5), which are expressed prevalently on the surface of tumour cells more than on the surface of normal cells and thus triggers the extrinsic apoptotic signal. This pathway involves caspases-8 and -10 in forming a death-inducing signaling complex. Caspase-8 can either activate caspase-3 in cooperation with Caspase-10 or participate in the mitochondrial apoptosis pathway (Ahmed *et al.*, 2015).

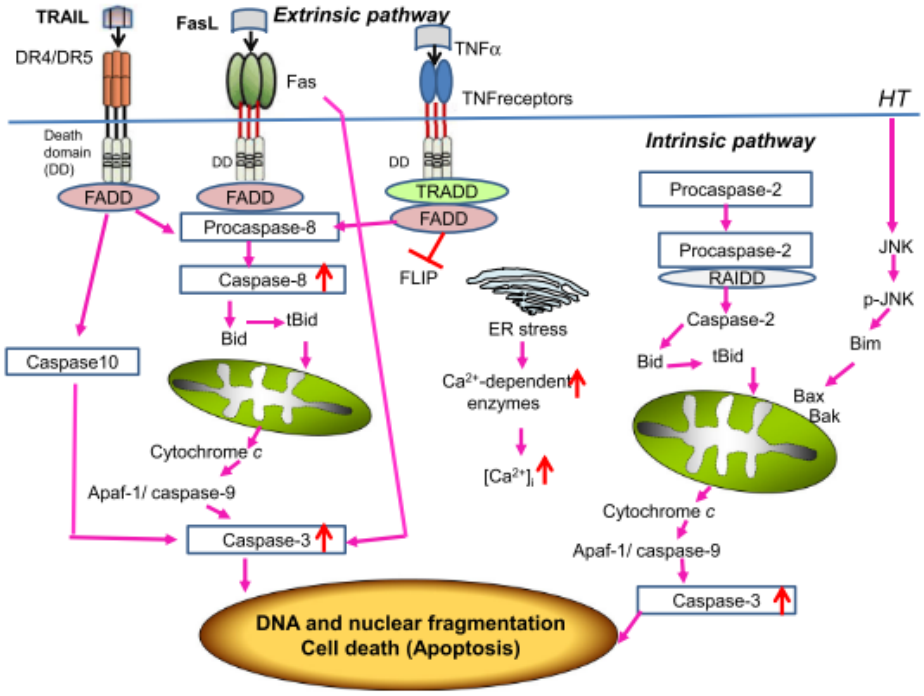

Figure 1-10: Extrinsic and intrinsic apoptotic pathways triggered by HT. *Extrinsic apoptotic pathway: HT activates the ligand TRAIL, Fas ligands, and the TNF-α ligand. TRAIL binds to death receptor DR4 and DR5, starting the apoptosis signal; as a consequence, the surface of FADD is exposed, and forms the death signalling complex with the help of caspase-8 and caspase-10. Caspase-8 can either activate caspase-3 in cooperation with Caspase-10 or participate in the mitochondrial apoptosis pathway. Fas could either activate the mitochondrial amplification loop (involving caspase-8, Bid and cytochrome c) or the downstream caspases. TNF-α binds THFR1 and TNFR2 receptors, inducing apoptosis through extrinsic pathway. The repetition of HT favours the down-regulation of the FLIP protein, which inhibits caspase-8 and favours the TNFR-mediated apoptosis signalling.*

Intrinsic apoptosis pathway: Caspase-2 acts on microtubules and forms a complex with RAIDD. The complex Caspase-2/RAIDD cleaves Bid, creating tBid, which stimulates the mitochondrial outer membrane potential (MOMP), cytochrome c release, and the formation of Apaf-1-caspase-9 apoptosome. The intrinsic apoptosis signalling could be triggered also by the independent pathway which involves Bim. Bim favours the Bax/Bak-independent activation of caspase-3 in the absence of MOMP, and it is also destroyed by heat stress, together with actin and tubulin.

Image taken from Ahmed et al. (2015).

1.6.4 Hyperthermia activates heat shock proteins (HSPs)

Molecular chaperones are needed for a range of major cellular functions including recovery from cellular stress. Heat shock proteins (HSPs) are molecular chaperones that act as "stress protein" due the wide range of stimuli able to cause stress induction such as heat, oxidative injury, sodium arsenite, heavy metals, amino acid analogues and serum deprivation (Fuller *et al.*, 1994). Based on their molecular weight, HSPs can be divided into six subfamilies: the large HSPs of 100- 110 kDa, the HSP90 family, the HSP70 family, the HSP60 family, the HSP40 family, and small HSPs of 18-30 kDa (Jäättelä, 1999). The HSP70 family is the most conserved and widely studied class of HSPs. Human cells contain several HSP70 family members including highly stress-inducible HSP70. The synthesis of stress-inducible HSP70 enhances the ability of stressed cells to deal with increased concentrations of unfolded and/or denatured proteins under various stress stimuli. Several studies either enhanced or reduced expression of HSP70 in a wide range of cell lines have suggested that HSP70 is a general survival protein capable to cover a prominent role in cell protection from heat as well as maintaining the resistance of most cells to apoptosis and/or necrosis (Fuller *et al.*, 1994; Jäättelä, 1999; Kaur *et al.*, 2000).

HT is known to induce HSPs. Since the expression of HSPs protects cells from heat-induced apoptosis, HSP expression is considered to be a critical factor in HT treatment. A connection between HSP-expression and hyperthermia came from a study investigating a stress-inducible form of HSP-70/72 that is expressed on the surface of cultured cells. The study suggested that HSP 70/72 was expressed either constitutively or heat-induced, and, is likely capable to stimulate an MHC-independent tumour cell-lysis, probably acting as foreign antigens by themselves and activating the immune response against tumour cells (Multhoff *et al.*, 1997, 1999; Botzler *et al.*, 1998). Impaired tumour immune responses could be due to poorly immunogenic tumour cells with insufficient concentrations of intracellular HSP–peptide complexes. Previous reports have demonstrated the importance of HSPs in immune reactions, including HSP70, HSP90 and gp96, and suggested that HSPs chaperon tumour antigens (Udono and Srivastava, 1993; Srivastava *et al.*, 1994; Vanaja *et al.*, 2000; Castelli *et al.*, 2001).

It was suggested that the antitumour activity of MNHT may consist of two possible mechanism: a direct killing effect by hyperthermia and an indirect, immune-mediated antitumour effect. In the latter case, MNHT increases immunogenicity during hyperthermia treatment which also improve the therapeutic outcome when combined with immunotherapy or chemotherapy. MNHT stimulates antigen presentation via the expression of intracellular HSP70-–peptide complexes as well as enhance function of the endogenous antigen-processing machinery and increases density of MHC class I–peptide complexes at cell surfaces (Ito *et al.*, 2001; Ito, Shinkai, *et al.*, 2003; Kobayashi *et al.*, 2014).

1.6.5 Hyperthermia stimulates production of reactive oxygen species

Reactive oxygen species (ROS) are a by-product of oxygen metabolism in the cell respiration system. In conditions of oxidative stress ROS levels are elevated as a consequence of an imbalance between the production of ROS and the available neutralizing antioxidants. ROS such as superoxide and hydrogen peroxide (H_20_2) are produced at low levels during normal cellular metabolism and play important roles in both physiological and pathological processes (Boveris and Chance, 1973). ROS are involved in regulation of cell death through various stimuli. It has been known that high levels of oxidative stress can kill tumour cells or at least prevent tumour growth. Therefore several studies have focused on increasing the formation of ROS under HT treatment and enhance tumour cell death (El-Orabi *et al.*, 2011; Franke *et al.*, 2013; Hou *et al.*, 2014; Fu *et al.*, 2017; Yang *et al.*, 2018). Recent reports investigating the HT application in human osteosarcoma (U-2 OS) cells showed that HT exposure at 43 °C for 60 min was able to induce apoptosis by triggering mitochondrial dysfunction, ROS accumulation, and caspase activation (Hou *et al.*, 2014). *In vivo* and *in vitro* HT induced radiosensitization in breast cancer stem-like cells (CSCs) and pancreatic CSCs was associated with increased intracellular ROS level in CSCs, which suggests a new approach for improving CSCs radiosensitivity (Fu *et al.*, 2017).

Recently MNHT was shown to efficiently induce higher ROS production when compared to conventional HT (extrinsic HT), leading to enhanced pancreatic cancer

cell death (Ludwig *et al.*, 2017). This study also demonstrated that increasing levels of ROS with increasing temperatures correlated well with the induction of apoptosis. Interestingly, the exposure of cells to bare MNP also increased formation of ROS which potentially could be a consequence of partial degradation of internalized MNP in endolysosomes. Besides being more efficient in increasing ROS production, MNHT exposure may also significantly reduce the expression of the proliferation markers Ki-67, TOP2A, and TPX2 compared to extrinsic HT (Ludwig *et al.*, 2017).

1.6.6 Basic physic of magnetic hyperthermia

Brownian-Néel relaxation and hysteresis losses are two main mechanism responsible for heat dissipation from magnetic nanoparticles in MNHT (Rosensweig, 2002; Suto *et al.*, 2009; Carrey *et al.*, 2011). Hysteresis losses are observed in multidomain MNP, whereas Brownian-Néel relaxation mainly occurs in single domain nanoparticles such as superparamagnetic nanoparticles. The Brownian-Néel relaxation mechanism is accomplished by rotating the magnetic moment of each particle against an energy barrier. In case the rotation results in the wholesale rotation of the particle itself, then the particle has gone through Brownian relaxation and thermal energy is promoted through shear stress in the surrounding fluid. On the other hand, if the moment rotates while the particle itself remains fixed, then the particle has undergone Néel relaxation and thermal energy is dissipated by the rearrangement of atomic dipole moments inside the crystal as can be seen in Figure 1-11 (Deatsch and Evans, 2014; Das *et al.*, 2019). The Néel (τN) and Brownian (τB) relaxation times are given by the following equations (Rosensweig, 2002; Suto *et al.*, 2009):

1) $\tau_N = \tau_0 e \frac{KV_M}{kT}$

2) $\tau_B = \frac{3\eta V_H}{kT}$

3) $\tau = \frac{\tau_B \tau_N}{\tau_B + \tau_N}$

where τ, τ_0, K, V_M,k,T, η, and V_H are the effective relaxation time, the characteristic flipping frequency, the magnetic anisotropy constant, the volume of the nanoparticle, the Boltzmann constant, the temperature, the viscosity of the fluid, and the hydrodynamic volume of nanoparticles, respectively.

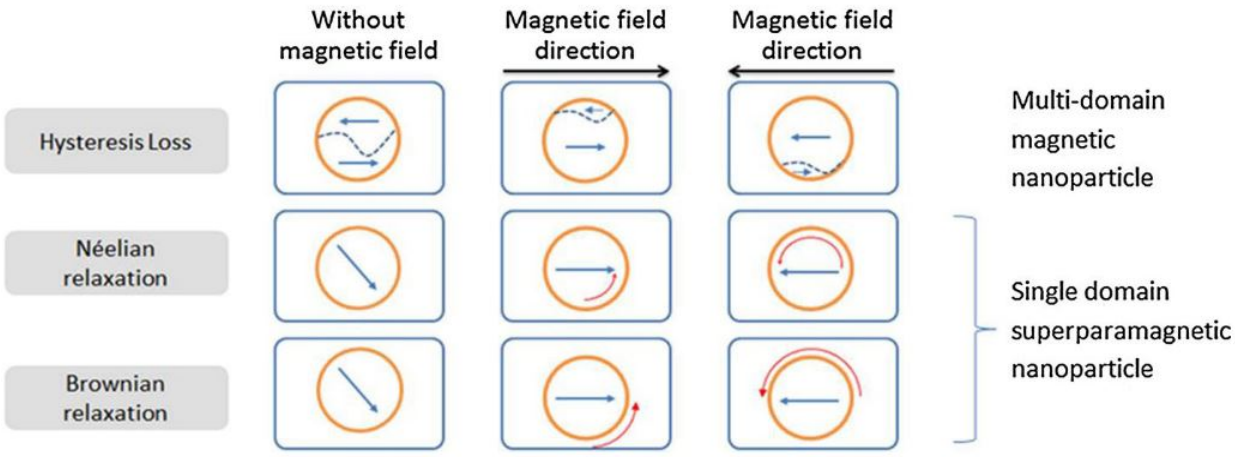

Figure 1-11: Schematic illustration of heat dissipation models in a magnetic nanoparticle in response to the alternating magnetic field. *The short straight arrows represent the magnetic moment direction, the curved arrows represent the movement or change in direction, and the dash lines represent the domain boundaries in multi-domain particles. In Néel rotation model, the magnetic moment rotates while the particle remains fixed, whereas in Brownian rotation, the magnetic moment remains fixed with respect to the crystalline axes while the particle rotates. Image taken from* Suriyanto *et al.* (2017).

The equations above demonstrate that the Néel relaxation time highly depends on the MNP size, whereas the Brownian relaxation time also depends on the hydrodynamic size of nanoparticle as well as strongly depends on the viscosity of the fluid. For this reason, smaller MNP will provide more effective intracellular hyperthermia due to less energy required for rotation of magnetic moments and low restriction of nanoparticles rotation in cellular environments of high viscosity (Das *et al.*, 2019). It was proposed that the ideal nanoparticle size to optimize the balance between Néel and Brownian contribution to thermal losses for maghemite nanoparticles should be around 15 nm (Lévy *et al.*, 2008).

When MNP exposed to external AMF, the heat dissipation occurs and is given by the following equation (Rosensweig, 2002; Suto *et al.*, 2009):

4) $P = \mu_0 \chi'' f H^2$

where P, μ_0, χ'', f, and H are the values of heat dissipation, the permeability of free space or the magnetic field constant, the magnetic susceptibility, the frequency of the applied magnetic field, and the strength of the applied magnetic field, respectively. This equation explains that the MNP under AMF produce heat because of delay in the relaxation of the magnetic moment under an external AMF with a time lapse required for magnetic reversal lower than relaxation times of nanoparticles. The equation also indicates that heat dissipation value depends on the frequency and amplitude of the applied magnetic field as well as the magnetic properties of nanoparticles.

The generated heat by AMF and its quantity from AMF are measured using SAR, also referred to as specific loss power (SLP), which is the amount of electromagnetic energy power absorbed per unit and mass (Suto *et al.*, 2009). SAR is described as the ability to produce heat through magnetic connection between the magnetic field and moments of MNP. Different types of MNP demonstrate varied heating mechanisms. The generated heat by such mechanisms are dependent on the intrinsic and extrinsic characteristics of MNP such as particle shape, particle size, types of coating material and surface functionalization, as well as AMF parameters, such as frequency and amplitude (Hedayatnasab *et al.*, 2017; Das *et al.*, 2019). The SAR value of nanoparticles in solution is calculated by using the following equation (Mornet *et al.*, 2004):

$$SAR = C\left(\frac{dT}{dt}\right)\left(\frac{m_s}{m_m}\right)$$

where C is the specific heat capacity of the solvent, dT/dt is the initial slope of the time-dependent heating curve, m_s is the mass of the solvent, and m_m is the mass of magnetic nanoparticles. Ideally, MNP capable of generating high SAR values are

desired for effective clinical application of MNHT as they allow using a lower dosage of nanoparticle solutions (Das *et al.*, 2019).

1.6.7 Types of magnetism

Understanding the behavior of magnetic nanomaterial is important to design optimal MNP for MNHT. Magnetism originates from the orbital and spin motions of electrons. The intensity of the interaction among them generated different magnetism strength, thus based on the arrangement of magnetic dipoles in absence or presence of an external magnetic field, nanomaterials are classified into five categories, such as diamagnetic, paramagnetic, ferromagnetic, ferrimagnetic and anti-ferromagnetic as can be seen in Figure 1-12 (Spaldin, 2003; Jeong *et al.*, 2007). If a material does not have magnetic dipoles in the absence of an external field, but generate magnetic dipole in opposite direction to the applied field the material is referred to as diamagnetic. Diamagnetic materials also exhibit little magnetization. In paramagnetic nanomaterials, the materials have randomly oriented dipoles in absence of magnetic field, but they can be aligned in the same direction upon interaction with an external magnetic field. For a ferromagnetic material, or material with a permanent magnetic moment, the magnetic dipoles always exist in the absence and presence of an external field. For ferrimagnetic material, some weak magnetic dipoles also exist in antiparallel to the neighboring stronger dipoles in absence of magnetic field. In contrast, antiferromagnetic material has zero net magnetization and the neighboring dipoles are antiparallel and neutralize each other in absence of magnetic field (Jeong *et al.*, 2007; Hedayatnasab *et al.*, 2017).The ferromagnetic and ferrimagnetic materials also display superparamagnetic behavior above the blocking temperature (T_B). The value of T_B is experimentally determined using SQUID (superconducting quantum interference device) measurement by the merging point of the zero-field-cooled (ZFC) and field-cooled (FC) magnetization curves (Jeong *et al.*, 2007).

Superparagnetism is a form of magnetism which appears in small ferromagnetic or ferrimagnetic nanoparticles. Nanomaterials with superparamagnetic behavior displays the magnetization drops to zero when the applied magnetic field is removed,

suggesting an external magnetic field is able to magnetize the nanoparticles, similarly to a paramagnet. However, their magnetic susceptibility is much larger than that of paramagnets. Due to this unique feature, nanomaterials which show superparamagnetic behavior are preferred in biomedical application as they can only be activated to generate heat by the applying external magnetic field. Due to this feature recent work on MNHT has focused more on superparamagnetic nanoparticles. These are nanosized particles with single-domain configuration due to the energetically instability of domain wall. The use of these particles for hyperthermia offers benefits of allowing better dispersion of particles and avoiding the formation of particle aggregations, which could lead to serious adverse problems derived from the formation of clots in the blood circulation system. (Lévy *et al.*, 2008; Villanueva *et al.*, 2010; Silva *et al.*, 2011; Bañobre-López *et al.*, 2013; Goya *et al.*, 2013; Sato *et al.*, 2014; Shevtsov *et al.*, 2014; Suriyanto *et al.*, 2017).

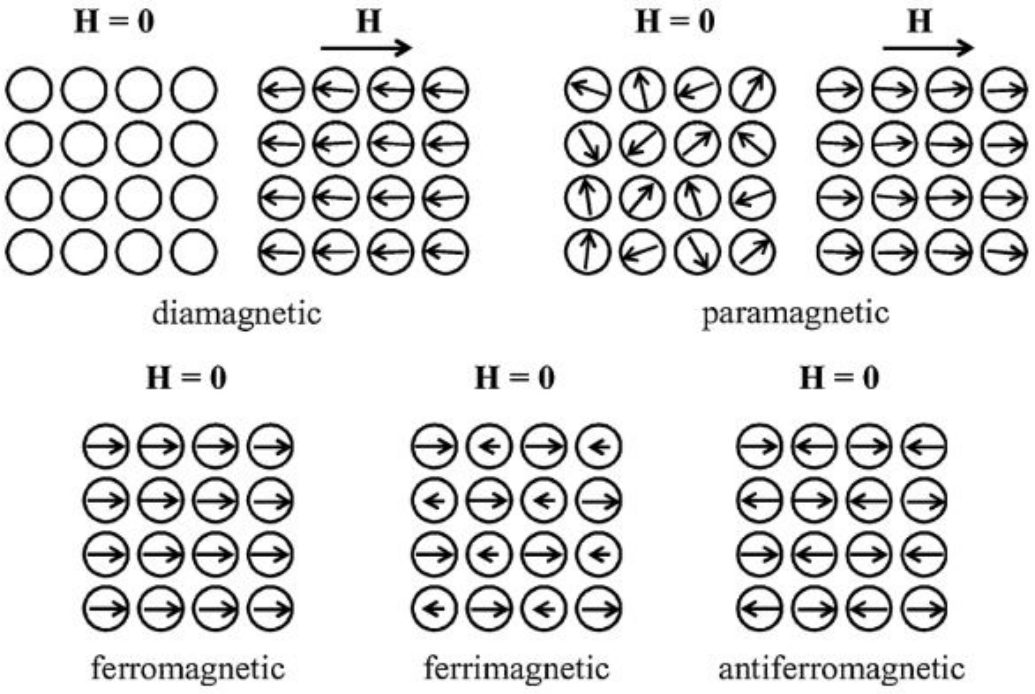

Figure 1-12: Alignment of the magnetic moment of individual atoms of iron. *Schematic representation of magnetic dipoles arrangements of different materials such as diamagnetic, paramagnetic, ferromagnetic, ferrimagnetic, and antiferromagnetic materials in absence and presence of external magnetic field (H). Image taken from Das et al. (2019).*

1.6.8 Magnetic hyperthermia for tumour therapy

The applicability of MNP with adequate heating properties for clinical application or *in vivo* trial is dependent on the evaluation of them in *in vitro* studies. In this regard, if the *in vitro* results were remarkable, giving sufficient heating capabilities in physiological tolerable range, then they would be applied for *in vivo* trials (Hedayatnasab *et al.*, 2017). As can be clearly seen in Figure 1-13, in most *in vitro* studies, MNP in fluid are placed in a micro-centrifuge tube or Petri dish in the center of a circular coil (with certain diameter). The sample is then exposed to AMF, and the temperature changes over time (dT/dt) throughout the process are measured by a thermocouple connected to a data processing system to record the temperature (T_H) (Khandhar *et al.*, 2012; Chiriac *et al.*, 2015; Liu *et al.*, 2015; Soetaert *et al.*, 2017; Zuvin *et al.*, 2019). In general, the MNP and experimental setup are designed to achieve desirable T_H at between 42 °C and 47 °C, because MNP within this range are prone to burn cancerous cells. Overheating may occur and thus causing some unwanted effect in healthy cells at over this secure temperature range (Hedayatnasab *et al.*, 2017).

Although it may be preferable to use a high magnetic field strength and frequency in order to produce a large amount of heat, however, it may cause side effects on the human body. Therefore, the magnetic frequency is generally set between 0.05 and 1.2 MHz (Rast and Harrison, no date; Suriyanto *et al.*, 2017). Based on an experimental study, it was suggested that the usable limit of applying the magnetic field on the human body was up to the magnetic field intensity of 35.8 Amp-turns/meter at a frequency of 13.56 MHz (Atkinson *et al.*, 1984). However, other experimental result also suggests that the acceptable values for the product between the magnetic field amplitude and frequency may be two to four times larger than the safety clinical setting of of 4.85 x 108A/m/s. This was suggested to enable lower dosage of nanoparticles needed for an effective treatment (Bellizzi *et al.*, 2016).

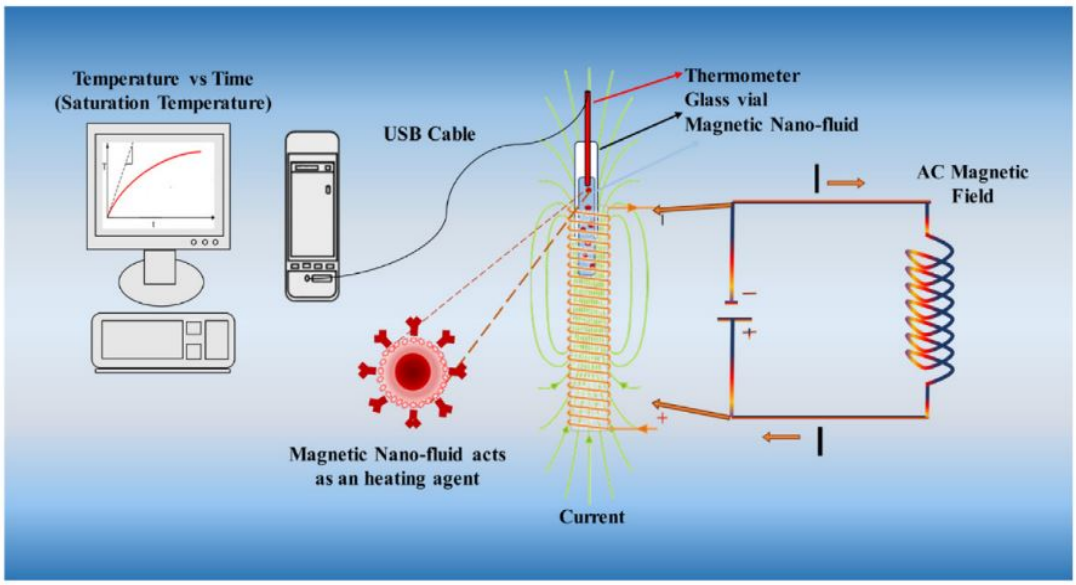

Figure 1-13: Schematic of experimental setup for in vitro magnetic hyperthermia application. *MNP in fluid are placed in a micro-centrifuge tube or Petri dish in the center of a circular coil (with certain diameter). The sample is then exposed to AMF, and the temperature changes over time (dT/dt) throughout the process are measured by a thermocouple connected to a data processing system to record the temperature (T_H). Image taken from Hedayatnasab et al. (2017).*

Several pre-clinical *or in vitro* magnetic hyperthermia studies have been performed in an attempt to improve the cancer treatment aiming at minimizing the side effects on healthy cells. Majeed *et al.* synthesized silica-coated iron oxide (Fe_3O_4-SiO_2) nanoparticles with tunable shell thickness and investigated the effect of surface coating on specific absorption rate (SAR) under AMF. They found that the coated Fe_3O_4 generate higher temperature than that by uncoated group, suggesting that the silica coated MNP can be attributed to extent of increase in Brownian motion. The synthesized MNP were also evaluated *in vitro* by assessing their MNHT effect on L929 and human cervical cancer cells (HeLa cells) using sulforhodamine-B assay, resulted in ~55% cell death more in cells treated with silica coated MNP under AMF as compared to untreated control (Majeed *et al.*, 2014). Similar approach was also tested by Rana and coworkers using other type of MNP coating such as cross-linked polyaniline to coat superparamagnetic Fe_3O_4 nanoparticles for MNHT application

(Rana *et al.*, 2014). The magnetic material was synthesized by cross-linking of polyaniline shell on the surface of carboxyl PEGy- lated Fe_3O_4 nanoparticles resulting in a high SAR of 120 W/g at low concentration due to the high magnetic sensibility and colloidal stability, suggesting the polyaniline shell of magnetic nanoparticles increased the heat activated toxicity toward fibrosarcoma cancer cell lines after AMF application.

Mondal *et al*. synthesized MNP coated with biocompatible hydroxyapatite and used them as a heat mediator for MNHT for cancer treatment. This MNP effectively killed the MG-63 cancer cells at a temperature between 42°C and 47°C after 30 min exposure to AMF. Moreover, the synthesized nanoparticles show minimal or no cytotoxic effect on cell lines when AMF was not applied. They also investigated the mechanism of cell death by transmission electron microscopy (TEM) analysis, which indicated that cell degradation and formation of blebs due to the generation of reactive oxygen species (ROS) by heat stress (Mondal *et al.*, 2017).

In order to study the thermal heating effects resulting from Brownian motion and hysteresis losses in cellular environment, Makridis *et al.* (2014) investigated $MnFe_2O_4$ nanoparticles at various concentrations and embedded the MNP in aqueous media of varying agar concentration that resemble the cellular environments. The study indicated that the heating profile of nanoparticles demonstrated by SLP values was significantly decreased compared to water due to the restriction of Brownian relaxation in high viscous media. Moreover, application of two subsequent MNHT cycles on human osteosarcoma Saos-2 cells incubated with manganese ferrite MNP resulted in cytotoxicity effect on Saos-2 osteoblasts cancer cell line (Makridis *et al.*, 2014).

Recent report in 2018 by Jang et al (2018) showed magnesium doped γ- Fe_2O_3 as a new strong hyperthermia agent which exhibited 100 times higher value of intrinsic loss power (ILP) compared to commercial Fe_3O_4 (Feridex) via controlled distribution and concentration of dopant ions in octahedral iron vacancy sites of γ- Fe_2O_3. Due to this high value, they then performed *in vitro* and *in vivo* magnetic hyperthermia studies using U87 glioblastoma cancer cell lines and Hep3B xenografted animal models, which revealed the complete destruction of the tumour via its exceptionally high

heating power under a biological safe range of applied magnetic field (Jang *et al.*, 2018).

Biomolecule functionalized MNP is advantageous in therapy due to higher selectivity and lower cytotoxicity compared to unconjugated nanoparticles. To increase the effectiveness of tumour-targeted therapy, Sadhukha and coworkers designed a peptide functionalized nanoparticle, which aimed to EFGR-tumour-targeted for magnetic hyperthermia of lung cancer. Inhalation delivery of EGFR-targeted MNP were performed and it was found that EGFR targeting enhances tumour retention of MNP. Moreover, the magnetic hyperthermia experiment resulted in significant inhibition of *in vivo* lung tumour growth in an orthotopic mouse lung tumour model (Sadhukha, Wiedmann, *et al.*, 2013). Other biomolecule such as galactose functionalized alginate-coated iron oxide nanoparticles (Fe_3O_4@Alg-GA) was also tested for targeted hyperthermia therapy by Liao *et al.* (2015), which showed that approximately 95% HepG2 cancer cells were killed by Fe_3O_4@Alg-GA MNP under AMF due to their enhanced cellular uptake via receptor-mediated endocytosis (Liao *et al.*, 2015). Other specific MNP uptake mechanism via lysosomes was also observed when synthesized glucose functionalized citric acid-coated iron oxide nanoparticles were internalized into CT26 colorectal cancer cells, as reported by Wydra and coworkers (2015). These cells were then exposed to an AMF to determine the potential to deliver therapy. Cellular ROS generation and apoptotic cell death was enhanced with field exposure. The nanoparticle coatings inhibit the Fenton-like surface generation of ROS suggesting that the cellular ROS measured is attributed to a thermal or mechanical effect of the internalized nanoparticles (Wydra *et al.*, 2015).

In recent times, studies have been focused on the development of innovative multimodal therapies to improve the efficiency of cancer treatments, such as combining anticancer action of MNHT and drug released under AMF to cancer cells. In attempt to design controllable drug released mediated by hyperthermia for cancer treatment, Aoyagi research group developed a smart nanofiber composed of a temperature-responsive polymer with both cytotoxic drug doxorubicin and MNP for enhanced hyperthermic chemotherapy. When the smart nanofiber exposed under

AMF, the MNP generate heat to collapse the polymer networks in the nanofiber, allowing the release of doxorubicin from the nanofiber into human melanoma cells. The result showed cell viability was decreased to 70% following 5 min exposure of AMF (Kim *et al.*, 2013). Other similar study investigating double effect of hyperthermia and chemotherapy also reported by Kim and coworkers (2015), who constructed magnetic micelles consisting of poly(ethylene glycol)-poly(lactide) (PEG-PLA), iron oxide nanoparticles, and encapsulated anticancer drug doxorubicin into hydrophobic PLA of PEG-PLA. At least 78% adenocarcinoma A549 cells cells were killed through the double effects of magnetic hyperthermia and rapidly released doxorubicin under AMF application (Kim *et al.*, 2015). Therefore, these works have shown the potential for combined synergistic effects of chemotherapy and hyperthermia.

1.6.9 Clinical trials of magnetic hyperthermia

The toxicity of MNP is one of important aspect to consider in the clinical trials of MNHT. Other aspects such as the safety of any technical equipment must also be considered because the AMF generators are electrical appliances that use high voltages and currents. Moreover, the safety of insulators which need to be carefully placed with a patient's body, as well as temperature-monitoring systems are also important for the safe use of MNHT (Kobayashi, 2011). Studies on mice has shown that the systemic administration of magnetite cationic liposomes (90 mg, i.p.) in mice resulted in over 50% of the magnetite had accumulated in the liver and 3% had accumulated in the spleen. However, there was no significant accumulation of magnetite in the liver or spleen at 14 days after injection, suggesting that the magnetite had been biodegraded by the reticuloendothelial system (Ito *et al.*, 2003).

In 2005, Johannsen *et al.* firstly reported clinical application of magnetite-nanoparticle-mediated hyperthermia in locally recurrent prostate cancer, using the sophisticated MFH 300F-type magnetic induction hyperthermia instrument. The core diameter of magnetic fluid is 15 nm, with aminosilicane coating. The concentration of iron particles is 112 mg/mL. The nanoparticles were injected transperineally into the

prostate of a 67-year-old patient under transrectal ultrasound and fluoroscopy guidance. Treatments were performed by using an alternating magnetic field of 100 kHz, 4.0–5.0 kA/m magnetic field strength, with once a week treatment, 60 min per treatment session, continuing 6 times. During the first treatment, the maximum and minimum intraprostatic temperatures were 48.5 and 40.0°C. While during the sixth treatment, the maximum and minimum intraprostatic temperatures were 42.5 and 39.4°C during the sixth treatment (Johannsen *et al.*, 2005).

In 2007, Johannsen and coworkers reported the phase I clinical study of magnetic hyperthermia treatment of 10 patients with local recurrence of prostate cancer who had received magnetic induction hyperthermia. The result indicated that hyperthermia nanoparticles can still be observed in the prostate within 1 year. No systemic toxicity was observed for 17.5 months (3–24 months) of the median follow-up. The acute urinary retention was found in four patients with a history of urethral stricture. No significant treatment-related discomfort was found, the effect on quality of life was only temporary. The study concluded that the MNHT treatment of local recurrence of prostate cancer is feasible, well tolerated without significant side effects (Johannsen *et al.*, 2007).

In 2007, Maier-Hauff *et al.* reported a clinical study of intracranial thermotherapy using MNP combined with external beam radiotherapy for treatment of 14 patients with recurrent glioblastoma multiforme. A 3-dimensional image guided intratumoural injection of MNP coated with aminosilane (15 nm; 112 mg/mL) was performed on patients. To design the specific treatment program and treatment dose based on the MNP distribution and expected heat distribution, data analysis using magnetic resonance imaging (MRI) and computed tomography (CT) were performed, then instillation of 0.1–0.7 mL (median 0.2 mL) of magnetic fluid per milliliter was injected into the tumour tissues. Patients then received 4-10 (median: 6) thermotherapy using 100 kHz magnetic frequency and 2.5-18 kA/m magnetic field strength of AMF. For the external beam radiation, patients without undergoing radiotherapy received 60 Gy irradiation and 10 Gy added boost, whereas patients with recurrent tumours received 20–30 Gy of irradiation. The result of the study indicated that thermotherapy using

magnetic nanoparticles was tolerated well by all patients without significant side effects. Intratumoural median maximum temperature reached median 44.6°C (42.4°C–49.5°C), suggesting that deep cranial thermotherapy using magnetic nanoparticles are feasible and can be safely applied on glioblastoma multiforme patients to increase the therapeutic effect (Maier-Hauff *et al.*, 2007).

The first study on the autopsy findings of two glioblastoma patients treated with MNHT following instillation of MNP was reported in 2009 by Van Landeghem and coworkers. Three patients with malignant glioma received local tumour magnetic fluid injection. MNHT treatment was applied to two patients, while the other one did not undergo the treatment. The autopsy conducted on the patient who died just before application of MNHT, which they found a significant decrease in phagocytic activity of the infiltrating macrophages compared to the patients receiving complete MNHT. The study concluded that the MNHT temperatures between 49.5 °C and 65.6 °C as obtained in both patients, result in extended tumour necrosis followed by enhanced infiltration of macrophages and subsequent phagocytosis of necrotic debris and nanoparticles (van Landeghem *et al.*, 2009).

One key challenge in MNHT application is how to obtain a homogenous distribution of MNP in tumour. To overcome this problem, Wust *et al.* (2006) conducted magnetic fluid magnetic induction hyperthermia treatment for 22 patients with relapsed tumour entities in different parts to determine and evaluate the temperature distributions using three different implantation methods: infiltration under CT fluoroscopy (group A), TRUS (transrectal ultrasound) – guided implantation with X-fluoroscopy (group B) and intra-operative infiltration under visual control (group C). 14 patients were in group A or B, while 8 patients were treated in group C. The MNP used is aminosilane coated superparamagnetic nanoparticle with 15 nm core diameter with 112 mg/mL iron particles concentration. The result indicated no discomfort or mild discomfort was observed in patients following the instillation of MNP. For the AMF application, the magnetic field strength selected was 3.0–6.0 kA/m for the pelvis tumours, 7.5 kA/m for neck and chest tumours and >10.0 kA/m for the head. Post-implantation analysis after nanofluid infiltration indicated that specific absorption rate (SAR) value was 60–

380 W/ kg with the tumour coverage of ≥ 40 °C distributed in 90 % tumour area in Group A) and in 85 % tumour area in Group B. However, the targeted tumour coverage of ≥ 42 °C unfortunately only distributed in 30% tumour area in Group A and significantly less with only 0.2 % tumour area in Group B. Although the targeted thermoablation temperature of ≥ 46 °C in in the whole target area was not obtained, the study indicated the decrease of nanoparticle mass of approximately 10% was observed in 100 days, or only 3% heating loss in one month if all other parameters remain constant, suggesting MNHT treatment could be potentially used for multimodal treatment concepts (Wust *et al.*, 2006).

In 2007, Matsumine and coworkers reported a clinical study aimed to develop novel hyperthermic treatment modality using magnetic materials for metastatic bone tumours. The study involved treatment of 16 bone lesions in 15 patients (HT group) with metastatic bone tumours. Seven lesions were fixed with intramedullary nailing after scraping out, one lesion was conducted with the prosthesis implantation after an excision and the remaining eight lesions were fixed by intramedullary nailing for the involved bones, and these lesions were filled with calcium phosphate bone cement containing Fe_3O_4 magnetic nanoparticles. The MNHT treatment was conducted at 1 week after the surgery. Moreover, for comparison purposes with MNHT patients, the study also assessed 8 patients (Op group) who did not undergo radiotherapy and hyperthermia treatment after surgery and 22 patients (Op + RT group) underwent postoperative radiotherapy. The result indicated that there were no significant complications in the MNHT group. On radiographs, 87 %, 38 %, and 91% were, considered to demonstrate an effective treatment outcome in HT group, Op group, and Op + RT group, respectively. The patients in HT group showed a statistically significant radiographic outcome than the surgery alone (Op) alone ($P = 0.0042$), whereas no significant differences were found in the postoperative magnetic induction hyperthermia group (HT) compared with the postoperative radiotherapy group (Op + RT), suggesting the MNHT treatment had a satisfactory local control rate for metastatic bone tumour (Matsumine *et al.*, 2007).

1.6.10 Magnotosomes for tumour therapy

Magnetosomes have potential use in MNHT because they provide the most powerful source of heat under AMF application due to their ferrimagnetic behavior, cubic shape, large structure and thermally stable magnetic moment (Alphandéry *et al.*, 2013). Alphandéry and coworkers found that magnotosomes are nontoxic, with rats surviving up to a quantity of magnetosomes administered of 480mg per kg of animal. When AMF applied to suspensions of magnetosomes, high loss power per cycle of 5–11 J/kg_{Fe} was observed suggesting that the magnetosomes are good candidates for MNHT treatments of tumours (Alphandéry *et al.*, 2013).

In 2011, Alphandéry *et al.* reported that the chains of magnetosomes extracted from AMB-1 magnetotactic bacteria have antitumoural activity. The study investigated the cell viability of MDA-MB-231 breast cancer cells in the presence of magnetosomes suspension under AMF application of 183 kHz and field strengths of 20, 40, or 60 mT. Results revealed that only chains of magnetosomes and not individual separated magnetosomes made the tumour fully disappeared after 30 days from treatment. The temperature reached during the treatment with chains of magnetosomes was 45 °C - 46 °C, suggesting that the specific arrangement of chains of magnetosomes likely crucial to induce the hyperthermia effect. In addition, the chains also prevent agglomerations, and the resulting toxic effect, while the heating is distributed more uniformly inside the cell. The author also concluded that higher efficiency of the extracted chains of magnetosomes compared with that of the other nanoparticles is attributed to three factors: 1) a specific absorption rate (SAR) higher for the magnetosomes than for the chemically synthesized superparamagnetic iron oxide nanoparticles, 2) a more uniform heating for the chains of magnetosomes than for the individual magnetosomes and 3) the ability of the chains of magnetosomes to penetrate within the cancer cells or bind at the cell membrane following the AMF application which enables efficient cell destruction. Moreover, *in vivo* experiment using mouse showed that following the injection of ~1 mg of chains of magnetosomes directly within the xenografted breast tumours under the skin of mouse and by applying an AMF of frequency 183 kHz and magnetic strength 40 mT, three times during 20 min,

total disappearance of tumour was observed, suggesting potential of chains of magnetosomes extracted from whole magnetotactic bacteria for application in MNHT for cancer therapy. Furthermore, biodistribution analysis result also indicated that extracted chains of magnetosomes administered directly within xenografted breast tumours progressively left the tumours during the 14 days following their administration and were then eliminated in large proportion in the feces (Alphandéry *et al.*, 2011).

Later in 2012, the same research group, Alphandéry *et al.* also reported the use of chains of magnetosomes isolated from *Magnetospirillum magneticum* strain AMB-1 for MNHT treatment of tumours. The application of 198 kHz frequency and average magnetic field strength of 20 or 30 mT AMF resulted in efficient inhibition of cell proliferation on HeLa and MDA-MB-231 cancer cells loaded with chain of magnetosomes. However, when the chains are heated during 5 hours at 90 °C in the presence of 1% SDS, to denature the filament binding of magnetosomes and to obtain individual magnetosome, and used them in MNHT treatment, no significant cell proliferation inhibition was observed. The result revealed that individual magnetosomes are prone to aggregation, are not stable in solution and do not generate efficient inhibition of cancer cell proliferation under application of AMF, suggesting the increased efficiency was related to much less particle aggregation for the magnetosome chains than for the individual magnetosomes, thus enabling efficient magnetosome internalization by cancer cells (Alphandéry *et al.*, 2012).

In agreement with the finding above, Liu and coworkers (2012) reported that magnetosomes could be new natural biologic magnetic nanoparticles to be used in MNHT. They investigated the properties of magnetosomes such as morphology, magnetic properties and their heating effects under magnetic field and compared them to the chemically synthesized magnetic nanoparticles (MNP). Cytotoxicity studies using human breast cancer cells MCF-7 loaded with magnetosomes indicated that 80% of cell population died following AMF application (300 kHz magnetic frequency and 110 Gs field amplitude) reaching a temperature of 47 °C. In addition, the acute toxicity evaluation in mice shows that the lethal dose magnetosomes is much higher than MNP,

suggesting the relatively high biocompatibility of magnetosomes (R. T. Liu *et al.*, 2012).

In contrast with the finding above, Manucci *et al*. (2014) found that the magnetosomes enter the cells not as chains but as single nanoparticles or short chains. They extracted magnetosomes from *Magnetospirillum gryphiswaldense* strain MSR-1 and investigated the interaction with cellular elements and anti-neoplastic activity both *in vitro* and *in vivo*, with the aim of developing a new theranostic approach for neoplastic diseases. *In vitro* result indicated a strong uptake of magnetosomes with no evident signs of cytotoxicity on human colon carcinoma HT-29 cell cultures and also showed three phases in the interaction: adherence, transport and accumulation in Golgi vesicles. Histological analysis showed fibrous and necrotic areas close to magnetosomes injection sites in mice subjected to a complete thermotherapy protocol using three AMF application (187 kHz and 23kA//m on alternate days, over a week), suggesting magnetosomes as promising candidates for theranostic applications in cancer therapy (Mannucci *et al.*, 2014).

In 2017, Alphandéry *et al* research group investigated the potential use of magnetosomes for MNHT treatment of tumour and found that 40% of mice bearing intracranial U87-Luc tumours display full tumour disappearance following only 10 % magnetosome distribution coverage of the whole tumour volume after intratumour administration of 40 μg of chains of magnetosomes and 12 to 15 magnetic sessions (30 mT; 198 kHz; 30 min). Even more interesting, the study measured the percentage of endotoxin release, which was at 1 to 3% during the first 2 magnetic sessions, then strongly increases to 11% and 32% following the third and fourth magnetic session respectively, suggesting that endotoxins, which are initially at magnetosome surface, are progressively released from magnetosomes under AMF application. Therefore, it seems possible to simultaneously produce heat and release an immune-stimulating substance such as endotoxins or anticancer drugs-conjugated to magnetosomes, which could improve the therapeutic effect (Alphandéry *et al.*, 2017a).

Other report by the same research group above also demonstrated an approach to design magnetosomes coated with poly-L-lysine (M-PLL) in order to stabilize the

magnetosomes in suspension (Alphandéry *et al.*, 2017b). M-PLL-enhanced antitumour efficacy was demonstrated by administering 500-700 mg in iron of M-PLL to intracranial U87-Luc tumours of 1.5 mm^3 and by exposing mice to 27 magnetic sessions each lasting 30 min, during which an AMF of 202 kHz and 27 mT was applied. Treatment conditions were adjusted to reach a typical hyperthermia temperature of 42 °C during the first magnetic session. The *in vitro* result revealed that the percentage of cell death of M-PLL increased from 60 % before AMF application to 90% after AMF application. For *in vivo* experiment, only 20 % of the treated mice showed antitumour efficacy following the administration of chemically synthesized MNP and 23 magnetic sessions. In contrast, living glioblastoma cells loaded with M-PLL were 100 % fully disappeared at 68 days following tumour cell implantation (D68) and AMF treatment. Even more interesting, histological analysis of their brain tissues revealed an absence of tumour cells, suggesting that they were fully healed (Alphandéry *et al.*, 2017b).

Recently, Mannucci *et al.* (2018) investigated the theranostic potential of chains of magnetosomes for AMF application on xenograft model of glioblastoma. They injected a single intratumoural magnetosomes into the mice, then conducted AMF application three times a week. The MRI analysis showed significant inhibition of the tumour growth in subjects exposed to the AMF, showing visible necrotic tissue at the tumour site. In contrast, tumour volume that was initially free from magnetosomes keeps growing. The MRI analyses also revealed inhomogeneous distribution of magnetosomes inside the tumour tissue which may strongly limit their therapeutic efficacy (Mannucci *et al.*, 2018).

1.7 HYPOTHESIS AND AIMS

The roles of Mms6 that have been described provide an insight into how Mms6 could function in magnetic nanoparticle synthesis. Moreover, the distinctive characteristic of MSC and the ability to perform genetic modification on these cells that have been described provide an insight into how MSC could be engineered to express certain protein and to target tumour site. Therefore, it was hypothesized that MSC could be engineered to express Mms6, thus enabling MSC able to self-express MNP which can be utilized for tumour targeting and MNHT.

The main aims of the study were:

1. To transfect AD-MSC with the MTB genes, *mms6,* using transient and stable transfection technique
2. To demonstrate Mms6 mRNA and protein expression in AD-MSC following the transfection
3. To investigate the effect of *mms6* gene expression on MSC functionality
4. To confirm whether the expression of *mms6* by MSC leads to the production of MNP, as seen for the MTB
5. To investigate whether MSC able to self-express MNP could be used in MNHT treatment.

2 MATERIALS AND METHODS

2.1 MAGISTER GENE DESIGN AND CLONING

2.1.1 MAGISTER gene design

A specific DNA sequence containing *M. magneticum* strain AMB-1 *mms6* DNA bacterial synthetic gene was used in this study. The *mms6* DNA fragment was optimised for mammalian cell expression by using *mms6* gene codon optimization and by adding a Kozak sequence at the N terminus of the *mms6* gene. This particular gene sequence was named MAGISTER (MAG) gene. In order to detect mms6 protein expression, protein tag markers were used. Two types of constructs were used:

1) *mms6* + single tag marker

   This construct has polyhistidine-tag at the N terminus of the *mms6* DNA fragment, as illustrated in Figure 2-1.

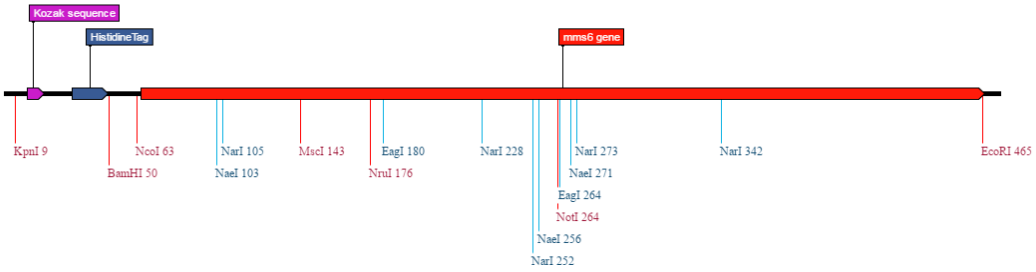

Figure 2-1: MAGISTER gene construct with a single tag marker. *The construct has polyhistidine-tag at the N terminus of the mms6 DNA fragment.*

2) *mms6* + double tag marker

   This construct has polyhistidine-tag at the N terminus and GFP-tag at the C terminus of the *mms6* DNA fragment, as illustrated in Figure 2-2.

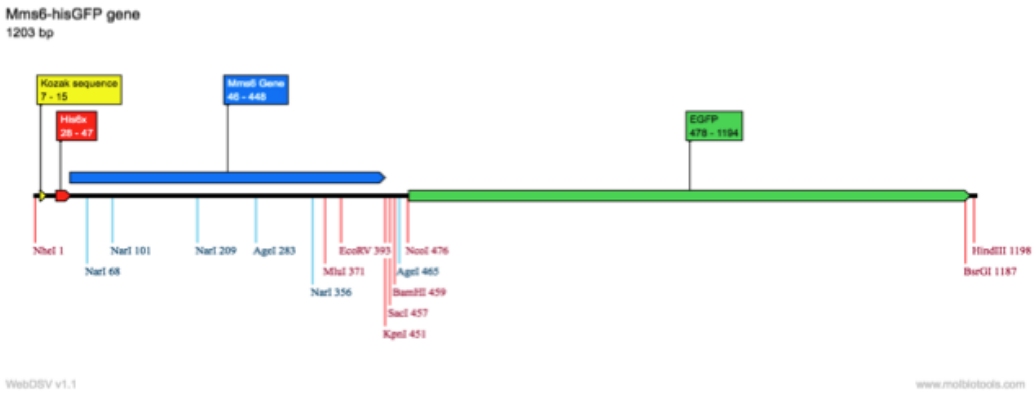

Figure 2-2: MAGISTER gene construct with double tag markers. *The construct has polyhistidine-tag at the N terminus and GFP-tag at the C terminus of the mms6 DNA fragment*

There were 4 different MAGISTER gene constructs with double tag markers, depending on different codon optimization of the *mms6* gene, used in this study (Table 2-1):

1) MagWT contains the original sequence of *M. magneticum* strain AMB-1 *mms6* gene
2) Mag01 was kindly designed by Dr. Greg Kudla (Group leader of RNA synthetic biology group, MRC Institute of Genetics & Molecular Medicine, University of Edinburgh)
3) Mag02 was designed by Dr. Chris Boyd (Group leader of gene therapy for cystic fibrosis research group, MRC Institute of Genetics & Molecular Medicine, University of Edinburgh)
4) Mag03 was designed by GeneArt® Gene Synthesis service (Thermo Fisher Scientific)

All of these MAG fragments were synthesized and cloned into pcDNA3.1 plasmid at NheI/HindIII restriction site by GeneArt® Gene Synthesis service. All these constructs were specifically used in the experimental works in Chapter 4.

For the MAGISTER gene construct with single tag marker, only Mag02 sequence was used. The sequence was synthesized and cloned into pcDNA3.1 plasmid at

KpnI/EcoRI restriction site by GeneArt® Gene Synthesis service. This construct was specifically used in the experimental works in Chapter 3.

Table 2-1 MAGISTER gene design with double tag markers

Gene/Plasmid Code	DNA Fragment
MAGISTER-WT (MagWT)	His - *mms6* Wild Type - GFP
MAGISTER-01 (Mag01)	His - *mms6* codon optimised 1 - GFP
MAGISTER-02 (Mag02)	His - *mms6* codon optimised 2 - GFP
MAGISTER-03 (Mag03)	His - *mms6* codon optimised 3 - GFP

2.1.2 Bacterial heat shock transformation

To clone the MAGISTER sequence, bacterial transformation was performed. In Brief, 2 µl of plasmid was added to 50 µl of DH5α competent cells (Thermo Fisher Scientific) in a microcentrifuge tube and incubated for 30 minutes on ice. The tube was then placed into the waterbath at 42°C for 70 seconds. Thereafter the tube was immediately transferred back on to ice and incubated for 3 minutes, then 900 µl of SOC (Super Optimal Broth with Catabolite repression) medium was added into the tube. Cells were incubated at 37°C with shaking for 1 hour to allow bacterial growth before being plated to Luria Broth (LB) agar medium. The bacteria were then centrifuged at 6000 rpm and 500 µl of supernatant was discarded. The remaining pellet and supernatant were then resuspended. 100 µl of the bacteria were then plated to Luria Broth (LB) agar medium. The bacteria were then centrifuged at 6000 rpm and 500 µl of supernatant was discarded. The remaining pellet and supernatant were then resuspended. 100 µl of the bacteria were then plated on to premade Luria Broth/ampicillin plate. The plate was incubated for overnight at 37°C.

2.1.3 Gene cloning and mini scale plasmid purification

Following overnight incubation, a single colony of DH5α cells were picked and put into 5 ml LB media supplemented with 5 µl (1000x concentration) ampicillin. Cells were incubated at 37°C with 225 rpm shaking for 16 hours to allow bacterial growth. Following 16 hours incubation, one colony from the plate was transferred into 5 ml of LB medium supplemented with 5 µl (1000x concentration) ampicillin. The bacterial culture was allowed to grow with shaking (225 rpm) at 37°C for overnight. Thereafter, 500 µl of culture was stored at -80ºC in 50% glycerol. The remaining cells were then collected via centrifugation at 4°C for 5 min at 13000 rpm, then the plasmid was purified from the DH5α cells using the standard protocol of QIAprep spin MiniPrep Kit (Qiagen) to obtain a high purity of plasmid.

In order to evaluate whether the MAG gene had been successfully amplified, restriction enzyme digestion by KpnI/EcoRI (for Mag gene with single tag marker) or HindIII/NheI (for Mag gene with double tag marker) restriction enzymes was performed. Briefly, 1 µg plasmid DNA, five units of restriction enzyme and 5 µl of 10x CutSmart buffers were used in each reaction. The reactions were made up to a volume of 50 µl in distilled water and incubated at 37 °C for 2 hours. Enzymes were heated for 20 min at 85°C after digestion. The digestion products were then visualized by conducting electrophoresis on 2% (w/v) agarose gels with SYBR™ Safe DNA gel stain.

2.1.4 Gene cloning and large-scale plasmid purification

In order to obtain an adequate amount of MAGISTER gene plasmid to be used in this study, a large scale of MAGISTER gene cloning and plasmid purification was performed. Briefly, the DH5α cells containing MAGISTER plasmid from glycerol stock were plated using streak method on to pre-made LB/Amp agar. The plates were then incubated at 37°C overnight.

Following incubation, a colony of DH5α cells was picked and put into 5 ml LB media supplemented with 5 µl (1000x concentration) ampicillin. Cells were incubated at 37 °C with 225 rpm shaking for 7 hours to allow bacterial growth. The bacteria culture was then added to 200 ml LB media supplemented with 200 µl Ampicillin (1000x) and left to grow overnight at 37°C on a 225 rpm shaker.

Following overnight incubation, plasmid purification was performed. Plasmid EndoFreeMaxi kit (Qiagen) was used to purify plasmids according to the manufacturer's instructions. Briefly, bacteria culture was centrifuged at 6000 rpm for 10 minutes and the supernatant was removed. Bacteria pellets were resuspended in 10 ml of Buffer P1, supplemented with RNase A and LyseBlue at 1:1000. 10 ml of Buffer P2 was added and was inverted 6 times and left to incubate at room temperature for 5 minutes, at which point the solution turns blue. 10 ml of Buffer P3 was added, inverted six times and incubated on ice for 20 minutes. The solution was centrifuged at 13000 rpm for 10 minutes at 4°C. At the same time, a Qiagen tip was equilibrated with 10 ml Buffer QBT and allowed to empty by gravity flow. The supernatant was removed from the sample into a Qiagen syringe, which was used to dispense the sample into the Qiagen tip and remove any suspended pellet that remained. The sample was allowed to flow through the tip and was washed twice with 30 ml of Buffer QC. The Qiagen tip was moved to a new 50 ml falcon tube and the DNA was eluted with 10 ml of Buffer QF. The tip was then discarded, and the eluted DNA was precipitated with 10.5 ml isopropanol and mixed. The sample was centrifuged at 16000 rpm for 30 minutes at 4°C. The supernatant was removed and 5 ml of 70% ethanol was added to the tube to wash the pellet. The sample was then centrifuged at 16000 rpm for 5 minutes. The pellet was dissolved in 500 µl of ddH_2O. DNA concentration was measured using the NanoDrop1000 spectrophotometer (Labtech).

In order to evaluate whether the MAGISTER gene has been successfully amplified without mutation, the gene was sequenced. DNA sequencing was carried by the Institute of Genetic and Molecular Medicine sequencing service, University of Edinburgh. Sanger Sequencing method was used using the following primers:

Primer Forward (5'-3'): CGCAAATGGGCGGTAGGCGTG

Primer Reverse (5'-3'): TCAGATCCGGTCGGCCACCCA

The sequencing information received was visualized and processed using DNA Baser Sequence Assembler. The sequencing results were then aligned to match the original sequence using the Basic Local Alignment Search Tool (BLAST) software.

2.2 LENTI-*mms6* GENE CONSTRUCTION

2.2.1 Lenti-*mms6* plasmid construct

To reprogram the AD-MSC stably expressing *mms6* gene, a lentiviral construct of MAGISTER gene was generated. The pSicoR-Ef1α-mCh-Puro lentiviral plasmid and the pcDNA 3.1 – *mms6* were used in the lenti-*mms6* plasmid construction. The pSicoR-Ef1α-mCh-Puro lentiviral plasmid was a gift from Dr. Chris Boyd, while the pcDNA 3.1 – *mms6* (Mag01 gene construct without his-tag and GFP-tag) was a gift from Dr. Lisa Lungaro (former member of Donald Salter research group, IGMM). The *mms6* gene insert was extracted with restriction enzymes XbaI/NotI (New England Biolabs) from the pcDNA 3.1 plasmid and the resulting product was ligated into the SpeI/NotI sites of pSicoR-Ef1α-mCh-Puro plasmid to create the Lenti-*mms6* construct. The protocol used as described in the following section.

2.2.2 *mms6* gene fragment extraction

For extraction of the DNA fragment containing *mms6* gene from pcDNA 3.1 plasmid, the plasmid was extracted with restriction enzymes XbaI/NotI (New England Biolabs) following the manufacturers protocol. The digestion product was then analysed by electrophoresis, then extracted from the gel using QIAquick gel extraction kit (Qiagen). To extract the DNA, the digestion DNA product from the agarose gel was excised with a clean, sharp scalpel. The weight of the gel slice was then measured in a colorless tube, then the gel slice was dissolved in 3 volumes Buffer QG to 1 volume

gel. After the gel slice has dissolved completely, 1 gel volume isopropanol was added to the sample and mixed. To bind the DNA, the sample was then applied to the QIAquick column and centrifuged for 1 min at 13000 rpm. The flow-through was discarded and 500 µl Buffer QG was added to the QIAquick column and centrifuged for 1 min at 13000 rpm. The flow-through was again discarded, then the QIAquick column was placed back into the same tube. To wash, 750 µl Buffer PE was added to QIAquick column and centrifuged for 1 min at 13000 rpm. After discarding the flow-through, the QIAquick column was then centrifuged again for 1 min at 13000 rpm to remove residual wash buffer. Afterwards, to elute DNA, 50 µl Buffer EB (10 mM Tris·Cl, pH 8.5) was added into the QIAquick membrane and centrifuged for 1 min. The DNA concentration was then measured using the NanoDrop1000 spectrophotometer.

2.2.3 Plasmid dephosphorylation and ligation.

The ligation of the *mms6* gene insert into the pSicoR-Ef1α-mCh-Puro plasmid was performed using Rapid DNA Dephos and Ligation Kit (Roche). The plasmid vector (1µg) was digested with restriction enzymes SpeI/NotI (New England Biolabs) following the manufacturer's protocol. Once digested with the enzymes, the vector sample was then dephosphorylated using a reaction as shown in Table 2-2. The mixture was left for 15 minutes at 37°C. For the ligation reaction, a 1:3 ratio of vector to insert was used. The ligation reaction was set up as shown in Table 2-3. The ligation mixture was left for 5 minutes at room temperature before used for the transformation process into DH5α cells to amplify the plasmid. Once the plasmid yield was purified, the samples were then sent to the IGMM sequencing department who sequenced vectors in both directions, using the following primers:

Primer Forward (5'-3'): CGCAAATGGGCGGTAGGCGTG

Primer Reverse (5'-3'): TCAGATCCGGTCGGCCACCCA

The sequences were checked against *mms6* DNA sequence (Mag01) using online BLAST software. Afterwards, the plasmid was then sent to Biomolecular Core Department – SURF, the University of Edinburgh who performed the lentivirus titer production.

Table 2-2: Dephosphorylation reagent concentration

Reagent	Final Concentration	Volume (µl)
Vector DNA	200 ng	10 µl
rAPID Alkaline Phosphatase Buffer, 10 x conc.	1 x	2 µl
rAPID Alkaline Phosphatase	1 U	1 µl
Water		7 µl
	Total	20 µl

Table 2-3: Ligation reagent concentration

Reagent	Final Concentration	Volume (µl)
Vector DNA	50 ng	5
Insert DNA	150 ng	3
DNA Dilution Buffer (5 x)	1 x	2 µl
T4 DNA Ligation Buffer (2x)	1 x	10 µl
T4 DNA Ligase	5 U	1 µl
	Total	21 µl

2.3 CELL CULTURE

All cell culture procedures were performed in laminar air flow hoods. Cells were cultured in their specific medium and incubated in the incubator at 37°C with 5 % CO_2. Adipose-derived human mesenchymal stem cells (AD-MSC) were purchased from American Type Culture Collection (ATCC). The Human Embryonic Kidney 293T (HEK293T) cell line was kindly provided by Micaela Rios Visconti, PhD (MRC Institute of Genetics & Molecular Medicine, University of Edinburgh). The cell culture media and the cell culture maintenance procedure can be found at the following sections.

2.3.1 Cell culture medium

Adipose-derived human mesenchymal stem cells (AD-MSC) standard culture medium: Mesenchymal Stem Cell Basal Medium for Adipose, Umbilical and Bone Marrow-derived MSC, supplemented with Mesenchymal Stem Cell Growth Kit for Adipose and Umbilical-derived MSC – Low Serum, 100U/ml penicillin and 100μg/ml streptomycin (P/S). The complete medium was prepared by adding 10 ml of Growth Kit and 5 ml of P/S into 485 ml of MSC basal medium.

HEK293T cell line culture medium: DMEM medium, high glucose, supplemented with 10% FBS and 1% of 100U/ml/100μg/ml P/S. The complete medium was prepared by adding 50 ml of FBS and 5 ml of P/S into 450 ml of DMEM medium.

Adipose-derived human mesenchymal stem cells (AD-MSC) FeQ doped medium: AD-MSC culture standard medium with the addition of 3.4 μl/ml of FeQ solution, to a final concentration 34 μM.

2.3.2 Passaging of cells

Cells were passaged when they reached the 80% of confluence. Cells were washed with 10 ml of 1x PBS and then incubated with 1 ml of Trypsin-EDTA 0.25% for 2 minutes in the incubator at 37°C with 5% CO_2. Cells were then resuspended and collected in 10 ml of complete medium. The cell suspension was then centrifuged at 1000 rpm for 5 minutes. The supernatant was discarded, and the cell pellet was resuspended in 1 ml of complete medium. Then 200 µl of cell suspension was put into T75 flask containing 10 ml of complete medium (1:5 ratio).

2.3.3 Storage of cells

The freezing medium was made by adding 1 part of DMSO to nine parts of FBS. 5 x 10^6 cells were added to each vial. Cells were stored to -80°C for one day and then transferred to liquid nitrogen for longer storage.

2.4 TRANSIENT GENE TRANSFECTION

In order to investigate the efficient way to transfect AD-MSC with MAGISTER genes, several approaches of transient transfection technique were used in this study. HEK293T cells, as a relatively easy cell line to transfect, were also used in this study as a positive control. A lipid-based transfection, a multi-component non-lipid transfection and an electroporation transfection technique were used as described in the following sections. The transfection efficiency was measured by flow cytometry to determine the most efficient technique to transfect AD-MSC with the MAGISTER gene construct.

2.4.1 Non-Lipid transfection

X-tremeGENE™ HP DNA (Roche), a multi-component non-lipid transfection reagent, was used to transfect cells. Briefly, cells were seeded at 1 x 10^5 cells per well

in 24-well plates one day prior to transfection. On the day of transfection, OptiMEM media (Gibco) was prepared in tubes at 100 µl per tube. DNA plasmid (3 µg) was put into the OptiMEM media, then 9 µl (1:3 ratio to the DNA concentration) of transfection reagent was added to the mixture. The complexes were then mixed and incubated for 20 minutes. Then, the complex solution was gently added into the cells. Each sample transfection was performed in triplicate. Cells mixed with transfection reagent without plasmid were used as negative control. The cells were then incubated at 37°C with 5% CO_2 for 48 hours before the transfection efficiency was quantified by flow cytometry.

2.4.2 Lipid-based transfection

Lipofectamine 3000® transfection

Lipofectamine 3000® (Life Technologies) transfection reagent is a lipid-based transfection reagent that has been commonly used to transfect eukaryotic cells. To perform the transfection, cells were seeded at 1 x 10^5 cells per well in 24-well plates one day prior to transfection. On the following day, 3 µg of MAGISTER plasmid was diluted in 50 µl of OptiMEM media. Separately, Lipofectamine 3000® (9 µl) solution was diluted in 50 µl of OptiMEM media. The individual solutions were then mixed gently and allowed to incubate for 5 minutes at room temperature, after which they were combined and allowed to incubate at room temperature for another 20 minutes. The cell medium was then replaced with prewarmed 500 µl media. Then, the complex solution was gently added into the cells. Each sample transfection was performed in triplicate. Cells mixed with transfection reagent without plasmid were used as negative control. The cells were then incubated at 37°C with 5% CO_2 for 4 hours, after which the cell media was replaced with standard growth media. After incubation for a total of 48 hours at 37°C with 5% CO_2, the transfection efficiency was quantified by flow cytometry.

Fugene® HD transfection

Fugene® HD (Promega) transfection reagent is a novel, non-liposomal complex designed to transfect DNA into a wide variety of cell lines with high efficiency and low toxicity. To perform the transfection, cells were seeded at 1 x 10^5 cells per well in 24-well plates one day prior to transfection. On the day of transfection, OptiMEM media was prepared in tube at 100 µl per tube. DNA plasmid from each construct (3 µg) was put into the OptiMEM media, then 9 µl of transfection reagent/plasmid was added to the mixture. The complexes were then mixed and incubated for 20 minutes. Then, the complex solution was gently added into the cells. Then, the complex solution was gently added into the cells. Each sample transfection was performed in triplicate. Cells mixed with transfection reagent without plasmid were used as negative control. The cells were then incubated at 37°C with 5% CO_2 for 48 hours before the transfection efficiency was quantified by flow cytometry.

2.4.3 Nucleofection

Electroporation, or electropermeabilization, is a physical transfection technique in which a specific electric field is applied to cells. Nucleofection, an electroporation-based technique, also uses electrical pulse but the nucleic acid is directly introduced into the nucleus of cells. When the cell is exposed to the electric shock, the permeability of the cell membrane is increased allowing the DNA entering the cells. The Human MSC Nucleofector™ Kit (Lonza) was used to transfect AD-MSC using this approach. Briefly, 24-well plates were prepared by filling the appropriate number of wells with 500 µl of culture medium then pre-incubated the plates in a humidified 37°C 5% CO_2 incubator. A pellet of cells was prepared at a density 1 x 10^5 cells in a tube, then mixed with 100 µl of Human MSC Nucleofector™ solution. The cell suspension was then mixed with 3 µg DNA plasmid. Afterwards, the nucleofection samples were transferred into an Amaxa™ certified cuvette. The cuvette then inserted into Nucleofector™ Device (Amaxa). The electroporation process was performed on the device by using the U-23 program. Thereafter, the cell suspension was taken out from the cuvette and seeded into prewarmed 24-well plates. Each sample transfection

was performed in triplicate. Cells transfected without plasmid were used as negative control. The cells were then incubated at 37°C with 5% CO^2 for 48 hours before the transfection efficiency was quantified by flow cytometry.

2.5 STABLE GENE TRANSFECTION

To assess whether AD-MSC can be reprogrammed to stably expressing *mms6* gene, a stable *mms6* gene transfection was performed. A lentiviral vector carrying *mms6* gene that was designed as described in section 2.2 was used to transduce AD-MSC. The preparation and the process of this technique is described in the following section.

2.5.1 Puromycin kill-curve

A standard protocol of puromycin kill-curve was performed as a first critical step to determine the minimum antibiotic concentration needed to kill all the cells over the course of two weeks. Briefly, Puromycin (Sigma) was dissolved in 10 ml of ddH_2O giving a stock concentration of 1 mg/ml. In order to set up a kill-curve assay, 5 x 10^4 cells were seeded in triplicate for 8 different puromycin concentrations in a 24-well plate and left overnight. The concentrations tested were 0, 0.5, 1, 2, 4, 6, 8, 10 µg/ml. The selection media containing Puromycin was added to cells providing selection pressure. The medium was changed every three days until 100% of cells had undergone cell death in the lowest concentration condition.

2.5.2 Virus transduction

For virus transduction, 1 x 10^4 AD-MSC and HEK293T cells as control were seeded in into one well of a 24-well plate and grown overnight. The virus-containing supernatant was diluted in growth medium supplemented with polybrene (final concentration: 8 mg/ml) and added to the cell culture. The MOI (Multiplicity of

Infection) number of 10, 15 and 30 were used for the transduction of AD-MSC, whereas MOI ratio of 5 and 10 were used for transduction of HEK293T cells.

The MOI was determined as virus volume (ml) x virus titer (TU/ml)/plated cell number. Two days later, the medium was refreshed with selection medium (growth medium supplemented with 2 µg/ml Puromycin) to generate stable cells expressing the *mms6* gene. The selection medium was changed every 3 days and cells were passaged each time they reached confluence. The mCherry red fluorescence produced by cells was then observed every 5-7 days during the selection process for three weeks. The successful cells stably expressing mCherry red fluorescence were then expanded for the later experiments.

2.6 RNA RELATED INVESTIGATION

2.6.1 RNA Extraction

RNA extraction was performed using RNAeasy Mini Kit (Qiagen). Briefly, cells were trypsinized and resuspended in PBS. Once the supernatant was removed, 350 µl of lysis buffer was used to resuspend the cells. The resuspend was then transferred to a 1.5 ml reaction tube. Then 350 µl of 70% ethanol was added to the lysate. The lysate was transferred into Mini spin column placed in the 2 ml collection tube, then was centrifuged at 13,000 rpm on a table top micro centrifuge for 15 seconds. After centrifugation, 700 µl of wash buffer (RW1) added into the spin column and centrifuged at 13,000 rpm for 15 seconds. Once the flow-through discarded, 500 µl of wash buffer (RPE) added into the spin column and centrifuged at 13,000 rpm for 15 seconds. The flow-through was discarded. Afterwards, 700 µl of wash buffer (RPE) added into the spin column and centrifuged at 13000 rpm for 2 minutes. After that, the spin column was then placed into 1.5 ml collection tube, then 50 µl of RNAase-free water was added to elute the RNA from the membrane into the collection tube and stored at -20°C for later use.

2.6.2 RNA Concentration Measurement

Yield and purity of RNA samples were determined using a Nanodrop1000 spectrophotometer. The absorbance was measured at wavelength 260 nm, 280 nm, and 230 nm. The absorbance ratio of RNA samples at 260/280nm of 0.8 - 1 and absorbance ratio at 260/230 nm in a range 2.0 – 2.2 were considered as highly pure.

2.6.3 Primer design

To determine the MAGISTER gene expression, a set of DNA primers were designed using *Primer3* Software. The human Glyceroaldehude-3-Phosphate Dehydrogenase (GADPH) was chosen as housekeeping gene. The primers were then purchased from Integrated DNA Technologies (USA).

Primers to be used with cDNA synthesized from RNA of cells transfected with MAG02 gene of *mms6* with single tag marker (His6x) was designed to generate amplicons of 142 bp:

Forward : 5’ GGA CCA AAG TGG CAC TGG 3’

Reverse : 5’ CCC ACT ACG CCC AAG ATG AT 3’

While Primers to be used with cDNA synthesized from RNA of cells transfected with MAGISTER gene of *mms6* with double tag marker (His-GFP) was designed to generate amplicons of ~150 - 230 base pairs. The DNA sequence of the primers can be seen at **Table 2-4**.

Table 2-4: Primers for PCR of MAGISTER Gene with His-GFP tag marker

Gene	Forward Primer (5' – 3')	Reverse Primer (5' – 3')	Product Size
MAGISTER - WT	CTCCTGCCAATG TTGCCG	CACGGCTCTTCATAT ACGCG	210 bp
MAGISTER - 01	GAAAGTGGTGGG CGGCAC	CCACTTCTTCATCGC TCTGC	167 bp
MAGISTER - 02	CAAAGTAGTGGG CGGCAC	CTAGGGCATCTCTCA GCTCC	185 bp
MAGISTER - 03	GCACAATCTGGA CAGGCAAA	TTCAACTTCCTCGTC GCTCT	155 bp

2.6.4 cDNA synthesis and DNAse I treatment

cDNA was synthesized by reverse-transcribing 1 µg of RNA. cDNA was synthesized following qScript^{TM}cDNA Synthesis kit (Quanta Biosciences) protocol as listed in Table 2-5. RNA samples (1ug/ µl) were added to 4 µl of x qScript cDNA superMix (which contained random oligo-dT), and then water was added up to 20 µL of final total volume. The reaction was then mixed using vortex and briefly centrifuged before running on the Thermocycler (Tetrad2 DNA Engine, Bio-Rad). Thermocycling conditions used are listed in

Table **2-6**. Then 1/10 of the reaction (2 µl) were used for RT-PCR amplification. Samples of cDNA were stored in -20°C.

2.6.5 Reverse Transcription Polymerase Chain Reaction (RT-PCR)

Amplification of MAGISTER DNA fragment was performed was using the Taq MasterMix kit (Qiagen) in a Thermocycler (Tetrad2 DNA Engine, Bio-Rad). Two reactions were run in parallel for MAGISTER internal gene amplification and for GAPDH amplification. Reactions were prepared on ice to a total volume of 25 µl according to the protocol provided by Qiagen as listed in Table 2-7. Reactions were run alongside a negative control where RNA was substituted for dH_2O. The PCR reaction was performed in the Thermocycler using condition as listed in Table 2-8.

2.6.6 DNA agarose gel electrophoresis

In order to investigate the MAGISTER amplified fragment, the PCR products were resolved in a 2% agarose gel. Briefly, 2 g of agarose were mixed with 150 ml of 0.5 x TBE and dissolved using microwave. Then, 0.01% diluted SYBR™ Safe stain (Invitrogen) was added to the gel to visualize the DNA under UV image analyzer. The gel then cooled at room temperature, and then 20 µl of the sample were loaded into the gel and run in running buffer made of 0.5 x TBE in horizontal gel electrophoresis system (Bio-Rad) at a constant voltage of 110V for 100 minutes. Samples were run alongside a 100bp DNA ladder (New England BioLabs) in order to determine the molecular weight (MW) of the PCR product. Then, the gel was then visualized under UV light to image the DNA bands.

Table 2-5: Reagent concentrations for cDNA production

Reagent	Volume (µl)
RNA (1 µg/µl)	Variable
qScript supermix	4

H_2O		Variable
	Total	20

Table 2-6: Thermocycler condition for qScript cDNA production

Temperature (°C)	Time (mm:ss)
25	05:00
42	30:00
85	05:00
4	Hold

Table 2-7: Reagent concentrations for End-Point PCR

Reagent	Volume (µl)
Taq MasterMix (2x)	12.5
Forward primer	1
Reverse primer	1
Control dye	2.5
dH_2O	6

Sample		2
	Total	25

Table 2-8: Thermocycler condition for End-Point PCR

Step	Temperature (°C)	Time (mm:ss)
Initial Denaturation	95	00:30
35 Cycles	95	00:45
	55	00:45
	70	01:00
Final Extension	72	05:00
Hold	4	Hold

2.7 PROTEIN RELATED INVESTIGATION

2.7.1 Protein extraction

Western blot technique was used in this study to investigate protein expression. For this, the protein extraction was performed on cell lysates from samples. In brief, cells were washed in cold PBS and scraped in cold RIPA buffer (Santa Cruz). The RIPA

reaction buffer was supplemented with protease and phosphatase inhibitors as listed in Table 2-9. The cell lysates were left on ice for 10 minutes before being centrifuged for 30 minutes at 13000 rpm (4°C). The supernatants were kept at -20 °C until future use.

Table 2-9: Reagent concentration for complete RIPA buffer

Reagent	Volume per 1 ml of RIPA buffer (µl)
Sodium orthovanadate (Na_3VO_4)	10
Phenylmethylsulfonyl fluoride (PMSF)	10
Proteinase Inhibitor	20

2.7.2 Protein Quantification

The protein concentration was then quantified from the cell lysates against a bovine serum albumin standard pre-diluted set (Thermo Fisher Scientific), based on the method of Bradford using Bio-Rad protein assay. Briefly, 10 µl of each standard and sample solution were loaded into 200 µl of diluted dye reagent in microtiter plates well. Once incubated at room temperature for 5 minutes, the plate was then read at 595 nm using FLUOstar Omega plate reader (Labtech).

2.7.3 Gel Electrophoresis

Western blots were performed in 4-15% Mini-Protean TGX gel (Bio-Rad), held in a vertical tank filled with 10% TGS (Bio-Rad) electrophoresis running buffer. The protocol was set-up according to the manufacturer's instructions. In brief, 20 µg of protein lysates was solubilized in 4x Laemmli (Bio-Rad) loading buffer (62.5 mM Tris-HCl, pH 6.8 sample buffer, 10% glycerol, 1% LDS, 0.005% Bromophenol Blue, 10% 2-mercaptoethanol). The protein samples were then denatured for 5 minutes at 95 °C. The samples then loaded along with a protein ladder (Licor) at 180V for 35 minutes.

2.7.4 Electrophoretic Transfers

Protein were then transferred on a nitrocellulose membrane (Sigma), using a wet transfer technique. Initially, a transfer buffer (Bio-Rad) was prepared and cooled to 4°C. A blotting sandwich of pre-soaked sponges, pre-soaked filter paper, polyacrylamide gel and pre-soaked nitrocellulose membrane were carefully prepared on the transfer tank to allow the negatively charges protein to transfer from the gel to the membrane. The transfer sandwich was set up with the following configuration: sponge, filter paper, nitrocellulose membrane, gel, filter paper and sponge. The sandwich was topped with a 1x transfer buffer, and the tank was programmed at 100 V for 60 minutes on an ice bucket.

2.7.5 Immunostaining and Antibody Detection

Once the transfer finished, the membrane was saturated in 5% non-fat dry milk (Marvel) diluted in 0.1% TBST buffer (0.05 M Tris-HCl, 0.15 M NaCl, 0.1% Tween-20, pH 7.6) for an hour at room temperature. The membrane was then incubated overnight at 4°C under slow agitation in the primary antibody (anti-His and anti-B-actin from Abcam) diluted at 1:1000 in 5% non-fat milk, in 0.1% TBST.

After being washed with 0.1% TBST every 10 minutes for half an hour, the membrane was then incubated with second antibody (HRP-linked anti-mouse IgG, Abcam) at a dilution of 1:1000 in 5% non-fat milk made in 0.1% TBST under slow agitation at room temperature for 1 hour.

The nitrocellulose membrane was then washed again with 0.1% TBST every 10 minutes for one hour before being visualized using Clarity Western ECL substrate (Bio-Rad) in Odyssey® Fc Imaging System (Li-Cor). The intensities of the bands were quantified ImageStudioLite software from Li-Cor.

2.8 FLUORESCENCE IMAGING OF GFP

The MAGISTER protein expression of transfected cells was investigated by observing GFP fluorescence under fluorescence microscope. 18mm glass coverslips were sterilized in 70% ethanol, air dried for 10 minutes, exposed to UV for 20 minutes, then added to 6-well plates. 4 x 10^4 transfected cells were used per well and once seeded grown for 48 hours. Cells were then washed with ice-cold PBS three times for five minutes. Cells were then fixed with formaldehyde 3.7% at 10 minutes at room temperature. Cells were washed three times for five minutes with PBS. Coverslips were then removed, washed in distilled H_2O and mounted on to microscope slides using VECTASHIELD® Antifade Mounting Medium with DAPI (Vector Laboratories) and dried overnight. Images were obtained using the Nikon E800 fluorescence microscope.

2.9 FLOW CYTOMETRY ANALYSIS OF GFP EXPRESSING CELLS

To measure the percentage of GFP-Positive cells following the transfection, flow cytometry was performed. Briefly, cells were washed with PBS two times, then trypsinized. Cells were collected and centrifuged at 1000 rpm for 5 minutes, then diluted in 200 µL of PBS supplemented with 5% FBS. The percentage of GFP positive cells were analysed using the Accuri C6 flow cytometry reader (BD Biosciences).

2.10 INDIRECT IMMUNOFLORESCENCE

Immunofluorescence was performed to characterise population of human MSCs using positive and negative selection markers provided by human MSC characterization kit (Merck). Briefly, 5 x 10^4 cells were seeded in 24 well-plate and grown overnight. Cells were then fixed with ice-cold methanol for 15 minutes at -20 °C. In order to reduce non-specific background staining, cells were incubated with PBS 3% BSA solution for 20 minutes. Cells were incubated with anti-CD44, anti-CD90, anti-CD14 and anti-CD19 1:500 diluted in PBS 1% BSA for one hour. Cells were washed three times for five minutes with PBS.

AlexaFluor 488 (Abcam) antibodies were diluted in PBS 1% BSA solution and added to cells for one hour in darkness. Cells were washed three times for five minutes with PBS. Cell were washed in distilled H_2O and counterstained with VECTASHIELD® Antifade Mounting Medium with DAPI (Vector Laboratories) and dried overnight. Images were obtained using the Nikon E800 fluorescence microscope.

2.11 TURBIDITY MEASUREMENT OF COMMERCIAL IRON-BASED MAGNETIC NANOPARTICLE IN CULTURE MEDIUM.

Following iron oxide-based MNPs were tested for their colloidal stability in PBS and in culture medium: NanoMAG®-D-Spio (Micromod, Germany), BNF-Dextran (Micromod, Germany), FluigMAG-CT (Chemicell, Germany) and Ferucarbotran (Meito Sangyo, Japan) as can be seen in **Table 2-14**.

NanoMAG®-D-Spio are ferrofluids, cluster-typed shape MNP, which have diameter size of 50 nm. They are prepared by precipitation of iron oxide in the presence of dextran. FluidMAG-CT are ferrofluids consisting of an aqueous dispersion of magnetic iron oxides with diameters of 50 nm. The particles are covered with hydrophilic polymers which protect them against aggregation by foreign ions. BNF-Dextran are 80 nm cluster-typed shape Bionized NanoFerrite particles which are

prepared via the core-shell method with a core of 75-80% (w/w) magnetite and a shell of dextran. Ferucarbotran is an aqueous suspension of multi-core carboxydextran-coated magnetite nanoparticles (54 nm), originally designed as a liver-targeting MRI contrast agent.

Colloidal stability of these MNP in PBS and culture medium was assessed by measuring turbidity of the MNP in medium over time. For this analysis, MNP samples were prepared in either 500 µl of culture medium or PBS (500 µg/ml) in 24-well plate. Turbidity measurement was performed over a period up to 24 h, namely 0, 2 h, 16 h and 24 h. The suspension was measured at 450 nm using a microplate reader.

2.12 PRUSSIAN BLUE STAINING

For Prussian blue staining, cells were seeded in 12-well plates (5 x 10^4 cells/well) in 1 ml medium and grown overnight. A day after, cells were loaded with 200 µg/ml Ferucarbotran nanoparticle in 500 µl medium and incubated overnight. Cells without MNP served as control. Following overnight incubation, cells were fixed with formaldehyde 4% and stained with HT20 Prussian blue iron stain kit (Sigma Aldrich). Briefly, equal volumes of Potassium Ferrocyanide Solution (15 ml) and Hydrochloric Acid Solution (15 ml) were mix to make 30 ml working Iron Stain Solution. Cells were then incubated in the working Iron Stain Solution (1 ml/ well) for 3 minutes. Thereafter, cells were washed with distilled water three times. Cells were then incubated with Pararosaniline solution (1ml/well) for 5 minutes. Thereafter, cells were washed with distilled water for three times and observed at light microscope. Cells were pictured using a coloured camera (Micropublisher camera, QIMAGING).

2.13 TRANSMISSION ELECTRON MICROSCOPY (TEM) SAMPLES PREPARATION

1 x 10^6 cells were collected and centrifuged at 1000 rpm for 5 minutes. The cell pellet was then resuspended in 50 µl of cell culture medium and transferred to a 1.5 ml

microcentrifuge tube. A sample blocking made of 1% agarose was prepared by dissolving 0.5 g agarose powder in 50 ml of 1x PBS in a glass beaker. The solution was put in microwave at 800 W for 3 minutes. In the meantime, the bottom of a 0.5 ml tube was cut with scissors and it was put upside down with the lid closed in an ice bucket. The 1% agarose solution was cooled down for 30 seconds at room temperature, then the cell pellet was slowly resuspended in 100 µl of agarose solution avoiding air bubbles. After the agarose was solidified, the sample was then immediately transferred in a 5 ml bijoux tube filled with 3% glutaraldehyde solution, under chemical hood.

For Transmission Electron Microscopy, sample preparation was done by Stephen Mitchell at Biology Scanning Electron Microscope facility, The University of Edinburgh. For this, cells were fixed in 3% glutaraldehyde in 0.1M Sodium Cacodylate buffer, pH 7.3, for 2 hours then washed in 3 x 10-minutes changes of 0.1M Sodium Cacodylate. Specimens were then post-fixed in 1% Osmium Tetroxide in 0.1M Sodium Cacodylate for 45 minutes, then washed in 3 x 10-minutes changes of 0.1M Sodium Cacodylate buffer. These samples were then dehydrated in 50%, 70%, 90% and 100% ethanol (X3) for 15 minutes each, then in 2 x 10-minute changes in Propylene Oxide. Samples were then embedded in TAAB 812 resin. Sections, 1µm thick were cut on a Leica Ultracut ultramicrotome, stained with Toluidine Blue, and viewed in a light microscope to select suitable areas for investigation. Ultrathin sections, 60nm thick were cut from selected areas, stained in Uranyl Acetate and Lead Citrate then viewed in a JEOL JEM-1400 Plus TEM. Representative images were collected on a GATAN OneView camera.

2.14 AD-MSC DIFFERENTIATION EXPERIMENT

2.14.1 Osteogenesis

AD-MSC expressing *mms6* (*mms6*-lenti-transduced AD-MSC) and untransfected AD-MSC were differentiated in osteogenic culture medium for 10 or 21 days, using StemPro Osteogenesis Differentiation Kit (Gibco). Cells cultured in standard growth medium were considered as a negative control. The differentiation experiments were

performed in the absence of FeQ doping. Briefly, cells were seeded in 24 wells plates in triplicate for each cell group. Cells were seeded at a density of $2x10^4$ cells/well cultured in standard culture medium. After 48 hours of incubation, the medium was replaced with osteogenic medium for the treated group. The medium was continuously replaced with fresh medium every 3 days.

At 10 Days and 21 Days of incubation time point, cells were fixed for the osteogenic staining. For this, cells were washed twice with 1 ml of 1xPBS and fixed in 4% PFA for 30 minutes at room temperature in fume hood. After fixation, cells were washed twice with 1 ml of ddH2O /well and stained with 2% Alizarin Red S solution (pH4.2) for 30 minutes. The cells were then washed three times with 1ml of ddH2O/well and observed under light microscope and scanned for the analysis.

2.14.2 Adipogenesis

AD-MSC expressing *mms6* (*mms6*-lenti-transduced AD-MSC) and untransfected AD-MSC were differentiated in adipogenic culture medium for 10 days, using StemPro Adipogenesis Differentiation Kit (Gibco). Cells cultured in standard growth medium were considered as a negative control. The differentiation experiments were performed in the absence of FeQ doping. Briefly, cells were seeded in 24 wells plates in triplicate for each cell group. Cells were seeded at a density of $2x10^4$ cells/well cultured in standard culture medium. After 48 hours of incubation, the medium was replaced with adipogenic medium for the treated group. The medium was continuously replaced with fresh medium every 3 days.

After 10 Days of incubation, cells were fixed for the adipogenic staining. For this, the medium was removed and plates were carefully washed twice with 1 ml of 1x PBS, to not disrupt the cells monolayer. The cells were fixated in 4% PFA under the chemical hood, then they were incubated for 1 hour at 37°C. After fixation, cells were washed twice with 1 ml of 1x PBS, then incubated with 1 ml of 60% isopropanol for 1 minute. Then, the isopropanol was disposed and the cells were let dry under the chemical hood. At this point, it was added the Oil Red O solution diluted 3:2 in distilled water for 20

minutes. Thereafter cells were washed with 1x PBS for three times and imaged immediately at light microscope. Cells were pictured using a coloured camera (Micropublisher camera, QIMAGING).

2.15 MAGNETIC RESONANCE IMAGING (MRI)

To perform MRI experiment, *mms6* transfected AD-MSC: Mag01-transfected and Mag-03 transfected; and lentiviral *mms6* transduced cells were prepared for the assay. Cells were incubated in FeQ medium for 10 days. Thereafter, 1 x 10^6 of cells were collected and centrifuged at 1000 rpm for 5 minutes. The cell pellet was then resuspended in 50 µl of PBS in microcentrifuge tube. A sample blocking made of 1% agarose was prepared by dissolving 2 g agarose powder in 200 ml of 1x PBS in a glass beaker. The solution was put in microwave at 800 W for 3 minutes. After that, the solution was loaded into 50 ml falcon tubes, 40 ml each tube, and cooled down for 5 minutes at room temperature. Once the solution almost solidified, a microcentrifuge tube was used to make a V shape hole on the surface of the gel. The cells were then loaded into the hole carefully, before adding 2 ml of agar solution to cover the cells. Cells after 24 hours loaded with Ferucarbotran MNP were used as positive control.

Magnetic resonance imaging was performed using the head matrix coil of a 3T MRI system (MAGNETOM Verio, Siemens AG, Healthcare Sector, Erlangen, Germany) by Dr. Scott Semple at Clinical Research Imaging Centre, Queen's Medical Research Institute, University of Edinburgh. Phantoms were suspended in a water bath to reduce artefact. Multi-gradient-echo T2* acquisitions were acquired from 2.7–21.3ms and used to generate T2* values (ms) using a standard least-squares fitting routine in Matlab (Mathworks).

2.16 SQUID (SUPERCONDUCTING QUANTUM INTERFERENCE DEVICE) MAGNETOMETRY ASSAY

SQUID magnetometer is a very high precision instrument which measures the total magnetic moment of a sample. A device called a MPMS is used to measure the magnetic moment of a sample by reading the output of the SQUID detector. To perform SQUID measurements, 3 x 10^6 cells were collected and centrifuged at 1000 rpm for 5 minutes. The supernatant was removed, and the pellet was washed with 1 ml of 1x PBS, then centrifuged again at 1000 rpm for 5 minutes. The supernatant was discarded, and the pellet was transferred in a 1.5 ml microcentrifuge tube sealed with parafilm. The pellet was desiccated at 60°C for 30 minutes in a vacuum-pump centrifuge (TVC 2-18, CHRIST). The parafilm that sealed each Eppendorf was punctured to avoid sample damage by vacuum. Then, a capsule method of SQUID preparation was used to prepare the samples by transferring the dry pellet into a non-magnetic gelatin capsule. The capsule was then inserted into a plastic straw. Then, the straw was mounted into the SQUID sample rod and inserted into MPMS device. Magnetization data were taken at temperatures 5K < T < 350 K, using a liquid-He-cooled variable-temperature installed in the commercial SQUID-magnetometer apparatus (MPMS, Quantum Design Inc., San Diego, USA). The temperature-dependent magnetization was determined in a small, (u0H = 0.01T) between body temperature, T = 310 K, and T = 5K. The measurement was performed at varying temperatures moving the samples through a pick-up coil system connected to the SQUID via a flux transformer in a constant magnetic field, generate by a superconducting coil.

2.17 MAGNETHERM SYSTEM DEVICE DESCRIPTION

To perform *in vitro* MNHT experimentation, an alternating magnetic field generated by a commercial system (Magnetherm™ V1.5, nanoTherics Ltd) was used in this study. The experimental setup consisted of the following components: a radiofrequency induction heater (magneTherm™ version 1.5 nanoTherics Ltd), an oscilloscope (ISO-TECH ISR622 20 MHz), a laboratory power supply (EA-PS 3032-

20B, EA Elektro Automatic), a function generator (SFG-2004, GW Instek), and a circulating water-cooling system.

The radiofrequency induction heater was used to generate AMF to expose the MSC by high-frequency induction through 9-turn water-cooled, copper coil inside the device.

Three different capacitors used in the magneTherm^{TM}: a 200 nF capacitance; a 22 nF capitance; and a 6.2 nF capitance to achieve the desired frequency range for the 9-turn coil. The function generator was used to generate a square waveform at three different frequencies: 178.3 kHz (23.89 mT), 540 kHz (24.87 mT), and 1030 kHz (13.37 mT).

The DC power supply was supplied by a Digimess Concept series DC power supply SM5020 device. An oscilloscope was used to monitor the signal voltage passing through the coil. A continuous circulating water from sink drain system was used as water-cooling system to prevent the sample being exposed to the non-specific heating caused by the heat induction by the high-frequency magnetic fields in the coils.

2.18 *IN VITRO* ALTERNATING MAGNETIC FIELD (AMF) EXPERIMENTATION

2.18.1 Media used in the experiments

Standard Medium: Mesenchymal Stem Cell Basal medium supplemented with Mesenchymal Stem Cell Growth Kit + Penicillin/streptomycin (100 U/ml/100µg/ml), and without FeQ.

Iron Source Medium: Mesenchymal Stem Cell Basal medium supplemented with Mesenchymal Stem Cell Growth Kit + Penicillin/streptomycin (100 U/ml/100ug/ml), and FeQ.

Ferucarbotran nanoparticles medium: Mesenchymal Stem Cell Basal medium supplemented with Mesenchymal Stem Cell Growth Kit + Penicillin/streptomycin (100 U/ml/100ug/ml), and with Ferucarbotran nanoparticle (200 µg/ml).

2.18.2 AD-MSC Monolayer Culture and AMF Exposure Experimentation.

AD-MSC expressing *mms6* monolayer culture and AMF exposure procedure

AD-MSC expressing *mms6* (lenti-transduced AD-MSC) were cultivated with the iron source medium in T75 flask for 10 days. After 10 days incubation, the cells were then collected and seeded in sterile 35 mm Petri dishes at the density of 5 x 10^5 cells each Petri dish in 2 ml of standard medium. The cells were incubated at 37°C, 5 % CO_2 overnight before the AMF exposure at the following day.

For the AMF exposure, six sterile 35mm Petri dishes, each containing a single monolayer of *mms6*-expressing MSC, were prepared as explained above. Then, three Petri dishes were exposed one by one to an AMF for 1 hour, in the magneTherm device, while the other three Petri dishes were placed in the magneTherm system under the similar conditions, but with the AMF switched off, as a control. After the AMF exposure, Petri dishes were incubated overnight in the incubator at 37°C and 5% CO_2. The next day, the cell viability was assessed by AlamarBlue cell viability assay. Experiments were set in three different frequencies of AMF: 178.3 kHz (23.89 mT), 540 kHz (24.87 mT), and 1030 kHz (13.37 mT).

Ferucarbotran nanoparticle-loaded MSC monolayer culture and AMF exposure procedure.

AD-MSC were seeded in sterile 35mm Petri dishes at the density of 5 x 10^5 cells each Petri dish in 2 ml of Ferucarbotran nanoparticles medium. The cells were incubated at 37°C, 5 % CO_2 overnight. The following day, the cells were washed with 1x PBS three times before replaced the medium with the standard medium and exposed the cells

with AMF exposure. After the AMF exposure, Petri dishes were incubated overnight in the incubator at 37°C and 5% CO_2.

For the AMF exposure, six sterile 35mm Petri dishes, each containing a single monolayer of Ferucarbotran nanoparticle-loaded MSC, were prepared as explained above. Then, three Petri dishes were exposed one by one to an AMF frequency for 1 hour, in the magneTherm device, while the other three Petri dishes were placed in the magneTherm system under the similar conditions, but with the AMF switched off, as a control. After the AMF exposure, Petri dishes were incubated overnight in the incubator at 37°C and 5% CO_2. The next day, the cell viability was assessed by AlamarBlue cell viability assay. Experiments were set in three different frequencies of AMF: 178.3 kHz (23.89 mT), 540 kHz (24.87 mT), and 1030 kHz (13.37 mT).

2.18.3 MSC in 3D Culture and AMF Exposure Experimentation

AD-MSC expressing *mms6* in 3D culture and AMF exposure procedure

AD-MSC expressing *mms6* (lenti-transduced AD-MSC) were cultivated with the iron source medium in T75 flask for 10 days. After 10 days incubation, the cells were then washed with 1x PBS twice before trypsinized and centrifuged at 1000 rpm for 5 minutes. Cells were then prepared in a 1.5 ml microcentrifuge tube at the concentration of 1 x 10^6 cells for each tube. The cells were then centrifuged again at 1000 rpm for 5 minutes, to create a cell pellet. The supernatant was discarded and replaced with 50 µl standard medium.

For the AMF exposure, six tubes of samples, each containing a single 3D cells of *mms6*-expressing MSC, were prepared as explained above. Then, three tubes were exposed one by one to an AMF of 540 kHZ frequency for 1 hour, in the magneTherm device, while the other three tubes were placed in the magneTherm system under the similar conditions, but with the AMF switched off, as a control. After the AMF exposure, cells were resuspended in 1 ml standard medium, then the 200 µl of

suspension cells were seeded into 6-well plate. The cells then incubated overnight in the incubator at 37°C and 5% CO_2.

After the AMF exposure, cells were resuspended in 1 ml standard medium, then the 200 µl of cell suspension were seeded into 6-well plate in triplicate and incubated overnight in the incubator at 37°C and 5% CO_2. The next day, the cell viability was assessed by AlamarBlue cell viability assay.

Ferucarbotran nanoparticle-loaded MSC in 3D culture and AMF exposure procedure

AD-MSC were cultivated in sterile T75 flask with the standard medium at the density of 5 x 10^5 cells each flask, until confluent. The medium was then replaced with the ferucarbotran nanoparticles medium. The cells were incubated at 37°C, 5 % CO_2 overnight. The following day, the cells were washed with 1x PBS three times before collected and centrifuged at 1000 rpm for 5 minutes. The cells were then prepared in a 1.5 ml microcentrifuge tube at the concentration of 1 x 10^6 cells for each tube. The cells were then centrifuged again at 1000 rpm for 5 minutes, to create a cell pellet. The supernatant was discarded and replaced with 50 µl standard medium.

For the AMF exposure, six tubes of samples, each containing a single 3D cells of ferucarbotran nanoparticle-loaded MSC, were prepared as explained above. Then, three tubes were exposed one by one to an AMF of 540 kHZ frequency for 1 hour, in the magneTherm device, while the other three tubes were placed in the magneTherm system under the similar conditions, but with the AMF switched off, as a control.

After the AMF exposure, cells were resuspended in 1 ml standard medium, then the 200 µl of cell suspension were seeded into 6-well plate in triplicate and incubated overnight in the incubator at 37°C and 5% CO_2. The next day, the cell viability was assessed by AlamarBlue cell viability assay.

2.18.4 Cell Viability determination by AlamarBlue assay

AlamarBlue Cell Viability Assay Description

AlamarBlue^{Tm} is a reagent used to quantify cellular metabolic activity. The kit employed for these experiments relies on the indicator dye which incorporates an oxidation-reduction (REDOX) indicator that both fluorescence and changes colour in response to the chemical reduction of growth medium, resulting from living cells. The reagent solution contains blue-coloured molecule resazurin, which is non-toxic and non-fluorescent. The solution also cell permeable, which, when the molecule enters inside the cells, and chemically reduced by a metabolic activity of cells, turns into the highly fluorescent red-coloured resorufin. Both the fluorescence and the colour change resulted from this reaction can be monitored on a plate reader of a fluorescence spectrophotometer. By comparing this change of two or more cell populations, it is possible to do direct measurement of cell metabolic activity as well as viable cell concentration.

AlamarBlue Cell Viability Assay experimental procedure

Following the AMF exposure and overnight incubation in the incubator at 37°C and 5% CO_2, AlamarBlue reagent was added to the cell medium at 1/10th ratio of cell medium volume. Then, the cells were incubated in the incubator at 37°C and 5% CO_2. After 4 hours incubation, the fluorescence change of the sample was then measured at the plate reader (FLUOstar Omega, BMG LABTECH) by excitation at 544 nm and emission at 590 nm.

Results are presented both as relative fluorescence units (RFU) than as the percentage of cell viability, against controls considered as 100% viable. This percentage was calculated according to (Zachari *et al.*, 2014):

$$\%\text{Viability} = \frac{RFU\ (exposed) - RFU\ (blank)}{RFU\ (not\ exposed) - RFU\ (blank)} \times 100\ \%$$

Blanks are represented by the medium without cells and with the addition of 10% AlamarBlue reagent.

2.18.5 Cell apoptosis by TUNEL assay

Cell apoptosis detection using TUNEL assay description

Terminal deoxynucleotidyl transferase (TdT) dUTP Nick-End Labeling (TUNEL) assay has been designed to detect apoptotic cells that undergo extensive DNA degradation during the late stages of apoptosis. The method is based on the ability of the enzyme terminal deoxynucleotidyl transferase to incorporate labeled dUTP into free 3'-hydroxyl termini generated by the fragmentation of genomic DNA into low molecular weight double-stranded DNA and high molecular weight single stranded DNA. TUNEL staining generally considered as a method for the detection of DNA damage (DNA fragmentation), and under the appropriate circumstances, more specifically as a method for identifying apoptotic cells.

Cell apoptosis detection using Click-iT® Plus TUNEL assay experimental procedure

AD-MSC expressing *mms6* (lenti-transduced AD-MSC) were cultivated with the iron source medium in T75 flask for 10 days. After 10 days incubation, the cells were then collected and seeded in sterile 35 mm Petri dishes at the density of 5 x 10^5 cells each Petri dish in 2 ml of standard medium. The cells were incubated at 37°C, 5 % CO_2 overnight before the AMF exposure at the following day.

For the AMF exposure, six sterile 35mm Petri dishes, each containing a single monolayer of *mms6*-expressing MSC, were prepared as explained above. Three Petri dishes were exposed one by one to an AMF of 540 kHZ frequency for 1 hour, in the magneTherm device. The other Petri dishes were placed in the magneTherm system without AMF exposure for an hour, as a control. After the AMF exposure, Petri dishes

were incubated overnight in the incubator at 37°C and 5% CO_2. The next day, the cell apoptosis was assessed by The Click-iT® Plus TUNEL Assay,

The assay was done based on the manufacturer's specifications. A day after AMF exposure, the cells were fixed for 10 minutes in 4% paraformaldehyde in PBS, at room temperature. The cells were carefully washed in PBS three times, to remove all traces of formaldehyde. Then, they were permeabilized using 0.5 % Triton X-100. After an incubation for 20 minutes, the cells were washed (×2) with DNase free ultrapure water. After which, TdT reaction buffer was added to each cover slips prior to 60 minutes incubation with tetrathionate reaction cocktail (TdT reaction buffer, EdUTP, TdT enzyme). Then, the Petri dishes were washed with 3% bovine serum albumin (BSA) in PBS and were added with click-iT reaction cocktail (click-iT reaction buffer with Alexa Fluor™ 488 dye–labeled and reaction buffer additive). After incubating for 30 minutes, the samples were washed with 3% BSA in PBS for 5 minutes. The cells were washed 3 times in PBS and stained with Hoechst staining (DAPI). Images were obtained using the Nikon E800 fluorescence microscope.

2.18.6 HSP70 gene expression analysis by western blot assay

HSP70 gene expression analysis by western blot assay description

The HSP70 family is a set of highly conserved proteins that are induced by a variety of biological stresses, including heat stress in all organism. These proteins are essential constituents of the cellular network of molecular chaperones and folding catalysts. HSP70 plays a vital role in several folding processes, such as the folding and assembly of newly synthesized proteins, refolding of misfolded and aggregated proteins. A protein analysis, western blot, was performed in this study to investigate the effect of the AMF exposure on HSP70 protein expression.

HSP70 gene expression analysis by western blot assay description

AD-MSC expressing *mms6* (lenti-transduced AD-MSC) were cultivated with the iron source medium in T75 flask for 10 days. After 10 days incubation, the cells were then washed with 1x PBS twice before trypsinized and centrifuged at 1000 rpm for 5 minutes. Cells were then prepared in a 1.5 ml microcentrifuge tube at the concentration of 1 x 10^6 cells for each tube. The cells were then centrifuged again at 1000 rpm for 5 minutes, to create a cell pellet in 1.5 ml centrifuge tube. The supernatant was discarded and replaced with 50 µl standard medium.

For the AMF exposure, cells in the microcentrifuge tube were then exposed to 540 kHZ frequency of AMF for 1 hour. After the AMF exposure, cells were resuspended in 1 ml standard medium, then reseeded into T75 flask. The cells then incubated overnight in the incubator at 37°C and 5% CO_2. AD-MSC expressing *mms6* not exposed to AMF were used as a control.

After one day incubation, cells were washed with cold PBS and collected, then western blot assay was performed. For this assay, Anti-Hsp70 antibody, rat mAb (Cell Signaling) diluted at 1:1000 in 5% non-fat milk, in 0.1% TBST, was used as primary antibody. HRP-linked Anti-rat IgG (Cell Signaling) at a dilution of 1:1000 in 5% non-fat milk made in 0.1% TBST was used as secondary antibody. The nitrocellulose membrane was then visualized using Clarity Western ECL substrate (Bio-Rad) in Odyssey® Fc Imaging System (Li-Cor). The intensities of the bands were quantified ImageStudioLite software from Li-Cor.

2.19 STATISTICAL ANALYSIS

Each experiment was conducted three times except where stated. The average, standard deviation (SD) were calculated from triplicate experiments. GraphPad prism was used for all statistical analyses. Student unpaired t-test was used to test between two independent variables.

2.20 MATERIAL

2.20.1 List of reagents

Table 2-10: Cell culture reagents

Reagents	Supplier
Mesenchymal Stem Cell Growth Kit for Adipose and Umbilical-derived MSC – Low Serum	ATCC, USA
DMEM (Dulbecco's Modified Eagle Medium)	Life Technologies, UK
FBS (Fetal Bovine Serum)	Life Technologies, UK
Trypsin with 0.25 % EDTA	Life Technologies, UK
100 x PenStrep (Penicillin/Streptomycin)	Life Technologies, UK
PBS (Phosphate Buffered Saline)	Life Technologies, UK
OptiMEM Reduced Serum Media	Life Technologies, UK

Table 2-11: RNA Isolation/DNA synthesis/agarose gel electrophoresis/PCR reactions/Western blot reagents

Reagents	Company
Ethanol	Sigma Aldrich, UK
DNA/RNAse free water	Life Technologies, UK
RNA Denaturating Loading Buffer	New England Biolabs, UK
Agarose	Sigma Aldrich, UK
Tris-Borate-EDTA buffer	Thermo Fisher Scientific, UK
RNAeasy Mini Kit	Qiagen, UK
DNAase I Kit	Qiagen, UK
Taq PCR Master Mix Kit (250 U)	Qiagen, UK
qScript cDNA Synthesis Kit	Quanta Biosciences/VWR, UK
SYBR Stain	Life Technologies, UK
DNA ladder/PCR Marker N3234S	New England Biolabs, UK
dNTPs	Thermo Fisher Scientific, UK
Anti-6X His tag® antibody [HIS.H8]	Abcam, UK
4–20% Mini-PROTEAN®TGX™ Precast Protein Gels, 10-well (30 µl/well)	Bio-Rad, UK
RIPA Lysis buffer system	Santa Cruz Biotechnology, UK
WesternSure® Pre-stained Chemiluminescent protein ladder	Li-Cor, UK

Anti-beta Actin antibody [mAbcam 8226]	Abcam, UK
m-IgGκ BP-HRP secondary antibody	Santa Cruz Biotechnology, UK
2x Laemmli Sample Buffer	Bio-Rad, UK
Clarity™ and Clarity Max™ Western ECL Blotting Substrates	Bio-Rad, UK
Pierce™ Bovine Serum Albumin Standard Pre-Diluted Set	Thermo Fisher Scientific, UK
Tris Buffered Saline (TBS) Tablets	Clontech Takara, USA
Bradford Reagent	Sigma Aldrich, UK

Table 2-12: Gene purification from agarose gel/restriction enzymes digestion/vector dephosphorylation and ligation

Reagents	Company
QIAquick Gel Extraction Kit	Sigma Aldrich, UK
EcoRI enzyme	New England Biolabs, UK
NotI enzyme	New England Biolabs, UK
KpnI enzyme	New England Biolabs, UK
XbaI enzyme	New England Biolabs, UK
HindIII enzyme	New England Biolabs, UK
NheI enzyme	New England Biolabs, UK
NEBuffer 3.1 (10x concentrated)	New England Biolabs, UK
Rapid DNA ligation kit	New England Biolabs, UK
DNA clean up Kit	New England Biolabs, UK

Table 2-13: MSC osteogenic/adipogenic differentiation

Reagents	Company
StemPro Osteogenesis Differentiation Kit	Gibco, UK
StemPro Adipogenesis Differentiation Kit	Gibco, UK
4% Paraformaldehyde	Sigma Aldrich, UK
Alizarin Red Alcian	Sigma Aldrich, UK
Oil Red O Solution	Sigma Aldrich, UK
Human Mesenchymal Cell Characterization Kit	Sigma-Aldrich, UK

Table 2-14: Transfection/MNP/TEM reagents

Reagents	Company
X-tremeGENE™ HP DNA	Invitrogen, UK
Lipofectamine 3000®	Invitrogen, UK
Fugene®HD	Promega, UK
MSC Nucleofection Kit	Lonza, UK
Polybrene	Santa Cruz Biotechnology, UK
3% Glutaraldehyde	Sigma Aldrich, UK
Formaldehyde	Sigma Aldrich, UK
Ferucarbotran Magnetic Nanoparticle, 54 nm	Meito Sangyo, Japan
FluidMAG-CT Magnetic Nanoparticle, 50 nm	Chemicell, Germany
BNF-Dextran Magnetic Nanoparticle, 80 nm	Micromod, Germany
NanoMAG D-Spio Magnetic Nanoparticle 50 nm	Micromod, Germany
HT20 Prussian Blue Iron Stain Kit	Sigma Aldrich, UK

Table 2-15: In vitro AMF experimentation

Reagents	Company
Alamar Blue Cell Viability Assay	Thermo Fisher Scientific, UK
Click-iT® Plus TUNEL Assay	Life Technologies, UK
HSP70 (6B3) Rat mAb	Cell Signaling Technology, UK
Anti-rat IgG, HRP-linked Antibody	Cell Signaling Technology, UK

Table 2-16: Bacteria transformation/plasmid amplification/plasmid purification

Reagents	Company
Subcloning Efficiency DH5α^{TM} Competent Cells	Invitrogen, UK
SOC medium	Invitrogen, UK
Agar	Sigma Aldrich, UK
Ampicilin 1000x	Sigma Aldrich, UK
LB Broth (Luria-Bertani medium)	Sigma Aldrich, UK
Plasmid MiniPrep Kit	Qiagen, UK
Endotoxin-Free Plasmid Maxi Kit	Qiagen, UK
Isopropanol	Sigma Aldrich, UK
Ethanol	Sigma Aldrich, UK

3 EXPRESSION OF *mms6* IN HUMAN ADIPOSE DERIVED-MESENCHYMAL STEM CELLS

3.1 SUMMARY

A magnetosome gene, *mms6,* has been known for its important roles in controlling the size and the shape of the nanosized crystal to be specifically cubo-octahedral in magnetotactic bacteria (MTB) (Amemiya *et al.*, 2007). Previous study has shown that *mms6* gene can be expressed in mammalian cells, 9L glioblastoma tumour cells, using lipid-based transfection (Zhang *et al.*, 2014). Other MTB gene, *magA*, which is known to be involved in iron transport process in MTB, also can be expressed in human cell line, 293FT (Zurkiya *et al.*, 2008). Therefore, the main goal of this chapter was to demonstrate the *mms6* gene expression in human adipose derived-mesenchymal stem cells (AD-MSC). To reach this goal, I performed synthetic *mms6* gene molecular cloning and examined whether this gene can be introduced and expressed in AD-MSC using a non-viral transient transfection technique. The *mms6* gene expression in AD-MSC was determined at mRNA and protein level. Moreover, cell morphology and cell viability, essential parameters in transfection techniques, were also investigated in this study.

In order to introduce an MTB gene, *mms6*, a foreign gene into AD-MSC, a suitable gene construct and vector are fundamental. Even more important, the protein must be functional since the Mms6 protein has a major role in binding iron to form magnetic nanoparticles. For these reasons, a codon optimised *mms6* gene was used in the synthetic *mms6* gene construct. Codon optimisation is the term given to the synthetic creation of a gene sequence primarily aim to obtain the optimal codon usage patterns for a specific host organism to enhance expression (Patterson *et al.*, 2005). This was essential as mammalian expression of foreign genes such bacterial genes is often low (Narum *et al.*, 2001).

A Kozak sequence, which plays a major role in the initiation of translation process in mammalian expression, was also added to the *mms6* gene construct positioned upstream of the start codon of the *mms6* gene. In addition, a polyhistidine-tag (6x)

sequence was also added into the synthetic *mms6* gene construct as a protein expression marker. This optimised gene construct was named MAGISTER-02 (Mag02) and the sequence map can be seen in Figure 3-1. The gene was synthesized by GeneArt® Gene Synthesis service and cloned into a mammalian vector plasmid pcDNA3.1(+). The name Mag02 was used as a previous codon-optimised *mms6* (Mag01) was designed and already investigated in a previous study by Lisa Lungaro, former PhD student in the group.

As other primary cells, MSC are difficult to transfect (de Carvalho *et al.*, 2018). Hence, a suitable transfection technique is required for efficient mammalian expression. This study involves transient and stable transfection. Transiently transfected genetic materials can be lost by environmental factors and cell division. However, it is important to start with transient transfection and evaluate the gene expression before moving into stable transfection. Therefore, in this Chapter, a transient transfection technique using X-tremeGENE™ HP DNA (Roche), a non-lipid complex polymer, was chosen to introduce the synthetic *mms6* gene, Mag02, into AD-MSC. Following the transfection, the Mag02 expression in AD-MSC was determined using end-point PCR and western blotting.

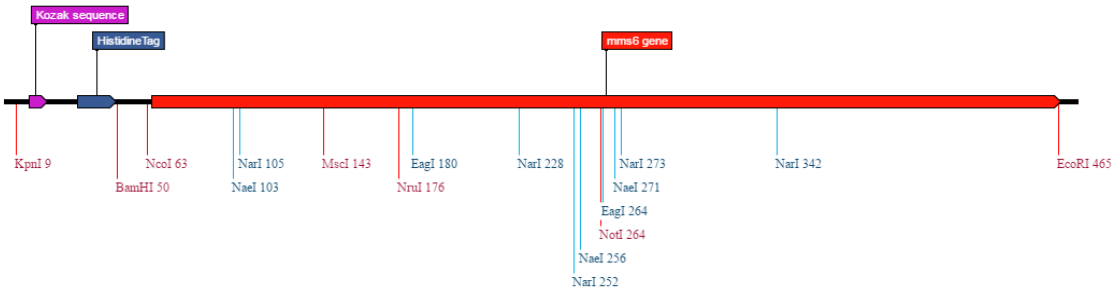

Figure 3-1: Gene construction map of Mag02 gene fragment*. The construct contains a synthetic codon optimized mms6 gene. It has polyhistidine-tag and Kozak sequence at the N terminus. The gene was cloned into a mammalian vector plasmid pcDNA3.1(+) at KpnI and EcoRi restriction site.*

3.2 AIMS

The aims of the experiments detailed in this chapter were:

1. To amplify the plasmid DNA containing Mag02 using molecular cloning techniques
2. To demonstrate expression of Mag02 mRNA in AD-MSC through end-point PCR experiments
3. To demonstrate *mms6* protein expression through western blot analysis
4. To investigate cell viability of AD-MSC following the *mms6* gene transient transfection

3.3 AMPLIFICATION OF PLASMID DNA CONTAINING MAG02

The use of high-quality plasmid DNA as DNA delivery vector that is free of proteins, RNA, and chemicals is crucial before starting the transfection procedure. In this study, the Mag02 DNA sequence was synthesized by GeneArt® Gene Synthesis service and had been cloned to pcDNA3.1 plasmid at KpnI and EcoRI restriction site. This particular plasmid was chosen as common mammalian vector. Once the plasmid had been amplified by bacterial transformation using DH5α competent *E. coli* cells, it was necessary to purify and analyse the plasmid yield and its DNA quality. Miniprep protocol and Maxiprep protocol, a standard commercial plasmid DNA Extraction kit via silica spin columns, were employed to purify the DNA plasmid containing Mag02 fragment.

Firstly, Miniprep was performed for rapid DNA plasmid isolation and to analyse the bacterial clones. This was an important step to determine whether or not the Mag02 plasmid can be amplified without mutation before conducting Maxiprep in order to obtain high quantity of plasmid DNA for the later transfection study. The DNA plasmid purified from Miniprep were digested using the restriction enzyme KpnI and EcoRI. The digestion products were then visualized via electrophoresis on 1.2% agarose gel. These steps were necessary so that I could quickly confirm that the Mag02 has been successfully amplified with a correct base pair length of 466 bp. Following the enzyme digestion, DNA sequencing analysis of the Mag02 gene sequence was also carried out to validate the successful of Mag02 DNA amplification.

Five samples of Miniprep purified plasmid from five different clones were analysed using KpnI and EcoRI restriction enzymes. As shown in Figure 3-2, all digested samples as indicated in lane 1, 3, 5, 7, 9 showed bands at around 500 bp, suggesting the presence of DNA fragment resulted from KpnI and EcoRI enzyme digestion. In contrast, the undigested control samples as indicated in lane 2, 4, 6, 8, and 10 did not show band. Therefore, this result confirmed that the digestion worked well and I was able to identify that all five clones of DH5α were carrying the Mag02 gene fragment. Moreover, all five samples showed DNA fragment with size around 500 bp of base pair length instead of 466 bp in correspondence to the original sequence. However, it

was possible that all of the sizes are correct but the DNA ladder and the DNA fragments may be running differently. This is thought to be due to the assumption that the amount of salts in the buffer of the DNA ladder and that of the samples loaded differ. Too much salt makes the sample run slower so fragments may look larger.

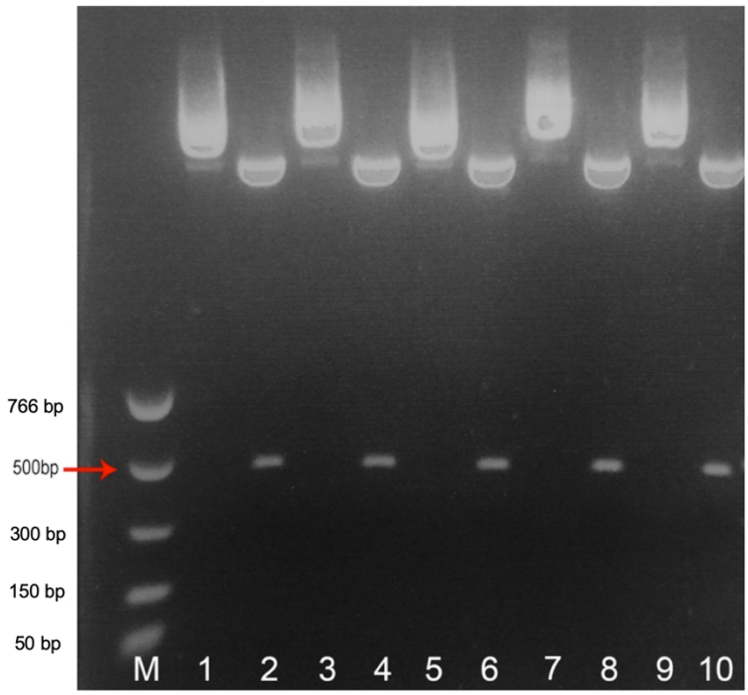

Figure 3-2: Restriction enzyme digestion analysis of plasmid DNA containing Mag02 obtained from Miniprep plasmid DNA extraction. *Agarose gel electrophoretograms demonstrating plasmid DNA containing Mag02 gene fragment successfully cut by KpnI and EcoRI restriction enzymes. Lane 2, 4, 6, 8, 10 = plasmid containing Mag02 gene fragment cut by KpnI and EcoRI) whereas Lane 1, 3, 5, 7, 9 = undigested plasmid as control.*

For closer inspection of the Mag02 fragment of the plasmid from the Miniprep, DNA sequencing of Mag02 was carried out. The sequencing results were then aligned to match the original sequence using the Basic Local Alignment Search Tool (BLAST). The DNA sequencing analysis of the plasmid, as shown in Figure 3-3 indicated that the sample sequence result (466 bases) was 100% identity (466/466) to the original sequences of Mag02 gene fragment. Therefore, these restriction enzyme digestion and DNA sequencing results confirmed the successful of Mag02 DNA amplification.

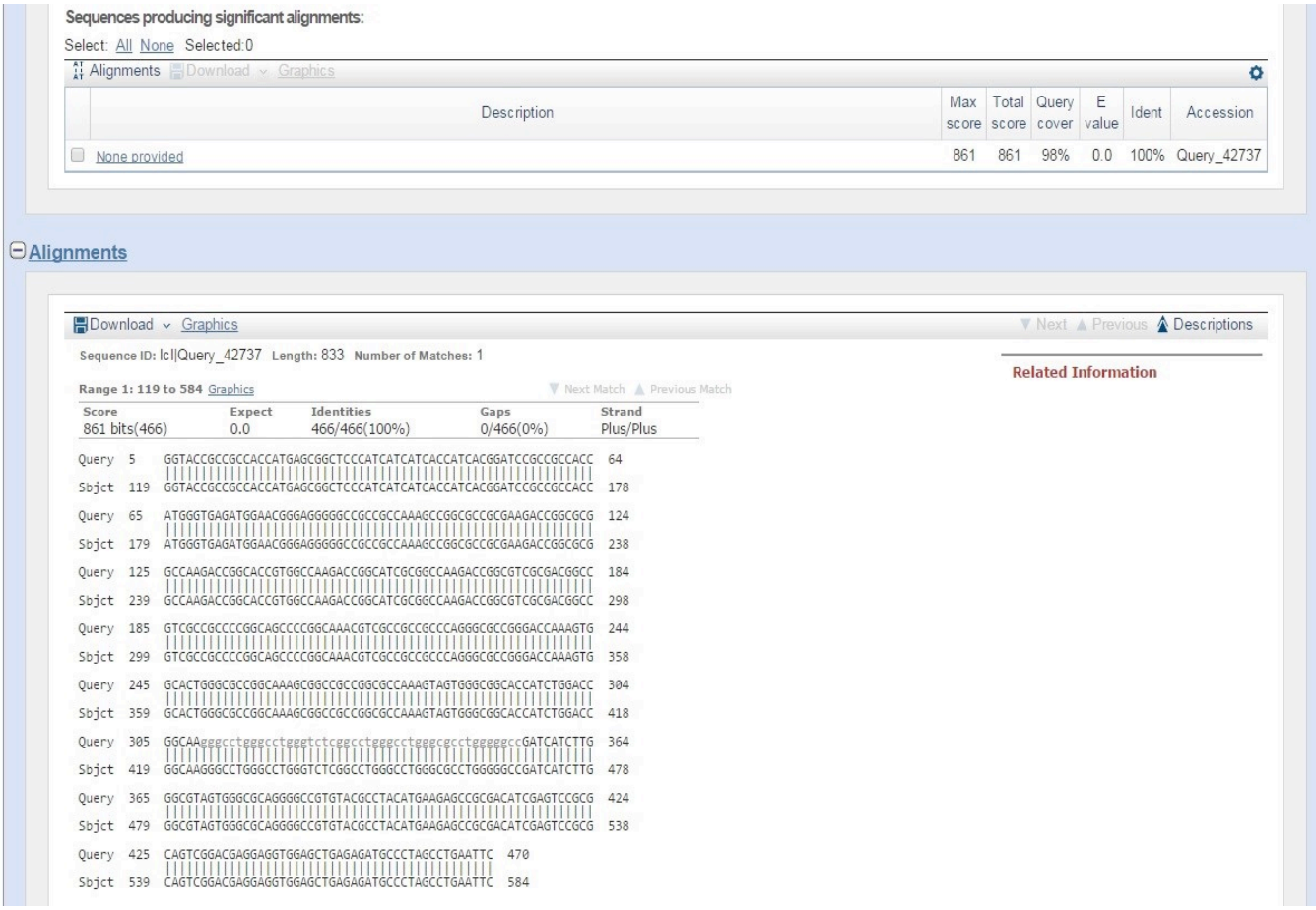

Figure 3-3: DNA sequencing analysis of plasmid DNA containing Mag02 obtained from Miniprep. *Detailed side by side alignment information for the DNA sequence result for sample (query) and known Mag02 gene sequence (subject). The sample sequence result (466 bases) was 100% identity (466/466) to the sequences of Mag02 gene fragment.*

After confirming the success of the Mag02 amplification using Miniprep, it was necessary to produce high-quantity of Mag02 DNA plasmid by performing Maxiprep. This was aimed to obtain a large stock of Mag02 DNA plasmid for later transfection experiments. Therefore, similar restriction enzyme digestion assay and DNA sequencing analysis were also carried out to analyse the purified plasmid DNA product from Maxiprep.

Two samples of Maxiprep purified plasmid from two different clones were analysed using KpnI and EcoRI restriction enzymes. As shown in Figure 3-2, the two digested samples as indicated in lane 1 and 3 showed DNA band at around 500 bp, suggesting

the presence of DNA fragment resulted from KpnI and EcoRI enzyme digestion. Whereas the undigested control samples as indicated in lane 1 and 4 did not show DNA band or digested DNA fragment. Therefore, this result confirmed that the Maxiprep purified plasmid contains Mag02 gene fragment.

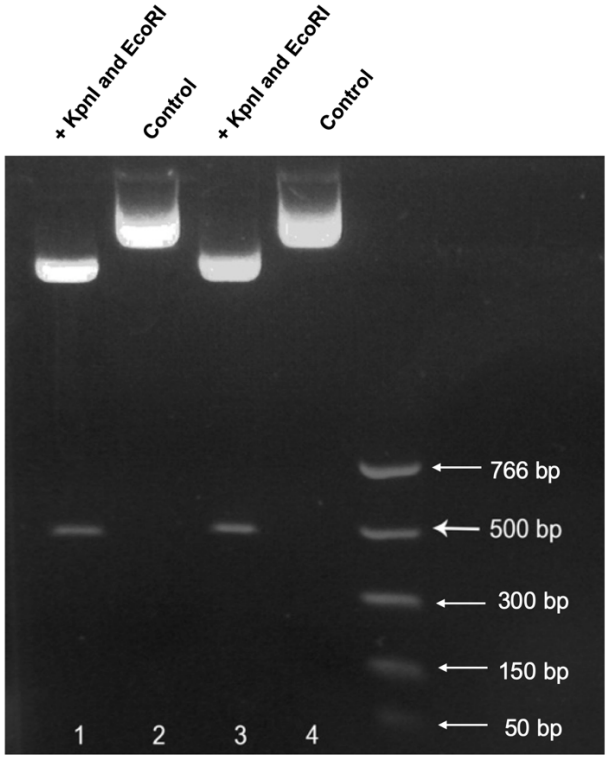

Figure 3-4: Restriction enzyme digestion analysis of plasmid DNA containing Mag02 obtained from Maxiprep. *Agarose gel electrophoretograms demonstrating plasmid DNA containing Mag02 gene fragment successfully cut by KpnI and EcoRI restriction enzymes. Lane 1 and 3 = plasmid containing Mag02 gene fragment cut by KpnI and EcoRI) whereas Lane 3 and 4 = undigested plasmid as control.*

The expected size of the DNA fragment from restriction enzyme digestion was 466 bp instead of ~500 bp as indicated in agarose gel electrophoretograms analysis. Therefore, DNA sequencing was conducted. BLAST analysis of DNA sequencing result, as presented in Figure 3-4, indicated that the sample sequence result (466 bases) was 100% identity (466/466) to the original sequences of Mag02 gene fragment. Overall, these results confirmed that the plasmid containing Mag02 gene fragment was successfully amplified and can be used for the later transfection experiments.

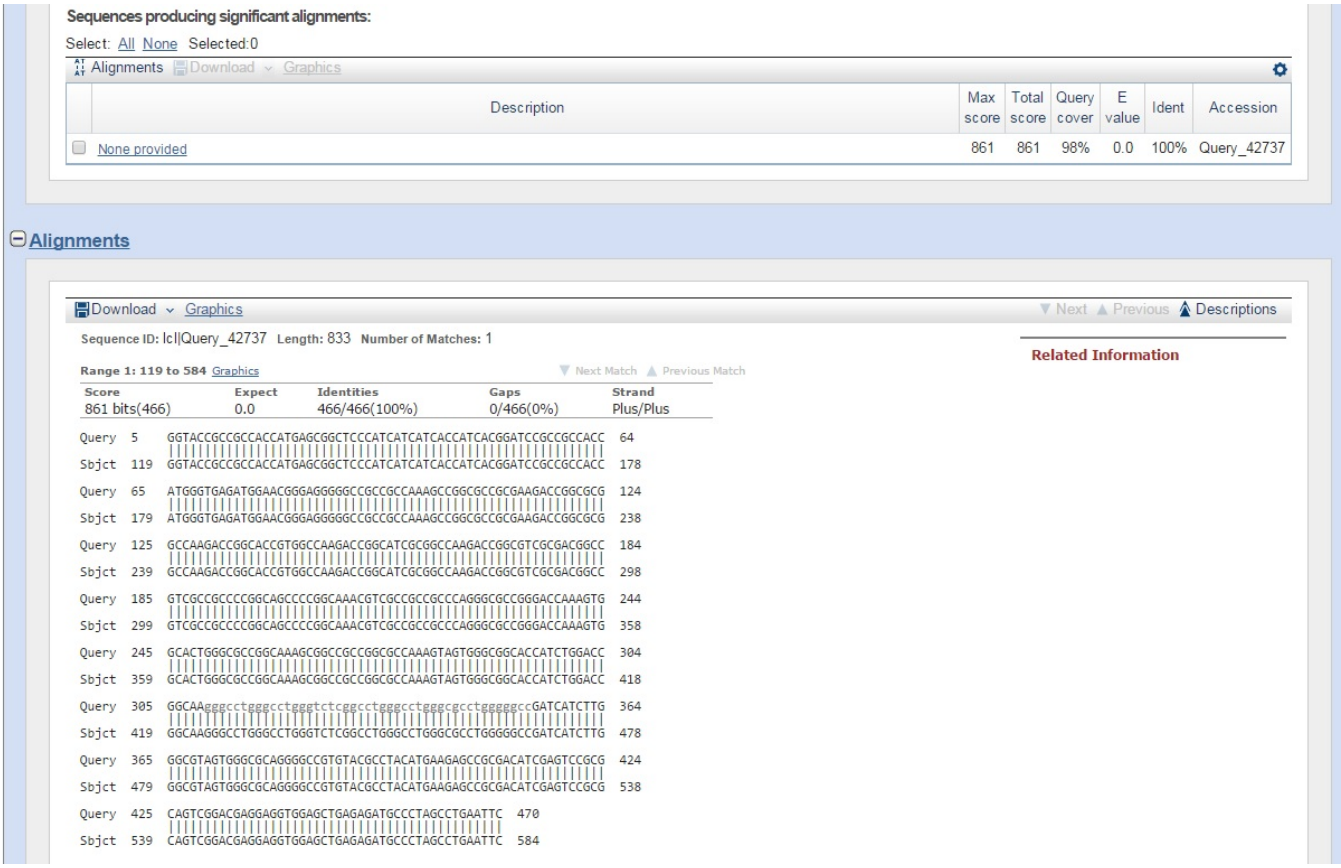

Figure 3-5: DNA sequencing analysis of plasmid DNA containing Mag02 obtained from Maxiprep. *Detailed side by side alignment information for the DNA sequence result for sample (query) and known Mag02 gene sequence (subject). The sample sequence result (466 bases) was 100% identity (466/466) to the sequences of Mag02 gene fragment.*

3.4 EXPRESSION OF MAG02 mRNA IN AD-MSC

In order to evaluate the *mms6* gene expression on AD-MSC, cells were transfected with Mag02 plasmid. For this, cells were seeded at 1 x 10^5 cells per well in 24-well plates one day prior to transfection. On the day of transfection, OptiMEM media was prepared in tubes at 100 µl per tube. DNA plasmid (3 µg) was put into the OptiMEM media, then 9 µl (1:3 ratio to the DNA concentration) of transfection reagent was added to the mixture. The complexes were incubated for 20 minutes, then gently added into the cells. Each sample transfection was performed in triplicate. Cells transfected with transfection reagent without plasmid were used as negative control. The cells were

then incubated at 37°C with 5% CO_2. Cells were cultured in a FeQ doped medium (34 µM) for 10 days. Non-transfected AD-MSC cultured for 10 days in similar FeQ doped medium (34 µM) were considered as a negative control. Ten days after the transfection, RNA was extracted from transfected AD-MSC, and cDNA was synthesized. Thereafter, the Mag02 mRNA expression in AD-MSC was determined by end-point PCR. To test this, a set of internal primers to obtain an amplicons length of 142 bp were designed using *PRIMER3* software:

Forward : 5' GGA CCA AAG TGG CAC TGG 3'
Reverse : 5' CCC ACT ACG CCC AAG ATG AT 3'

Glyceraldehyde 3-phosphate dehydrogenase (GAPDH) gene, a popular housekeeping standard gene in expression studies, was used as an internal control.

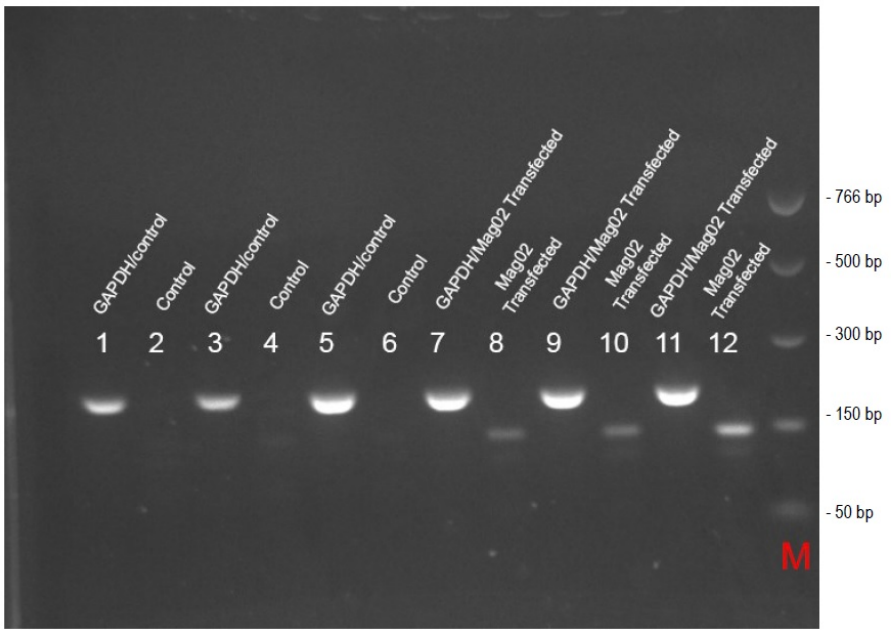

Figure 3-6: Mag02 mRNA expression in AD-MSC determined by end-point PCR. *A set of internal primers to obtain an amplicons length of 142 was used to determine Mag02 mRNA expression in AD-MSC. GAPDH was used as internal control. Mag02 mRNA expression was detected in AD-MSC at 10 days after transfection, as indicated in lane 8, 10, and 12 (tripilicate). Lane 1-6 = Untransfected cells as control; Lane 7-12 = AD-MSC transfected with Mag02 plasmid. N = 3.*

As shown in Figure 3-6, the end point-PCR result showed bands in all three samples of AD-MSC transfected with Mag02 plasmid, as indicated in lane 8, 10 and 12. All the three bands sat around a little less than 150 bp marker on the ladder, suggesting the correct expected size of 142 bp DNA. As for negative control, band was absence in untransfected cells, as shown in lane 2, 4, and 6. Whereas bands of GAPDH internal control was shown consistently in all samples both transfected and untransfected cells, confirming the validity of the end-point PCR experiment. Therefore, these results confirmed Mag02 mRNA expression in AD-MSC at 10 days after transfection.

3.5 EXPRESSION OF MAG02 PROTEIN IN AD-MSC

After confirming the *mms6* expression at transcriptional level as indicated by Mag02 mRNA in AD-MSC following the transfection, it was necessary to determine whether translation was occurring leading to production of Mms6 protein by the transfected cells. For this, AD-MSC were transfected with Mag02 plasmid using X-tremeGENE™ HP DNA transfection reagent. Briefly, cells were seeded at 1 x 10^5 cells per well in 24-well plates one day prior to transfection. On the day of transfection, OptiMEM media was prepared in tubes at 100 µl per tube. DNA plasmid (3 µg) was put into the OptiMEM media, then 9 µl (1:3 ratio to the DNA concentration) of transfection reagent was added to the mixture. The complexes were incubated for 20 minutes, then gently added into the cells. The cells were then incubated at 37°C with 5% CO_2. Two days after the transfection, total protein was extracted from the cells, then the Mag02 protein expression was evaluated using Western blot assay. Since the Mms6 antibody is not available commercially for the western blot assay, polyhistidine tag antibody was used to detect his-tag Mms6 protein expression in AD-MSC. Non-transfected AD-MSC were considered as negative control, while ß-actin was used as internal control in this experiment.

As shown in Figure 3-7, no his-tag protein was observed on both Mag-02 transfected AD-MSC and control cells at 2 days after transfection. The expected size of his-tag protein was 35.71 kDA protein. The internal control, ß-actin, was shown in both transfected and control cells, showing the expected size of 42 kDA protein. This result

suggested that Mag02, or his-tag Mms6 protein expression in particular, was absence after the transfection, suggesting AD-MSC were not able to express Mms6 protein. Another possibility could be a low transfection efficiency at the level where the Mms6 protein amount was too low to be detected by Western blot technique.

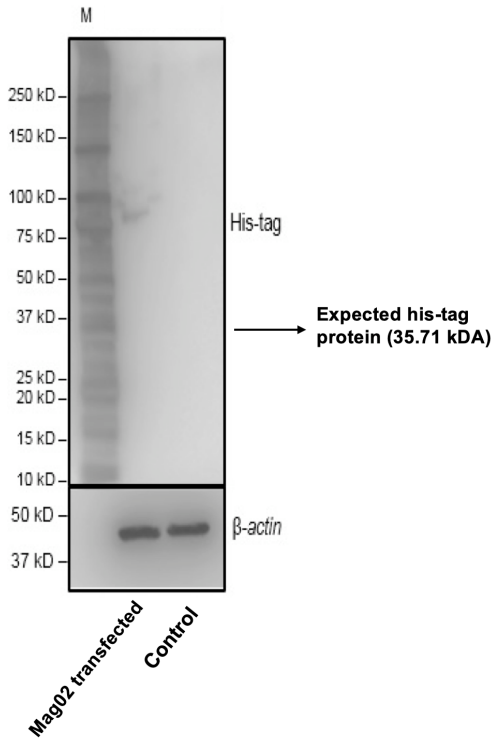

Figure 3-7: Mag02 protein expression in AD-MSC. *Image of western bloting assay indicating no his-tag protein with the expected size of 35.71 kDA was detected in Mag02-transfected AD-MSC at 2 days after initial transfection. β-actin serves as internal control. N = 3.*

3.6 EFFECT OF MAG02 GENE TRANSFECTION ON CELL VIABILITY AND MORPHOLOGY OF AD-MSC

The ideal method for an optimal transfection technique should have high transfection efficiency, low cell toxicity, minimal effects on normal physiology, and be easy to use and reproducible. In this section, cell toxicity and morphology of the AD-MSC were evaluated following the transfection with Mag02 plasmid using using X-

tremeGENE™ HP DNA Transfection reagent. Cell viability assay was determined at 1, 3 and 5 days after transfection using AlamarBlue assay.

As shown in Figure 3-8, AlamarBlue fluorescence intensity average values were 7863±97.07 for transfected cells, and 8578±25.48 for control at day 1 after transfection, showing 8.33% decreased of cell viability on the transfected cells. At day 3, AlamarBlue fluorescence intensity average values were 7820±94.16 for transfected cells, and 11128±67.42 for control. Whereas at day 5, AlamarBlue fluorescence intensity average values were 8550±98.33 for transfected cells, and 11762±56 for control. This result demonstrated that the cell viability difference between transfected and control group become greater over time after transfection as the fluorescence intensity average value of transfected cells were 29.72% and 27.31% significantly less compared to control group at 3 days and 5 days after transfection, respectively .

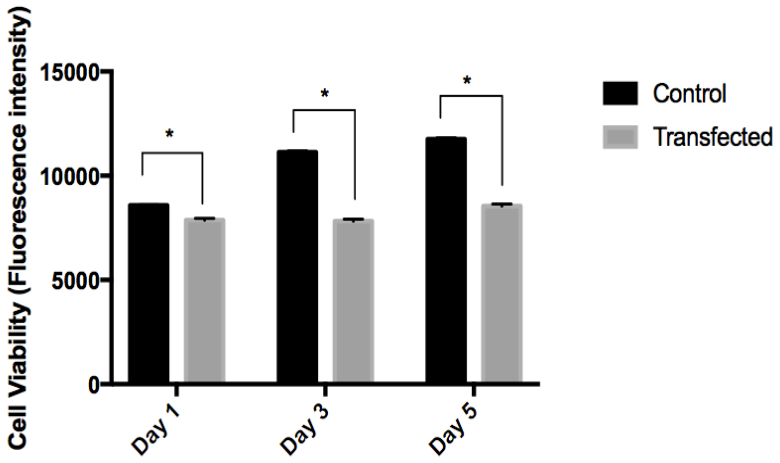

Figure 3-8: Cell viability analysis of AD-MSC transfected with Mag02 plasmid.

*AlamarBlue data showing average of fluorescence intensity of Mag-02 transfected AD-MSC compared to untransfected cells. Significant decreased of cell viability was observed at 1, 3, and 5 days after transfection using X-tremeGENE™ HP DNA transfection reagent. *P<0.0001. Values are presented as mean ± SD. N=3*

The cell morphology was also observed up to 10 days after transfection and imaged by light microscopy. As shown in Figure 3-9, cells with either a triangular shape, star-

like cell shape or spindle-shaped morphology were observed in both transfected and control cells. No observable morphological differences between two groups, indicating the transfection of AD-MSC using X-tremeGENE™ HP DNA transfection reagent and the expression of Mag02 mRNA have no effect on AD-MSC morphology at 10 days after transfection.

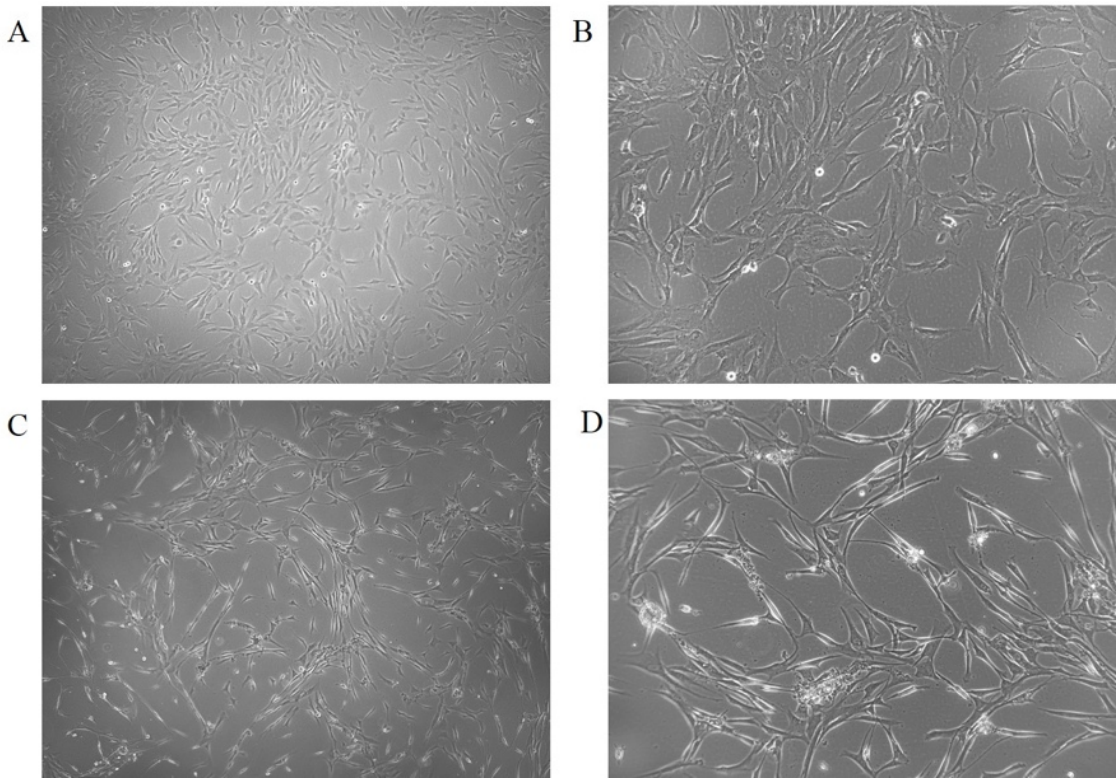

Figure 3-9: Representative image of AD-MSC cell mophology at 10 days after transfection with Mag02. *Light microscopy image showing either triangular or spindle-shaped morphology of cells on both transfected and control cells. No observable morphological differences between two groups, indicating the transfection of AD-MSC using X-tremeGENE™ HP DNA transfection reagent does not have effect on AD-MSC cell morphology. A) Untransfected AD-MSC (5x magnification); B) Untransfected AD-MSC (10X magnification); C) Mag02-transfected AD-MSC (5x magnification); D) Mag02-transfected AD-MSC (10x magnification). N = 3.*

3.7 DISCUSSION

The aims of this chapter were as follows:

1. To amplify the plasmid DNA containing Mag02 gene fragment using molecular cloning technique
2. To demonstrate expression of Mag02 mRNA in AD-MSC through end-point PCR experiments.
3. To demonstrate *mms6* protein expression through western blotting analysis
4. To investigate cell viability and morphology of AD-MSC following the *mms6* gene transient transfection

My first aim was successful in that I was able to amplify the Mag02 plasmid using standard molecular techniques. It was important to amplify and obtain high-quality plasmid DNA without any mutation or gene changes on the *mms6* gene sequence before starting the transfection procedure. The enzyme restriction digestion and DNA sequencing result confirmed that the Mag02 plasmid was succesfully amplified. The DNA band indicated that Mag02 fragment from all samples have around 500 bp of base pair length instead of 466 bp in correspondence to the original sequence, the DNA sequencing result demonstrated that the sample have 100% identity to the original sequence, which confirms the successful of Mag02 DNA amplification.

The end-point PCR result answers the second aim of this chapter as it demonstrates that MTB genes, *mms6,* can be expressed in AD-MSC. This result was in aggrement with the result from previous work by Elfick *et al.* (2017) using another MTB gene, *mmsF* and a different codon optimised *mms6* gene (Mag01) (Elfick *et al.*, 2017). The study demonstrated *mms6* mRNA expression in Mag01-transfected human bone marrow-derived MSC cells at 10, 15 and 21 days post-transfection using similar transfection reagent as in my study. Sanger DNA sequencing of the PCR transcripts of the *mms6* gene at 10, 15 and 21 days post-transfection also showed 100% identity with the inserted gene (Elfick et al., 2017). However, despite validating *mms6* gene

expression at the RNA level, that study did not provide evidence of Mms6 protein expression although intracellular nanoparticles were identified by TEM.

Considering the importance of Mms6 protein in binding the iron to form magnetic nanoparticles (Wang *et al.*, 2012; Rawlings *et al.*, 2016), it was necessarry to confirm Mms6 protein expression through Western blotting assay. Unfortunately, despite the successful *mms6* mRNA expression up to 10 days after transfection, the Western blot assay failed to identify expression of a His-tag Mms6 protein at 2 days after transfection. There are a few possible explanations for this: it could be due to low transfection efficiency, or it could be the Mms6 protein expression being at low level which can not detected by Western blotting. It may also be possible that *mms6* mRNA, for unknown reason, is not translated into functional Mms6 protein by AD-MSC or that the Mms6 protein might be directly degraded by AD-MSC cell system.

Furthermore, there was also a high likelihood that the bands in end-point PCR result reflect the plasmid DNA as contaminant, which potentially resulting in a false positive result. The plasmid concentration used in the transfection was 3 µg, which is a lot and could contaminate the RNA isolation and end-point PCR assays. To negate this issue, DNAse should be used during RNA isolation process to degrade plasmid DNA contaminant (Añez-Lingerfelt *et al.*, 2009). Negative control should be also performed in the end-point PCR experiments, such as: 1) A no template control omits any DNA or RNA template from a reaction, and serves as a general control for extraneous nucleic acid contamination, and 2) A no reverse transcriptase control or minus reverse transcriptase control involves carrying out the reverse transcription step of a PCR experiment in the absence of reverse transcriptase. This control assesses the amount of DNA contamination present in an RNA preparation.

Zhang *et al* (2014) investigated the possibility of using *mms6* as an MR reporter gene. They designed a transgenic mammalian cell line, gliosarcoma cell line, that stably expresses *mms6* by using Lipofectamine 2000® transfection reagent followed by Zeocin antibiotic selection (Zhang *et al.*, 2014). In similar way to my study, their *mms6* gene construct also has polyhistidine epitope tag to be used for verifying the expression of Mms6 protein. The study was able to demonstrate His-tag Mms6 protein being

expressed as well as the ability of the transfected cells to produce intrinsic magnetic nanoparticle. However, in my study, unlike cancer cell line or other primary cell types, MSC are known difficult cells to transfect (Baek *et al*., 2016). Common non-viral transfection methods used for mammalian cells, such as a cationic lipid-based reagent transfection system, still generally show low-to-moderate (less than 15%) gene transfer efficiency in transfecting MSC (Wang *et al*., 2015). The absence of Mms6 protein expression in this chapter is likely to be related to this.

Zaragosi and coworkers (2007) reported that only fewer than 5% of AD-MSC were successfully transfected using calcium phosphate precipitation and lipofectants transfection reagent (i.e., Lipofectamine 2000® and FuGENE transfection reagents) (Zaragosi *et al.*, 2006). Similarly, previous study using human bone marrow-derived MSC (BM-MSC) also demonstrate poor transfection efficiency of 4.4% with FuGENE6 and 6.8% for DOTAP, two commonly used lipid-based non-viral transfection reagents (Aluigi *et al.*, 2006). Unsuccessful attempt to generate AD-MSC expressing Mms6 protein in this chapter was thought to be related to the low transfection efficiency using the X-tremeGENE™ DNA Transfection Reagent, thus it was necessary to investigate a more effective transfection approach that suits AD-MSC which will be discussed in the next chapter.

Since the *mms6* gene was clearly expressed at transcriptional level and not proven to be expressed at the translational level, it was speculated that the codon optimised *mms6* of Mag02 gene construct may be not be optimal for mammalian cell expression. To further investigate these possibilities, different codon optimised of *mms6* needs to be considered. Therefore, further attempts of using different technique of transfection, different codon optimised, and different synthetic *mmm6* gene construct using double protein-tag marker His-GFP-tag are presented in Chapter 4.

4 EXPRESSION OF MMS6 PROTEIN IN AD-MSC AND IMPROVING AD-MSC TRANSFECTION STRATEGIES.

4.1 SUMMARY

In this chapter, the focus of the study was to investigate the expression of different codon optimised *mms6* in AD-MSC. It was hypothesized that certain codon optimisation or transfection approaches might be more suitable and efficient for expressing *mms6* in AD-MSC.

In Chapter 3, transfected AD-MSC appeared to show no Mms6 protein expression, despite *mms6* mRNA being detected up to 10 days after transfection using X-tremeGENE™ Transfection Reagent. Since AD-MSC are recognised as a difficult to transfect cell type, a likely reason is low transfection efficiency from using a chemical-based transfection reagent. Therefore, several non-viral based transfection approaches both chemical-based and physical-based, were further investigated in an attempt to express Mms6 protein in AD-MSC.

As discussed in Chapter 3, the absence of Mms6 protein expression could also be due to the codon optimisation of *mms6* gene (Mag02) which may not allow translation in the mammalian cells. Hence, different codon-optimised *mms6* were designed and investigated: MagWT, Mag01, Mag02 and Mag03.

MagWT contains the original sequence *mms6* gene of *M. magneticum* strain AMB-1 *mms6* gene without codon optimisation. Mag01 was kindly designed by Dr. Greg Kudla (Group leader of RNA synthetic biology group, MRC Institute of Genetics & Molecular Medicine, University of Edinburgh). Mag02 was designed by Dr. Chris Boyd (Group leader of gene therapy for cystic fibrosis research group, MRC Institute of Genetics & Molecular Medicine, University of Edinburgh). Mag03 was designed by GeneArt® Gene Synthesis service (Thermo Fisher Scientific).

Each of these constructs also have a polyhistidine-tag at the N terminus and a GFP-tag at the C terminus of the *mms6* DNA fragment. The use of these double marker tags

was important for investigating Mms6 protein expression due to the non-availability of a Mms6 antibody. Each of this construct was cloned into pcDNA 3.1 plasmid at at NheI/HindIII restriction site. The details of these codon optimised *mms6* gene constructs can be seen in Chapter 2.

End-point PCR, flow cytometry, western blot and GFP imaging analysis were carried out to determine the expression of both *mms6* mRNA and Mms6 protein. Alamar Blue cell viability assays were used to determine the effect of the transfection on AD-MSC cell viability. In addition, a lentiviral vector carrying the *mms6* gene was also designed in order to perform AD-MSC viral transduction. This technique was used to achieve stable expression of *mms6* in AD-MSC owing to the integration of the virus DNA into the host genome. This may be important for increasing Mms6 protein production which should improve the internal synthesis of magnetic nanoparticles in AD-MSC.

4.2 AIMS

The aims of the experiments detailed in this chapter were:

1. To demonstrate the mRNA expression of different codon optimised *mms6* in AD-MSC
2. To demonstrate the protein expression of different codon optimised *mms6* in AD-MSC
3. To improve the transfection approach of AD-MSC for transient Mms6 protein expression using nonviral-based transfection.
4. To develop AD-MSC stably expressing *mms6* using Lentiviral transduction.

4.3 EXPRESSION OF DIFFERENT CODON OPTIMISED *mms6* IN AD-MSC

End-point PCR method was used to investigate the *mms6* gene expression in AD-MSC. For this, cells were transfected with each of MAGISTER plasmids using X-tremeGENE™ Transfection Reagent. Both transfected cells and non-transfected cells as a control were cultured in a FeQ doped medium (34 μM) for 10, 15, and 21 days. Following the incubation, RNA of the cells from each time point was extracted. Thereafter, cDNA was obtained by reverse transcription, and was used for end-point PCR.

A set of internal primer pairs for each of the MAGISTER genes were designed using *Primer3* software. The amplicon lengths of each primer were the following: 210 bp, 229 bp, 185 bp and 155 bp for MagWT, Mag01, Mag02, and Mag03, respectively, as described in **Error! Reference source not found.** in Chapter 2. Glyceraldehyde 3-phosphate dehydrogenase (GAPDH) primer was used as an internal control. The experiment was performed for three times.

As shown in the Figure 4-1, the bands of *mms6* under (+) marks were present in all MAGISTER-transfected AD-MSC at 10, 15 and 21 days after transfection. These bands were found to be consistent for each sample with the expected size which were 210 bp for MagWT, 167 bp for Mag01, 185 bp for Mag02 and 155 bp for Mag03, respectively.

As an internal control, the GAPDH bands under (-) marks were also present in all MAGISTER-transfected AD-MSC at 10, 15 and 21 days after transfection. These bands were found to be consistent for all samples with the expected size of 210 bp. Moreover, all negative controls under (#) marks show no bands, confirming the validation of the experiment. As an overall result, the end-point PCR demonstrates the expression of *mms6* mRNA in AD-MSC up to 21 days following transfection with each of MAGISTER plasmid using X-tremeGENE™ DNA Transfection Reagent.

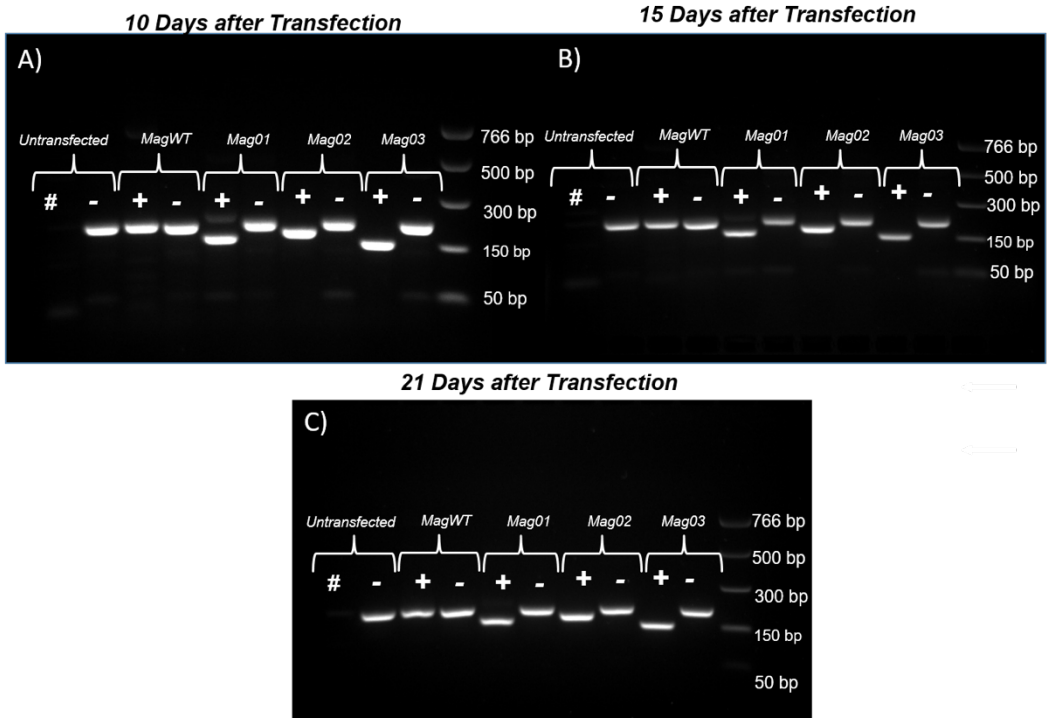

Figure 4-1: Image for end point-PCR reaction for different codon optimised mms6 gene expression in AD-MSC at 10 days (A), 15 days (B) and 21 days (C) after transfection with X-tremeGENE™ Transfection Reagent. *The end-point PCR demonstrates the expression of mms6 mRNA in AD-MSC up to 21 days after transfection using X-tremeGENE™ DNA Transfection Reagent. Panel A = 10 days after transfection; Panel B = 15 days after transfection; Panel C = 21 days after transfection. (+) = MAGISTER-transfected cells; (-) = GAPDH internal control for MAGISTER-transfected cells; (#) = negative control/untransfected cells. 766 bp NEB marker used in the gel electrophoresis. N=3.*

4.4 MMS6 PROTEIN IS NOT EXPRESSED IN AD-MSC, BUT EXPRESSED IN HEK293T CELLS.

The expression of Mms6 protein in AD-MSC was assessed using Western blot and GFP imaging. For this, AD-MSC were transfected with each of MAGISTER plasmids using X-tremeGENE™ Transfection Reagent. A common easy to transfect cell line, HEK293T cells, were also used and transfected with MAGISTER plasmids using the same method. The cells were then incubated in a growth medium for 2 days.

For the Western blot assay, 20 µg of protein lysates of cells extracted at 2 days after transfection were used. The non-transfected cells of both AD-MSC and HEK293T cells were considered as a negative control. Protein lysates were run on a Western blot with antibodies specific to His(6x)-tag protein and ß-actin as loading control. For the GFP imaging, the cells were fixed at 2 days after transfection, then observed under fluorescence microscope. Cells transfected with pmaxGFP plasmid were used as a positive control. Nuclei were counterstained using DAPI. The experiment was performed at least three times.

As shown in the Figure 4-2, no protein bands were detected in AD-MSC transfected cells after the transfection with all the four MAGISTER plasmids. However, four bands of His-tag protein were found around the expected size of interest (44 KDa) in HEK293T transfected cells. The His-tag protein was also absent in the negative controls of both AD-MSC and HEK293T cells, while ß-actin proteins with the expected size (42 KDa) were consistently expressed in all samples, confirming the validation of the experiment. Overall, this result demonstrates Hig-tag Mms6 protein expression in each of MAG-transfected HEK293T cells, but absence in MAG-transfected AD-MSC.

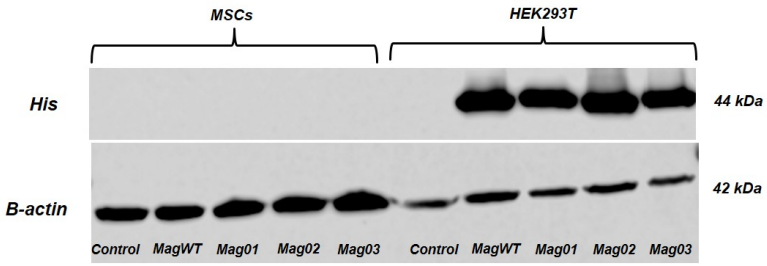

Figure 4-2: Western blot showing His-tag Mms6 protein expression in HEK293T cells at 2 days after transfection with X-tremeGENE™ Transfection Reagent. *Hig-tag Mms6 protein expression was absence in all four MAG-transfected AD-MSC. Blots probed for His-tag protein and β-actin as a loading control. N = 3.*

In agreement with the Western blot result, Figure 4-3 shows that HEK293T cells transfected with each of MAGISTER plasmids were expressing green fluorescence signal which confirmed the expression of GFP-tag Mms6 protein. The GFP expression

was also found in the positive control, but absence in the negative control, confirming the validation of the experiment.

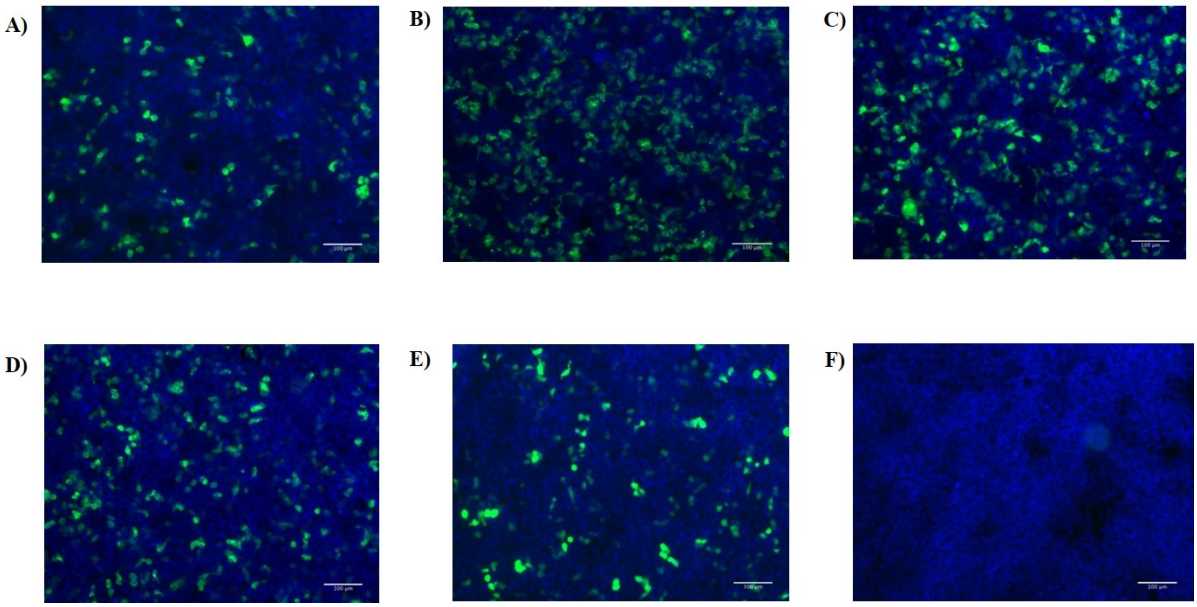

Figure 4-3: Image for GFP imaging analysis for GFP-tag Mms6 protein expression in HEK293T cells at 2 days after transfection with X-tremeGENE™ Transfection Reagent. *A = MagWT-transfected HEK293T cells; B = Mag01-transfected HEK293T cells; C = Mag02-transfected HEK293T cells; D = Mag03-transfected HEK293T cells; E = pmaxGFP-transfected HEK293T cells /positive control; F = control/untransfected cells. Scale bar = 100 µm. N = 3.*

These results confirm that both non-codon optimised *mms6* gene (MagWT) and codon optimised *mms6* gene (Mag01, Mag02 and Mag03) can be expressed in mammalian cells such as HEK293T cells. Unfortunately, this result also confirmed the absence of both His-GFP tag Mms6 protein, either non-codon optimised *mms6* or codon optimised *mms6,* in transfected AD-MSC. Therefore, this may suggest that the use of X-tremeGENE™ Transfection Reagent might not be sufficient to transfect AD-MSC for the Mms6 protein expression.

4.5 NUCLEOFECTION IMPROVES THE EFFICIENCY OF AD-MSC TRANSFECTION.

After having had difficulties in expressing the Mms6 protein in AD-MSC, it was necessary to test other nonviral-based transfection approaches in order to ascertain whether this approach could allow a higher transfection efficiency. In general, the nonviral-based transfection approach can be classified into chemical and physical transfection methods. For this, common chemical-based transfection reagent such as FugeneHD®, Lipofectamine 3000® and X-tremeGENE™ HP DNA Transfection Reagent were used. In additio, nucleofection, a physical-based transfection method using Human Mesenchymal Stem Cell Amaxa™ Nucleofection kit was also performed. The transfection efficiency was measured using Flow cytometry to analyse the percentage of cells positively expressing GFP from each of transfection approaches.

For the three chemical-based transfections, AD-MSC were plated into 24-well plates a day before transfection. Thereafter, 3µg of Mag01 plasmid was used to transfect the cells in the following day. For the nucleofection method, AD-MSC were collected from cell culture and directly transfected using the Amaxa™ Nucleofection kit. All of these transfections were undertaken on the same day. The transfected cells were then incubated at 37^{o}C in 5% CO_2 incubator for 2 days. The cells were then collected and analysed by Flow cytometry. Untransfected cells from each group was used as a negative control. The experiment was repeated twice.

As shown in the Table 4-1, the Flow cytometry result indicated that the percentage of GFP-positive cells were 59.6±1.9 %, 6.6±0.6 %, 15.5±3.9%, and 2.6±0.2% for Mag01-transfected AD-MSC with Amaxa™ Nucleofection, Lipofectamine 3000®, X-tremeGENE™ HP DNA, and FugeneHD® Transfection reagent, respectively. It was observed that the use of Amaxa™ Nucleofection resulted in the highest percentage of AD-MSC positively expressing GFP-tag Mms6 protein with value of 59.6±1.9 %. This number was 3.8 times higher than the number of GFP positive cells from Mag01-transfected cells using X-tremeGENE™ transfection reagent which was only 15.5±3.9%. Compare to lipid-based transfection, Nuclofection techniques was 8.9

times more efficient than Lipofectamine 3000® in transfecting AD-MSC as Lipofectamine 3000® only generates 6.6±0.6% of GFP positive cells. The lowest transfection efficiency was 2.6±0.2% from Mag01-transfected AD-MSC using FugeneHD® Transfection Reagent, which was 22 times less efficient compared to Amaxa™ Nucleofection. Overall, Nucleofection technique improves the efficiency of AD-MSC transfection.

Table 4-1: Percentage of GFP-positive cells after Mag01 transfection of AD-MSC using different transfection reagent.

Method	Percentage of GFP-positive cells
Amaxa™ Nucleofection	59.6±1.9%
Lipofectamine 3000®	6.6±0.6%
X-tremeGENE™ HP DNA	15.5±3.9%
FugeneHD®	2.6±0.2%

4.6 MMS6 PROTEIN IS EXPRESSED IN AD-MSC AFTER NUCLEOFECTION.

Following the above observations that transfection efficiency of AD-MSC was improved using Nucleofection, it was necessary to investigate Mms6 protein expression in AD-MSC after Nucleofection with each of MAGISTER plasmids to identify which, if any, resulted in maximal protein production. Flow cytometry, GFP imaging and Western blotting were used to assess Mms6 protein expression.

For the Flow cytometry and GFP imaging, AD-MSC were transfected with each of the MAGISTER plasmid using Amaxa™ Nucleofection kit. As a positive control, AD-MSC were transfected with pMax GFP plasmid. Untransfected cells were used as negative control. After 2 days of incubation, cells were either collected for Flow cytometry analysis or fixed for GFP imaging. Each experiment was repeated three times.

For the Western blot, AD-MSC were transfected with each of the MAGISTER plasmid using Amaxa™ Nucleofection kit. After 2 days of incubation, 20 µg of protein lysates from each sample were used for the Western blot assay. The non-transfected cells of both AD-MSC were considered as a negative control, while ß-actin was used as an internal control. The experiment was repeated three times.

As shown in the Figure 4-4, the Flow cytometry result shows that around 45–55% of AD-MSC from each group of MAG-trasfected AD-MSC were expressing GFP-tag Mms6 protein after the Nucleofection. The percentage of cells expressing GFP were 47.3±4.1%, 49.4±3.5%, 53.9±1.2%, and 47.3±3.7% for cells nucleofected with MagWT, Mag01, Mag02 and Mag03, respectively. The percentage of GFP positive cells which transfected with pmaxGFP plasmid was 87.9±2.9%, which was significantly higher than cells nucleofected with MAGISTER plasmids. Overall, this result confirmed the previous result that nucleofection technique improves the efficiency of AD-MSC transfection. Moreover, all of transfected AD-MSC showed GFP-tag Mms6 protein expression in all samples which was the ultimate goal of the experiment.

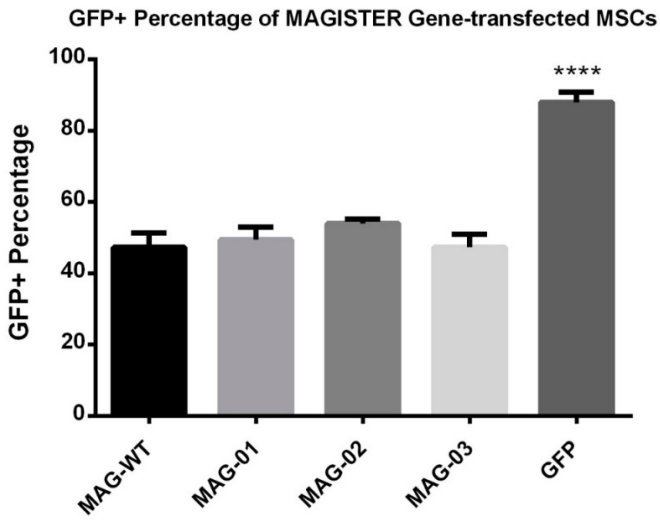

Figure 4-4: Flow cytometry analysis of positive MAGISTER-transfected AD-MSC expressing GFP. *No statistical difference in percentage of GFP positive MAGISTER-transfected AD-MSC cell in all samples but pmaxGFP-transfected AD-MSC. Values are presented as mean ± SD from one independent experiment in triplicates. ****p<0.0001 from all.*

Figure 4-5 shows the results for GFP imaging assay. Cells expressing green fluorescence were found in nucleofected-AD-MSC with each of MAGISTER plasmids and pmaxGFP plasmid. This result agrees with the previous Flow cytometry result, confirming the successful of Mms6 protein expression in AD-MSC using nucleofection technique.

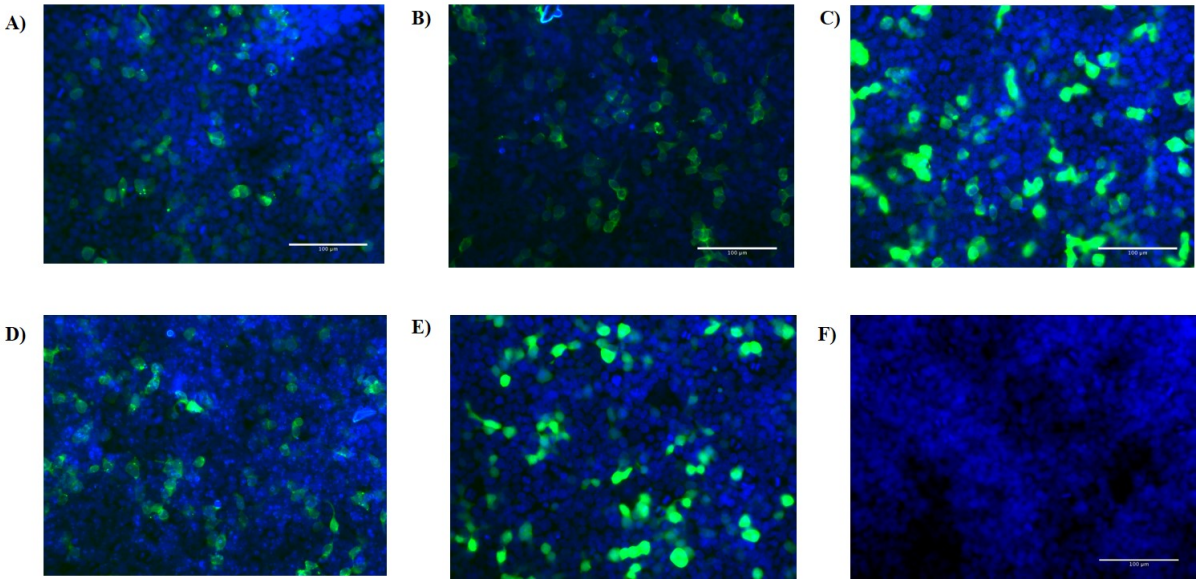

Figure 4-5: Image for GFP imaging analysis for GFP-tag Mms6 protein expression in AD-MSC at 2 days after nucleofection. *All MAG-transfected AD-MSC samples successfully expressing GFP-tag Mms6 protein green following nucleofection.. A = MagWT-transfected AD-MSC; B = Mag01-transfected AD-MSC; C = Mag02-transfected AD-MSC; D = Mag03-transfected AD-MSC; E = pmaxGFP-transfected AD-MSC /positive control; F = control/untransfected AD-MSC. Scale bar = 100 µm. N= 3*

Further experiment also confirmed the Mms6 protein expression in AD-MSC. As shown in **Figure 4-6**A, Westen blot result shows His-tag protein bands were identified around the expected size of interest (44 KDa) in each of MAG-transfected AD-MSC sample. The His-tag protein was absent in the negative controls, while ß-actin protein bands with the expected size (42 KDa) were shown in all samples. This result, finally, confirmed the expression of His-GFP-tag Mms6 protein in AD-MSC after

nucleofection. **Figure 4-6**B shows the deduced levels of His-tag Mms6 protein for each band, corrected by ß-actin. Although, it seems that the expression of His-tag Mms6 protein was found to be highest in AD-MSC transfected with Mag03 compared to the other three plasmids, no statistically significant variation of expression was observed.

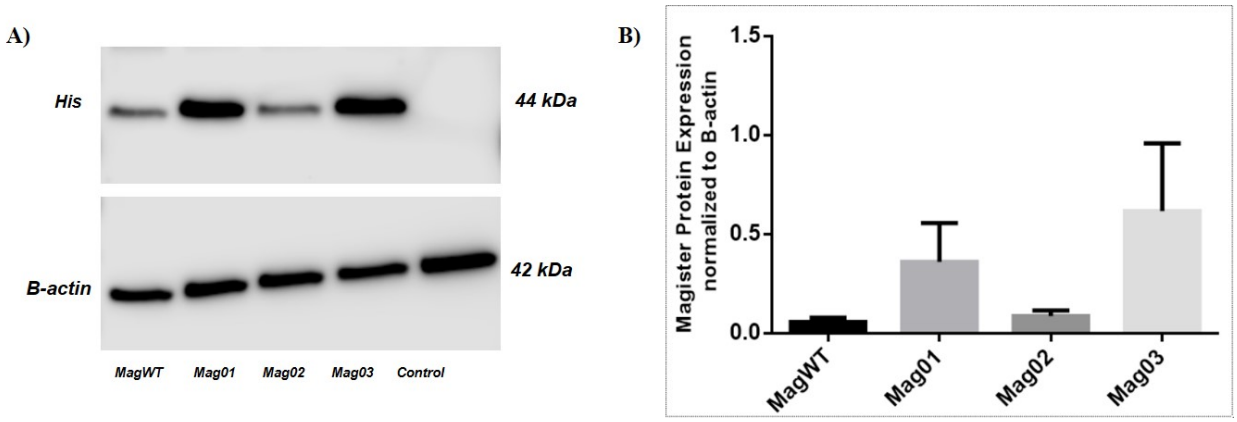

Figure 4-6: Western blot analysis for His-GFP-tag Mms6 protein expression in AD-MSC at 2 days after nucleofection. *A) Image for western blot of three independent experiments. B) Protein levels of His-tag Mms6 from each of MAGISTER-transfected AD-MSC were normalised by Actin. Values are presented as mean ± SD from three independent experiments. N = 3*

4.7 DECREASED AD-MSC CELL VIABILITY AFTER NUCLEOFECTION

The effect of nucleofection on the cell viability of AD-MSC was assessed by the AlamarBlue Cell Viability assay. For this, AD-MSC cell samples were transfected with either Mag03 or the pmaxGFP plasmid using Amaxa™ Nucleofection kit. The non-transfected cells were considered as a negative control. A day after nucleofection, cell viability determination was performed.

The results are shown in Figure 4-7. AlamarBlue fluorescence intensity average was 7040 ± 231% for cells nucleofected with Mag03, and 8627±373% for cells nucleofected with pmaxGFP, against mean fluorescence intensity of 10356±410 % for

control untransfected cells. The results are statistically significant ($p<0.0001$) for cells nucleofected with Mag03 and ($p<0.01$) for cells nucleofected with pmaxGFP plasmid. Cell viability percentage of transfected cells was calculated as a ratio between transfected and controls cells, and it is shown in considering controls as 100% viable. Results reveal that the viability of cells nucleofected with Mag03 was 66.2±2.5% of that of controls, while the viability of cells nucleofected with pmaxGFP was 82.3±6.5% of that of controls

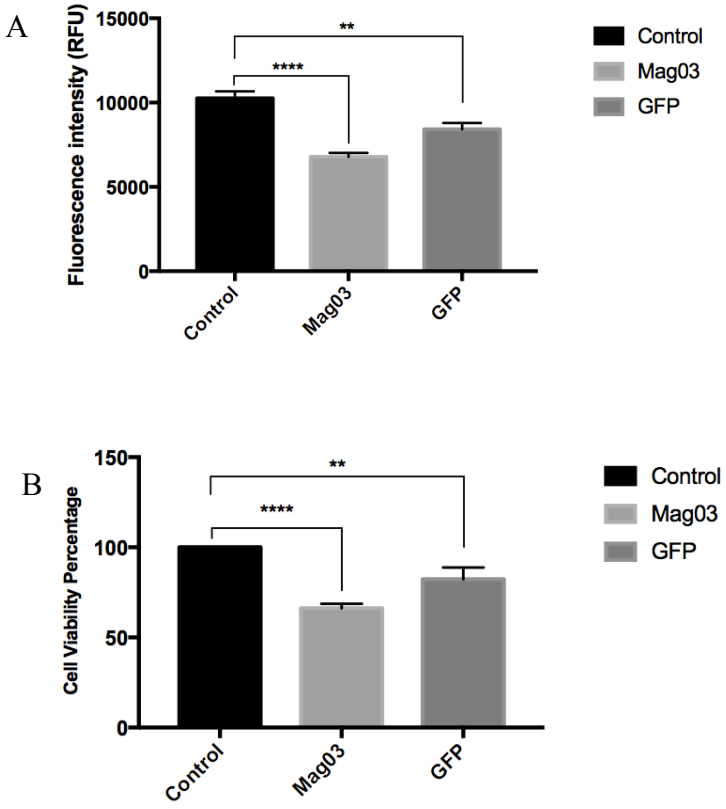

Figure 4-7: Cell viability measurement of Mag03-transfected and pmaxGFP-transfected AD-MSC by AlamarBlue Cell Viability Assay. *AD-MSC nucelofected with Mag03 plasmid (light grey column), or with pmaxGFP plasmid (dark grey column), or not nucleofected (controls - black column). A = fluorescence intensity; B = Cell viability percentage of transfected cells against controls. Values are presented as mean ± SD from one experiment undertaken in triplicate. **p<0.01, **** p<0.0001.*

4.8 DECREASED MMS6 PROTEIN PRODUCTION WITH TIME IN CULTURE

Consistent with the known transient nature of plasmid-based transfection, transgene expression generally decreased rapidly over time, lasting usually 2 to 3 weeks. To assess the stability of Nucleofection-based transfection of the transfected His-GFP-tag *mms6,* the time course and level of expression were determined. For this analysis, nucleofected cells were analyzed and sorted for GFP expression from day 2 up to day 21 after nucleofection. Specifically, on d 2, 7, 14, and 21, cells were trypsinized and reanalyzed for GFP-positive cells.

As shown in **Figure 4-8**, the number of positive GFP-expressing cells dropped to 29.3% by day 7 and to 4.6 % by day 14, then declined to only 0.6% by day 21, for MagWT nucleofected cells. For Mag01-nucleofected cells, the number of positive GFP-expressing cells dropped to 25.5% by day 7 and to 3.4 % by day 14, then went down to 0.2% by day 21. In Mag02-nucleofected cells, the number of positive GFP-expressing cells also dropped to 24.7% by day 7 and to 4.3 % by day 14, then declined to only 0.3% by day 21. Similar result also observed in Mag03-nucleofected cells, as the number of positive GFP-expressing cells also dropped to 25.9% by day 7 and to 4.1 % by day 14, then declined to only 1% by day 21. Thus, nucleofection tecnhique exhibited a time course that declined over time, as would be expected for a transient transfection with no subsequent expression-based selection. However, it is noteworthy that a substantial level of His-GFP tag Mms6 expression was detected even after 7 days of culture.

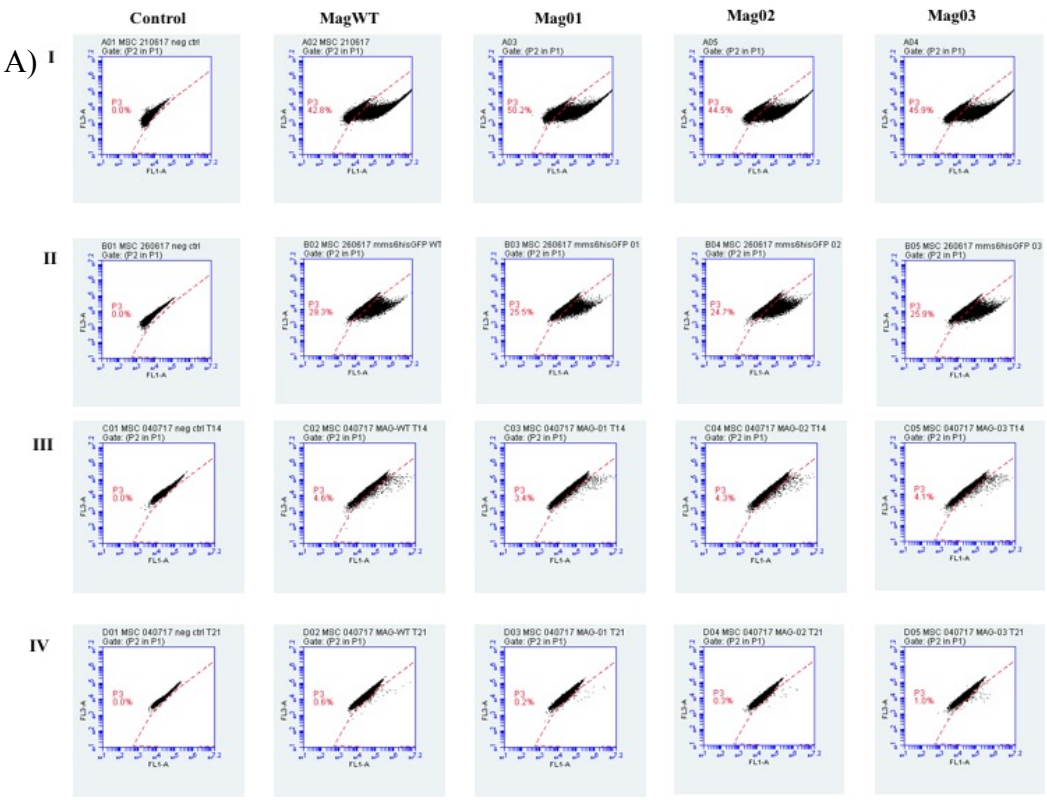

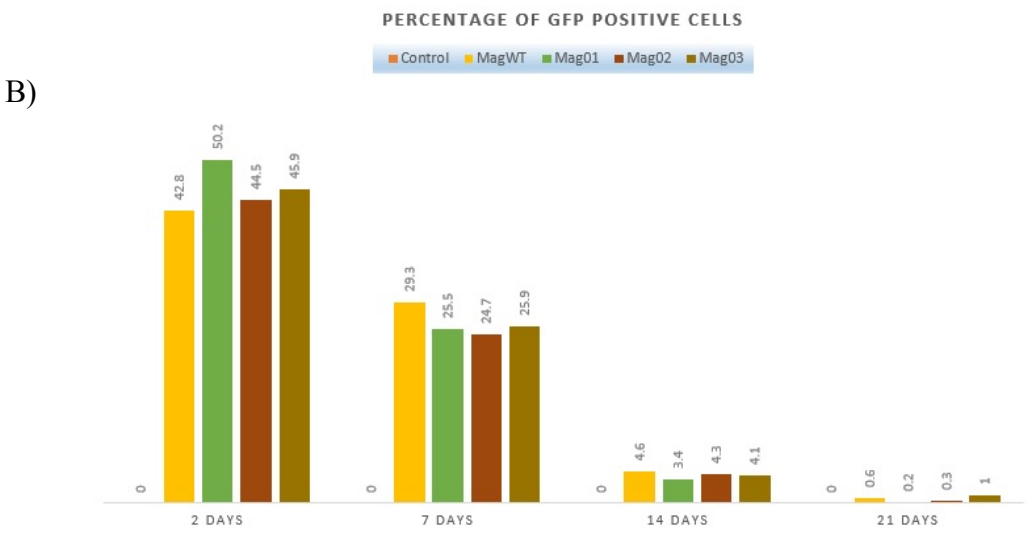

Figure 4-8: Flow cytometry analysis of GFP-positive MAG-transfected AD-MSC at different time point after nucleofection. *A) Image of percentages of positive cells for His-GFP-tag Mms6 protein expression at different time point: I = 2 days; II = 7 days; III = 14 days; and IV = 21 days after nucleofection. B) His-GFP-tag Mms6 expression decreases with time in culture. Values were obtained by Flow cytometry analysis from one independent experiment.*

4.9 LENTIVIRAL TRANSDUCED AD-MSC STABLY EXPRESSING *mms6*

Having confirmed that Mms6 protein can be expressed in AD-MSC but only transiently, it was necessary to generate AD-MSC stably expressing *mms6*. For this, viral transduction was performed using lentivirus carrying codon optimized *mms6* (Mag01, without His-GFP tag). The *mms6* sequence was cloned into pSicoR-Ef1α-mCh-Puro lentiviral transfer plasmid. This vector has two important markers which were Puromycin selection marker and mCherry red fluorescence marker, allowing for selection of the transduced cells.

For virus transduction, AD-MSC and HEK293T cells were seeded in into 24-well plate and grown overnight. HEK293T cell line were used as a positive control due to their feature as 'easy to transfect' cell line. A day after incubation, cells were then transduced with the virus particle. For HEK293T cells, MOI (multiplicity of infection) ratios of 5 and 10 were used, while MOI ratios of 10, 15 and 30 were used for AD-MSC.

After 2 days of incubation, the medium was refreshed with 2 μg/ml Puromycin selection medium to generate stable cells expressing the *mms6* gene. The selection medium was changed every 3 days. The mCherry red fluorescence produced by cells was observed every 5-7 days during the selection process for three weeks. Moreover, mCherry red fluorescence imaging and end-point PCR assay were performed to confirm the *mms6* expression. The successful cells stably expressing mCherry red fluorescence were then expanded for the later experiments.

As shown in Figure 4-9, AD-MSC were expressing red fluorescence in all samples at 1 week after lentiviral transduction. It seems that the higher the MOI ratio, the brighter the red fluorescence. Similar to this result, cells expressing red fluorescence was also observed in transduced HEK293T cells, as shown in Figure 4-10, suggesting the successful of lenti-*mms6* transduction.

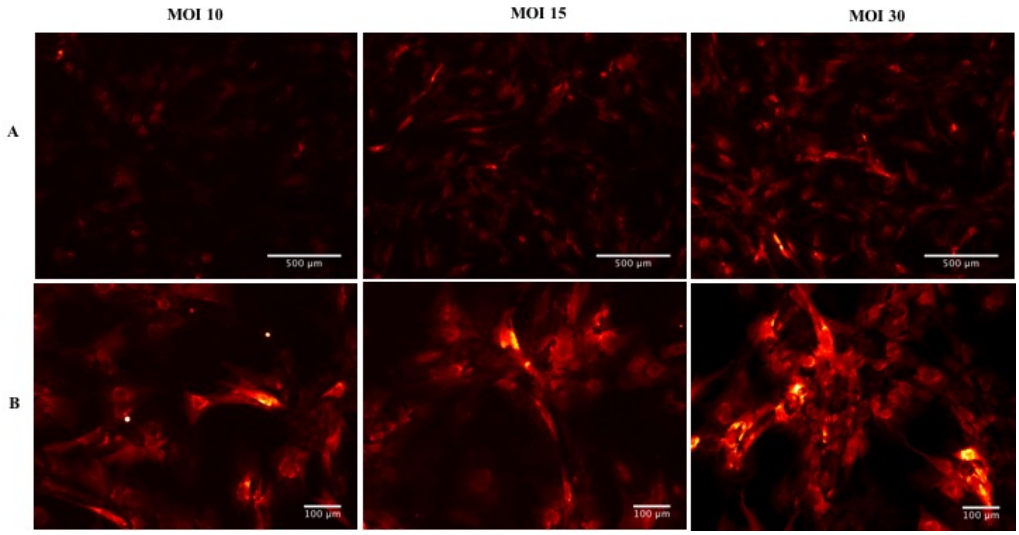

Figure 4-9: mCherry red fluorescence analysis of AD-MSC a week after lenti-mms6 transduction. *AD-MSC expressing mCherry red fluorescence after lenti-mms6 transduction using three different MOI ratio. A = Magnification 5x, scale bar 500 µm. B = Magnification 10x, scale bar 100 µm. N = 3.*

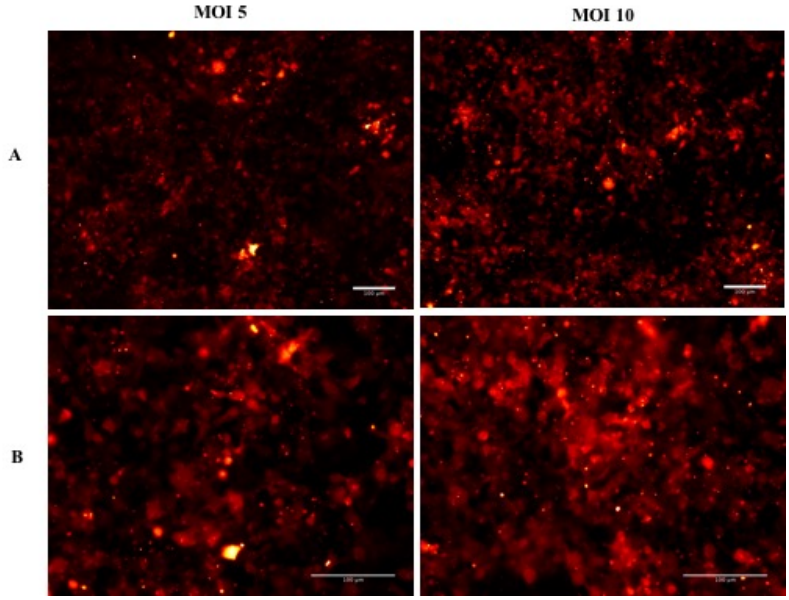

Figure 4-10: mCherry red fluorescence analysis of HEK293T cells a week after lenti-mms6 transduction. *HEK293T cells expressing mCherry red fluorescence after lenti-mms6 transduction with two different MOI ratio. A = Magnification 5x; B = Magnification 10x. Scale bar 100 µm. N = 3*

Figure 4-11 shows transduced AD-MSC were expressing mCherry red fluorescence expression at 3 weeks after lenti-*mms6* viral transduction. By visual inspection brighter red fluorescence signal was also observed in higher MOI used for the transduction. Overall, this result suggests that the lentiviral transduction approach was able to generate AD-MSC stably expressing *mms6* gene as confirmed by the constant expression of mCherry red fluorescence.

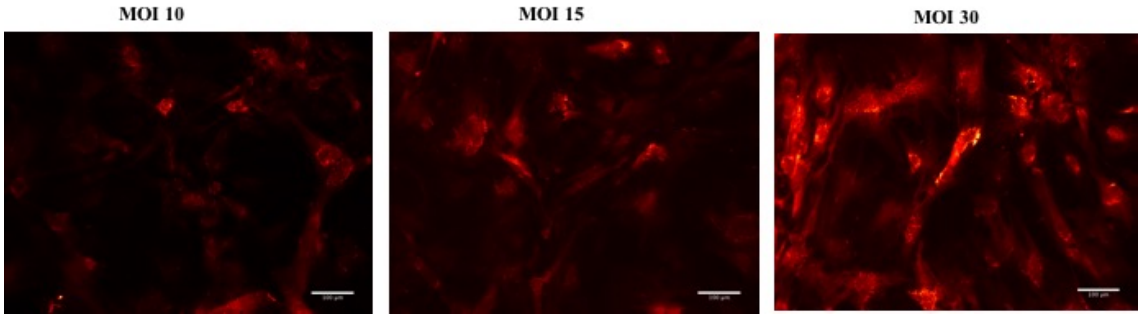

Figure 4-11: mCherry red fluorescence analysis for AD-MSC at three weeks after lenti-mms6 transduction. *AD-MSC stably expressing mCherry red fluorescence at three weeks after lenti-mms6 transduction with three different MOI ratio. Scalebar 100 µm. N = 3*

To further confirm the *mms6* expression, end-point PCR was also performed at 3 weeks after transduction. To test this, a set of internal primers to obtain an amplicons length of 167 bp were used:

Forward : 5' GAA AGT GGT GGG CGG CAC 3'
Reverse : 5' CCA CTT CTT CAT CGC TCT GC 3'

Glyceraldehyde 3-phosphate dehydrogenase (GAPDH) primers was used as an internal control.

As shown in **Figure 4-12**, the DNA bands of *mms6* were present in all transduced cell samples, as indicated by lane D, F and H for cells transduced with MOI 10, 15 and 30 of lenti-*mms6* viral titer, respectively. These DNA bands were found at position slightly above 150 bp of the PCR marker. This was found to be consistent in each

sample with the expected DNA band of 167 bp. No *mms6* DNA bands was observed in untransfected cells, as indicated in lane B. As for the internal control, GAPDH DNA bands were also present both in all samples, both untransfected cells and in lenti-*mms6* transduced AD-MSC. These DNA bands were also found to be consistent for all samples with the expected size of 210 bp, confirming the validation of the experiment. Overall, the end-point PCR demonstrates the expression of *mms6* mRNA in AD-MSC up to 3 weeks following the lentiviral transduction, suggesting the integration of viral DNA which carries *mms6* into the host DNA of AD-MSC allowing the cells to to stably express *mms6*.

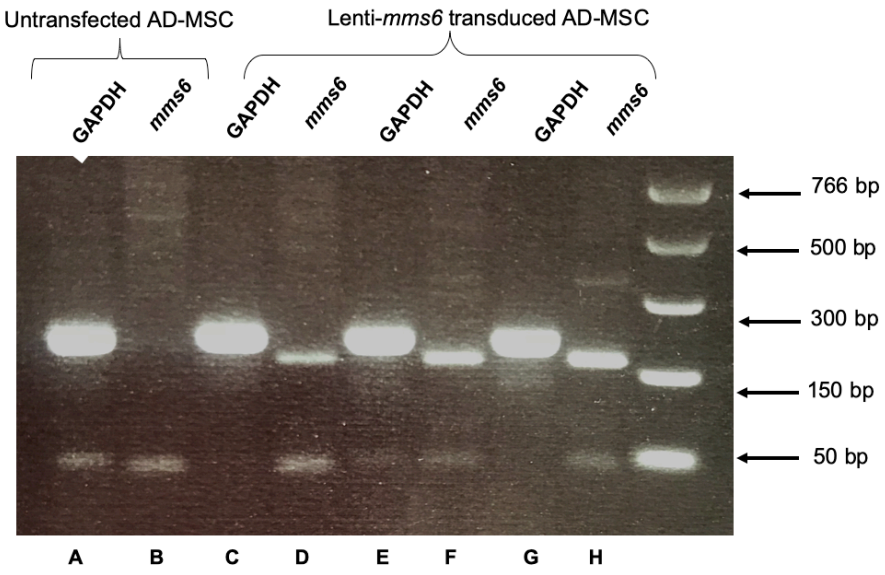

Figure 4-12: mms6 gene expression in AD-MSC at 3 weeks after lentiviral transduction. *The end-point PCR demonstrates the expression of mms6 (Mag01) mRNA in AD-MSC following lenti-mms6 transduction. A-B = Control; C-D = MOI 10; E-F = MOI 30. N = 3.*

4.10 DISCUSSION

The aims of the experiments detailed in this chapter were:

1. To demonstrate mRNA expression of different codon optimised *mms6* in AD-MSC
2. To demonstrate protein expression of different codon optimised *mms6* in AD-MSC
3. To improve the transient transfection approach for Mms6 protein expression in AD-MSC using nonviral-based transfection.
4. To develop AD-MSC stably expressing *mms6* using Lentiviral transduction.

Regarding the first aim, the end-point PCR results indicate that both non-codon optimised and codon optimised *mms6* can be expressed in AD-MSC. The mRNA of *mms6* was constantly expressed in AD-MSC up to 21 days after the transfection with each of the MAG plasmid using X-tremeGENE™ DNA Transfection Reagent.

Initially, it was hypothesised that certain codon optimised *mms6* for mammalian cell expression might be more preferable than non-optimised mms6 by AD-MSC cell system for the protein expression. Indeed, codon optimization can affect protein conformation and function, thus the optimal codon usage patterns for a specific host organism can be used to enhance expression (Patterson *et al.*, 2005; Mauro and Chappell, 2014).

However, the initial Western blot result showed that the His-GFP-tag Mms6 protein expression was found to be absent in all samples after the transfection with X-tremeGENE™ DNA Transfection Reagent. Nonetheles, the His-GFP-tag Mms6 protein was observed to be expressed in HEK293T cells, as indicated by Western blot and GFP imaging assay. This result confirms that the absence of His-GFP-tag Mms6 protein in all samples might not be related to the codon optimisation of the mms6.

Instead, this most likely as a consequence of low transfection effiency since AD-MSC has been known as difficult to transfect cells.

It is also important to note that, as discussed in Chapter 3, there was also a high likelihood that the bands in end-point PCR result could reflect the plasmid DNA as contaminant, giving a false positive result. The high concentration of MAG plasmid DNA used in the transfection which was 3 µg may contaminate the RNA isolation and end-point PCR assays. Therefore, it is important to use DNAse during RNA isolation process to avoid this issue. Moreover, negative control should be also performed in the end-point PCR experiments, such as: 1) A no template control omits any DNA or RNA template from a reaction, and serves as a general control for extraneous nucleic acid contamination, and 2) A no reverse transcriptase control or minus reverse transcriptase control involves carrying out the reverse transcription step of a PCR experiment in the absence of reverse transcriptase. This control assesses the amount of DNA contamination present in an RNA preparation.

In an attempt to improve the transient transfection efficiency of AD-MSC, several nonviral-based transfection approaches were investigated. Based on the Flow cytometry analysis, it was observed the electroporation method using Amaxa™ Nucleofection was able to generate 59.6±1.9% of GFP-positive cells at 2 days after transfection with Mag01 plasmid. This was the highest percentage of transfection efficiency compared to the previously used method using X-tremeGENE™ transfection reagent with only 15.5±3.9% GFP-positive cells. Other methods using Lipofectamine 3000® and FugeneHD® only generated relatively low transfection efficiency with only 6.6±0.6% and 2.6±0.2%, respectively. This low transfection efficiency result was in agreement with other report which suggests lipid and polymeric agents typically can transfect only 2–35% of MSC (Santos *et al.*, 2011). Moreover, the conventional cationic liposome method was not effective for MSC transfection as it resulted in very low transfection efficiency even close to 0 % (Mun *et al.*, 2016). In contrast, Haleem-smith and coworkers reported that the application of electroporation method using Amaxa™ Nucleofection was able to enhance the transfection efficiency of adult human MSC. With this method, transfection

efficiencies of 50 to 80% were achieved using two different GFP expression plasmid constructs (Haleem-Smith *et al.*, 2005). Similar to this finding, my work also shows that nucleofection using Amaxa™ Nucleofection was able to produce high transfection efficiency, as the percentage of AD-MSC expressing GFP were 47.3±4.1%, 49.4±3.5%, 53.9±1.2%, and 47.3±3.7% for cells nucleofected with MagWT, Mag01, Mag02 and Mag03, respectively. Other group also tried to overexpress CXCR4 in human MSC using mRNA nucleofection approach and obtained 90% expression of the surface receptor, suggesting high effectivity of nucleofection technique for modification of human MSC (Wiehe *et al.*, 2013).

The result of experiments described in this chapter confirm the protein expression of His-GFP-tag Mms6 protein in AD-MSC after electroporation. The GFP fluorescence expressed by AD-MSC evaluated by both Flow cytometry and GFP imaging analysis confirmed the success of expressing Mms6 protein in AD-MSC. This was also confirmed by Western blot analysis which shows the expression of His-GFP-tag protein in all cell samples nucleofected with MagWT, Mag01, Mag02 and Mag03 plasmid.

It was also hypothesized that different codon optimised *mms6* may improve Mms6 protein expression, hopefully resulting in increased MNP production. To test this hypothesis, a semi-quantitative protein quantification analysis was performed using western blot. Even though the result reveals the expression of His-GFP-tag Mms6 protein was found to be highest in AD-MSC transfected with Mag01 and Mag03 compared to the other two plasmids, statistically no significant variation of Mms6 protein expression was observed. More replicates may be needed to measure whether there is a significant difference of Mms6 protein expression level due to certain codon optimisation of *mms6.*

AD-MSC cell viability was found to be affected by electroporation which results in reducing its cell viability. AlamarBlue cell viability analysis reveals that the viability of cells nucleofected with Mag03 was significantly decreased to 66.2±2.5% against 100% cell viability of control. This was expected as, generally, the disadvantage of using electroporation method is the tendency for high level of damaged cells (Kaestner

et al., 2015). In agreement with the finding in my study, Helledie *et al.* (2008) also had optimized the parameters of electroporation of human MSC (hMSC), using exponential decaying pulses. The result of the study indicated up to 90% stable transfection efficiency. However, the main disadvantage of this electroporation approach was that it decreased 50% cell viability, suggested that this technique is rather harsh and caused a high rate of cell mortality, especially in MSC (Helledie *et al.*, 2008). The significant effect on cell viability following the electroporation may be due to the large surface area of the electrode (Halim *et al.*, 2014).

Moreover, it was also noticed that the Mms6 protein production was decreased over time in culture, which was expected for a transient transfection method. In general, transiently transfected genes are only expressed for a limited period of time. This most likely as a consequence of the transfected genetic material are not integrated into the genome and affected by cell division and environmental factors (Kim and Eberwine, 2010). Moreover, the drop off in expression is also likely due to cytomegalovirus (CMV) promoter used in the plasmid. CMV promotor has been known its advantage to direct a high level of transient gene expression. However, a potential drawback of the CMV promoter is that it is prone to silencing over time after being introduced into the genome of host cells (Damdindorj *et al.*, 2014). Previous study has demonstrated that the CMV promoter in plasmid vectors directs a prominently high level of transient gene expression, but such gene expression does not persist for a long period of time in human cell lines (Damdindorj *et al.*, 2012). For long term expression, mammalian promoter such as elongation factor-1α (EF1α) may be a more suitable for this work as it offers more stable expression (Norrman *et al.*, 2010).

However, it is noteworthy that over 20% level of His-GFP tag Mms6 expression at 7 days after transfection was observed in all nucleofected cell samples, suggesting high efficiency of the approach. In agreement with this finding, a study also reported that following the MSC electroporation using Amaxa™ Nucleofection, a drop in the number of GFP expression cells was observed over time, corresponding to 21% at day 13 and 12% at day 23, resulting a significant number of GFP- positive MSC cells remained by 3 weeks post transfection (Haleem-Smith *et al.*, 2005)

The final aim of this chapter was to develop AD-MSC stably expressing *mms6* using Lentiviral transduction. It has been well known that classical transfection methods are generally less efficient than viral-based techniques, in particular for AD-MSC transfection (Halim *et al.*, 2014). Previous studies investigating human-periodontal-ligament-stem-cell (hPDLSC) transfection using nonviral-based transfection method such Lipofectamine 3000® and X-tremeGENE DNA Transfection Reagent compared to lentiviral vectors harboring a green-fluorescent-protein gene indicated that transfection efficiency of nonviral-based transfection was unsatisfactory (<6%) compared to that of lentiviral vectors (95%) (Wang *et al.*, 2015). Taken together all this evidence, it was then decided to clone the *mms6* into a lentiviral vector in order to develop AD-MSC stably expressing *mms6.* In my study, I did not perform transfection efficiency measurement following the lentiviral transduction. Instead, I performed antibiotic selection started at day 2 after transduction and continuously for 2 weeks in order to obtain colony of AD-MSC expressing *mms6*.

The results of lentiviral transduction experiment described in this chapter confirm that AD-MSC can be modified to stably expressing *mms6* as shown by continuous mCherry red fluorescence protein marker expression and *mms6* mRNA expression at 3 weeks after transduction. This was as expected due to the fact that viral vector has nature of integration into the host genome, providing high efficiency of gene transfection. The integrated viral DNA replicates as the host genome does. Consequently, it segregates into daughter cells, which enables sustainable transgene expression (Kim and Eberwine, 2010).

In summary, nucleofection, although rather harsh and leading to excessive cell death, is highly effective for transient expression of Mms6 in AD-MSC. Morevor, viral-based transduction, using lentiviral carrying *mms6*, was also able to generate AD-MSC stably expressing *mms6.* These cells were utilized for the later MNHT experiments in the following chapter. Importantly, this chapter has succeeded to demonstrate expression of an MTB gene, *mms6,* in AD-MSC both in transcriptional and translational level which was the ultimate goal of the study.

5 THE EFFECT OF *mms6* EXPRESSION ON THE AD-MSC STEMNESS, MULTIPOTENCY, NANOPARTICLES PRODUCTION AND MAGNETISM.

5.1 SUMMARY

In chapter 4, experiments successfully showed that it is possible to express a bacterial magnetic gene, *mms6*, in AD-MSC. However, the main aim of the research was to produce biogenic magnetic human AD-MSC which can be used for MNHT or MRI applications. Therefore, in this chapter, it was determined if the *mms6* expression of AD-MSC could cause any detrimental effect on the nature characteristic of AD-MSC by investigating MSC stemness and its multipotency. Further investigations on magnetic nanoparticles produced in AD-MSC expressing *mms6* was then assessed by Transmission Electron Microscopy (TEM) analysis. This work also involved investigations using commercial iron-based MNP for comparison of magnetic properties between AD-MSC expressing *mms6* and iron-based nanoparticle labelled AD-MSC.

To determine whether lenti-*mms6* transduced AD-MSC could still be considered stem cells and have utility in the clinical setting, experiments were carried out to confirm MSC stemness and the ability of the cells to differentiate into the osteogenic and adipogenic lineage.

For the iron-based nanoparticle-labelled AD-MSC studies, several commercial iron-based MNP, NanoMAG-D-Spio, BNF-Dextran, FluigMAG-CT and Ferucarbotran nanoparticles, were used. The stability of these nanoparticles in culture medium as well as cell viability analysis of AD-MSC loaded with these nanoparticles were then performed. To look further on the nanoparticle uptake ability of MSC, Prussian blue staining and TEM analysis were performed.

For the TEM analysis, AD-MSC expressing *mms6* were cultured in a ferric quinate (FeQ) doped medium (3.4 µl FeQ/ml), following the standard protocol for the culture

of MTB, to provide non-magnetic iron necessary to create nanoparticle material. In this experiment, three group of AD-MSC expressing *mms6* were used: lenti-*mms6* transduced-cells, Mag01-nucleofected cells, and Mag03-nucleofected cells. They were cultured in FeQ medium for 10 days, allowing incubation time for the cells to bind the iron. Furthermore, the magnetism of AD-MSC expressing *mms6* and MNP labelled AD-MSC were evaluated by Superconducting Quantum Interference Device (SQUID) upon zero field cooling (ZFC) and field cooling (FC) magnetic measurement.

5.2 AIMS

The aims of the experiments detailed in this chapter were:

1. To investigate the effect of *mms6* expression in AD-MSC stemness and differentiation potential.
2. To study magnetic nanoparticle production by AD-MSC expressing *mms6* and commercial magnetic nanoparticle-labelled AD-MSC.
3. To demonstrate magnetic properties of AD-MSC expressing *mms6.*

5.3 ANALYSIS OF STEM CELL SURFACE MARKERS OF AD-MSC EXPRESSING *mms6.*

In order to investigate whether AD-MSC expressing *mms6* are still able to express typical mesenchymal stem cell surface markers, immunofluorescence analysis was performed. This was important to define whether the stable expression of *mms6* could affect the ability of stem cells in maintaining their stemness and differentiation potential.

Immunofluorescence was performed on lentiviral transduced AD-MSC expressing *mms6* cell samples. Cells were stained with anti-CD44, anti-CD90, anti-CD14 and anti-CD19, followed by Alexa Fluor 488-conjugated goat anti-mouse IgG (green) secondary antibody. CD44 or homing cell adhesion molecule (HCAM) and CD90 are MSC positive surface markers, while CD14 (present on leukocytes) and CD19 (present on B-lymphocytes) are negative markers for MSC. The non-transfected or wild type AD-MSC were used as a positive control. The experiment was run in triplicates.

As shown in Figure 5-1 A-B, both AD-MSC expressing *mms6* and control cells stained with anti-CD44 or anti-CD-90 shows green fluorescence signal. On the other hand, the green fluorescence signal was not detected in both cell lines stained with anti-CD14 or anti-CD-19 (Figure 5-1 C-D). This result indicates the expression of MSC positive markers and the lack of negative markers expression on both AD-MSC expressing *mms6* and control cells. This suggests that AD-MSC expressing *mms6* are still able to express the typical mesenchymal stem cell surface markers, and the expression of *mms6* may not affect the ability of stem cells in maintaining their stemness and differentiation potential.

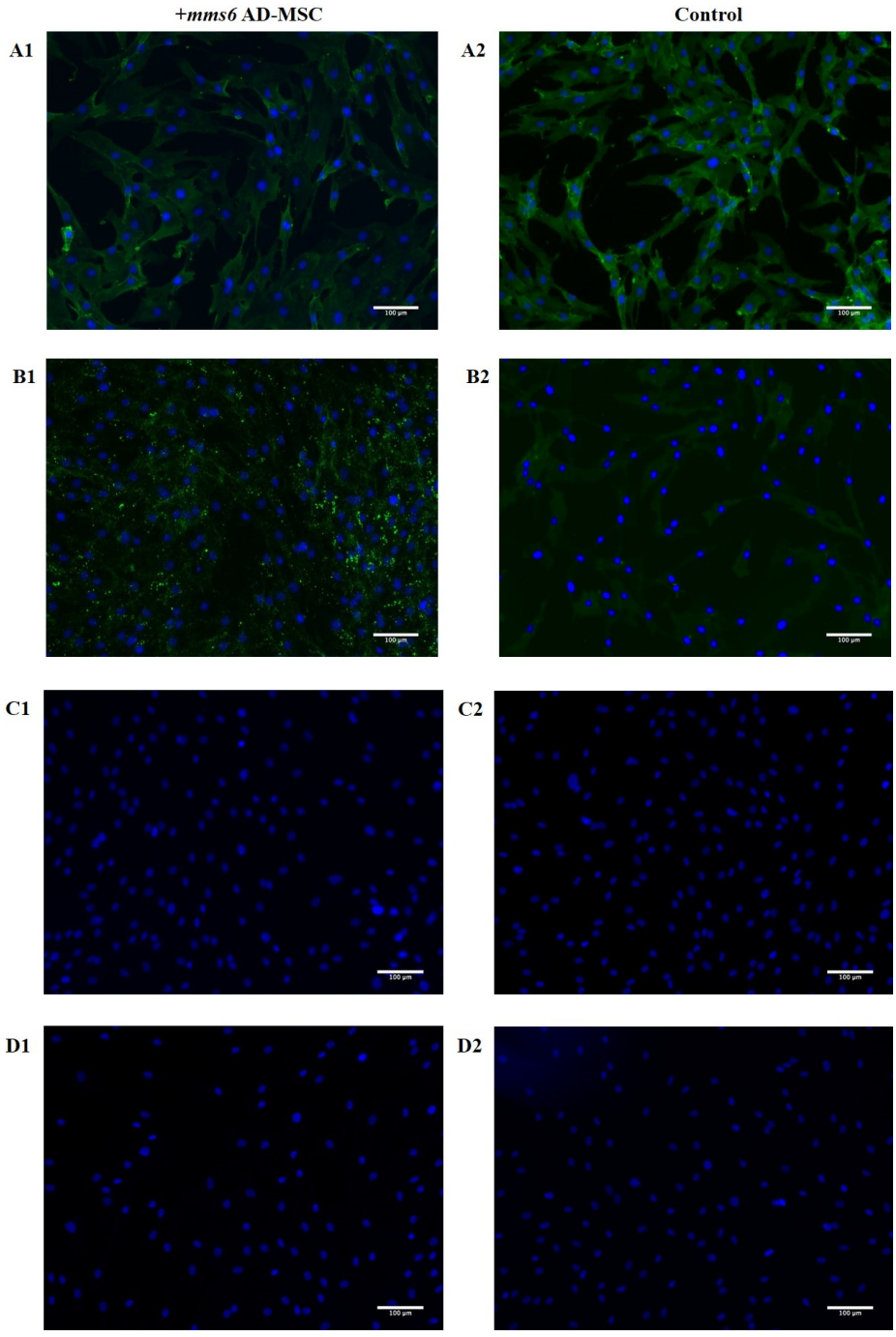

Figure 5-1: Analysis of mesenchymal stem cell surface markers. *Immunofluorescence image showing both AD-MSC expressing mms6 (left panel) and untransduced AD-MSC as control (right panel) stained with A) anti-CD44, B) anti-CD90, C) anti-CD14, and D) anti-CD19, followed by Alexa Fluor 488-conjugated goat anti-mouse IgG (green) secondary antibody. Cell nuclei is shown in blue (DAPI) and surface markers positivity is shown in green. Scale bar = 100 µm. N=3.*

5.4 ASSESSMENT OF ADIPOGENIC AND OSTEOGENIC DIFFERENTIATION POTENTIAL OF AD-MSC EXPRESSING *mms6*.

In order to evaluate whether stable expression of *mms6* could cause any adverse effect on MSC pluripotency, *in vitro* functional differentiation experiments were carried out on AD-MSC expressing *mms6* and wild-type AD-MSC. Both cells group were differentiated into the osteogenic and adipogenic lineage using the appropriate medium for each lineage. The results were then compared, using the wild-type AD-MSC as a positive control.

For osteogenic differentiation, AD-MSC expressing *mms6* and control cells were incubated with osteogenic differentiation medium for 14 and 21 days. Cells grown in standard medium served as negative controls. At each time point, osteogenic differentiation of both cell lines was assessed by identification of calcium deposits stained by the Alizarin Red dye. The experiment was run in triplicates.

For adipogenic differentiation, AD-MSC expressing *mms6* and wild-type AD-MSC were incubated with adipogenic differentiation medium for 10 days. Cells grown in standard medium served as negative controls. Following the incubation, cells were fixed in 4% paraformaldehyde and stained by Oil Red O. Pictures of cells were taken in light microscopy and photographed using a coloured camera. The experiment was run in triplicates.

As shown in **Figure 5-2**, following 14 days in osteogenic and standard culture medium calcium deposits were not detected in either AD-MSC expressing mms6 or wild-type AD-MSC. At 21 days AD-MSC expressing mms6 and wild-type AD-MSC in osteogenic media showed extensive calcium deposition whereas cells in control media did not show calcium deposition. The result indicates no difference was observed between AD-MSC expressing *mms6* and wild-type AD-MSC both at 14 days and 21 days incubation with osteogenic differentiation medium, indicating successful differentiation of both cell lines into osteoblasts and *in vitro* bone-formation. This result demonstrates the expression of *mms6* did not affect the ability of AD-MSC in maintaining their osteogenic differentiation potential.

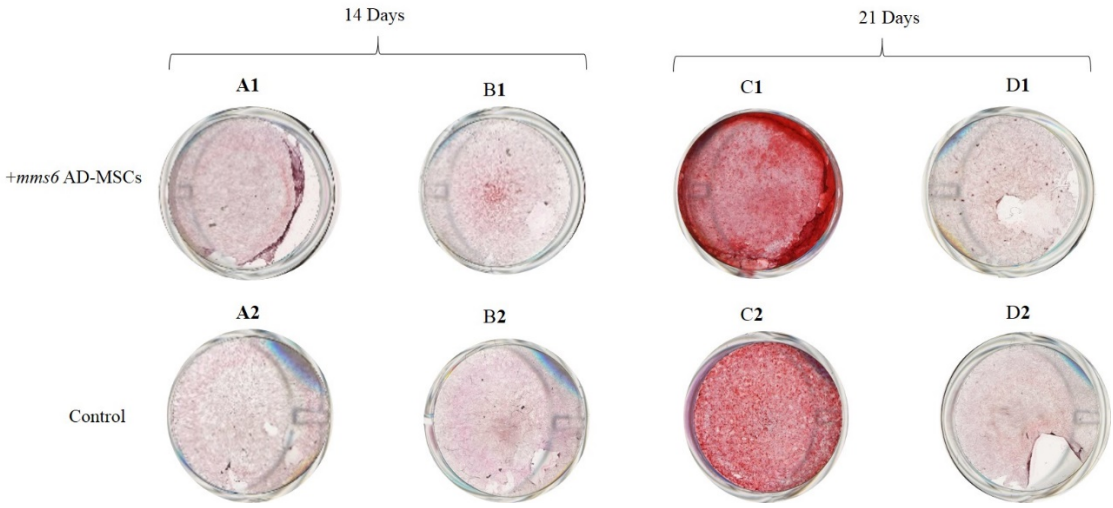

Figure 5-2: AD-MSC expressing mms6 differentiate into osteogenic lineage. *Alizarin staining data showing both AD-MSC expressing mms6 (upper panel) and wild-type AD-MSC as control (lower panel) cultured for 14 days and 21 days in osteogenic medium (A & C) or in standard medium (B & D). N=3.*

After being cultured in adipogenic medium for 10 days, both AD-MSC expressing *mms6* and wild-type AD-MSC began to form small intracellular translucent vacuoles, which then gradually filled the cytoplasm along the cell membrane, exhibiting adipogenic phenotype. As shown **Figure 5-3**, both cell lines show formation of intracellular lipid droplets, stained in bright red colour by Oil Red O. No formation of lipid droplets and morphological changes were noticed in both cell lines cultured in standard medium. Therefore, this result confirms the expression of *mms6* did not affect the ability of AD-MSC in maintaining their adipogenic differentiation potential and could differentiate into adipocytes.

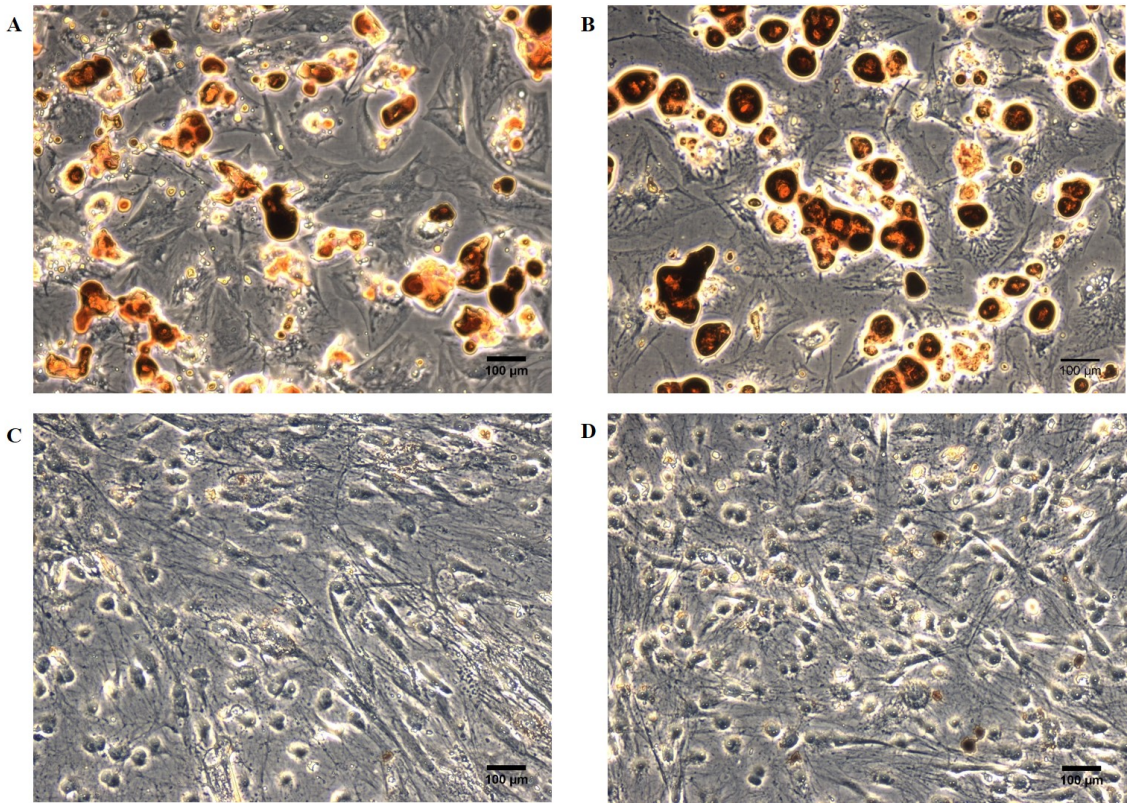

Figure 5-3: AD-MSC expressing mms6 differentiate into adipogenic lineage. *Oil Red O staining data showing both AD-MSC expressing mms6 (left panel) and control cells (right panel) cultured for 10 days in adipogenic medium (A-B) or in standard medium (C-D). Scale bar = 100 µm. N=3.*

5.5 ASSESSMENT OF COMMERCIAL IRON-BASED MNP STABILITY IN THE CULTURE MEDIUM.

In vitro studies using chemically synthesized MNP were also performed. The experiment aimed to find the best candidate of MNP for MNP-loaded AD-MSC. This will allow a comparison study of MNP-loaded AD-MSC and AD-MSC expressing *mms6* being able to self-produce nanoparticles. For this purpose, fully synthetic commercial iron oxide-based MNP were investigated: NanoMAG D-Spio, BNF-Dextran, FluigMAG-CT and Ferucarbotran nanoparticle.

Since MNP colloidal stability in culture medium is a crucial factor in *in vitro* assay, the colloidal stability of each of these MNP was measured. Colloidal stability of MNP

in medium is indicated by consistent turbidity over time. Therefore, turbidity measurement of these nanoparticles in culture medium was performed to assess their colloidal stability. For this analysis, a turbidity assay was monitored over a period up to 24 h, namely 0, 2 h, 16 h and 24 h, with MNP concentration of 500 µg/ml. MNP were suspended in culture medium or in PBS. The turbidity of MNP suspension was measured at 450 nm using a microplate reader. The experiment was conducted in quadruplicates and repeated twice.

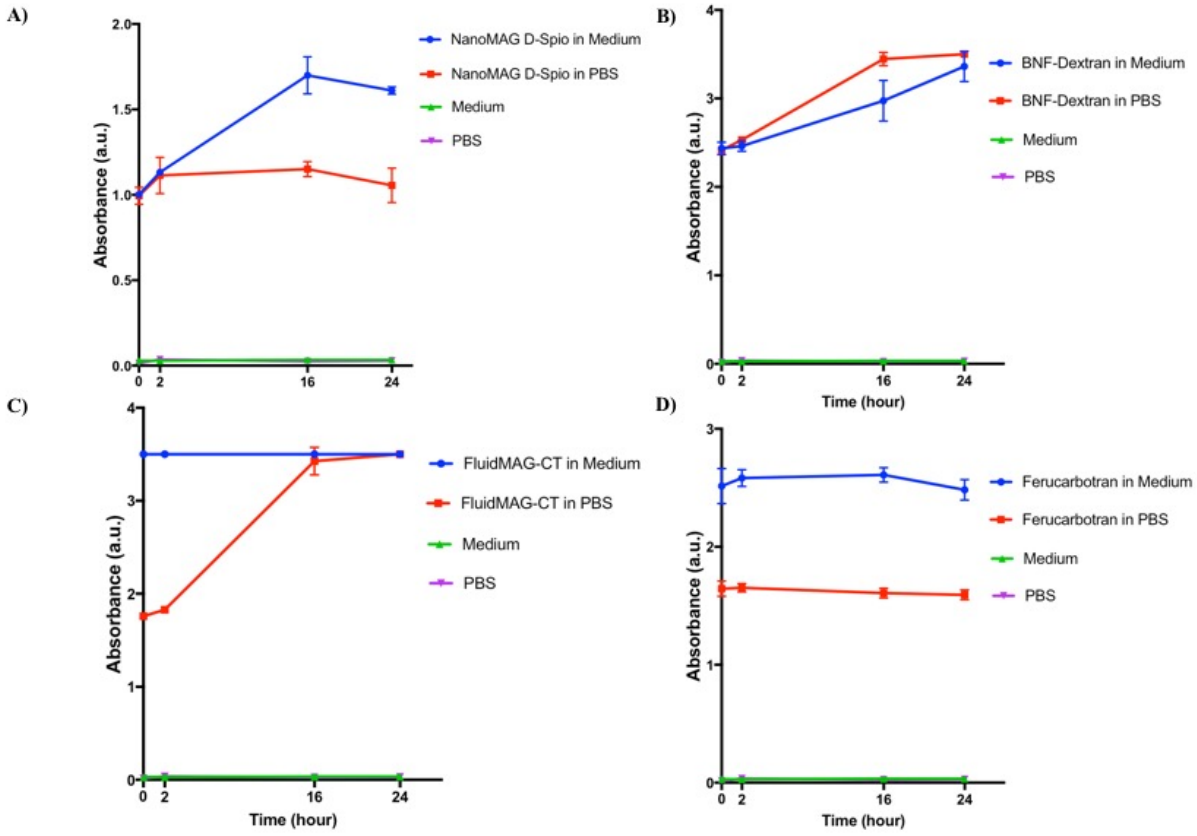

Figure 5-4: Spectroscopy of 450 nm of iron-based MNP in PBS and in basic culture medium. *Turbidity analysis data showing absorbance value of A) NanoMAG D-Spio in culture medium and PBS; B) BNF-Dextran in culture medium and PBS; C) FluidMAG-CT in culture medium and PBS; D) Ferucarbotran in culture medium and PBS. Values are presented as mean ± SD. N = 4.*

As shown in **Figure 5-4**, both NanoMAG D-Spio and BNF-Dextran showed increasing absorbance value in culture medium over period of 24 hours, suggesting the turbidity of the nanoparticle was increased or not stable in the medium. This was also confirmed

with debris formation at the bottom of culture plate after 16 hours of incubation by visual inspection. On the other hand, despite increased turbidity over time in PBS, FluidMAG-CT showed consistent turbidity in culture medium over period of 24 hours. Meanwhile, the turbidity measurement of Ferucabotran nanoparticles in both PBS and culture medium showed consistent values over 24 hours, indicating Ferucarbotran nanoparticles were the only colloidally stable MNP in both PBS and the culture medium. Based on these results, FluidMAG-CT and Ferucabotran nanoparticles were the most stable MNP in culture medium suspension among those four MNP, thus they were chosen for the later *in vitro* experiment.

5.6 CELL VIABILITY OF MNP-LOADED AD-MSC

Cellular viability of AD-MSC loaded with Ferucarbotran or FluigMAG-CT nanoparticles was assessed to investigate whether these iron-based MNP had cytotoxic effect on AD-MSC. For this, cells were seeded in 48-well plates (5×10^4 cells/well in 500 µl medium) for 24 hours after which they were loaded with 25, 50, 100, 250, 500 or 1000 µg/ml nanoparticles. Cells without MNP added were used as control. Following 24 hours of incubation, cell viability determination was performed using an AlamarBlue assay. The experiment was run in triplicates and repeated three times.

As shown in ***Figure 5-5***, AlamarBlue fluorescence intensity average decreased with increasing FluidMAG nanoparticle concentration. The fluorescence intensity average values were 6364±414, 5974±389, 5528±340, 4727±182, 4365±657, and 3381±245 for cells incubated with 25, 50, 100, 250, 500 and 1000 µg/ml nanoparticle concentration, respectively, against average fluorescence intensity of 6940±548.99 for control cells. The fluorescence intensity was found to be statistically significant against control with value ($p<0.01$) for cells incubated with 100 µg/ml, ($p<0.001$) for cells incubated with 250 µg/ml, and ($p<0.0001$) for cells incubated with 500 and 1000 µg/ml. This suggests that FluidMAG-CT nanoparticles are toxic for AD-MSC at MNP concentration higher than 100 µg/ml.

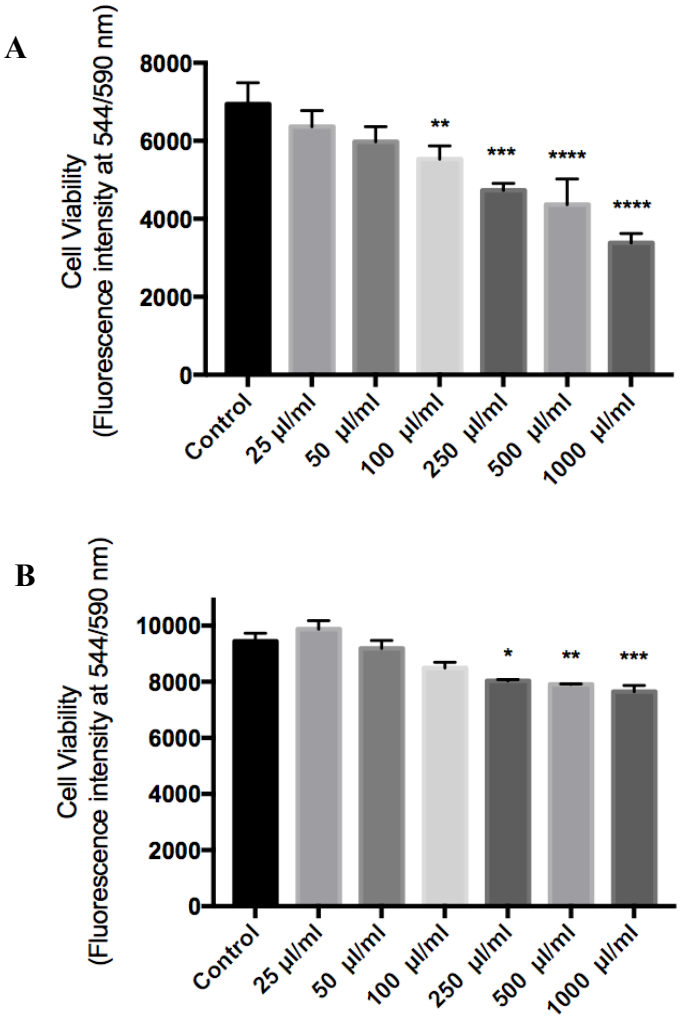

Figure 5-5: Cell Viability of MNP-loaded AD-MSC. *AlamarBlue data showing fluorescence intensity of A) AD-MSC loaded with FluigMAG nanoparticles, and B) AD-MSC loaded with Ferucarbotran nanoparticles, cultured for 24 hours in standard medium. Values are presented as mean ± SD. *p≤0.05, **p≤0.01, *** p≤0.001, **** p≤0.0001 from control. N=3*

AlamarBlue fluorescence intensity average values were 9878±302, 9189±288, 8488±209, 8037±43, 7903±20, and 7653±220 for cells incubated with 25, 50, 100, 250, 500 and 1000 µg/ml Ferucarbotran nanoparticle concentration, respectively, against average fluorescence intensity of 9115.33±858.53 for control cells. The fluorescence intensity was found to be statistically significant against control with value ($p \leq 0.05$) for cells incubated with 250 µg/ml, ($p < 0.01$) for cells incubated with

500 µg/ml, and ($p<0.001$) for cells incubated with 1000 µg/ml Ferucarbotran nanoparticle. This result indicated that Ferucarbotran nanoparticles are toxic for AD-MSC at MNP concentration higher than 250 µg/ml. In addition, it was noticed the reduction in cell viability of AD-MSC incubated with Ferucarbotran nanoparticles was less dramatic than that of AD-MSC incubated with FluidMAG-CT nanoparticles. Overall, Ferucarbotran nanoparticles appeared to be less toxic compared to FluidMAG-CT nanoparticles. Therefore, Ferucarbotran nanoparticles were chosen for subsequent experiments.

5.7 ASSESSMENT OF FERUCARBOTRAN NANOPARTICLE UPTAKE BY AD-MSC

Cellular labeling was evaluated using Prussian blue staining for iron assessment. This was important to assess the ability of MNP uptake by AD-MSC. Successful AD-MSC cellular labeling is necessary for comparative studies with AD-MSC expressing *mms6*.

For Prussian blue staining, cells were seeded in 12-well plate (5×10^4 cells/well) and grown overnight. A day after, cells were loaded with 200 µg/ml Ferucarbotran nanoparticle in 500 µl medium. Cells without MNP served as control. Following overnight incubation, cells were fixed with formaldehyde and stained with Prussian blue dye. The experiment was conducted in triplicate and repeated at least three times.

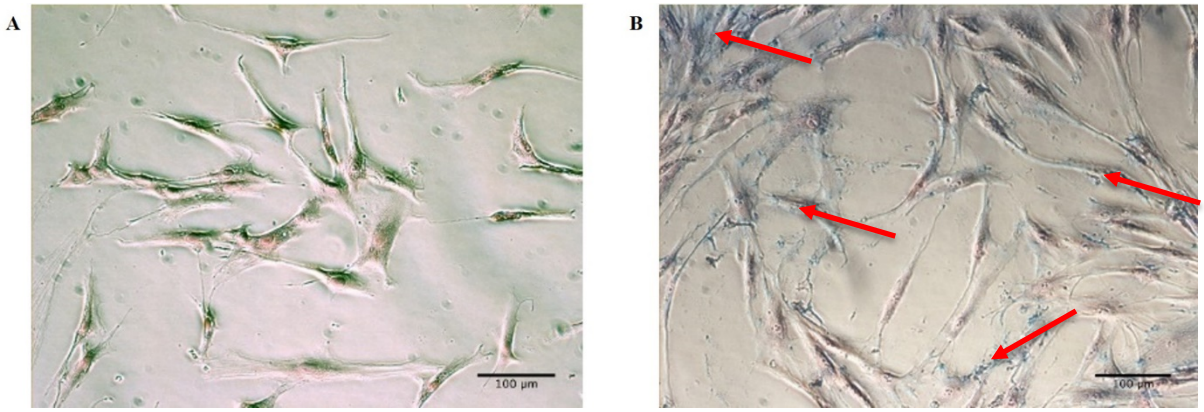

Figure 5-6: Ferucarbotran nanoparticles uptake by AD-MSC. *Prussian blue data showing A) AD-MSC control, and B) AD-MSC loaded with 100 µg/ml Ferucarbotran nanoparticles stained with Prussian blue. Both cells cultured in standard medium for 24 hours; the colour blue indicates the presence of iron; arrows indicate representative intracellular iron accumulation. Scale bar = 100 µm. N =3.*

As shown in Figure 5-6, under light microscopy blue-colored granules are identifiable distributed along the cell cytoplasm, indicating the presence of iron in Ferucarbotran-loaded AD-MSC. These blue granules were not detected in control cells. This result shows the successful of AD-MSC cellular labeling with Ferucarbotran MNP, confirming the ability of iron uptake by AD-MSC after overnight incubation of AD-MSC with Ferucarbotran nanoparticles.

5.8 TRANSMISSION ELECTRON MICROSCOPY ANALYSIS OF AD-MSC EXPRESSING *mms6* AND FERUCARBOTRAN-LOADED AD-MSC.

To evaluate whether the expression of *mms6* could induce AD-MSC to produce intracellular biogenic MNP, electron micrographs were acquired. This was also important to further evaluate the location and distribution of the Ferucarbotran nanoparticles within cells for comparative purposes.

Mag01-nucleofected AD-MSC, Mag03-nucleofected AD-MSC, and lenti-*mms6* transduced AD-MSC were cultured in medium doped with FeQ (34 µM) for 10 days. Untransfected AD-MSC cultured in medium doped with FeQ (34 µM) for 10 days were used as a control. AD-MSC cultured with Ferucarbotran (100 µg/ml) for 24 hours

were also assessed by TEM. Following 10 days incubation, cells were dehydrated and embedded in Eponate resin. Thereafter, ultrathin sections of samples were produced and viewed on a transmission electron microscope.

As shown in Figure 5-7, dispersed electron dense nanocrystal-like structures are present in the cytoplasm of all transfected cells samples, both MAG-nucleofected cells (Figure 5-7 B & C) and lenti-*mms6*-transduced cells (Figure 5-7 D). The nanocrystals appear homogenous in size. The vesicles size varies from 100 nm to more than 1 μm. No electron dense intracytoplasmic particles are present in untransfected AD-MSC (Figure 5-7 A). It was also noticed some nanocrystals appear to form clusters within the vesicle. The nanoparticle clusters look denser in AD-MSC stably expressing *mms6* compared to Mag01- and Mag03- nucleofected AD-MSC. Similar to this result, the same nanocrystal materials within vesicles were also found in AD-MSC incubated with Ferucarbotran nanoparticles, as indicated in Figure 5-7 E. Overall, the TEM analysis demonstrates that AD-MSC expressing *mms6* could induce iron binding to promote intracellular biogenic MNP within AD-MSC.

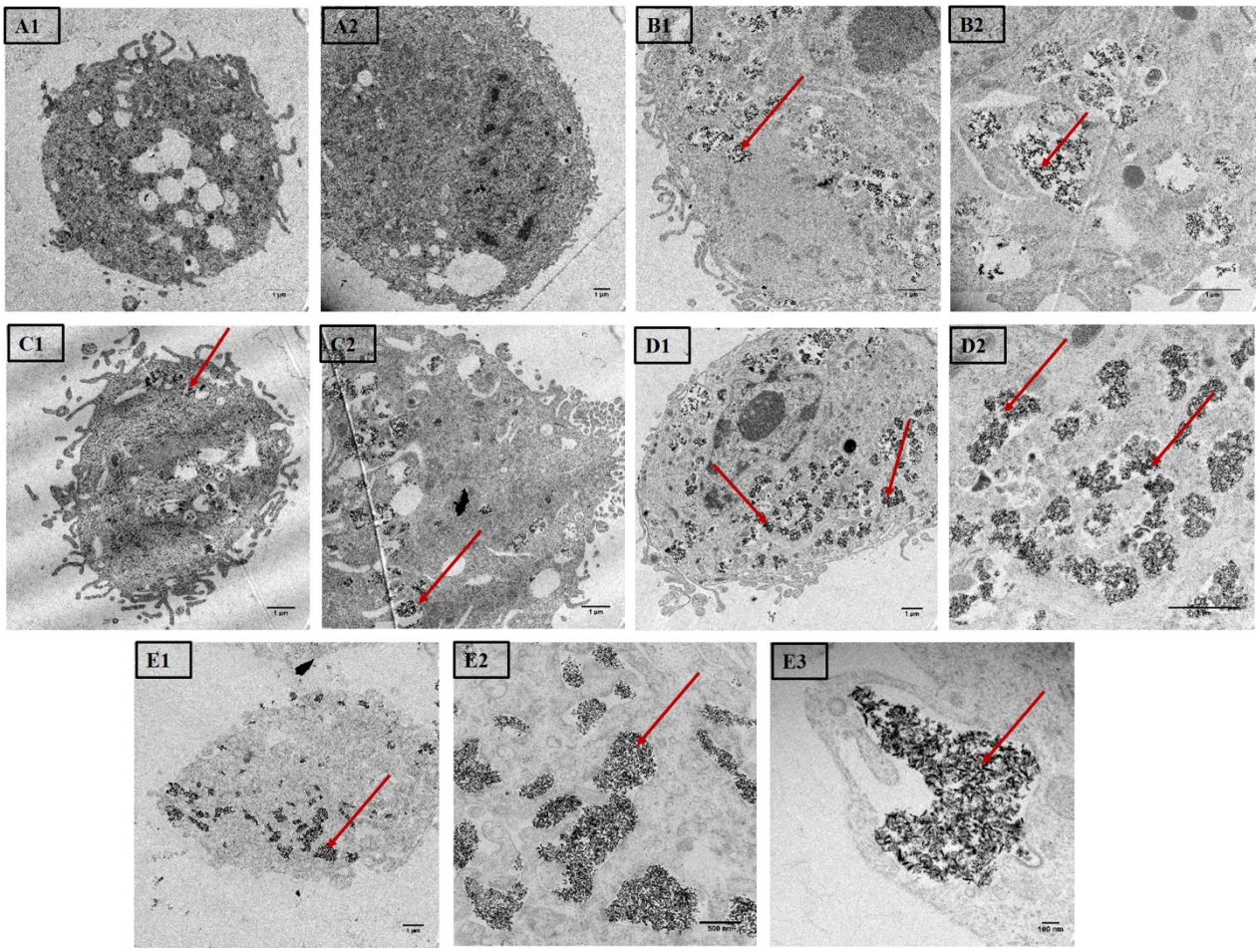

Figure 5-7: TEM Analysis of AD-MSC. *Representative TEM pictures of A1-A2) AD-MSC control cells; B1-B2) Mag01-nucleofected AD-MSC; C1-C2) Mag03-nucleofected D1-D2) Lenti-mms6—transduced AD-MSC; E1-E3) Ferucarbotran-loaded AD-MSC. Scale bar = 100 µm (A1-E1); 500nm (E2); 100 nm (E3). N = 2.*

5.9 MAGNETISATION ANALYSIS OF AD-MSC EXPRESSING *mms6* AND FERUCARBOTRAN-LOADED AD-MSC

The magnetization of AD-MSC expressing *mms6* and Ferucarbotran-loaded AD-MSC was measured upon zero field cooling (ZFC) and field cooling (FC) in magnetic fields by Superconducting Quantum Interference Device magnetometer (SQUID) magnetometry. This was important to evaluate the magnetism of both AD-MSC expressing *mms6* and Ferucarbotran-loaded AD-MSC.

For AD-MSC expressing *mms6* cell magnetization analysis, 3 x 10^6 cells were incubated for 10 days in culture medium doped with FeQ (3.4 µl FeQ/ml). Wild-type AD-MSC incubated under identical conditions were used as a control. For Ferucarbotran-loaded AD-MSC, 3 x 10^6 cells were incubated with Ferucarbotran (100 µg/ml) for 24 hours. Following the incubation time, cells were collected in a pellet form then air-dried and transferred into SQUID capsule for the measurement.

The zero-field-cooled (ZFC) and field-cooled (FC) measurements were performed under an applied field of 100 Oe between 5 up to 400 K. Firstly, the sample was cooled down to the lowest temperature (5K) in zero magnetic field, so that the nanoparticles were randomly oriented. Then, at 5K, a very low field was applied (100 Oe) and the recording started. In the second run, the measurement was taken under FC condition.

Figure 5-8 shows the temperature dependence of magnetization plot, at an applied field of 100 Oe, measured for the Ferucarbotran-loaded AD-MSC. The resulting plot shows a lower branch (ZFC) and an upper branch (FC). It can be clearly seen from the ZFC branch, raising temperature increases the magnetisation of the sample. However, above a certain temperature (around 135 K), the magnetization was decreasing. This transition shows a ferromagnetic behavior at low temperatures and superparamagnetism at higher temperature. The transition at low temperature named the blocking temperature *T*b that appear in the ZFC curve is a typical characteristic of superparamagnetic nanoparticles. At low temperatures, the nanoparticles are disoriented and frozen. Then the heating makes the nanoparticles more mobile, so they tend to orient themselves in the field, and reaching the maximum at the blocking temperature (*T*b). Upon further heating of the sample, the Brownian motion brings so much disorder that the nanoparticles start to move randomly and they disorient again, causing the magnetisation decreasing. Further, in cooling in a 100 Oe magnetic field, the magnetic moment of the sample will permanently increase, as shown by FC curve. Overall, this result demonstrates superparamagnetic behavior of Ferucarbotran-loaded AD-MSC at room temperature, suggesting AD-MSC were succesfully labelled with Ferucabotran magnetic nanoparticle.

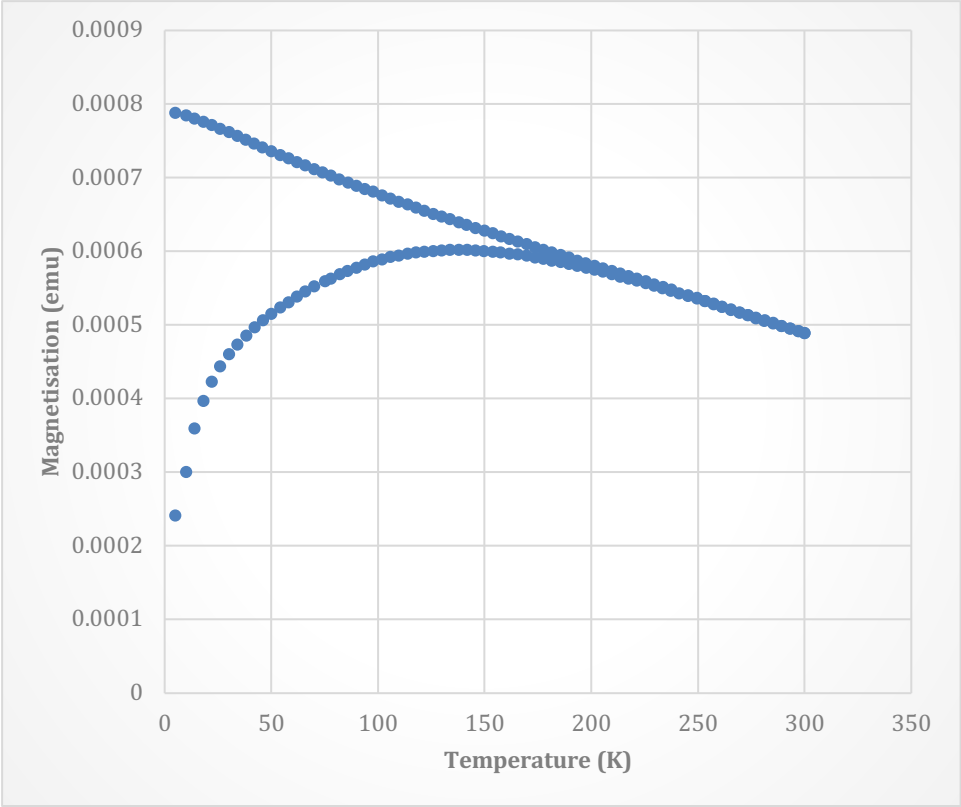

Figure 5-8. The M-T measurements in ZFC & FC mode under the field of 100 Oe in temperature range 5 K-300 K for Ferucarbotran-loaded AD-MSC sample*. The resulting plot displays a lower branch (ZFC) and an upper branch (FC) which indicates blocking temperature (Tb) reached at around 135 K. This transition at Tb demonstrates that Ferucarbotran-loaded AD-MSC has superparamagnetic behavior at higher temperature.*

Figure 5-9 shows the temperature dependence of magnetisation plot, at an applied field of 100 Oe, measured for the AD-MSC expressing *mms6* (blue lines) and wild-type AD-MSC as control (red lines). ZFC curves of both samples show no blocking temperature in the range of 5 to 400 K, confirming no superparamagnetic behavior detected on both samples. However, it can be seen that the magnetization of AD-MSC expressing *mms6* is higher than control, as indicated by higher position of the curve of AD-MSC expressing *mms6* (blue) compared to wild-type AD-MSC (red).

When cooling down from 400 K, both the ZFC and FC data follow similar trend, that is, slow increase of magnetisation until 60 K followed by a sharp rise. The ZFC and

FC curves from both samples are separated and continue to persist up to room temperature, indicating that the Curie temperature of the sample is expected to exceed 300 K. Note that the ZFC-FC curve separation gap of AD-MSC expressing *mms6* is a consequence of the large distribution of energy barriers, which can be associated with the particle size distribution. Most importantly, it can be clearly seen that the temperature-dependent magnetisation of AD-MSC expressing *mms6* (blue curve) is stronger than that of wild-type AD-MSC (red curve).

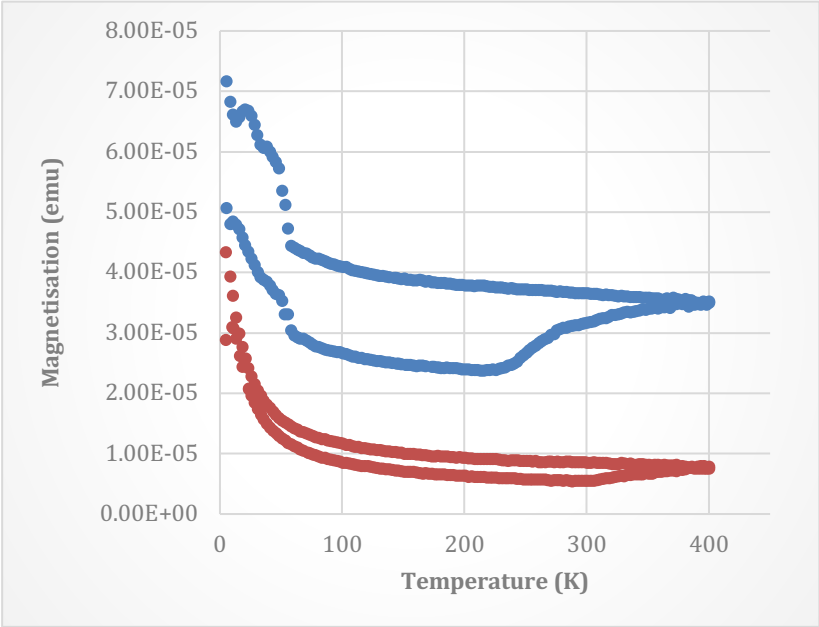

Figure 5-9:The M-T measurements in ZFC & FC mode under the field of 100 Oe in temperature range 5 K-400 K for AD-MSC expressing mms6 (blue) and wild-type AD-MSC (red). *Blocking temperature in the range of 5 to 400 K was not detected on both AD-MSC expressing mms6 and control cells, confirming no superparamagnetic behavior observed on AD-MSC expressing mms6.*

Overall, the magnetic measurement based on ZFC-FC indicate two important results: 1) the existence of room temperature ferromagnetism of both AD-MSC expressing *mms6* and control cells. This is likely to be due to the incubation of both cell samples in FeQ doped medium 2) The temperature-dependent magnetisation of AD-MSC expressing *mms6* is stronger than that of wild-type AD-MSC, revealing the expression of *mms6* may improve iron binding ability of the cells, which then increased the ferromagnetism of the cells.

5.10 DISCUSSION

In this chapter, it was determined if:

1. The *mms6* expression of AD-MSC could cause any detrimental effect on the cells by investigating MSC stemness and MSC differentiation potential.
2. The *mms6* expression of AD-MSC could promote iron binding in order to produce magnetic nanoparticles inside the cells.
3. The *mms6* expression of AD-MSC could generate a magnetic behavior similar to commercial MNP or magnetosomes in MTB.

Regarding the point 1, immunofluorescence experiments revealed no observable difference between AD-MSC expressing *mms6* and control cells. It was observed the expression of *mms6* did not alter the presentation of typical surface antigens on human MSC. Both cell groups were positive for the typical MSC markers CD44 and CD90, and negative for CD14 and CD19. In addition, both AD-MSC expressing *mms6* and control cells showed a similar differentiation capacity into adipogenic and osteogenic lineages. Adipogenesis was demonstrated by the accumulation of lipid vacuoles after 10 days of adipogenesis induction, indicated by a positive Oil Red O staining. In addition, Alizarin red staining also confirmed osteogenic differentiation after 21 days of osteogenic induction.

A previous study has shown that differentiation of MSC is affected with increasing MNP dose (Henning *et al*., 2009). Confirming this finding, a study using Citrate SPIONs for magnetic labeling of human MSC bu Andreas and coworkers (2012) indicated that the nanoparticle labeling did not affect cell proliferation, presentation of typical cell surface marker antigens and differentiation into the adipogenic and osteogenic lineages. However, chondrogenic differentiation and chemotaxis were significantly impaired with increasing SPIONs incorporation (Andreas *et al*., 2012). Hence, in this chapter, the investigation of MSC stemness and differentiation potential was also crucial to assess whether such genetic modification for inducing magnetic

nanoparticles synthesize in AD-MSC could alter the functionality of cells. Overall, the results show that the MSC stemness and multipotency are unaffected by the expression of this magnetobacterial genes

Regarding point 2, a separate investigation on iron-based MNP was also performed before performing TEM analysis for both AD-MSC expressing *mms6* and iron-based MNP-loaded AD-MSC. A prior study by Kasten et al (2014) has suggested AD-MSC can be labelled with iron-based MNP. In their study, AD-MSC were loaded with bionized nanoferrite (BNF) starch and Nanomag®-D-spio and differentiated into adipogenic lineage. The result showed the successful *in vivo* MRI visualization of magnetically labeled AD-MSC seeded onto collagen scaffolds for adipose tissue engineering in a SCID mice model (Kasten *et al.*, 2014).

A further study looking at potential use of MSC as cellular therapy for vascular injury also showed successful MSC labelling with FluidMAG and Ferucarbotran nanoparticles (Riegler *et al.*, 2013). The study revealed that MSC labelled with MNP increased cell retention after balloon angioplasty leading to reduced restenosis in a rabbit model. A recent study by Kalber et al (2016) also demonstrated that MSC can be used as carriers of Ferucarbotran MNP, that following an injection into tumour in a mouse model, these labeled MSC can be retained in the tumour tissue over a matter of weeks before a magnetic hyperthermia treatment. Indeed, Ferucarbotran has recently been used in a number of hyperthermia studies (Araya, T, 2013; Kalber *et al*., 2016; Sato, I., 2014). Most importantly, a study by Kallumadil *et al.* (2009) in investigating a number of commercial colloids for magnetic hyperthermia also suggested three best magnetic fluids in terms of magnetic heating capability, which were Nanomag-D-Spio 100 nm, FluidMAG-D 50 nm and Resovist Carboxydextran or Ferucarbotran (Kallumadil *et al.*, 2009).

Taken together all the evidence above, several commercial iron-based MNP NanoMAG-D-Spio, BNF-Dextran, FluigMAG-CT and Ferucarbotran nanoparticles were investigated in this study. Firstly, since their stability in culture medium is a crucial factor affecting their further use, the colloidal stability of each of these MNP was measured. Turbidity measurement revealed only Ferucabotran and FluidMAG-

CT were stable over 24 hours. In contrast, Nanomag-D-Spio and BNF-Dextran showed an increase of turbidity of the medium, suggesting they are not colloidally stable in the medium culture. The use of both MNP also raised technical issue during MNP-loaded AD-MSC experiments. There is a high likelihood that the increasing turbidity over time was due to MNP in contract with FBS or protein-containing media. This interaction could generate protein corona and form larger aggregates of MNP, as opposed to in PBS (Gorshkov *et al.*, 2019). Therefore, Feruarbotran and FluigMAG-CT were then used in the later experiments.

The cell viability analysis was performed on FluidMAG-CT-loaded and Ferucabotran-loaded AD-MSC. The result indicated that AD-MSC cell viability was dramatically lower with increasing FluidMAG nanoparticle concentration. Despite the result showing that Ferucarbotran nanoparticles at concentration higher than 250 µg/ml was statistically affected the cell viability, only slight decrease was observed even up to 1000 µg/ml concentration compared to the FluidMAG-CT sample. In good agreement with this result, a previous report suggested that the amount of iron in living cells is remarkably increased by increasing the concentration of carboxy-dextran MNP in the cell culture media and no toxicity was noticed up to 250 µg Fe/ml (Mahmoudi *et al.*, 2011). In contrast, a contradictive study has shown that the labeling of Ferucarotran nanoparticles is advantageous to stem cell growth. The study showed that instead of inducing cellular toxicity, the Ferucarbotran can accelerate cell cycle progression and promote cell growth which likely due to its ability to diminish intracellular H_2O_2 through intrinsic peroxidase-like activity (Huang *et al.*, 2009). For this reason, Ferucarbotran nanoparticles were chosen for subsequent experiments as it was expected that the MNP should be non-toxic and can be retained within cells before magnetic hyperthermia treatment.

Ferucarbotran MNP used in this study is similar to the dextran-coated Endorem and carboxydextran-coated Resovist MNP, which are the most commonly used MNP as MRI contrast agent and are clinically applied for liver and spleen imaging by MRI. These nanoparticles have range of 50-200 nm size, which are easily phagocyted by

Kupffer cells of the reticuloendothelial system (RES) upon intravenous administration (Reimer and Balzer, 2003).

To investigate the Ferucarbotran nanoparticles uptake of AD-MSC, Prussian blue staining was conducted. The result showed blue-colored granules inside the cells, revealing the presence of iron and the ability of nanoparticle internalisation by AD-MSC. This result agrees with a numerous studies that showed MSC can be labelled with Ferucarbotran after overnight incubation without the need of transfection reagent, and can be visually detected by Prussian blue staining (Mailänder *et al.*, 2008; Bauer *et al.*, 2009; Henning *et al.*, 2009; Yang *et al.*, 2009; Kalber *et al.*, 2016). The presence of carboxyl groups in Ferucarbotran structure was known increases the cellular uptake as compared with non-functionalized MNP (Mahmoudi *et al.*, 2011).

Further investigation on nanoparticles cellular uptake of Ferucarbotran-loaded AD-MSC showed accumulation of membrane-bound, intracytoplasmic electron-dense nanoparticles identified by TEM. Similar electro-dense material was also found in both AD-MSC stably expressing *mms6* after lentiviral transduction and AD-MSC transiently expressing *mms6* after nucleofection with Mag01 or Mag03. Although the number of nanoparticles formed inside the cells were not deeply quantified or analysed in this study, by visual inspection the electro-dense material in AD-MSC stably expressing *mms6* appeared to look denser than the nucleofected ones. This may be possible due to the stable expression of *mms6* which may induce more iron binding during 10 days of cell incubation with FeQ doped medium.

In agreement with this result, a previous study by Elfick *et al.* (2017) has shown that bone marrow-derived MSC expressing *mms6* and *mmsF genes* contain vesicles filled with both dispersed and larger electron-dense material. Image analysis studies show an increase in the amount of electron-dense material within cytoplasmic vesicles of *mms6* transfected cells from day 10 to day 15 (Elfick *et al.*, 2017). In addition, Zhang et al (2014), using a gliosarcoma cell line stably expressing *mms6,* showed 3 types nanoparticle distribution within cells after 3 days incubation in ferric citrate doped medium: 1) Some clusters of nanoparticles within membrane-enclosed structures, 2)

few clusters of nanoparticles without membrane enclosures, and 3) few scattered nanoparticles throughout the cytoplasm.

Although the mechanism of formation those nanoparticle clusters remains unclear, the intracellular membrane-enclosed structures are likely endosomes or lysosomes in which waste materials are disposed (Pieber *et al.*, 2009). Furthermore, the distribution of nanoparticle clusters formed in AD-MSC expressing *mms6* appeared to look the same as the AD-MSC loaded with Ferucarbotran. Studies using carboxydextran Resovist demonstrated that the nanoparticle clusters were not found in the cell core, Golgi or mitochondria, and were found only localized in intracellular compartments resembling endosomes of MSC (Mailänder *et al.*, 2008). Other TEM analysis of human MSC loaded with Citrate SPIONs study also displayed internalization into endosomes suggesting an endocytotic uptake mechanism (Andreas *et al.*, 2012).

Regarding point 3, the magnetic measurement based on ZFC-FC demonstrated a strong ferromagnetic behavior of AD-MSC expressing *mms6*. The temperature-dependent magnetisation of AD-MSC expressing *mms6* was stronger than that of untransfected AD-MSC control cells, indicating the expression of *mms6* may promote iron binding ability of the cells, which then increased the ferromagnetism of the cells. In contrast, the magnetic measurement on Ferucarbotran-loaded AD-MSC displayed a superparamagnetic behavior, confirming different magnetic properties between AD-MSC expressing *mms6* and Ferucabotran-loaded AD-MSC.

A study comparing the magnetic properties of MNP modified with amino silane with bacterial magnetosomes revealed that synthetic MNP show superparamagnetic characteristics while magnetosomes are ferromagnetic. The study suggested that the different magnetic properties of magnetosomes and MNP may be largely due to their different size (R.-T. Liu *et al.*, 2012). The large sizes of magnetosome result in a ferromagnetic behavior at physiological temperature, while the SPION of sizes below 20 nm are superparamagnetic at this temperature. (Arakaki et al., 2008; Alphandéry et al., 2010). The ferromagnetic behaviour displayed by AD-MSC expressing *mms6* could mean that the Mms6 protein binds iron and form a bigger nanocrystal aggregates, instead of smaller superparamagnetic nanocrystal. It should be also underlined that the

Mms6 alone would not be able to synthesise ferromagnetic magnetosome structure similar to the one in MTB.

Despite the ferromagnetic properties of bacterial magnetosomes, numerous studies have attempted to synthesize superparamagnetic nanoparticle using Mms6 protein (Prozorov *et al.*, 2007; Wang *et al.*, 2012; Feng *et al.*, 2013). It was demonstrated that Mms6 binds iron in order to form superparamagentic nanoparticles in vitro (Wang *et al.*, 2012). The high affinity for iron ions and negative charges of the Mms6 protein was believed give the protein a unique ability to self-assemble, making it a key regulator of crystal size and morphology (Arakaki *et al.*, 2010, 2014).

A study by Prozorov *et al.* showed the Mms6 protein-mediated nanoparticle synthesis was found to be able to promote shape-selective formation of uniform superparamagnetic nanocrystals. In their study, recombinant Mms6 facilitates formation of single-domain, uniform magnetite nanocrystals in solution, as confirmed by using TEM and magnetization analysis. In contrast, the nanoparticles formed in the presence of iron binding protein such as mammalian ferritin, lipocalin, and bovine serum albumin, do not exhibit the uniform sizes and shapes observed for those formed in the presence of Mms6. Most importantly, Mms6 protein-mediated synthesis magnetite nanoparticles displayed the largest magnetization values above the blocking temperature, as well as the largest magnetic susceptibility compared to those of the nanomaterials synthesized with other proteins (Prozorov *et al.*, 2007).

It should be underlined that MNP for the use in biomedical applications are preferable to have superparamagnetic properties (SPIONs) (Corot *et al.*, 2006; Markides *et al.*, 2012; Ludwig *et al.*, 2014b). SPIONs are typically small particles composed of either a magnetite (Fe_3O_4) or maghemite (γ-Fe_2O_3) core coated with a biocompatible organic/inorganic polymer (Pardoe *et al.*, 2001; Mahmoudi *et al.*, 2010). Both maghemite and magnetite are commonly ferromagnetic in nature. However, they lose their permanent magnetism and become superparamagnetic when they decrease in size to 30nm or smaller (Mahmoudi *et al.*, 2011). For biomedical application, it was suggested that the superparamagnetic properties may prevent the nanoparticles to not

be attracted each other, thus the risk of agglomeration in a its medical use could be avoided (Markides *et al.*, 2012).

The mechanism by which *mms6*, as a single gene, is able to provide the human AD-MSC with magnetic properties is still not well understood. However, there are some specific properties of the Mms6 protein which could justify its ability to confer such fascinating properties to the cells. Mms6 was described as a protein able to bind iron and generate uniform magnetic crystals with a high affinity for iron ions and bearing negative charges which give to the protein the peculiar ability to self-assemble (Prozorov *et al.*, 2007). Moreover, Mms6 is not the only protein able to generate magnetic properties to mammalian cells. Previous work expressing *MagA* in mammalian cells also showed the ability to increase the iron retention and to create magnetic structures inside mouse and human cancer cells, as well as in human embryonal kidney cell line. The magnetic structures generated by *MagA* in the cells produced contrast at MRI of 11T, suggesting the gene has a potential use as reporter gene for MRI applications (Zurkiya *et al.*, 2008; Goldhawk *et al.*, 2009). Therefore, all of these evidence support the idea that a single gene could be sufficient to generate magnetic properties to mammalian cells.

In summary, this chapter have demonstrated that the expression *mms6* gene could promote the intracytoplasmic vesicles formation in AD-MSC, which contain magnetic nanocrystal material. Most importantly, the expression of this bacterial gene does not affect cells stemness, proliferation and differentiation ability. Morever, the nanocrystal in AD-MSC expressing *mms6* appeared to showed a ferromagnetic behaviour. In addition, AD-MSC was also successfully labelled with commercial iron-based Ferucarbotran-loaded AD-MSC, and showed a superparamagnetic characteristic. Further investigation in the use of these cells in MRI and MNHT application will be discussed in Chapter 6.

6 *IN VITRO* APPLICATION OF ALTERNATING MAGNETIC FIELD ON AD-MSC EXPRESSING *mms6*.

6.1 SUMMARY

The hypothesis underlying this study was that the nanoparticles produced inside AD-MSC expressing *mms6* could induce cell cytotoxicity or cell death when the cells are exposed to an alternating magnetic field (AMF). It is expected that in its biomedical application, when the AD-MSC have successfully homed to tumours, the magnetic hyperthermia application would activate the nanoparticle-mediated cell death mechanism. Hence it could cause the death of the neighbouring cancer cells or induce an antitumour immune response.

To test this concept, this chapter is focusing on *in vitro* application of an alternating magnetic field (AMF) to AD-MSC expressing *mms6*. To conduct this study, a MagneTherm^{TM} device was used to create an *in vitro* model of magnetic hyperthermia application. The device is specifically designed for nanoparticle heating applications, operating within with a wide frequency range from 100 kHz to 1MHz.

In this chapter, the two important questions I address are the following: 1) could the interaction between nanoparticles produced inside the AD-MSC expressing *mms6* and AMF application have a magnetic hyperthermia effect? 2) Can I achieve the desired magnetic hyperthermia effect at three different AMF frequencies of 178.3 kHz (23.89 mT), 540 kHz (24.87 mT), and 1030 kHz (13.37 mT). To answer these questions, AD-MSC cell viability, cell apoptosis and HSP70 expression following the AMF application were investigated.

In chapter 5, it was observed that Ferucarbotran-loaded AD-MSC have superparamagnetic behavior, while AD-MSC expressing *mms6* has Feromagnetic behavior. Therefore, the magnetic hyperthermia effect of AMF application on Ferucarbotran-loaded AD-MSC was also determined. This was important since the heating capacity of magnetic nanoparticles will vary, depending on size, shape and material properties (Ludwig *et al.*, 2014a; Patsula *et al.*, 2016).

The magnetic hyperthermia effect of the AMF on cell viability was assessed using the AlamarBlue Cell Viability assay. For this, cells were arranged in two experimental designs: 1) AMF application on cells in 2-D monolayer model as cells arranged in a Petri dish, 2) in attempt to create an *in vitro* model of an *in vivo* situation, AMF application on cells in a 3-D model were performed. Furthermore, to determine the AMF effect on cell apoptosis, In Situ Apoptosis Detection was conducted using The Click-iT Plus TUNEL assay. For HSP70 expression analysis, a western blot assay was conducted.

In order to investigate whether the nanoparticles created in AD-MSC expressing *mms6* could be utilized as contrast agent for magnetic resonance imaging (MRI), an *in vitro* model of MRI experiment was also performed. In this experiment, the following AD-MSC were used for the MRI analyses: 1) Mag01-transfected AD-MSC, 2) Mag03-transfected AD-MSC 3) lentiviral-*mms6* tranduced AD-MSC and 4) Ferucarbotran-loaded AD-MSC. This experiment may elucidate the future potential use of cells expressing *mms6* for MRI detection or cell tracking.

6.2 AIMS

The aims of the experiments detailed in this chapter were:

1. To investigate the effect of AMF on cell viability of AD-MSC expressing *mms6* and Ferucarbotran-loaded AD-MSC arranged in 2-D and 3-D culture.
2. To investigate the effect of AMF application on cell apoptosis and HSP70 expression of AD-MSC expressing *mms6*.
3. To demonstrate the potential use of AD-MSC expressing *mms6* in magnetic resonance (MR) imaging.

6.3 HEATING CAPACITY OF FERUCARBOTRAN NANOPARTICLE.

In this study, the heating capacity of free Ferucabotran nanoparticles in colloid under different frequencies of AMF was performed. Previous report has shown Ferucarbotran MNP (Resovist) have higher magnetic heating capability compared to several MNP manufactured by Chemicell and Micromod. Intrinsic loss power (ILP) measurement of 28 mg/mL Fe concentration of Ferucarbotran (60nm) showed ILP value of 3.1 nHm^2/kg (Kallumadil *et al.*, 2009). Furthermore, specific absorption rate (SAR) measurement, which is dependent on the field amplitude and frequency, indicated Ferucarbotran have 90 W/g SAR value under 5.7 kA/m field amplitude and 900 kHz frequency (Blanco-Andujar *et al.*, 2016).

The main goal of this experiment was to demonstrate the interaction between AMF and free Ferucabotran nanoparticles in rising the temperature of nanoparticle suspension. This was also important particularly to test whether the MagneTherm™ device is suitable for this *in vitro* magnetic hyperthermia (MH) experiment in this study and to provide a positive control for future experiments with *mms-6* expressing cells.

For this, three group samples of Ferucarbotran nanoparticle suspensions were prepared in microcentrifuge tubes. Each tube contains 5 mg/ml of Ferucarbotran nanoparticle in 500 µl sterile water. Each sample was then exposed for 50 minutes, each with three different frequencies of AMF: 178.3 kHz (23.89 mT), 540 kHz (24.87 mT), and 1030 kHz (13.37 mT). The samples were exposed under AMF for 40 minutes then allowed to rest in the MagneTherm™ device without AMF for a further 10 minutes. The temperature changes during the experiment were recorded every 5 minutes using a Fibre Optic Probe and USB data logging Temperature sensor (MagneTherm™) allowing data capture of the sample temperature. The experiment was repeated three times.

As shown in Figure 6-1, all samples showed temperature increase as soon as samples were exposed to AMF. In Ferucarbotran suspension exposed under 178.3 kHz AMF, the temperature goes up from 25.8±1.2 °C to 38.5±1.0 °C in 20 minutes. The maximum

temperature hits 40.2±0.8 at 40 minutes before going down to 33.8±1.5 after the AMF was turned off. Similar temperature profile was also shown in sample exposed to 1030 kHz, which showed temperature raising from 26.2±0.6 °C to 39.8±0.3 °C in just 10 minutes. The maximum temperature hits 43.5±0.9 °C at 35 minutes time point before going down to 34±0.9 °C when the AMF exposure has stopped. For 540 kHz AMF, the Ferucarbotran nanoparticles generates a temperature rise from 26.2±3.1 °C to 51.7±31.9 °C in just 5 minutes. Afterwards, the temperature continues to rise up to 67.5±1.3 °C at 40 minutes, then goes down to 49.5±2.8 °C in the end.

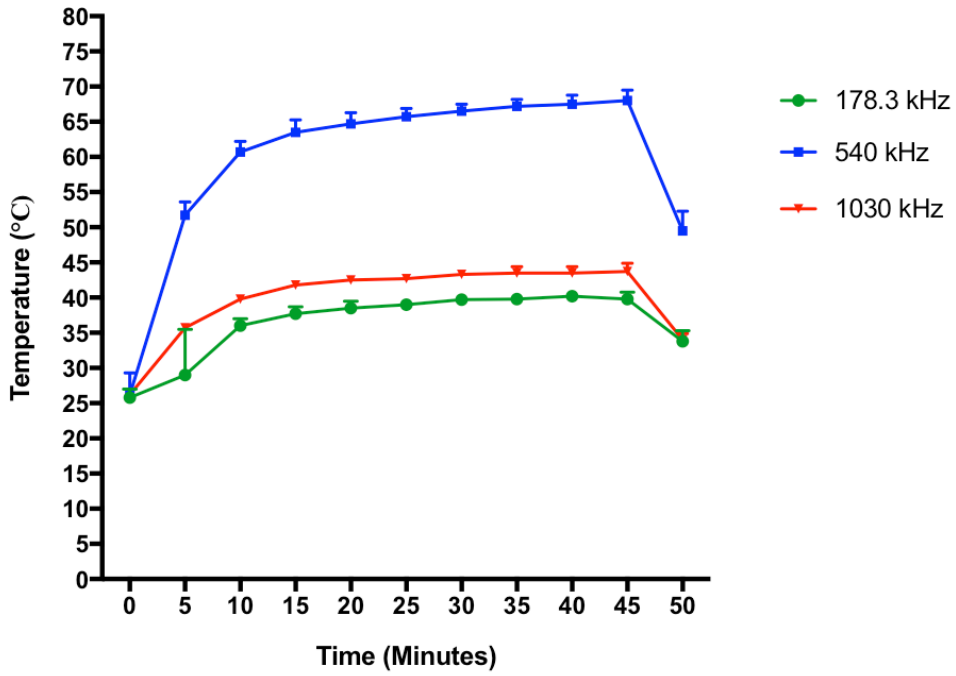

Figure 6-1: Temperature profile of Ferucarbotran nanoparticle. *Temperature measurement analysis showing the temperature increase of Ferucarbotran nanoparticle suspension over 40 minutes of AMF exposure. Ferucarbotran suspension samples were exposed to 178.3 kHz (green line), 540 kHz (blue line), and 1030 kHz (red line). Values are presented as mean ± SD. N=3*

In general, the experiment successfully demonstrated the heating capacity of free Ferucarbotran nanoparticles under AMF application in the MagneTherm™ device. The result was important to demonstrate that the MagneTherm™ device was suitable

to be used in this *in vitro* magnetic hyperthermia (MH) study. All the samples showed the temperature rise above physiological temperature when they were exposed to 178.3 kHz, 540 kHz, and 1030 kHz of AMF.

The highest temperature was shown in sample exposed to 540 kHz AMF with a temperature value over 60 °C for less than an hour of AMF exposure. This was likely due to this particular setting generate the highest magnetic field which was 24.87 mT, compared to 23.89 mT and 13.37 mT generated by 178.3 kHz and 1030 kHz setting, respectively.

However, the ultimate aim of the study was to use the AD-MSC as a cell delivery system to deliver magnetic nanoparticles instead of using free magnetic nanoparticles. Therefore, it was still not clear whether the nanoparticles inside the cells would give similar heating capacity as the free nanoparticle in colloid suspension. Indeed, it would have been better to measure the temperature of Ferucarbotran-loaded AD-MSC rather than the free Ferucarbotran nanoparticles. However, due to the lack of instrument specifically measuring cell temperature, the experiment was not possible to be done.

6.4 THE EFFECT OF ALTERNATING MAGNETIC FIELD ON FERUCARBOTRAN-LOADED AD-MSC ARRANGED IN 2-D CULTURE.

To determine the effect of AMF on Ferucarbotran-loaded AD-MSC arranged in 2-D monolayer culture, Ferucarbotran-loaded AD-MSC were exposed in three different frequency of AMF: 178.3 kHz (23.89 mT), 540 kHz (24.87 mT), and 1030 kHz (13.37 mT). The effect of the AMF on AD-MSC cell viability was then determined with AlamarBlue Cell Viability Assay.

6.4.1 Cell viability analysis of Ferucarbotran-loaded AD-MSC in 2-D culture following one-hour exposure of 178.3 kHz AMF.

For 2-D monolayer culture, AD-MSC were seeded in Petri dishes and incubated 37 °C CO_2 incubator for overnight. Cells were then loaded with 500 ug/ml Ferucarbotran in

culture medium and incubated overnight in 37 °C CO_2 incubator. On the next day, the medium was then removed and replaced with fresh culture medium. Cells were then exposed to 178.3 kHz AMF for one hour. Ferucabotran-loaded AD-MSC exposed to 0 kHz AMF (cells placed in MagneTherm^{TM} device without AMF) were used as control. After the exposure, cells were then incubated in 37°C CO_2 incubator for overnight. The cell viability was then determined with Alamar Blue Cell Viability Assay. The experiment was run in triplicate and repeated three times.

The result of this experiment is illustrated in Figure 6-2, where the fluorescence intensity average values registered for the exposed cells was 6114±365, while for control was 6181±360. Cell viability percentage of exposed cells was calculated as a ratio between AMF exposed cells and controls cells, and it is shown in considering controls as 100% viable. The result reveals that the viability of AMF exposed cells was 99.58±0.66% of that of controls and not statistically significant. This result confirmed that the 178.3 kHz of AMF application on the Ferucarbotran-loaded AD-MSC arranged in a 2-D monolayer culture leads to no cytotoxicity effect.

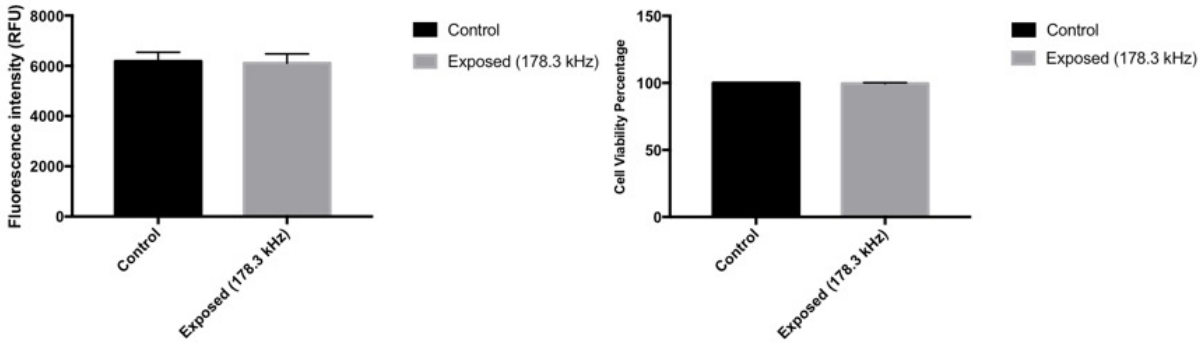

Figure 6-2: Cell Viability of Ferucarbotran-loaded AD-MSC in 2-D culture following one-hour exposure of 178.3 kHz AMF. *Ferucarbotran-loaded AD-MSC cell were exposed to 178.3 kHz (grey column) or exposed to 0 kHz as control (black column). AlamarBlue data showing average of fluorescence intensity of cells following AMF exposure (left panel) and average of cell viability percentage of exposed cells against controls (right panel). Values are presented as mean ± SD. N=3*

6.4.2 Cell viability analysis of Ferucarbotran-loaded AD-MSC in 2-D culture following one-hour exposure of 540 kHz AMF.

AD-MSC were seeded in Petri dishes and incubated 37 °C CO_2 incubator for overnight. Cells were then loaded with 500 µg/ml Ferucarbotran nanoparticle in culture medium and incubated overnight in 37 °C CO_2 incubator. On the next day, the medium was then removed and replaced with fresh culture medium. Cells were then exposed to 540 kHz AMF for one hour. Ferucabotran-loaded AD-MSC placed in MagneTherm™ device without AMF application for one hour were used as control. After the exposure, cells were then incubated in 37 °C CO_2 incubator for overnight. The cell viability was then determined with AlamarBlue Cell Viability Assay. The experiment was run in triplicate and repeated at least three times.

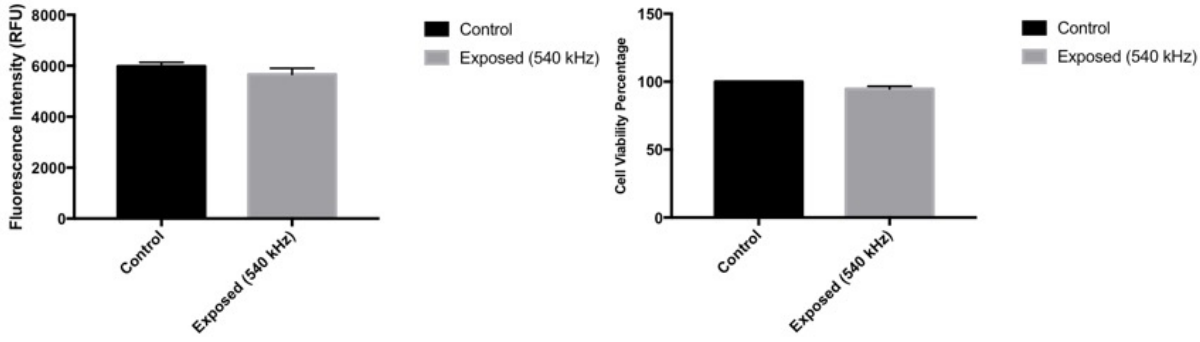

Figure 6-3: Cell viability of Ferucarbotran-loaded AD-MSC in 2-D culture following one-hour exposure of 540 kHz AMF*. Ferucarbotran-loaded AD-MSC cell were exposed to 540 kHz (grey column) or exposed to 0 kHz as control (black column). AlamarBlue data showing average of fluorescence intensity of cells following AMF exposure (left panel) and average of cell viability percentage of exposed cells against controls (right panel). Values are presented as mean ± SD. N=3*

The result of this experiment is illustrated in Figure 6-3, where the fluorescence intensity average values registered for the exposed cells was 5665±235, while for control was 5984±153. Cell viability percentage of exposed cells was calculated as a ratio between AMF exposed cells and controls cells, and it is shown in considering controls as 100% viable. The result indicated that the viability of AMF exposed cells

was 94.65±2.03% of that of controls and not statistically significant. This result confirmed that the 540 kHz AMF exposure on the Ferucarbotran-loaded AD-MSC arranged in 2-D monolayer culture does not have an effect on AD-MSC cell viability.

6.4.3 Cell viability analysis of Ferucarbotran-loaded AD-MSC in 2-D culture following one-hour exposure 1030 kHz AMF.

AD-MSC were seeded in Petri dishes and incubated 37 °C CO_2 incubator for overnight. Cells were then loaded with 500 ug/ml Ferucarbotran nanoparticle in culture medium and incubated overnight in 37 °C CO_2 incubator. On the next day, the medium was then removed and replaced with fresh culture medium. Cells were then exposed to 1030 kHz AMF for one hour. Ferucabotran-loaded AD-MSC exposed to 0 kHz AMF for one hour were used as control. After the exposure, cells were then incubated in 37°C CO_2 incubator for overnight. The cell viability was then determined with Alamar Blue Cell Viability Assay. The experiment was run in triplicate and repeated three times.

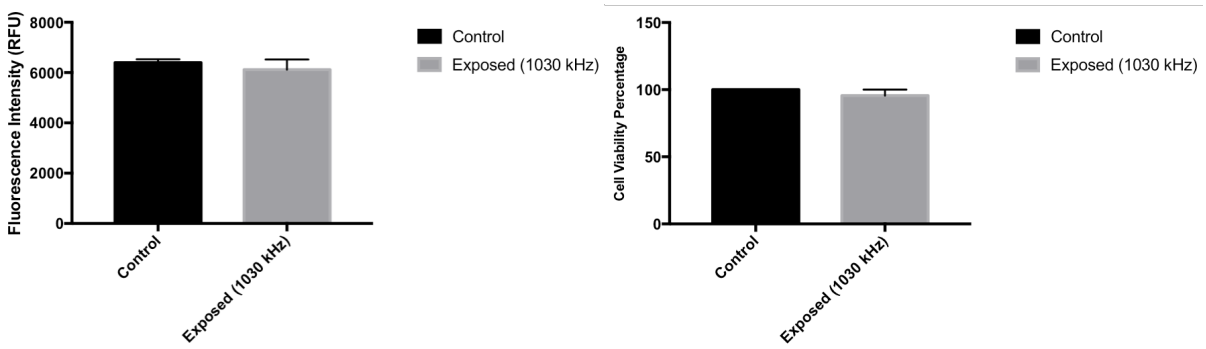

Figure 6-4: Cell viability of Ferucarbotran-loaded AD-MSC in 2-D culture following one-hour exposure of 1030 kHz AMF*. Ferucarbotran-loaded AD-MSC cell were exposed to 1030 kHz (grey column) or exposed to 0 kHz as control (black column). AlamarBlue data showing average of fluorescence intensity of cells following AMF exposure (left panel) and average of cell viability percentage of exposed cells against controls (right panel). Values are presented as mean ± SD. N=3*

The result of this experiment is illustrated in Figure 6-4, where the fluorescence intensity average values registered for the exposed cells is 6120±406, while for control is 6397±133. Cell viability percentage of exposed cells was calculated as a ratio between AMF exposed cells and controls cells, and it is shown in considering controls as 100% viable. This result demonstrated that the viability of AMF exposed cells was 95.5±4.4% of that of controls and not statistically significant. The experiment failed to show a magnetic hyperthermia effect on cell viability even using a higher frequency (1030 kHz) of AMF on Ferucarbotran-loaded AD-MSC.

6.5 THE EFFECT OF ALTERNATING MAGNETIC FIELD ON AD-MSC EXPRESSING *mms6* IN 2-D CULTURE.

To determine the effect of AMF on AD-MSC expressing *mms6* arranged in 2-D monolayer culture, three group of cells were exposed in three different frequencies of AMF: 178.3 kHz (23.89 mT), 540 kHz (24.87 mT), and 1030 kHz (13.37 mT). The effect of the AMF on cell viability was then determined with AlamarBlue Cell Viability Assay.

6.5.1 Cell viability analysis of AD-MSC expressing *mms6* in 2-D culture following one-hour exposure of 178 kHz AMF.

AD-MSC expressing *mms6* were cultured in medium doped with FeQ (34 μM) for 10 days in cell culture flask. Afterwards, the cells were then collected and seeded in Petri dishes in a 2-D monolayer culture and incubated in 37°C CO_2 incubator for overnight. In the following day, cells in the Petri dishes were exposed under 178 kHz of AMF for one hour. AD-MSC expressing *mms6* exposed to 0 kHz AMF for one hour were used as control. After the AMF application, cells were then incubated in 37°C CO_2 incubator for overnight. In the next day, the cell viability was then determined using AlamarBlue Cell Viability Assay.

The result of the experiment is illustrated in Figure 6-5, where the fluorescence intensity average values registered for the exposed cells is 6591±523, while for control is 7063±315. Cell viability percentage of exposed cells was calculated as a ratio between AMF exposed cells and controls cells, and it is shown in considering controls as 100% viable. The result reveals that the viability of AMF exposed cells was 93.24±3.79% of that of controls and not statistically significant. This result confirms that the low frequency (178.3 kHz) of AMF application on the AD-MSC expressing *mms6* arranged in 2-D monolayer culture does not have an effect on AD-MSC cell viability.

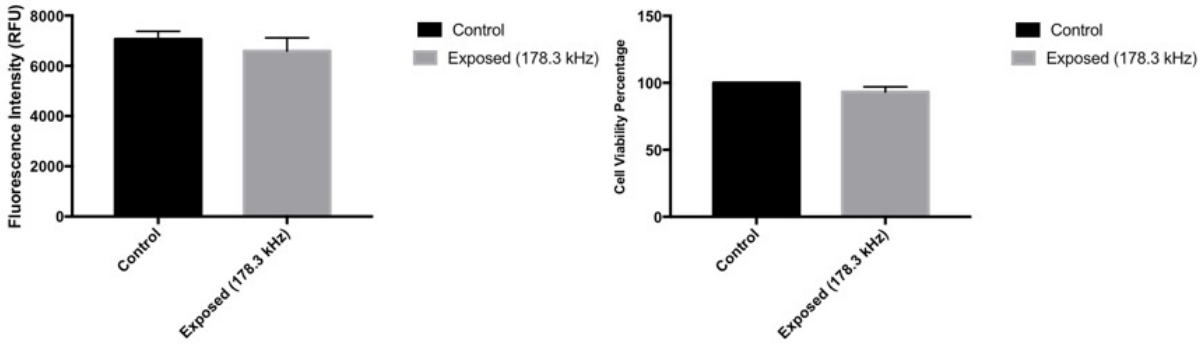

Figure 6-5: Cell viability of AD-MSC expressing mms6 in 2-D culture following one-hour exposure of 178.3 kHz AMF*. AD-MSC expressing mms6 cell were exposed to 178.3 kHz (grey column) or exposed to 0 kHz as control (black column). AlamarBlue data showing average of fluorescence intensity of cells following AMF exposure (left panel) and average of cell viability percentage of exposed cells against controls (right panel). Values are presented as mean ± SD. N=3*

6.5.2 Cell viability analysis of AD-MSC expressing *mms6* in 2-D culture following one-hour exposure of 540 kHz AMF.

AD-MSC expressing *mms6* were cultured in medium doped with FeQ (34 μM) for 10 days in cell culture flask. The cells were then collected and seeded in Petri dishes in a 2-D monolayer culture and incubated in 37°C CO_2 incubator for overnight. In the following day, cells were exposed with 540 kHz AMF for one hour. AD-MSC

expressing *mms6* exposed to 0 kHz AMF for one hour were used as control. After the exposure, cells were then incubated in 37°C CO_2 incubator. In the following day, the cell viability was then determined with AlamarBlue Cell Viability Assay.

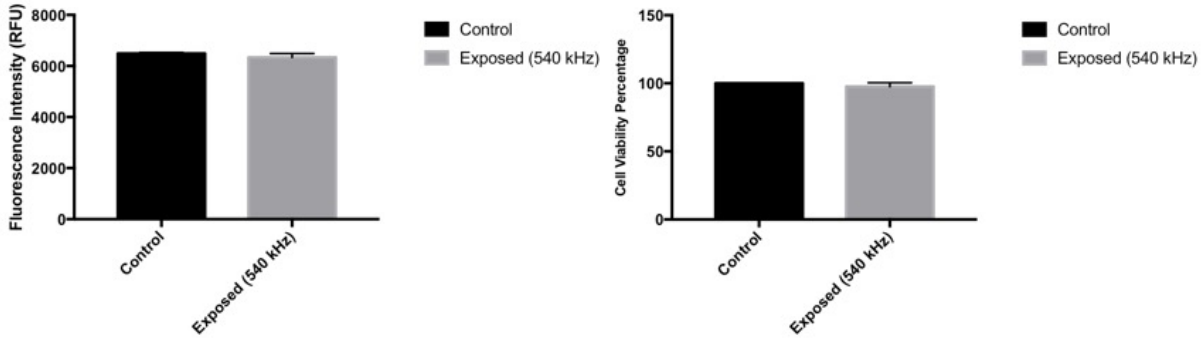

Figure 6-6: Cell viability of AD-MSC expressing mms6 in 2-D culture following one-hour exposure of 540 kHz AMF*. AD-MSC expressing mms6 cell were exposed to 540 kHz (grey column) or exposed to 0 kHz as control (black column). AlamarBlue data showing average of fluorescence intensity of cells following AMF exposure (left panel) and average of cell viability percentage of exposed cells against controls (right panel). Values are presented as mean ± SD. N=3*

The result of this experiment is illustrated in Figure 6-6, where the fluorescence intensity average values registered for the exposed cells is 6334±158, while for control is 6489±39. Cell viability percentage of exposed cells was calculated as a ratio between AMF exposed cells and controls cells, and it is shown in considering controls as 100% viable. It was noticed that the viability of AMF exposed cells was 97.62±2.79% of that of controls. No significance difference was observed between exposed and control group. Thus, this result confirmed that 540 kHz AMF application does not generate cell cytotoxicity on AD-MSC expressing *mms6* arranged in 2-D monolayer culture.

6.5.3 Cell viability analysis of AD-MSC expressing *mms6* in 2-D culture following one-hour exposure of 1030 kHz AMF.

AD-MSC expressing *mms6* were cultured in medium doped with FeQ (34 μM) for 10 days in cell culture flask. The cells were then collected and seeded in Petri dishes in a 2-D monolayer culture and incubated in 37°C CO_2 incubator for overnight. In the following day, cells were exposed at low frequency of AMF (1030 kHz) for one hour. AD-MSC expressing *mms6* exposed to 0 kHz AMF for one hour were used as control. After the exposure, cells were then incubated in 37°C CO_2 incubator. Following one day of incubation, the cell viability was then determined with AlamarBlue Cell Viability Assay.

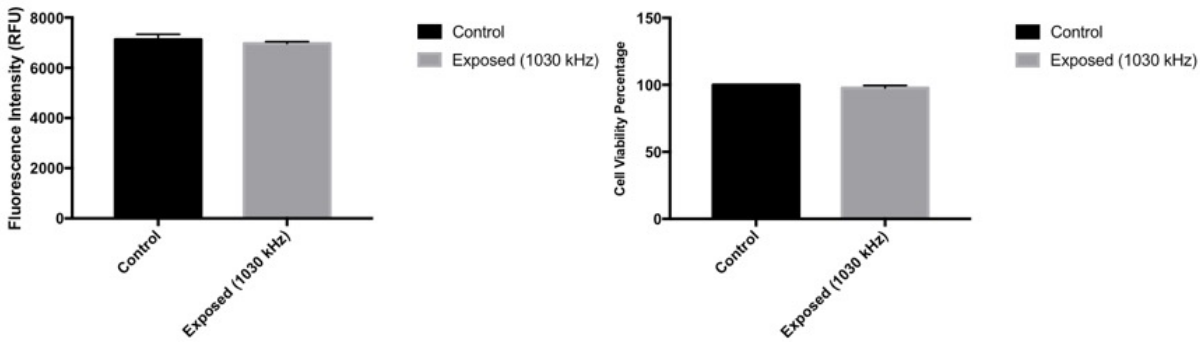

Figure 6-7: Cell viability of AD-MSC expressing mms6 in 2-D culture following one-hour exposure of 1030 kHz AMF*. AD-MSC expressing mms6 cell were exposed to 1030 kHz (grey column) or exposed to 0 kHz as control (black column). AlamarBlue data showing average of fluorescence intensity of cells following AMF exposure (left panel) and average of cell viability percentage of exposed cells against controls (right panel). Values are presented as mean ± SD. N=3*

The result of the experiment is illustrated in Figure 6-7, where the fluorescence intensity average values registered for the exposed cells is 6968±77, while for control is 7131±208. Cell viability percentage of exposed cells was calculated as a ratio between AMF exposed cells and controls cells, and it is shown in considering controls as 100% viable. The result revealed that the viability of AMF exposed cells was 97.75±1.79% of that of controls and not statistically significant. In summary, the

experiment failed to show a significance difference on cell viability of AD-MSC expressing *mms6* even using 1030 kHz of AMF.

6.6 THE EFFECT OF ALTERNATING MAGNETIC FIELD ON FERUCARBOTRAN-LOADED AD-MSC IN 3-D CULTURE.

AD-MSC were loaded with 500 µg/ml Ferucarbotran nanoparticle and incubated in 37 °C CO_2 incubator for overnight. On the next day, the cells were washed three times, then pelleted in microcentrifuge tube in 100 µl medium. The cells were then exposed to 540 kHz AMF for two hours. Ferucabotran-loaded AD-MSC exposed to 0 kHz AMF for two hours were used as control. AD-MSC exposed in 45 °C in block heater for 2 hours were used as positive control. After the exposure, cells were then incubated in 37 °C CO_2 incubator for overnight. The cell viability was then determined with Alamar Blue Cell Viability Assay. The experiment was run in triplicate and repeated three times.

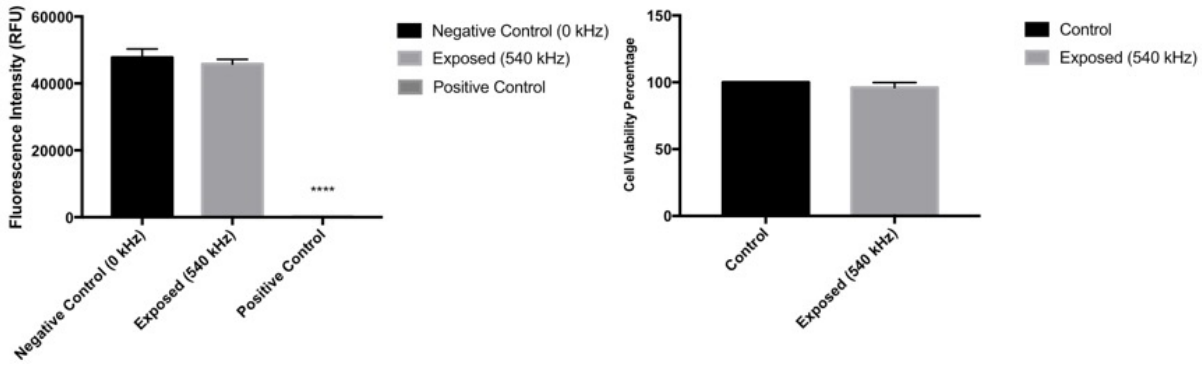

Figure 6-8: Cell viability of Ferucarbotran-loaded AD-MSC in 3-D culture following two-hour exposure of 540 kHz AMF*. Ferucarbotran-loaded AD-MSC cell were exposed to 540 kHz (light grey column) or exposed to 0 kHz as negative control (black column) or exposed to 45 °C in block heater as positive control (dark grey column). AlamarBlue data showing average of fluorescence intensity of cells following AMF exposure (left panel) and average of cell viability percentage of exposed cells against controls (right panel). Values are presented as mean ± SD. N=3*

The result of the experiment is illustrated in Figure 6-8, where the fluorescence intensity average values registered for the exposed cells is 45999±1406, while for negative control and positive control are 47751±2386 and 106±35, respectively. Cell viability percentage of exposed cells was calculated as a ratio between AMF exposed cells and controls cells, and it is shown in considering controls as 100% viable. The result revealed that the viability of AMF exposed cells was 96.09±3.76% of that of controls. The experiment failed to show any significant difference on cell viability of Ferucarbotran-loaded AD-MSC arranged in 3-D culture following the 540 kHz AMF application.

6.7 THE EFFECT OF ALTERNATING MAGNETIC FIELD ON AD-MSC EXPRESSING *mms6* IN 3-D CULTURE.

The effect of alternating magnetic field on AD-MSC expressing *mms6* in 3-D culture were determined using 3 different assays: 1) AlamarBlue Cell Viability assay, 2) Apoptosis assay, and 3) HSP70 expression analysis.

6.7.1 Cell viability analysis of AD-MSC expressing *mms6* in 3-D culture following two-hour exposure of 540 kHz AMF.

AD-MSC expressing *mms6* were cultured in medium doped with FeQ (34 μM) for 10 days. The cells were washed three times, then pelleted in microcentrifuge tube in 100 μl medium. The cells were then exposed to 540 kHz AMF for two hours. AD-MSC expressing *mms6* exposed to 0 kHz AMF for two hours were used as control. AD-MSC exposed in 45 °C in block heater for 2 hours were used as positive control. After the exposure, cells were then incubated in 37 °C CO_2 incubator for overnight. The cell viability was then determined with Alamar Blue Cell Viability Assay. The experiment was run in triplicate and repeated three times.

The results of the experiments are illustrated in Figure 6-9, where the fluorescence intensity average values registered for the exposed cells is 44434±702, while for negative control and positive control are 45307±1074 and 411±239, respectively. Cell viability percentage of exposed cells was calculated as a ratio between AMF exposed cells and controls cells, and it is shown in considering controls as 100% viable. The result reveals that the viability of AMF exposed cells was 97.42±2.25% of that of controls and not statistically significant. This result confirms that the 540 kHz AMF exposure on AD-MSC expressing *mms6* arranged in 3-D culture results in no cytotoxic effect.

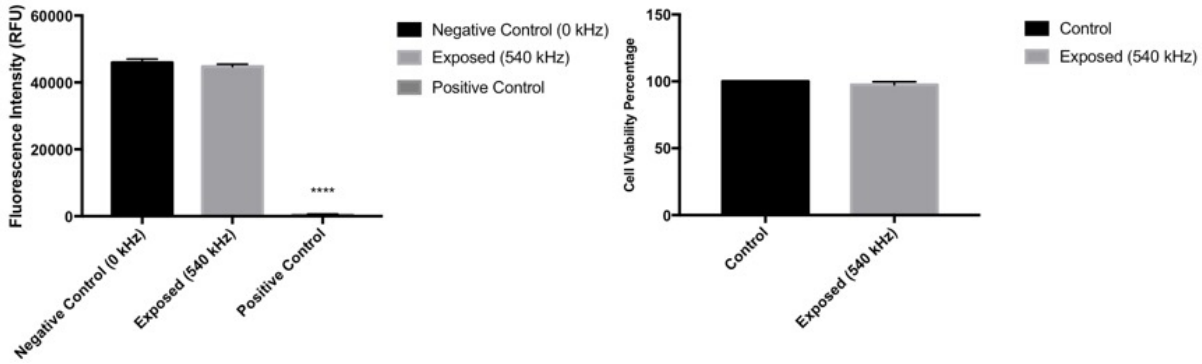

Figure 6-9: Cell viability of AD-MSC expressing mms6 in 3-D culture following one-hour exposure of 1030 kHz AMF*. AD-MSC expressing mms6 cell were exposed to to 540 kHz (light grey column) or exposed to 0 kHz as negative control (black column) or exposed to 45 °C in block heater as positive control (dark grey column). AlamarBlue data showing average of fluorescence intensity of cells following AMF exposure (left panel) and average of cell viability percentage of exposed cells against controls (right panel). Values are presented as mean ± SD. N=3*

6.7.2 Cell apoptosis analysis of AD-MSC expressing *mms6* in 3-D culture following two-hour exposure of 540 kHz AMF.

AD-MSC expressing *mms6* were cultured in medium doped with FeQ (34 μM) for 10 days. The cells were washed three times, then pelleted in microcentrifuge tube in 100 μl medium. The cells were then exposed to 540 kHz AMF for two hours. AD-MSC

expressing *mms6* exposed to 0 kHz AMF for two hours were used as control. After the exposure, cells were then seeded in Petri dish and incubated in 37 °C CO_2 incubator for overnight. The cell apoptosis was then determined with Click-iT™ Plus TUNEL Assay for in situ apoptosis detection with Alexa Fluor™ 488 dye. AD-MSC treated with DNase I were used as positive control. The experiment was run in triplicate and the experiment was only done once.

From the visual inspection of fluorescent microscopy as shown in Figure 6-10, the green fluorescent signal was clearly noticed in the positive control cells confirming the apoptosis mechanism by DNA strand breaks from DNAse treatment. Meanwhile, green fluorescent signals were not found on the cells exposed to 0 kHz AMF. For the cells exposed to 540 kHz AMF, only a few numbers of cells showing the green fluorescence. Moreover, it was not clear whether the green fluorescence was the result of DNA strand break or autofluorescence. This result confirmed that the two-hour 540 kHz AMF exposure on the AD-MSC may not induce cell apoptosis. It was also important to note that due to limited time and money, the experiment was only done once. Therefore, a further investigation using this method or other different methods of apoptosis assay need to be done to verify the result.

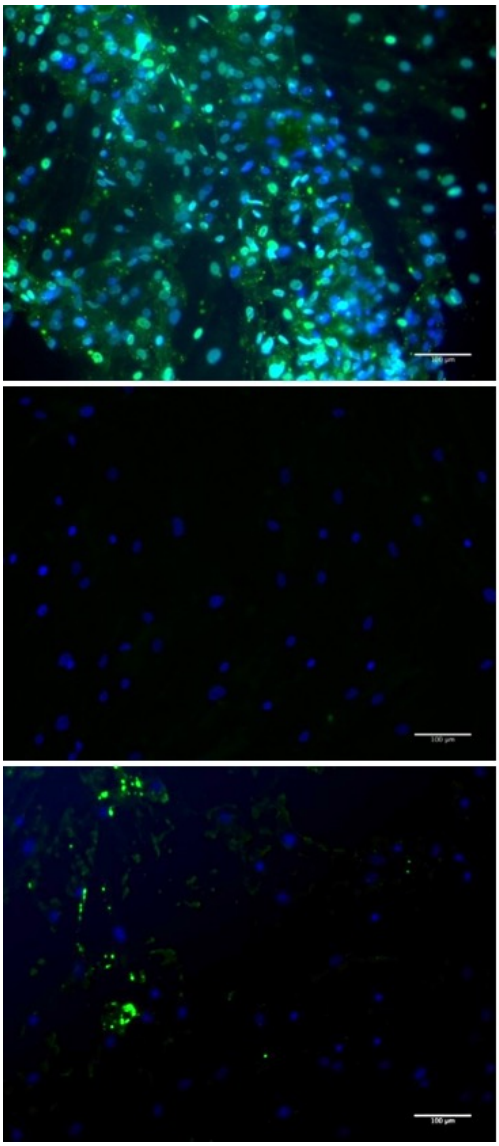

Figure 6-10: Cell apoptosis analysis of AD-MSC expressing mms6. *Click-iT™ Plus TUNEL Assay analysis showing cell apoptosis detection of AD-MSC expressing mms6 after two-hour of 540 kHz AMF exposure. Alexa Fluor™ 488 dye was utilized to detect the fragment DNA (green). DAPI was used to stain the cell nuclei (blue). Scale bar = 100 µm. N=3.*

6.7.3 HSP70 analysis of AD-MSC expressing *mms6* in 3-D culture following two-hour exposure of 540 kHz AMF.

AD-MSC expressing *mms6* were cultured in medium doped with FeQ (34 µM) for 10 days. The cells were washed three times, then pelleted in microcentrifuge tube in 100 µl medium. The cells were then exposed to 540 kHz AMF for two hours. AD-MSC

expressing *mms6* exposed to 0 kHz AMF for two hours were used as control. After the AMF treatment, cells were incubated in 37 °C CO_2 incubator for overnight. Afterwards, cells were collected and 20 µg of protein lysates from each sample were used for the western blot. ß-actin was used as an internal control. The experiment was repeated three times.

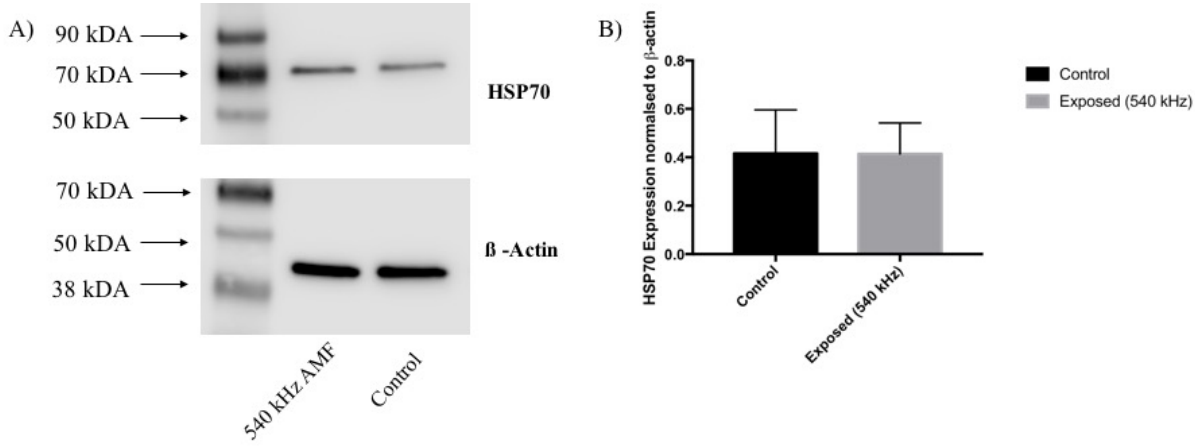

Figure 6-11: HSP70 expression of AD-MSC expressing mms6.

A) Representative image of western blot analysis showing HSP70 expression in AD-MSC expressing mms6 following two-hour of 540 kHz exposure. B) Protein level of HSP70 of AMF exposed AD-MSC expressing mms6 against control normalised by ß-actin. Values are presented as mean ± SD from three independent experiments N=3.

Based on the western blot result as shown in Figure 6-11, HSP70 protein band was found around the expected size of interest 70 KDa both in the AMF exposed cells and in the control cells. Meanwhile ß-actin protein bands with the expected size (42 KDa) were shown in both samples, confirming the validation of the experiment. From a visual inspection, it can be seen that the thickness of HSP70 protein band on both samples were similar without a clear difference. Using a semi quantitative method measuring the average expression of HSP70 normalised by ß-actin expression, it was found that the average expression of AMF exposed was 0.416±0.179 against 0.414±0.128 for control. This result confirms that the 540 kHz AMF exposure for two hours does not induce the expression of HSP70.

6.8 *IN VITRO* MAGNETIC RESONANCE IMAGING ANALYSIS OF AD-MSC EXPRESSING *mms6*

To determine whether AD-MSC expressing *mms6* would enhance MR contrast, magnetic resonance imaging experiment was performed. For this, following AD-MSC were prepared for the experiment: 1) Mag01-transfected AD-MSC, 2) Mag03-transfected AD-MSC 3) lentiviral-*mms6* tranduced AD-MSC and 4) Ferucarbotran-loaded AD-MSC.

Transfected cells or AD-MSC expressing *mms6* were cultured in medium doped with FeQ (34 μM) for 10 days. For Ferucarbotran-loaded AD-MSC, cells were incubated in 500 μg/ml Ferucarbotran for overnight. The cells were then harvested and fixed in 1% agarose gel in 50 ml falcon tubes. The tubes were then arranged in imaging phantoms and were suspended in a water container to reduce artefact. Multi-gradient-echo T2* acquisitions were acquired to generate T2* values (ms) using a standard least-squares fitting routine in Matlab (Mathworks)

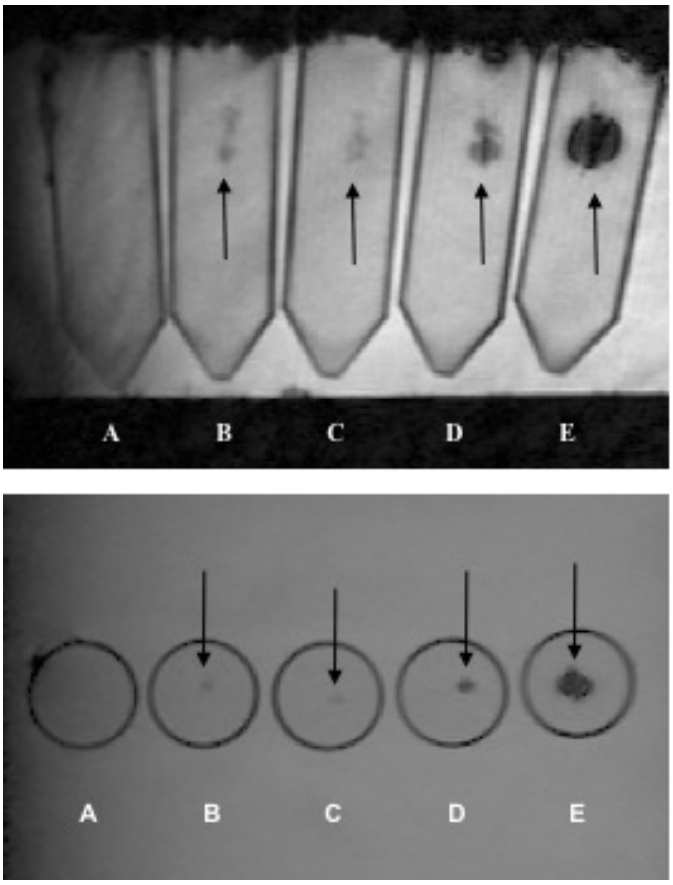

Figure 6-12: AD-MSC expressing mms6 produce intracellular nanoparticles which are identifiable by magnetic resonance imaging (MRI). *MRI analysis showing untransfected AD-MSC as control (A), Mag01-transfected AD-MSC (B), Mag03-transfected AD-MSC (C), Lenti-mms6 transduced AD-MSC (D), and Ferucarbotran-loaded AD-MSC (E).*

As shown Figure 6-12, all the AD-MSC expressing *mms6* samples: Mag-01 transfected (Tube B), Mag-03 transfected (Tube C), and Lenti-*mms6* transduced (Tube D) cells produced visually detectable changes at 3 T compared to control (Tube A). Meanwhile, Ferucarbotran-loaded AD-MSC (Tube E) cells produced the strongest contrast compared to all samples. This result confirms that the approach to magnetize AD-MSC using *mms6* gene has been successful and could be potentially useful in MRI application. However, it was clear that the use of chemically synthesized nanoparticle like Ferucarbotran nanoparticles was superior than using AD-MSC expressing *mms6*.

6.9 DISCUSSSION

The discussion in this chapter is focusing on cell delivered nanoparticle-mediated magnetic hyperthermia as an alternative to conventional hyperthermia. The basic concept of hyperthermia therapy is relying on targeting temperatures above 43°C which can cause necrosis of cancer cells. However, the main drawback of this approach is that adjacent normal tissues are also severely damaged under this conventional hyperthermia treatment. Thus several groups have attempted to use magnetic-nanoparticle-mediated hyperthermia which has the potential to overcome these shortcomings (Armijo *et al.*, 2012; Lemine *et al.*, 2014; Moros *et al.*, 2015; Blanco-Andujar *et al.*, 2016)

While much work on developing magnetic nanoparticle for hyperthermia are promising, MNP as a foreign material also have potential side effects in their clinical application (Huang *et al.*, 2017). Moreover, the previous approaches are still afflicted by the difficulty of delivering the magnetic nanoparticles to the tumour site *in vivo* (Gao *et al.*, 2013; Huang and Hainfeld, 2013). As such, there is a need for more selective hyperthermia agents, prevention of the necrosis of normal tissues and better nanoparticle delivery systems. To overcome this challenge, the ultimate purpose of this chapter was to investigate the potential use of engineered-MSC cells for cancer treatment via intracellular magnetic hyperthermia. Therefore, two group of cells were used in this *in vitro* magnetic hyperthermia study: 1) AD-MSC expressing *mms6* cultured in medium doped with FeQ (34 μM) for 10 days, 2) AD-MSC loaded with Ferucarbotran nanoparticle for overnight.

In this chapter, experiments were aimed to test the hypothesis that the nanoparticle produced inside AD-MSC expressing *mms6* could generate a magnetic hyperthermia effect by applying AMF into the cells. Cell viability, cell apoptosis and HSP70 expression were investigated as the parameter of magnetic hyperthermia effect. Furthermore, the experiment also aimed to demonstrate the potential use of AD-MSC expressing *mms6* as a contrast agent for MRI.

Regarding the magnetic hyperthermia experiment, the heating capacity of Ferucarbotran nanoparticle in water suspension were investigated. The experiment was conducted simply to measure the temperature increase of free nanoparticle in colloid. The nanoparticles were exposed under AMF each with three different frequency: 178.3 kHz (23.89 mT), 540 kHz (24.87 mT), and 1030 kHz (13.37 mT). Afterwards, the same AMF frequencies were used to evaluate the effect of AMF exposure on single layer of Ferucabotran-loaded AD-MSC and AD-MSC expressing *mms6*.

The three different frequencies above were considerably low to medium range radio frequencies. The different identifications of radio frequency sub-regions in terms of their frequency can be seen at Table 6-1. In magnetic hyperthermia, the heat generation involves the interaction between the magnetic moment of the MNP and the magnetic component of the applied electromagnetic wave.

As for the interaction between electromagnetic fields and the exposed cells, it is known that living organisms are mostly composed of molecules with a dipolar electric moment, and therefore can interact with the electric component of the radio frequency radiation. This interaction at a molecular level depends on the characteristic energy levels that can be excited at certain frequency range of the electromagnetic spectrum (Silver *et al.*, 1964; Goya *et al.*, 2013). As an example, conventional hyperthermia treatment based on microwave ranges for deep tumour treatment, is using dielectric heating at higher frequency (Silver *et al.*, 1964). In magnetic hyperthermia, however, the low RF frequency range (from approximately 100 kHz to 1 MHz) is commonly used. At his range, the interaction of both the electrical and magnetic components of RF waves with living organisms is not relevant and can be neglected.

Table 6-1: The different identifications of the RF sub-regions in terms of their frequency. Adapted from Radiation Advisory Group on Non-ionising Radiation.

Frequency	Wavelength	Designation
3–30 kHz	100–10km	Very low frequency
30–300 kHz	10–1km	Low frequency
300 kHz–3MHz	1 km–100m	Medium frequency
3–30MHz	100–10m	High frequency
30–300MHz	10–1m	Very high frequency
300 MHz–3GHz	1 m–10cm	Ultra high frequency
3–30GHz	10–1 cm	Super high frequency
30–300GHz	1 cm–1mm	Extremely high frequency
300 GHz–3000GHz	1 mm–0.1 mm	Tremendously high frequency

The result of the heating capacity of free Ferucarbotran nanoparticle experiment successfully showed that the temperature of the sample suspension was raised above physiological temperature when they were exposed under three different RF of AMF: 178.3 kHz, 540 kHz, and 1030 kHz. The highest temperature was shown in sample exposed to 540 kHz AMF with temperature value over 60 °C for less than an hour of AMF exposure. However, this result does not represent the real condition once the nanoparticles enter the cells. In addition, the concentration used in this experiment was 5 mg/ml which was too high and may not suitable for this *in vitro* intracellular magnetic hyperthermia experiment.

Although many studies have been demonstrating the heating mechanism of MNP when submitted to AC magnetic field, the translation of these theoretical model into *in vitro* MH is still lacking. Factors such hydrodynamic size, intracellular distribution and the degree of agglomeration once the nanoparticles enter the cells are important in *in vitro* magnetic hyperthermia study. A study by Ge and coworkers in 2009, investigating the effect of surface charge and agglomerate degree of MNP on Oral Squamous Carcinoma Cell KB as an *in vitro* model revealed that cellular uptake of MNP by KB cells was dependent on incubation time, nanoparticle concentration and properties (Ge *et al.*, 2009). In addition, another problem related to *in vitro* MH is the complex nature

of the interaction between nanoparticles and the biological media in *in vitro* MH. Therefore, the *in vitro* MH greatly depends on the cell type, nanoparticle design and the biological set up in the experiment.

The novelty of the present study is the use of engineered-AD-MSC as a potential cell delivery system and agent to induce magnetic hyperthermia. A similar approach was undertaken in an *in vitro* study reported by Asin and coworkers in 2013. The study was investigating the potential use of dendritic cells as cells to target tumours for magnetic hyperthermia. Interestingly, the study showed that cell death was observed following AMF exposure specifically to MNP-loaded dendritic cells (DCs) in culture and that this was caused by the release of unknown toxic agents into the cell culture supernatants without a significant temperature increase in the medium (Asín *et al.*, 2013).

Other studies using synthesized MNP which were incorporated into human breast cancer cells (MCF-7) showed cellular death following an AMF exposure (4 kW, 250 kHz, 20 minutes), achieving temperatures as high as 46 °C (Baba *et al.*, 2012). Another type of cells which has been tested for magnetic hyperthermia was caco-2 (human epithelial colorectal adenocarcinoma) cells. This study demonstrated that MNHT treatment (magnetic field of 20 kA/m; 237 kHz; for 30 minutes) significantly increases cell membrane fluidity which was believed to have contributing factor to the increase of cisplatin uptake in magnetic fluid hyperthermia-treated Caco-2 cells and enhance cytotoxic effect of the chemotherapeutic agent (Alvarez-Berríos *et al.*, 2013). Rodríguez-Luccioni and coworkers also showed a significant decrease in MCF-7 cell viability when the cells loaded with carboxymenthyl dextran iron oxide nanoparticles and exposed to a magnetic field amplitude (20 kA/m; 238 kHz for 120 minutes. Interestingly, cell viability decreased with time after a single application of AMF indicating possible secondary effects on cell viability which are seen after only a further period of culture (Rodríguez-Luccioni *et al.*, 2011). Other cells types, A549 (human lung adenocarcinoma) and MDA-MB-231 (human mammary adenocarcinoma) cells have also been tested in *in vitro* MNHT. The study showed that magnetic hyperthermia application (6 kA/m and frequency of 386 kHz) for 30 minutes

using custom design SPIO nanoparticles prepared from iron chlorides can induce cell death 88% in A549 and 90% in MDA-MB-231 cells (Sadhukha, Niu, *et al.*, 2013). The previous studies have shown promising potential in *in vitro* work of intracellular MH using various tumour cell lines however it may be that a significant component of the hyperthermia effect may be due to the presence of extracellular nanoparticles. The use of AD-MSC in the present work was found to be challenging for intracellular hyperthermia as the experiments failed to show any significant difference on the AMF treated and control group.

For the AMF application on 2-D monolayer culture experiment, no observable difference was seen in cell viability of Ferucarbotran-loaded AD-MSC following the AMF application. It was observed that the viability of AMF exposed cells were 99.58±0.66%, 94.65±2.03%, and 95.5±4.4% against controls after the cells were exposed to 178.3 kHz, 540 kHz and 1030 kHz of AMF, respectively (***Figure 6-2***, **Figure 6-3**, **Figure 6-4**). Therefore, the interaction of Ferucarbotran nanoparticles and considerably low frequency of AMF has not been found to influence cell viability of AD-MSC.

In contrast to this finding, a study by Kalber and coworkers indicated that human MSC can be used as cell delivery system of Ferucarbotran. In the *in vivo* test using a mouse model, the internalized Ferucarbotran was found to induce heating at 2 weeks after the Ferucarbotran-loaded MSC cells (60 pg/cell) Ferucarbotran were injected into OVCAR-3 tumour tissue and AMF of 10 mT at 1.05 MHz applied. Interestingly, despite the 4.3°C rise was observed in surface temperature of the tumour, the AMF application did not result in measurable retardation of tumour growth (Kalber *et al.*, 2016). The study, however, did not test the effect of AMF on MSC viability *in vitro*.

In another *in vivo* study by Araya and coworkers, Ferucarbotran nanoparticles (150 µl dose; 7.5 ml/kg) were injected into lung cancer xenografts in nude mice. The result revealed that the intratumour temperature rose rapidly and was maintained at 43 °C – 45 °C for 20 minutes under AMF (20 – 24 mT; 142 kHz), which significantly suppressed tumour size by necrosis (Araya *et al.*, 2013). However, the finding on this study is not relevant to the present study since the approach that they used was injecting

the Ferucabotran directly into the tumour site without using vector cells to deliver the Ferucarbotran nanoparticles. In addition, the study also declared its drawback which was the surface of the induction heating applicator was set at 2 cm from tumour site, thus it does not represent AMF application on deep organ cancers in clinical practice.

Regarding the experiment on AD-MSC expressing *mms6*, it was observed that the viability of AMF exposed cells was 93.24±3.79%, 97.62±2.79%, and 97.75±1.79% against controls after the cells were exposed under 178.3 kHz, 540 kHz and 1030 kHz of AMF, respectively. Therefore, the interaction of nanoparticles created in AD-MSC expressing cells and the AMF has not been found to influence cell viability of AD-MSC.

A previous report investigating the potential use of magnetosomes isolated from *Magnetospirillum magneticum* strain AMB-1 magnetotactic bacteria for extracellular MNHT indicated an efficient magnetic hyperthermia treatment of tumour cells (Alphandéry *et al.*, 2012). The study used two different approaches to treat the cancer cells: 1) addition of chains of magnetosomes to the cells, and 2) using individual separated magnetosomes to treat the MDA-MB-231 breast cancer cells. When the chain of magnetosomes (1 mg/ml) were incubated in the presence of cancer cells and exposed to AMF (~20 mT; 198 kHz; 5 – 20 min), they generate heat as indicated by increased SAR value and produce efficient inhibition of cancer cell proliferation, showing the percentage of inhibition increased by factor ~7 – 16 as indicated by MTT viability assay. By contrast, when the chain of magnetosomes were separated into individual magnetosomes, they were prone to aggregation, and did not produce efficient inhibition of cancer cell proliferation under application of AMF (Alphandéry *et al.*, 2012). In a further study, the chain of magnetosomes nanoparticles were injected into mice bearing intracranial U87-Luc glioma tumour. After 12 to 15 cycles of 30 min AMF (30 mT; 200 kHz) application, the experiment showed full tumour disappearance in 40% of mice. The study identified that the tumour destruction by the chain of magnetosome could be explained by extracelluar MH by a larger production of heat and possibly endotoxins released following cell death under alternating magnetic field application (Alphandéry *et al.*, 2017a).

Indeed, the use of *mms6* in the present work was not aimed to create the complete structure of magnetosomes inside AD-MSC. In fact, the use of *mms6* alone will not be able to create the complex natural structure of magnetosomes. Therefore, the use of magnetosomes for magnetic hyperthermia both *in vitro* and *in vivo* study as discussed above is not comparable to the magnetic hyperthermia results in the present study as they were aimed at comparing the utility of naturally produced magnetic nanoparticles by bacteria as a potential for use for clinical magnetic hyperthermia in contrast to chemically synthesized nanoparticles. However, the studies clearly described the superior characteristic of magnetosomes as a heating capacity agent in magnetic hyperthermia is highly dependant on its chain structure. Thus, it may be possible that the lack of observable difference of effect betweenAMF exposed and non-exposed AD-MSC expressing *mms6* could be due to the poor structure or shape of the synthesized nanoparticles, relatively low number of intracellular nanoparticles which results in insufficient heating capacity.

For the AMF application on 3-D model cells experiment, the result revealed that the viability of AMF exposed Ferucarbotran-loaded AD-MSC was 96.09±3.76% against controls. While the viability of AMF exposed AD-MSC expressing *mms6* was 97.42±2.25% against control. Consistent with the previous 2-D model experiment, both results showed no observable difference in AMF application effect on cell viability of Ferucarbotran-loaded AD-MSC and AD-MSC expressing *mms6*, suggesting no cell necrosis or cytoplasmic lysis following the 540 kHz AMF exposure. Furthermore, the investigation on cell apoptosis and HSP70 expression of AD-MSC expressing *mms6* following the AMF application also showed no observable difference. Unfortunately, the experiment was only done once due to limited time and money. However, it can be concluded that the 540 kHz application of AMF on 3-D pellet of AD-MSC expressing *mms6* does not induce cell apoptosis mechanism and does not increase the HSP70 expression.

The 3-D model experiment was developed to mimic the *in vivo* condition. The experiment, however, did not use a proper 3-D cell culture system, such as 3-D well plate as culture plates could not be fitted into the MagneTherm^{TM} device for the AMF

application. For this reason, one million cells were simply collected, pelleted and placed inside a microcentrifuge tube. The tube was then placed at the center position of the coil of MagneTherm^{TM} device for the AMF application.The theoretical reason behind using a 3-D cell pellet experiment was also due to the hypothesis that a larger number of cells in close proximity is required for intracellular magnetic hyperthermia and triggering the hyperthermia effect. In 2013, a study by Hedayati and coworkers hypothesized that cytotoxicity increased with increasing cell number (Hedayati *et al.*, 2013). In their study, starch-coated magnetite (Fe_3O_4) core shell particles (Bionized NanoFerrite) or BNF were loaded into cultured DU145 prostate cancer cells. Then, the cell pellets of variable size were treated with AMF amplitude fixed at 1100 Oe for 30-min duration. The study demonstrated that smallest cell pellet in which hyperthermia-mediated cytotoxicity was observed contained 250,000 cells, revealing there is a minimum number of cells within a pellet required for cytotoxic hyperthermia. The study also concluded that the intracellular magnetic hyperthermia has the same scaling effect to the extracellular or macroscopic magnetic hyperthermia. As a result, the intracellular magnetic hyperthermia approach would be less effective for smaller cell pellets or heating micro-metastatic cancer in medical application (Hedayati *et al.*, 2013). In short, the smaller heating system will result in less magnetic heating effect.

In agreement with the finding above, Wilhelm and coworkers (2007) investigated the relative cytotoxicity of maghemite anionic nanoparticles on human prostatic tumour cells. The study used 20 million cells of loose pellet and exposed to AMF (31 mT; 700 kHz; 1 hour duration), and found that more than 80% of the cells were killed after being submitted twice to AMF. Interestingly, when magnetic cells coexist with non-magnetic ones, the same proportion of cytotoxicity was found on both populations after the AMF application, suggesting the cytotoxic hyperthermia is a function of total iron particle content in the pellet (Wilhelm *et al.*, 2007).

As the studies above suggest, the negligible cytotoxicity associated with AMF treatment both on Ferucarbotran-loaded AD-MSC and AD-MSC expressing *mms6* in this chapter is likely related to cell number or cell pellet size. The interpretation of this result is that the one million cells used in this experiment could be not sufficient to

achieve the AMF treatment scale for increasing the temperature. In this regard, how many Ferucarbotran particles each individual AD-MSC cell absorbs could determine the cytotoxicity following AMF application. It might be also possible that some cells at least take up only a few or none of the particles whereas others take up a large portion. While for AD-MSC expressing *mms6*, it could be possible that some cells produce Mms6 protein to a lesser degree than others which results in only limited nanoparticle in the cells. In summary, the experimental set-up in the present study might be inadequate to provide an *in vitro* environment to obtain a proper magnetic heating effect which result in no detectable changes in cell viability, cell apoptosis and HSP70 expression.

Gordon *et al.* in in 1979 declared that intracellular hyperthermia is superior to extracellular hyperthermia by causing calamitous heating and triggering the intracellular space to reach higher temperatures. It is believed that the cell membrane may have a key role as a thermal insulator due to its low thermal conductivity, thus only intracellular heating can overcome this thermal barrier (Gordon *et al.*, 1979). In 2002, the hypothesis was rejected by Rabin and his co-workers who found that nanoscale heating effects are negligible in their study, suggesting a single magnetic nanoparticle does not have a practical effect on hyperthermia. Interestingly, the study also revealed that the heating generation in a single cell, which is loaded with a huge number of nanoparticles, is not sufficient to create the conditions for hyperthermia unless it is a part of a larger cellular structure of similar cells (Rabin, 2002). In short, macroscopic hyperthermia or extracellular hyperthermia is still superior to intracellular hyperthermia in the thermal sense, assuming that the same number of nanoparticles are present in both situations.

Recent controversial reports also suggested that AMF can trigger cytotoxicity without any macroscopic temperature increase, which strongly suggest that cell death by AMF is not just a matter of temperature increase, but through other specific mechanism (Villanueva *et al.*, 2010, Creixell, 2011). It is believed that the cell death is related either to chemical effects triggered by the presence of the nanoparticles, or mechanical damage caused to the cell by intracellular vibrations or movement of the nanoparticles.

Only 1 or 2 °C temperature increase was observed when nanoparticle-loaded dendritic cells (DCs) exposed under to AMF (260 kHz and 12.7 kA/m) for 15 min, yielding almost 100% of cell death (Asín *et al.*, 2012). Interestingly, the toxicity of the supernatant of AMF-exposed cells was observed to have the potential to kill control cells (Asín *et al.*, 2013). It was explained that the MNP might generate the disruption of the endocytic vesicles/lysosomes membranes during AMF exposure, allowing the unknown toxic vesicle´s content to be released into the cytoplasmic region and triggering cell death (Asín *et al.*, 2013). Another non-thermal explanation could be the disruption of cell membrane by the nanoparticles. It was suggested that the increasing cell membrane fluidity could trigger a heat shock protein response which may modulate positively or negatively apoptotic cell death (Csoboz *et al.*, 2013). The fact that no observable difference in HSP70 expression in the present study suggesting that the AMF application does not have direct effect to membrane fluidity of AD-MSC expressing *mms6*.

Work assessing cell apoptosis following AMF exposure needs to be optimised. An interesting observation comparing apoptotic effects of water-based hyperthermia (WH) and magnetic nanoparticle-mediated hyperthermia (MNHT) demonstrated that the apoptotic effect was slow and its effects on viability were not found until 48 hours after 2 hours of treatment. In contrast, an effect due to MNHT on cell viability was detected 24 hours after 2 hours of treatment (Rodríguez-Luccioni *et al.*, 2011). As explained it may have been preferable that apoptosis was assessed in the present study at several time points after AMF application. In addition, several AMF cycles might be needed to obtain the magnetic hyperthermia effect. For example, 10-15 magnetic session for several days; 30 minutes per session. This was suggested in a previous report which used magnetosome-loaded tumour exposed to 12 to 15 cycles of 30 min AMF applications to achieve full tumour disappearance. (Alphandéry *et al.*, 2017a).

Regarding the MRI experiment, it was obvious that the use of Ferucarbotran-loaded AD-MSC was superior to AD-MSC expressing *mms6* in terms of detectable magnetic signal, providing the same number of cells used in the experiment. Having said that, the fact that MR contrast was detected in the transfected cells, the experiment

successfully demonstrated a promising potential of *mms6* as a reporter gene. In agreement with this finding, a previous report using *mms6* transfected gliosarcoma cell line showed detectable MR changes in both *in vitro* and *in vivo* experiments. Even more interesting, the study revealed that tumour cells stably expressing *mms6* can produce MR contrast in the absence of iron supplementation by accumulating endogenous iron efficiently in the *in vivo* experiments (Zhang *et al.*, 2014) in contrast to earlier reports which used iron supplementation with cells transfected with *magA*, cloned from both MS-1 and AMB-1 species of MTB, to display increased MR contrast in stably transfected mammalian cells (Zurkiya *et al.*, 2008; Goldhawk *et al.*, 2009).

In conclusion, this chapter successfully showed the potential use of *mms6* as MR reporter gene for AD-MSC. However, future work both *in vitro and in vivo* is still needed in order to achieve a detectable magnetic hyperthermia effect in AD-MSC expressing *mms6*.

7 GENERAL DISCUSSION AND FUTURE PERSPECTIVE

Due to their small size and high surface-to-volume ratio, magnetic nanoparticles (MNP) have attracted great interest for their potential biomedical applications either alone or through cell-based therapies (Gao *et al.*, 2013). One of the most promising approaches is magnetic nanoparticle-mediated hyperthermia (MNHT) for cancer treatment, where magnetic nanoparticles (MNP) absorb energy from alternating magnetic fields (AMF) and transform this energy into heat. While they are promising, MNP have disadvantages of variable uptake by cells and may have potential side effects in its clinical application (Huang *et al.*, 2017). Another key challenge is the difficulty of delivering the magnetic nanoparticles to the tumour site due to their rapid removal from blood and biological barriers at tissue and cellular level (Gao *et al.*, 2013; Huang and Hainfeld, 2013). All these problems represent the need to find less toxic or more biocompatible nanoparticles and to improve strategies to deliver to and distribute nanoparticles within tumours for optimal MH treatment.

To overcome these problems, the use of MNP-labelled mesenchymal stem cells (MSC) has been proposed due to their inherent tumour-tropic and migratory properties, thus enabling cell-based MNP vehicle for the targeted delivery into tumour (Roger *et al.*, 2010; Duchi *et al.*, 2013; Gao *et al.*, 2013; Huang and Hainfeld, 2013). However, a drawback to the use of MSC so far is that MSC have limited phagocytic capability, yielding poor intrinsic capacity to ingest extrinsically applied MNP (Yin *et al.,* 2016; Boutry *et al.,* 2008). Therefore, a genetic engineering approach was utilized in this study, allowing MSC cells to intrinsically produce biogenic nanoparticles.

7.1 SYNTHETIC CODON OPTIMISED *mms6* GENE FOR MAMMALIAN EXPRESSION

In the present work, I investigated the potential use of a magnetosome gene, *mms6*, as the candidate gene for genetically engineered-cells producing intrinsic biogenic nanoparticles. In MTB, *mms6* encodes an iron binding protein which has a key role in initiating magnetite crystal nucleation within magnetosomes (Arakaki *et al.*,

2003) and helps regulate the crystal morphology of magnetite during the formation of magnetosomes (Prozorov *et al.*, 2007; Kashyap *et al.*, 2014; Yamagishi *et al.*, 2016). Having known the function of this gene, therefore, the ultimate aim of my project was to develop MSC able to self-express MNP by genetically modifying them with the *mms6* gene.

In Chapter 3, the main aims were to amplify the plasmid DNA containing synthetic codon-optimised *mms6,* which was called Mag02, using molecular cloning techniques and to demonstrate expression of Mag02 in AD-MSC after transfection. In particular, this chapter explains all the initial work performed in the 1st year of my PhD project. In this work, only one type of codon-optimised *mms6* was used called Magister02 (Mag02). The name Mag02 was used due to previous codon-optimised *mms6*, named Mag01, was designed and investigated in a previous study by Lisa Lungaro, former PhD student in the group. The Mag02 gene construct was designed by Dr. Christopher Boyd and was synthesized by GeneArt® Gene Synthesis service. In the previous work by Lisa Lungaro, the synthesised *mms6* (Mag01) does not have a protein marker in the construct, thus a polyhistine-tagged (6x) was added in the Mag02 construct which aimed for easier protein detection by Western blot.

Using molecular cloning techniques, I was able to amplify the plasmid which was important before starting the transfection experiment. To confirm this, using specific restriction enzyme digests in combination with DNA sequencing result, I was able to demonstrate that Mag02 plasmid was successfully cloned without mutation.

7.2 EXPRESSION OF *mms6* IN HUMAN ADIPOSE DERIVED-MESENCHYMAL STEM CELLS

For the transfection experiment, I explored a variety of transfection techniques in an attempt to improve the transfection efficiency. Initially, the experiments started with the X-tremeGENE™ HP DNA Transfection Reagent. This was the standard transfection reagent in our lab and had been previously optimised by Lisa Lungaro, showing successful transfection of bone marrow-derived MSC. Using this transfection

technique, I was able to demonstrate *mms6* expression in AD-MSC at 10 days after transfection with Mag02 plasmid. This result was in agreement with the result from previous work by Lisa Lungaro, showing MSC and MG63 cells were able to express these MTB genes at 10 days after transfection with each of *mmsF* and *mms6* genes. In addition, using the same technique, previous work by Elfick and co-workers (2017) also demonstrated expression of the *mms6* in transfected MSC cells at 10, 15 and 21 days post-transfection by RT-PCR and Sanger DNA sequencing of the PCR transcripts (Elfick *et al.*, 2017). However, despite mRNA of Mag01 being successfully displayed in previous work, they did not provide evidence of Mms6 protein expression. In my work, it was necessary to demonstrate the evidence that a foreign protein like Mms6 protein can be expressed in human AD-MSC.

Previous work by Liu *et al.* (2016) indicates that a direct comparison between protein and mRNA abundances from the same location or from the same cell type may not be appropriate. This is mainly due to multiple processes beyond mRNA concentration that contribute to establishing the expression level of a protein including translation rates, translation rate modulation, modulation of a protein's half-life or autophagy which may influence protein concentrations independent of transcript concentrations, protein synthesis delay and protein transport which disconnects proteins from the transcripts they were synthesized from (Liu *et al.*, 2016). Therefore, confirming Mms6 protein expression was important for the two following reasons: 1) To confirm that the synthesis of biogenic nanoparticle in AD-MSC was mainly because of the expression of Mms6 protein which acts as an iron binding protein and not due to another unknown mechanism; 2) To establish if mRNA expression equates with levels of expression of protein. My results showed that the His-tagged Mms6 protein was absent following the transfection procedure despite positive mRNA expression being evident up to 10 days after transfection. Indeed, it needs to be stated that the limitation of the experiment was that a specific Mms6 antibody for protein-based detection assay was not available commercially. It would have been great to use custom-designed Mms6 antibody for direct detection of Mms6 expression. However, such option was not available and thus polyhistidine-tag method was preferred. Nonetheless, such option should be considered in the future work.

In Chapter 4, the experiments conducted aimed to overcome the problems related to the absence of Mms6 protein expression discussed in Chapter 3. It was thought that the absence of His-tagged Mms6 protein expression could be due to low transfection efficiency or could be due to an as yet unidentified problem possibly related to the codon-optimised *mms6* construction. Therefore, the experiments in Chapter 4 aimed to demonstrate the *mms6* mRNA and protein expression in AD-MSC using different codon-optimised *mms6* and different technique of transfection. For this, additional codon-optimised *mms6* were designed and investigated: MagWT, Mag01, Mag02 and Mag03. MagWT contains the original sequence *mms6* gene of *M. magneticum* strain AMB-1 *mms6* gene. Mag01 was kindly designed by Dr. Greg Kudla (Group leader of RNA synthetic biology group, MRC Institute of Genetics & Molecular Medicine, University of Edinburgh). Mag02 was designed by Dr. Chris Boyd (Group leader of gene therapy for cystic fibrosis research group, MRC Institute of Genetics & Molecular Medicine, University of Edinburgh). Mag03 was designed by GeneArt® Gene Synthesis service.

Each of these constructs also included a polyhistidine-tag at the N terminus and a GFP-tag at the C terminus of the *mms6* DNA fragment. These double markers were essential to provide a quick and informative assessment of Mms6 protein expression following the transfection.

Regarding the *mms6* mRNA expression in AD-MSC, the end-point PCR result showed mRNA of *mms6* was constantly expressed in AD-MSC up to 21 days after the transfection using X-tremeGENE™ DNA Transfection Reagent after the transfection with each of those 4 types of MAGISTER genes. However, Western blotting demonstrated that the His-tagged Mms6 protein expression was found to be absent in all samples with this transfection reagent. It was speculated that false positive results due to plasmid DNA contamination were obtained during end-point PRC experiment, hence Mms6 protein expression was absence on the western blot assay. In the later experiments, when HEK293T cells were used in combination with similar transfection methodology, His-tagged Mms6 protein expression was successfully detected. These results indicate that the expression of Mms6 protein is likely to be cell-dependent. In

this case, HEK293 cells are relatively easy to transfect cells, while MSC are widely known as difficult to transfect cells, unlike other primary cell types, (Baek *et al*., 2016). Indeed, common non-viral transfection methods used for mammalian cells, such as a cationic lipid-based reagent transfection system, still generally show low-to-moderate (less than 15%) gene transfer efficiency in transfecting MSC (Wang et al. 2014). Therefore, there was a need to improve the transfection strategy to be able to generate AD-MSC expressing *mms6*.

7.3 NUCLEOFECTION IMPROVES THE EFFICIENCY OF AD-MSC TRANSFECTION.

In the later experiments in Chapter 4, a physical-based transfection, nucleofection, was used. The GFP fluorescence expressed by AD-MSC as evaluated by both Flow cytometry and GFP imaging analysis confirmed the success of expression of His-GFP tag Mms6 protein in AD-MSC. This was also confirmed by Western blot analysis which shows the expression the His-GFP tag Mms6 protein in all cell samples nucleofected with MagWT, Mag01, Mag02 and Mag03 plasmid, resulting Mag01 and Mag03 expression higher than the other two, as indicated by a semi-quantitative protein quantification analysis on Western blot result.

Flow cytometry analysis also showed that the nucleofection method was highly efficient as the method was able to generate 59.6±1.9 % of AD-MSC positively expressing His-GFP-tagged Mms6 protein at 2 days after transfection with Mag01 plasmid. This was the highest percentage of transfection efficiency compared to the previously used method using X-tremeGENE™ transfection reagent with only 15.55±3.9 % GFP-positive cells. This result is consistent with transfection efficiencies of 50 to 80% achieved using nucleofection method to transfect adult human MSC as reported by Haleem-Smith and co-workers (Haleem-Smith *et al.*, 2005).

However, a major drawback to the use of the nucleofection method was the reduction of cell viability. It was demonstrated the viability of AD-MSC nucleofected with Mag03 was significantly decreased to 66.2±2.5% against 100% cell viability of

control. This was expected as the disadvantage of using nucleofection method is the tendency for high level of damaged cells (Kaestner *et al*., 2015). It should be underlined that this cell viability problem alone technically made it difficult to use these transfected cells for *in vitro* MNHT experiments. Longer culture period may be needed to increase the cell number. However, it also means reduced protein expression overtime. Therefore, it still remains a challenge to find a high-transfection method with less effect in cell viability for the transient expression of *mms6* in AD-MSC.

7.4 AD-MSC STABLY EXPRESSING *mms6* AFTER LENTIVIRAL TRANSDUCTION

In regard to the stable expression of *mms6,* a lentiviral vector carrying *mms6* was designed. Using enzyme restriction digests, Mag01 gene fragment was successfully cloned into pSicoR-Ef1α-mCh-Puro lentiviral vector. Initially, it was aimed to clone Mag01 and Mag03 gene fragments into lentiviral vector as the expression of His-tag Mms6 protein was found to be higher in AD-MSC transfected with each of Mag01 and Mag03 compared to the other Magister plasmids, as shown by a semi-quantitative protein quantification analysis on western blot result. However, it was unfortunate that for unknown technical reason, I was unable to clone Mag03 into pSicoR-Ef1α-mCh-Puro lentiviral vector, thus only Mag01 was used for the later experiments. Following the viral transduction of AD-MSC, puromycin antibiotic selection was conducted in order to generate colonies of AD-MSC expressing *mms6*. This was also confirmed by the constant expression of mCherry red fluorescence under fluorescence microscope. These cells were then expanded for the later experiments.

In summary, my aims to demonstrate the *mms6* mRNA and protein expression in AD-MSC were largely successful and the experiments conducted in Chapter 3 and Chapter 4 have improved understanding of the transfection approach for expressing MTB genes in adult human stem cells.

For future studies it would be beneficial to investigate different techniques to optimally generate human stem cells stably expressing *mms6*. It will be interesting to use new

gene engineering tools such as zinc finger nucleases (ZFNs), transcription activator-like effector nucleases (TALENs), and CRISPR (clustered regularly interspaced short palindromic repeat)-Cas9(CRISPR-associated nuclease 9) system in order to improve the precision of genome editing, prevent mutations and maintain stable, long-term gene expression (Baek *et al*., 2016). Using these approaches, *mms6* could be integrated into a specific site in MSC genome in a more accurate way than using chemical-based transfection or lentiviral-based transduction, allowing better understanding of gene and protein expression (Ding et al., 2016).

7.5 THE *mms6* EXPRESSION ON THE AD-MSC DOES NOT ALTER STEMNESS AND MULTIPOTENCY CAPABILITY.

In Chapter 5, I aimed to investigate the effect of *mms6* expression in lenti-*mms6* transduced AD-MSC stemness and differentiation potential following the lentiviral transduction. In addition, I also aimed to demonstrate the formation of nanoparticles inside the cells as well as the magnetic behaviour of AD-MSC expressing *mms6*. It was found that expression of *mms6* gene by AD-MSC does not change cell stemness, and their capability to differentiate into the osteogenic and adipogenic lineage. However, due to technical problems, chondrogenesis differentiation was not shown in this study. It would be also interesting to compare these results with Ferucarbotran-loaded or MNP-loaded AD-MSC in terms of their cell stemness and differentiation capability.

Indeed, a previous study by Lima and co-workers demonstrated that MNP-loaded AD-MSC have shown the potential to induce differentiation towards the osteogenic and chondrogenic lineages under the influence of an external magnetic field (Lima *et al.*, 2015). Ferucarbotran nanoparticles have also been reported to accelerate cell cycle progression and promote cell growth of MSC (Huang *et al.*, 2009).

7.6 AD-MSC EXPRESSING *mms6* CONTAIN CLUSTERS OF NANOPARTICLES WITHIN MEMBRANE-ENCLOSED STRUCTURES

The TEM result showed accumulation of membrane-bound, intracytoplasmic electron-dense nanoparticles in Ferucarbotran-loaded AD-MSC. Similar electro-dense material was also found in AD-MSC expressing *mms6*, both virally transduced cells and nucleofected cells using Mag01 and Mag03 plasmid. However, unlike the highly ordered cubo-octahedral crystals of magnetite crystals of magnetosome in MTB, the nanoparticles produced by the AD-MSC expressing *mms6* appeared unstructured. Nonetheless, my aim to demonstrate the formation of intracellular nanoparticle-like structure in AD-MSC were largely successful.

This result was consistent with previous study by Elfick and co-workers which showed vesicles in *mms6*-transfected bone marrow-derived MSC filled with both dispersed and larger electron-dense material at day 10 to day 15 post-transfection (Elfick *et al.*, 2017). In addition, this was also in a good agreement with previous work by Zhang and co-workers, showing gliosarcoma cell lines stably expressing *mms6* contain clusters of nanoparticles within membrane-enclosed structures after 3 days incubation in ferric citrate doped medium (Zhang *et al.*, 2014).

7.7 FERROMAGNETIC BEHAVIOUR DISPLAYED BY AD-MSC EXPRESSING *mms6*

In Chapter 5, the magnetic measurement based on ZFC-FC successfully showed the existence of room temperature ferromagnetism of AD-MSC expressing *mms6* and superparamagnetic behaviour in Ferucarbotran-loaded AD-MSC. This result might be related to the previous study by Liu and co-workers demonstrating that magnetosomes have ferromagnetic behaviour. The study suggested that the different magnetic properties of magnetosomes and MNP may be largely due to their different size (Liu *et al.*, 2012). The large sizes of magnetosomes results in a ferromagnetic behaviour at physiological temperature, while the SPION of sizes below 20 nm are superparamagnetic at this temperature (Arakaki *et al.*, 2008; Alphandéry *et al.*, 2010).

Although it should be stated that the expression of *mms6* alone in AD-MSC would not be able to synthesise ferromagnetic magnetosome structure similar to the one in MTB, the ferromagnetic behaviour displayed by AD-MSC expressing *mms6* could mean that the Mms6 protein binds iron and form bigger nanocrystal aggregates, instead of smaller superparamagnetic nanocrystal.

For future experimentation, it would have been useful to use Atomic force microscopy/magnetic force microscopy (AFM/MFM) to analyse the magnetization of the cells, instead of using ZFC FC analysis alone. Moreover, it will be interesting to quantify the amount of iron in cells by using mass spectrometry, an analytical technique that measures the mass of different molecules within a sample. This quantification works by ionizing the chemical species and sorting the ions based on their mass-to-charge ratio; the mass spectrum indicates the masses within a sample (Glish and Vachet, 2003).

7.8 THE POTENTIAL USE OF AD-MSC EXPRESSING *mms6* FOR MRI AND MNHT APPLICATION

In Chapter 6, experiments were aimed to test the hypothesis that the nanoparticle produced inside AD-MSC expressing *mms6* could generate a magnetic hyperthermia effect by applying AMF into the cells. Cell viability, cell apoptosis and HSP70 expression were investigated as the parameter of magnetic hyperthermia effect. The experiments also aimed to demonstrate the potential use of AD-MSC expressing *mms6* as a contrast agent for MRI.

To confirm the potential use of *mms6* as a reporter gene for MRI, an *in vitro* MRI experiment successfully showed that MR contrast was detected in AD-MSC expressing *mms6*, indicating the promising use of *mms6* as a reporter gene. This result was consistent with the previous report by Zhang and co-workers which showed *mms6* transfected gliosarcoma cells displaying MR changes in both *in vitro* and *in vivo* experiments (Zhang *et al.*, 2014). However, due to limited time, this experiment was

only done once, thus more experiments are needed to improve the reliability and the reproducibility of the data.

Using both 2-D monolayer and 3-D models, the *in vitro* AMF experiments revealed no observable difference in AMF application effect on cell viability of AD-MSC expressing *mms6*. In addition, similar negative results were also found on Ferucarbotran-loaded AD-MSC, despite these nanoparticles showing superparamagnetic behaviour as discussed in Chapter 5. The investigation on cell apoptosis and HSP70 expression of AD-MSC expressing *mms6* following the AMF application also showed no observable difference. However, it was unfortunate that the cell apoptosis experiment was only performed once due to limited time and costs. Indeed, using TUNEL (terminal deoxynucleotidyl transferase mediated dUTP nick end labeling) analysis alone to detect cell apoptosis based on DNA fragmentation may not be enough to demonstrate cells undergoing apoptosis. Typical apoptosis hallmarks are: cell shrinkage, membrane blebbing, mitochondrial alteration, metabolic changes, nuclear condensation and genomic DNA fragmentation, activated caspases, and the eventual engulfment of the cell by phagosomes (Mukhopadhyay *et al.*, 2014). Therefore, for the future experimentation, it would be useful to perform cell apoptosis detection techniques such as analysing the plasma membrane changes using AnnexinV, followed by fluorescence, confocal microscopy or, together with propidium iodide, by FACS (Gu *et al.*, 2017); measuring the mitochondrial integrity using MitoTrackerRed, Rhodamine 123 followed by confocal microscopy or FACS (Gorojod *et al.*, 2017); or analysis of caspase-3 activation (Wang *et al.*, 2013; Zhang *et al.*, 2013).

Another important parameter assessed is the expression of heat shock proteins (HSP). HSPs represent one of the most conserved groups of proteins throughout evolution, and are classified on the basis of their molecular weight and funtions, HSP are divided into five major families. HSP60, HSP70, HSP90 and HSP100 are the most studied members of the family. Each family is comprised of several members, with similar molecular weights, but different patterns of induction and expression (Fuller *et al.*, 1994; Dubey *et al.*, 2015). It has been shown that HSP70 expression by hyperthermia

induced antitumour immunity in the T-9 rat glioma (Ito *et al*., 2003). Moreover, HSP70 transcriptional activation analysis can be used as molecular thermometer to sense cells response to magnetic hyperthermia (Moros *et al*., 2015). For the future experimentation, it would have been beneficial to investigate the expression of few families of HSP at certain time point. Also, instead of using semi quantitative measurement based on western blot result performed in this study, other techniques such as qRT-PCR could be more accurate way to quantify the HSP expression (Moros *et al*., 2015).

While the use of *mms6* for cells innately producing intracellular nanoparticles has potential, the present study indicates continuing difficulty and reliability of actually demonstrating the use of such an approach for magnetic hyperthermia treatment. It was believed that the negligible magnetic hyperthermia effect associated with AMF treatment both on Ferucarbotran-loaded AD-MSC and AD-MSC expressing *mms6* could be related to low number of cells or small cell pellet size used in this study. The interpretation of this result is that the one million cells used in this experiment is not sufficient to achieve the AMF treatment scale for increasing the temperature. In 2002, Rabin declared that nanoscale heating effects are negligible, suggesting a single magnetic nanoparticle does not have a practical effect on hyperthermia. Using a simple diffusive heat transfer model, he predicted that the maximum temperature change incurred by an isolated cell is negligible, even if the cells are packed to capacity with AMF-treated magnetic nanoparticles. Furthermore, he integrated experimentally achievable intracellular nanoparticle concentrations and heating efficiencies (150 mW/g Fe for iron oxide nanoparticles at 500 pg Fe/cell) to predict the achievable steady-state temperature increase of collections of such cells. He revealed that a high concentrated nanoparticle-containing cells, approximately 1 mm in diameter or containing no less than 200000 cells, would be crucial for therapeutic levels of hyperthermia to be achieved (Rabin, 2002). In agreement with this, Wilhelm and co-workers showed more than 80% of the cells were killed after being submitted twice to AMF (31 mT; 700 kHz; 1 hour duration), using 20 million cells of loose pellet. Interestingly, their study showed when magnetic cells coexist with non-magnetic ones, the same proportion of cytotoxicity was found on both populations following the AMF

application, suggesting the cytotoxic hyperthermia is a function of total iron particle content in the pellet (Wilhelm et al. 2007). In short, it is believed that macroscopic hyperthermia or extracellular hyperthermia is still far superior to intracellular hyperthermia in the thermal sense, assuming that the same number of nanoparticles are present in both situations. Therefore, future experimentation using a larger number of cells might be useful to test this hypothesis. Furthermore, several sessions of AMF may have more benefit than only performing one session of AMF application. This has been suggested in a previous report which use magnetosome-loaded tumour exposed 12 to 15 of 30 min AMF applications to achieve full tumour disappearance (Alphandéry *et al.*, 2017b)

7.9 CONCLUSION

In conclusion, the presented study, although it does not lead to a significant *in-vitro* magnetic hyperthermia effect, has significantly contributed to our knowledge on genetically modified AD-MSC expressing magnetic nanoparticles. This approach is remains promising for MR imaging and could yet be optimised for magnetic targeting in biomedical application.

8 APPENDICES

8.1 MAGISTER PLASMID CONSTRUCT

mms6 gene used in this study belongs to *Magnetospirillum. Magneticum*. The *mms6* DNA fragment was optimised for mammalian cell expression by using *mms6* gene codon optimization and by adding a Kozak sequence at the N terminus of the *mms6* gene. This particular gene sequence was named MAGISTER (MAG) gene and. Two types of constructs were used:

1) ***mms6* + single tag marker**

   This construct has polyhistidine-tag at the N terminus of the *mms6* DNA fragment. The construct was synthesized and cloned into pcDNA3.1 plasmid at KpnI/EcoRI restriction site by GeneArt® Gene Synthesis service.

The nucleotide sequence of this construct is the following:

CAAGGGTACCGCCGCCACCATGAGCGGCTCCCATCATCATCACCATCACGGATCCGCC
GCCACCATGGGTGAGATGGAACGGGAGGGGGCCGCCGCCAAAGCCGGCGCCGCGAA
GACCGGCGCGGCCAAGACCGGCACCGTGGCCAAGACCGGCATCGCGGCCAAGACCG
GCGTCGCGACGGCCGTCGCCGCCCCGGCAGCCCCGGCAAACGTCGCCGCCGCCCAG
GGCGCCGGGACCAAAGTGGCACTGGGCGCCGGCAAAGCGGCCGCCGGCGCCAAAGT
AGTGGGCGGCACCATCTGGACCGGCAAGGGCCTGGGCCTGGGTCTCGGCCTGGGCC
TGGGCGCCTGGGGGCCGATCATCTTGGGCGTAGTGGGCGCAGGGGCCGTGTACGCC
TACATGAAGAGCCGCGACATCGAGTCCGCGCAGTCGGACGAGGAGGTGGAGCTGAGA
GATGCCCTAGCCTGAATTCATCC

CATCATCATCACCATCAC : Polyhistidine Tag.

GGTACC: KpnI Restriction Site

GAATTC: EcoRI Retriction Site

ATG : Start Codon

TAG : Stop Codon

2) *mms6* + double tag marker

This construct has polyhistidine-tag at the N terminus and GFP-tag at the C terminus of the *mms6* DNA fragment. The construct was synthesized and cloned into pcDNA3.1 plasmid at NheI/HindIII restriction site by GeneArt® Gene Synthesis service. There were 4 different MAGISTER gene constructs with double tag markers, depending on different codon optimization of the *mms6* gene, used in this study

The nucleotide sequence of this construct is the following:

1. His-GFP *mms6 wild type/ non-codon optimized (MagWT)*

GCTAGCGCCGCCACCATGAGCGGCTCCCATCATCATCACCATCACATGGGCGAG
ATGGAGCGCGAGGGCGCCGCCGCCAAGGCCGGGGCTGCCAAGACGGGCGCCGC
CAAGACCGGAACCGTCGCCAAGACCGGCATCGCCGCCAAGACGGGTGTTGCCAC
CGCCGTTGCCGCTCCGGCGGCTCCTGCCAATGTTGCCGCCGCCCAGGGCGCCGG
GACCAAGGTCGCCCTTGGCGCGGGCAAGGCCGCCGCCGGTGCCAAGGTCGTCGG
TGGAACCATCTGGACCGGTAAGGGGCTGGGCCTCGGTCTGGGTCTCGGTCTGGG
CGCGTGGGGGCCGATCATTCTCGGCGTTGTTGGCGCCGGGGCGGTTTACGCGTA
TATGAAGAGCCGTGATATCGAATCGGCGCAGAGCGACGAGGAAGTCGAACTGC
GCGACGCGCTGGCCTTGGTACCGAGCTCGGATCCACCGGTCGCCACCATGGTGA
GCAAGGGCGAGGAGCTGTTCACCGGGGTGGTGCCCATCCTGGTCGAGCTGGACG
GCGACGTAAACGGCCACAAGTTCAGCGTGTCCGGCGAGGGCGAGGGCGATGCC
ACCTACGGCAAGCTGACCCTGAAGTTCATCTGCACCACCGGCAAGCTGCCCGTG
CCCTGGCCCACCCTCGTGACCACCCTGACCTACGGCGTGCAGTGCTTCAGCCGCT
ACCCCGACCACATGAAGCAGCACGACTTCTTCAAGTCCGCCATGCCCGAAGGCT
ACGTCCAGGAGCGCACCATCTTCTTCAAGGACGACGGCAACTACAAGACCCGCG
CCGAGGTGAAGTTCGAGGGCGACACCCTGGTGAACCGCATCGAGCTGAAGGGC
ATCGACTTCAAGGAGGACGGCAACATCCTGGGGCACAAGCTGGAGTACAACTAC
AACAGCCACAACGTCTATATCATGGCCGACAAGCAGAAGAACGGCATCAAGGT
GAACTTCAAGATCCGCCACAACATCGAGGACGGCAGCGTGCAGCTCGCCGACCA
CTACCAGCAGAACACCCCCATCGGCGACGGCCCCGTGCTGCTGCCCGACAACCA
CTACCTGAGCACCCAGTCCGCCCTGAGCAAAGACCCCAACGAGAAGCGCGATCA
CATGGTCCTGCTGGAGTTCGTGACCGCCGCCGGGATCACTCTCGGCATGGACGA
GCTGTACAAGTAAAAGCTT

2. His-GFP *mms6 codon optimized 01 (Mag02)*

GCTAGCGCCGCCACCATGAGCGGCTCCCATCATCATCACCATCACATGGGCGAA
ATGGAACGTGAAGGCGCGGCGGCGAAAGCGGGCGCGGCGAAAACCGGCGCGGC
GAAAACCGGCGCGGTGGCGAAAACCGGCATTGCGGCGAAAACCGGCGTGGCGA
CCGCGGTGGCGGCGCCGGCGGCGCCGGCGAACGTGGCGGCGGCGCAGGGCGCG
GGCACCAAAGTGGCGCTGGGCGCGGGCAAAGCGGCGGCGGGCGCGAAAGTGGT
GGGCGGCACCATTTGGACCGGCAAAGGCCTGGGCCTGGGCCTGGGCCTGGGCCT
GGGCGCGTGGGGCCCGATTATTCTGGGCGTGGTGGGCGCGGGCGCGGTGTATGC
GTATATGAAAAGCCGTGATATTGAAAGCGCGCAGAGCGATGAAGAAGTGGAAC
TGCGTGATGCGCTGGCGCCACCATTGGTACCGAGCTCGGATCCACCGGTCGCCA
CCATGGTGAGCAAGGGCGAGGAGCTGTTCACCGGGGTGGTGCCCATCCTGGTCG
AGCTGGACGGCGACGTAAACGGCCACAAGTTCAGCGTGTCCGGCGAGGGCGAG
GGCGATGCCACCTACGGCAAGCTGACCCTGAAGTTCATCTGCACCACCGGCAAG
CTGCCCGTGCCCTGGCCCACCCTCGTGACCACCCTGACCTACGGCGTGCAGTGCT
TCAGCCGCTACCCCGACCACATGAAGCAGCACGACTTCTTCAAGTCCGCCATGC
CCGAAGGCTACGTCCAGGAGCGCACCATCTTCTTCAAGGACGACGGCAACTACA
AGACCCGCGCCGAGGTGAAGTTCGAGGGCGACACCCTGGTGAACCGCATCGAG
CTGAAGGGCATCGACTTCAAGGAGGACGGCAACATCCTGGGGCACAAGCTGGA
GTACAACTACAACAGCCACAACGTCTATATCATGGCCGACAAGCAGAAGAACG
GCATCAAGGTGAACTTCAAGATCCGCCACAACATCGAGGACGGCAGCGTGCAGC
TCGCCGACCACTACCAGCAGAACACCCCCATCGGCGACGGCCCCGTGCTGCTGC
CCGACAACCACTACCTGAGCACCCAGTCCGCCCTGAGCAAAGACCCCAACGAGA
AGCGCGATCACATGGTCCTGCTGGAGTTCGTGACCGCCGCCGGGATCACTCTCG
GCATGGACGAGCTGTACAAGTAAAAGCTT

3. His-GFP *mms6 codon optimized 02 (Mag02)*

GCTAGCGCCGCCACCATGAGCGGCTCCCATCATCATCACCATCACATGGGTGAG
ATGGAACGGGAGGGGGCCGCCGCCAAAGCCGGCGCCGCGAAGACCGGCGCGGC
CAAGACCGGCACCGTGGCCAAGACCGGCATCGCGGCCAAGACCGGCGTCGCGA
CGGCCGTCGCCGCCCCGGCAGCCCCGGCAAACGTCGCCGCCGCCCAGGGCGCCG
GGACCAAAGTGGCACTGGGCGCCGGCAAAGCGGCCGCCGGCGCCAAAGTAGTG
GGCGGCACCATCTGGACCGGCAAGGGCCTGGGCCTGGGTCTCGGCCTGGGCCTG
GGCGCCTGGGGGCCGATCATCTTGGGCGTAGTGGGCGCAGGGGCCGTGTACGCC
TACATGAAGAGCCGCGACATCGAGTCCGCGCAGTCGGACGAGGAGGTGGAGCT
GAGAGATGCCCTAGCCTTGGTACCGAGCTCGGATCCACCGGTCGCCACCATGGT
GAGCAAGGGCGAGGAGCTGTTCACCGGGGTGGTGCCCATCCTGGTCGAGCTGGA
CGGCGACGTAAACGGCCACAAGTTCAGCGTGTCCGGCGAGGGCGAGGGCGATG
CCACCTACGGCAAGCTGACCCTGAAGTTCATCTGCACCACCGGCAAGCTGCCCG
TGCCCTGGCCCACCCTCGTGACCACCCTGACCTACGGCGTGCAGTGCTTCAGCCG
CTACCCCGACCACATGAAGCAGCACGACTTCTTCAAGTCCGCCATGCCCGAAGG
CTACGTCCAGGAGCGCACCATCTTCTTCAAGGACGACGGCAACTACAAGACCCG
CGCCGAGGTGAAGTTCGAGGGCGACACCCTGGTGAACCGCATCGAGCTGAAGG
GCATCGACTTCAAGGAGGACGGCAACATCCTGGGGCACAAGCTGGAGTACAACT
ACAACAGCCACAACGTCTATATCATGGCCGACAAGCAGAAGAACGGCATCAAG
GTGAACTTCAAGATCCGCCACAACATCGAGGACGGCAGCGTGCAGCTCGCCGAC
CACTACCAGCAGAACACCCCCATCGGCGACGGCCCCGTGCTGCTGCCCGACAAC
CACTACCTGAGCACCCAGTCCGCCCTGAGCAAAGACCCCAACGAGAAGCGCGAT
CACATGGTCCTGCTGGAGTTCGTGACCGCCGCCGGGATCACTCTCGGCATGGAC
GAGCTGTACAAGTAAAAGCTT

4. His-GFP *mms6 codon optimized 03 (Mag03)*

GCTAGCGCCGCCACCATGTCTGGATCTCACCACCACCATCACCACATGGGCGAG
ATGGAAAGAGAAGGCGCTGCTGCTAAAGCCGGCGCTGCTAAAACAGGTGCCGC
AAAAACAGGCGCCGTGGCCAAAACAGGCATTGCCGCTAAAACTGGCGTGGCCA
CAGCTGTTGCTGCTCCAGCTGCTCCTGCTAATGTGGCTGCTGCTCAAGGCGCCGG
AACAAAAGTTGCCCTTGGAGCCGGAAAAGCCGCCGCTGGTGCAAAAGTTGTTGG
CGGCACAATCTGGACAGGCAAAGGCCTCGGTCTTGGCCTTGGACTCGGACTTGG
AGCCTGGGGACCTATCATCCTGGGAGTTGTTGGAGCTGGCGCCGTGTACGCCTA
CATGAAGTCCAGAGATATCGAGAGCGCCCAGAGCGACGAGGAAGTTGAACTTA
GGGACGCTCTGGCTCCTCCACTGGTGCCTAGTTCTGATCCTCCAGTGGCCACAAT
GGTGTCCAAGGGCGAAGAACTGTTTACCGGCGTGGTGCCCATCCTGGTGGAACT
GGATGGGGATGTGAACGGCCACAAGTTCTCTGTGTCTGGCGAAGGCGAAGGGG
ATGCCACATACGGCAAGCTGACCCTGAAGTTCATCTGCACCACCGGAAAGCTGC
CCGTGCCTTGGCCTACACTGGTCACAACACTGACCTACGGCGTGCAGTGCTTCAG
CAGATACCCCGACCACATGAAGCAGCACGATTTCTTCAAGAGCGCCATGCCTGA
GGGCTACGTGCAAGAGCGGACCATCTTCTTCAAGGACGACGGCAACTACAAGAC
CAGAGCCGAAGTGAAGTTCGAGGGCGACACCCTGGTCAACAGAATCGAGCTGA
AGGGCATCGACTTCAAAGAGGATGGCAACATCCTGGGCCACAAGCTCGAGTACA
ACTACAACAGCCACAACGTGTACATCATGGCCGACAAGCAGAAGAACGGCATC
AAAGTCAACTTCAAGATCCGGCACAACATCGAGGACGGCTCTGTGCAGCTGGCC
GACCACTATCAGCAGAACACACCTATCGGAGATGGCCCCGTGCTGCTGCCCGAT
AATCACTACCTGTCTACCCAGAGCGCCCTGTCCAAGGATCCCAACGAGAAGAGG
GATCACATGGTGCTGCTGGAATTCGTGACAGCCGCCGGAATCACACTCGGCATG
GACGAGCTGTACAAGTGAAAGCTT

NheI: GCTAGC

Kozak sequence: GCCGCCACC

HisTag: CATCATCATCACCATCAC

ATG: actual gene starts at nt 46

HindIII: AAGCTT

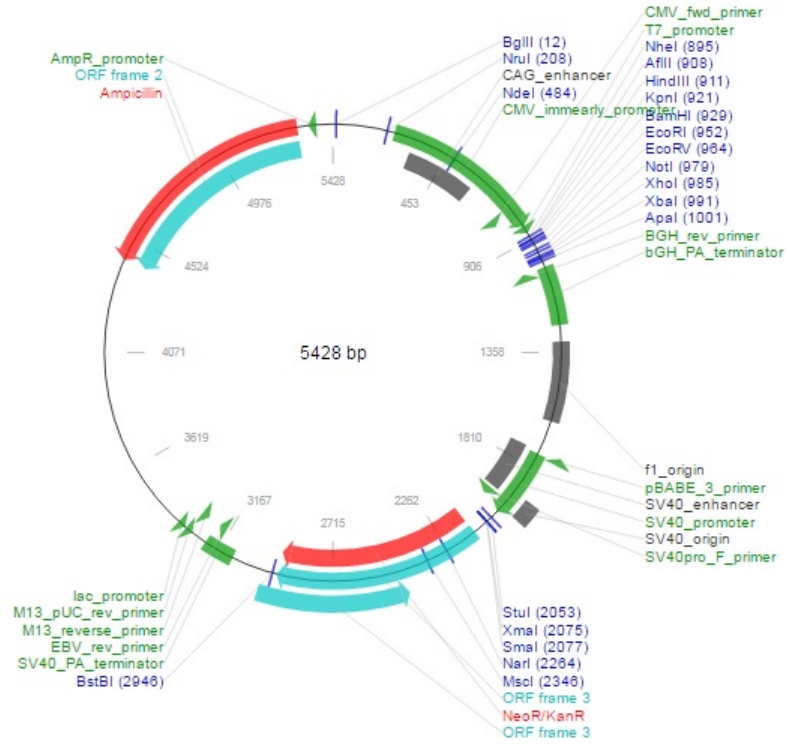

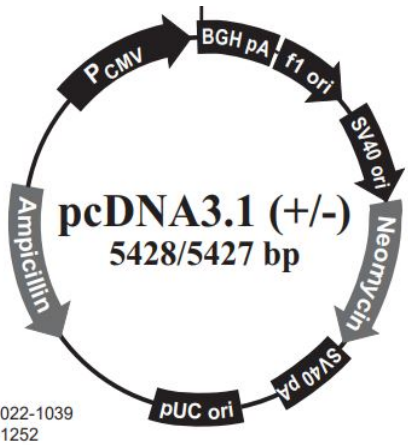

Comments for pcDNA3.1 (+)
5428 nucleotides

CMV promoter: bases 232-819
T7 promoter/priming site: bases 863-882
Multiple cloning site: bases 895-1010
pcDNA3.1/BGH reverse priming site: bases 1022-1039
BGH polyadenylation sequence: bases 1028-1252
f1 origin: bases 1298-1726
SV40 early promoter and origin: bases 1731-2074
Neomycin resistance gene (ORF): bases 2136-2930
SV40 early polyadenylation signal: bases 3104-3234
pUC origin: bases 3617-4287 (complementary strand)
Ampicillin resistance gene (*bla*): bases 4432-5428 (complementary strand)
ORF: bases 4432-5292 (complementary strand)
Ribosome binding site: bases 5300-5304 (complementary strand)
bla promoter (P3): bases 5327-5333 (complementary strand)

Figure 8-1: pcDNA3.1(+) Vector map. *Original picture taken from: https://tools.thermofisher.com/content/sfs/manuals/pcdna3_1_man.pdf*

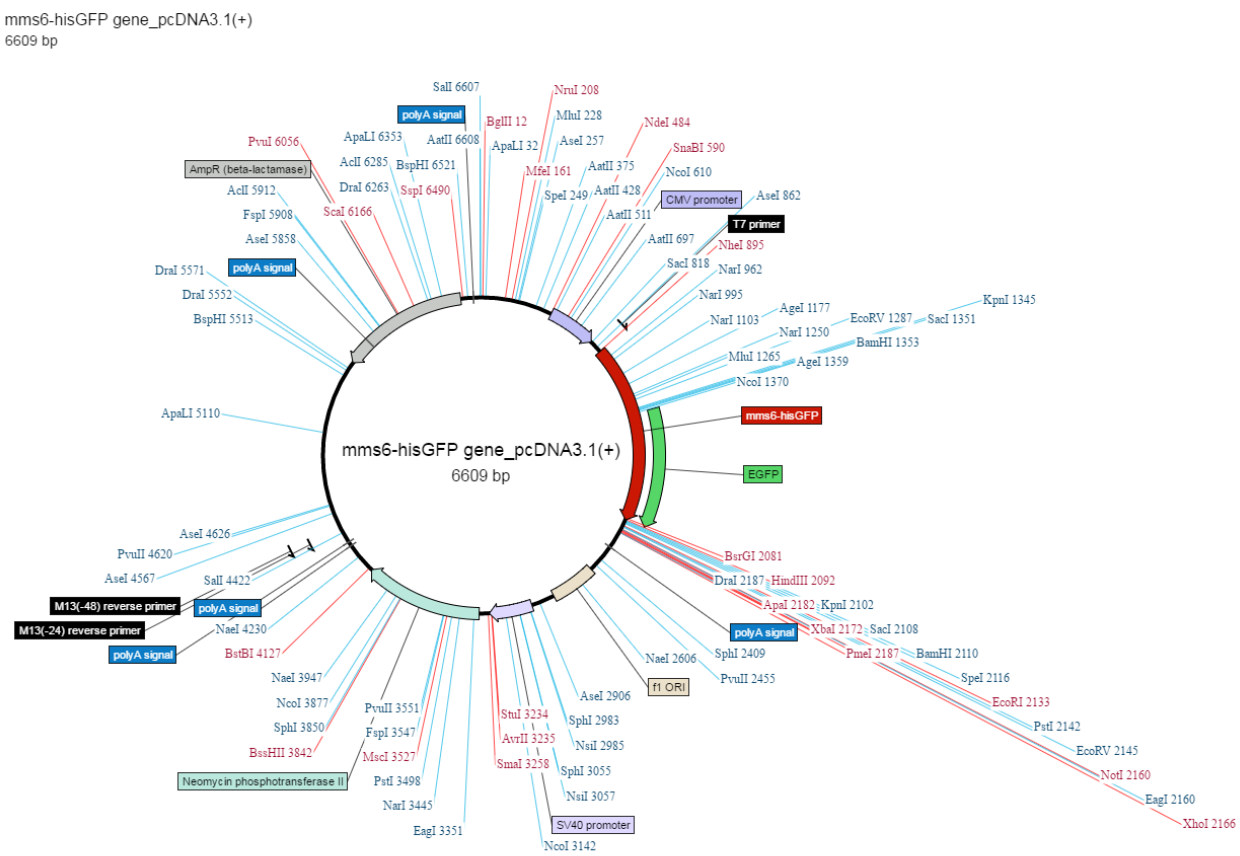

Figure 8-2: pcDNA3.1(+) Vector containing His-GFP mms6 gene construct. *The His-GFP mms6 gene was cloned into pcDNA3.1 plasmid at NheI/HindIII restriction site.*

8.2 MAGISTER PLASMID PURIFICATION

In order to evaluate whether the MAG plasmid containing His-GFP *mms6* had been successfully amplified, restriction enzyme digestion by HindIII/NheI (for Mag gene with double tag marker) restriction enzymes was performed. Briefly, 1 µg plasmid DNA, five units of restriction enzyme and 5 µl of 10x CutSmart buffers were used in each reaction. The reactions were made up to a volume of 50 µl in distilled water and incubated at 37 °C for 2 hours. Enzymes were heated for 20 min at 85°C after digestion. The digestion products were then visualized by conducting electrophoresis on 2% (w/v) agarose gels with SYBR™ Safe DNA gel stain.

Figure 8-3 showed DNA band at around 1200 bp, suggesting the presence of DNA fragment resulted from NheI and HindIII enzyme digestion, as indicated by Lane B, D, F, H. The expected size of the DNA digested with NheI/HindIII was 1181 bp. Therefore, this result confirmed the successful of MAGISTER plasmid cloning and purification.

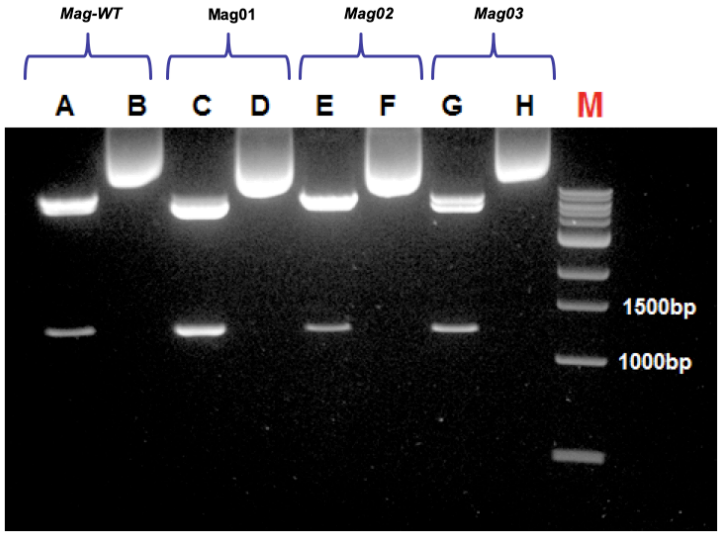

Figure 8-3: Agarose gel electrophoretograms demonstrating the plasmid DNA containing His-GFP mms6 gene fragment cut by NheI and HindIII restriction enzymes. *Lane B, D, F, H = Control/Uncut; Lane A, C, E, G = plasmid containing His-GFP tag mms6 gene cut by NheI and HindIII. M = Marker*

8.3 LENTI-*mms6* PLASMID CONSTRUCT

A lentiviral vector, pSicoR-Ef1a-mCh-Puro plasmid was used to construct lenti-*mms6* plasmid. The *mms6* insert fragment was cut from pcDNA3.1 (+) plasmid containing codon optimized *mms6* gene (Mag01). This Mag01 plasmid was kindly provided by Lisa Lungaro, former PhD student in the group.

This *mms6* insert sequence from pcDNA3.1 (+) is start from CAG enhancer region (or SpeI restriction enzyme site) to NotI restriction enzyme site.

The insert sequence is ligated to pSicoR-Ef1a-mCh-Puro plasmid at XbaI (2626) and NotI (2982) restriction enzyme site.

The actual *mmms6* nucleotide sequence of this construct is the following:

ATGGGCGAAATGGAACGTGAAGGCGCGGCGGCGAAAGCGGGCGCGGCGAAAAC
CGGCGCGGCGAAAACCGGCGCGGTGGCGAAAACCGGCATTGCGGCGAAAACCG
GCGTGGCGACCGCGGTGGCGGCGCCGGCGGCGCCGGCGAACGTGGCGGCGGCG
CAGGGCGCGGGCACCAAAGTGGCGCTGGGCGCGGGCAAAGCGGCGGCGGGCGC
GAAAGTGGTGGGCGGCACCATTTGGACCGGCAAAGGCCTGGGCCTGGGCCTGG
GCCTGGGCCTGGGCGCGTGGGGCCCGATTATTCTGGGCGTGGTGGGCGCGGGCG
CGGTGTATGCGTATATGAAAAGCCGTGATATTGAAAGCGCGCAGAGCGATGAAG
AAGTGGAACTGCGTGATGCGCTGGCGCCACCAUGG

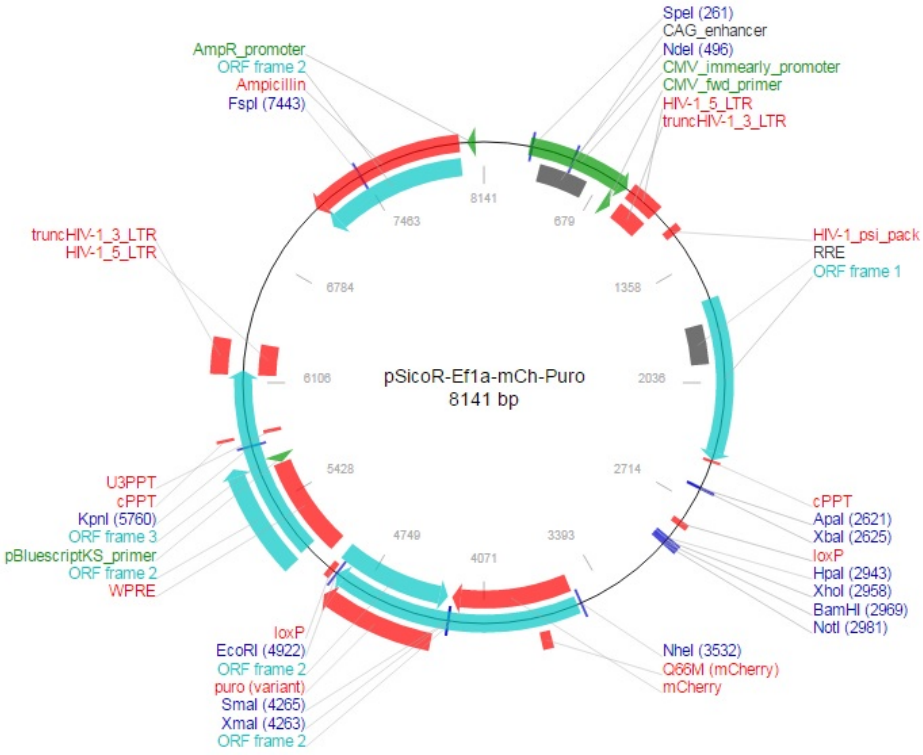

Figure 8-4: PsicoR-Ef1a-mCh-Puro Vector map.

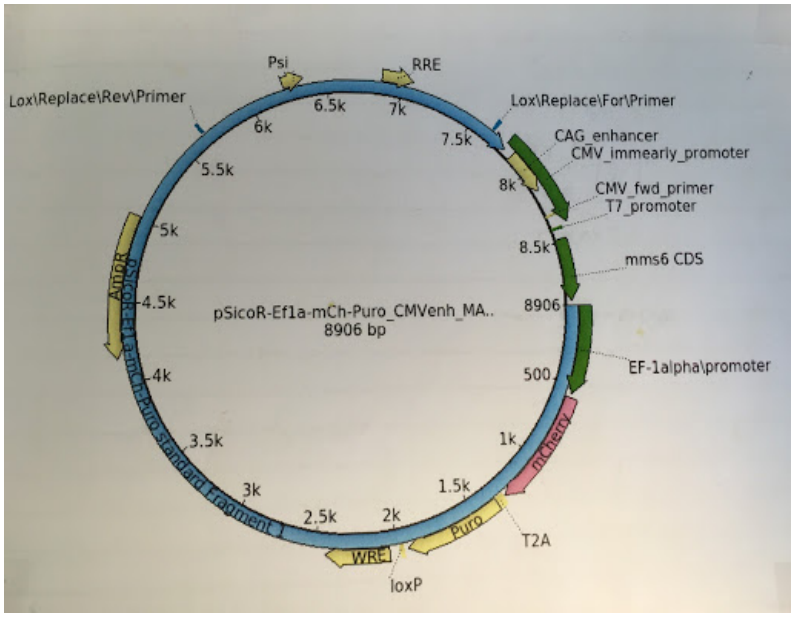

Figure 8-5: PsicoR-Ef1a-mCh-Puro Vector containing codon optimised mms6 (Mag01) gene construct.

Figure 8-6 DNA shows DNA sequencing analysis of the PsicoR-Ef1a-mCh-Puro vector containing codon optimised *mms6* (Mag01). The sequencing results were aligned to match the original sequence using the Basic Local Alignment Search Tool (BLAST).

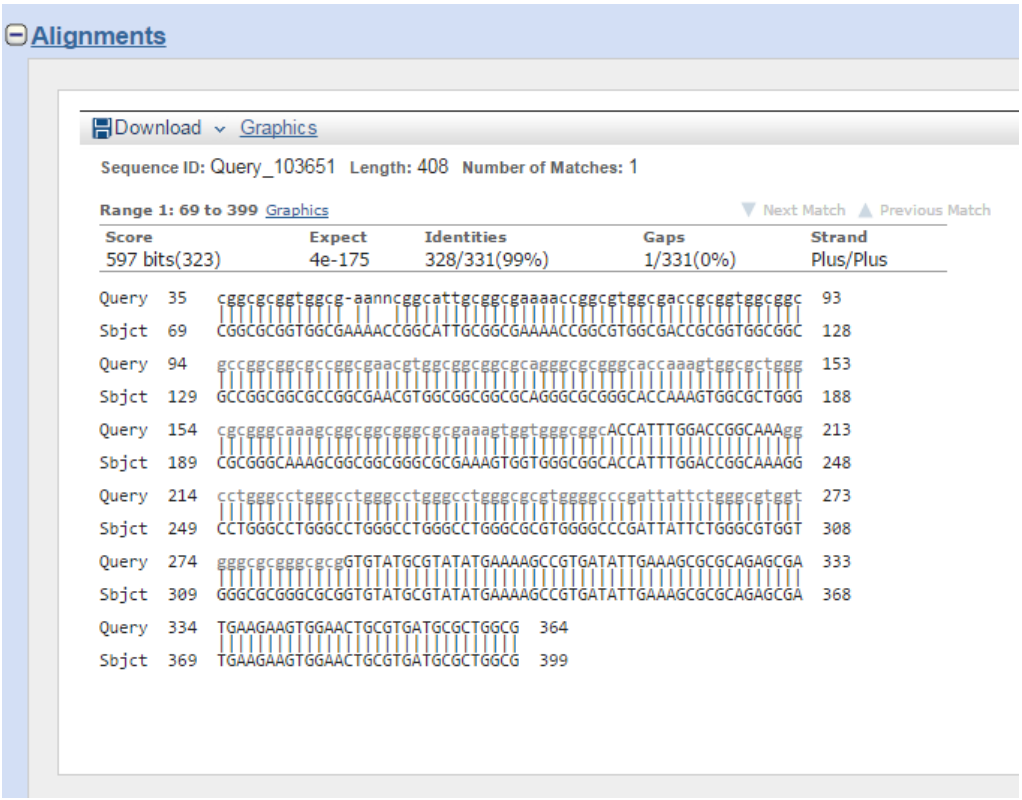

Figure 8-6: DNA sequencing analysis of plasmid DNA containing Mag02 obtained from Miniprep. *Detailed side by side alignment information for the DNA sequence result for sample (query) and known Mag01 gene sequence (subject). The sample sequence result was 99% identity to the sequences of Mag01 gene fragment.*

8.4 LENTI-*mms6* TRANSDUCTION EFFICIENCY TEST ON HT1080 HUMAN FIBROBLAST CELLS.

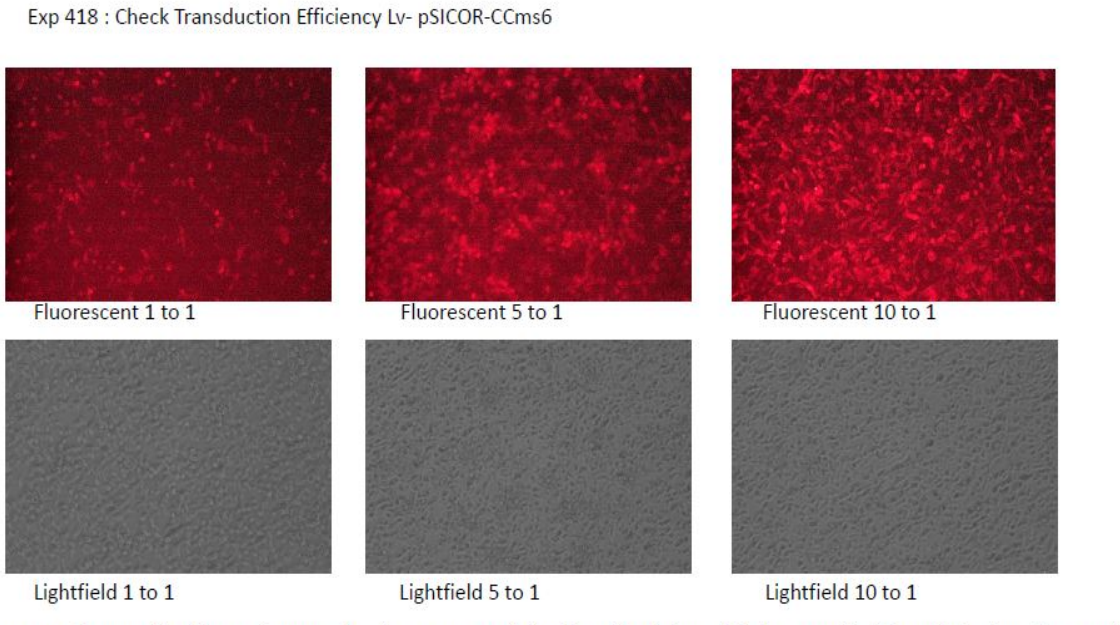

Figure 8-7: Lenti-mms6 transduced efficiency test on HT1080 human fibroblast. *Cells were plated at 2 x 10^5 cells/well and lentivirus added at a multiplicity of infection of 1, 5, and 10 vieruses per cell. Images were captures 72 hours later.*

8.5 FLOW CYTOMETRY ANALYSIS OF MAG01-NUCLEOFECTED AD-MSC

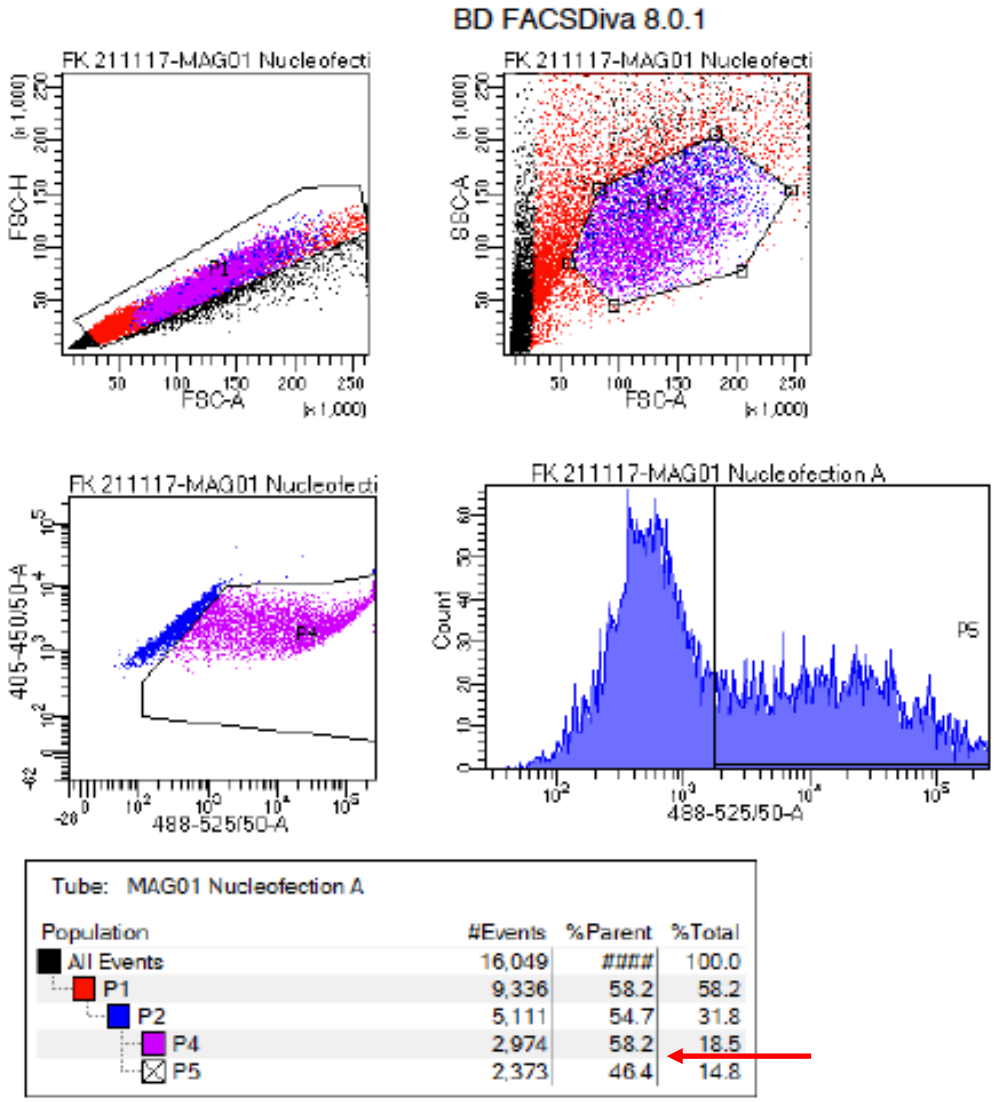

Figure 8-8: **Representative image for Flow cytometry analysis of Mag01-transfected AD-MSC at 2 days after nucleofection.** *P1 gate set for total cell population. P2 gate set for live cells. P4 gate set for GFP positive cells by using untransfected control cells to set the gate excluding GFP-negative population. Percentage of GFP-positive expression are indicated by the red arrow in the panel. The result shows 58.2% GFP-positive cells after nucleofection.*

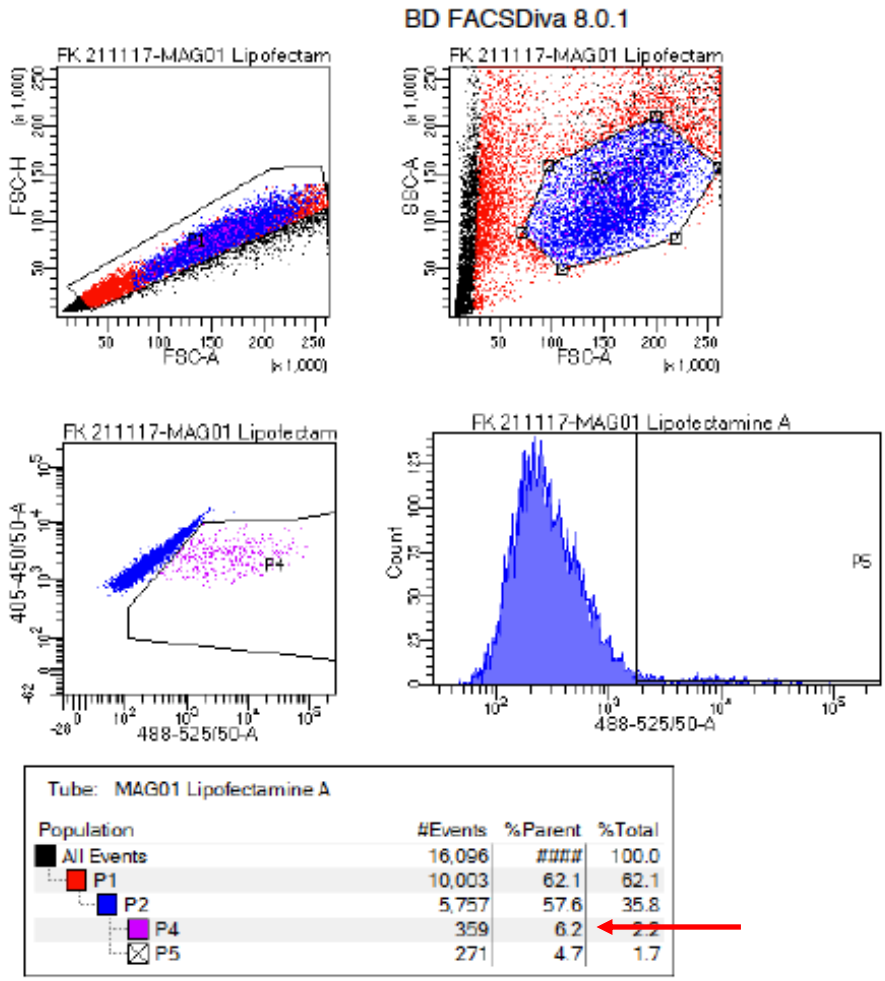

Figure 8-9: Representative image for Flow cytometry analysis of Mag01-transfected AD-MSC at 2 days after transfection using Lipofectamine 3000. *P1 gate set for total cell population. P2 gate set for live cells. P4 gate set for GFP positive cells by using untransfected control cells to set the gate excluding GFP-negative population. Percentage of GFP-positive expression are indicated by the red arrow in the panel. The result shows 6.2% GFP-positive cells after transfection using Lipofectamine 3000.*

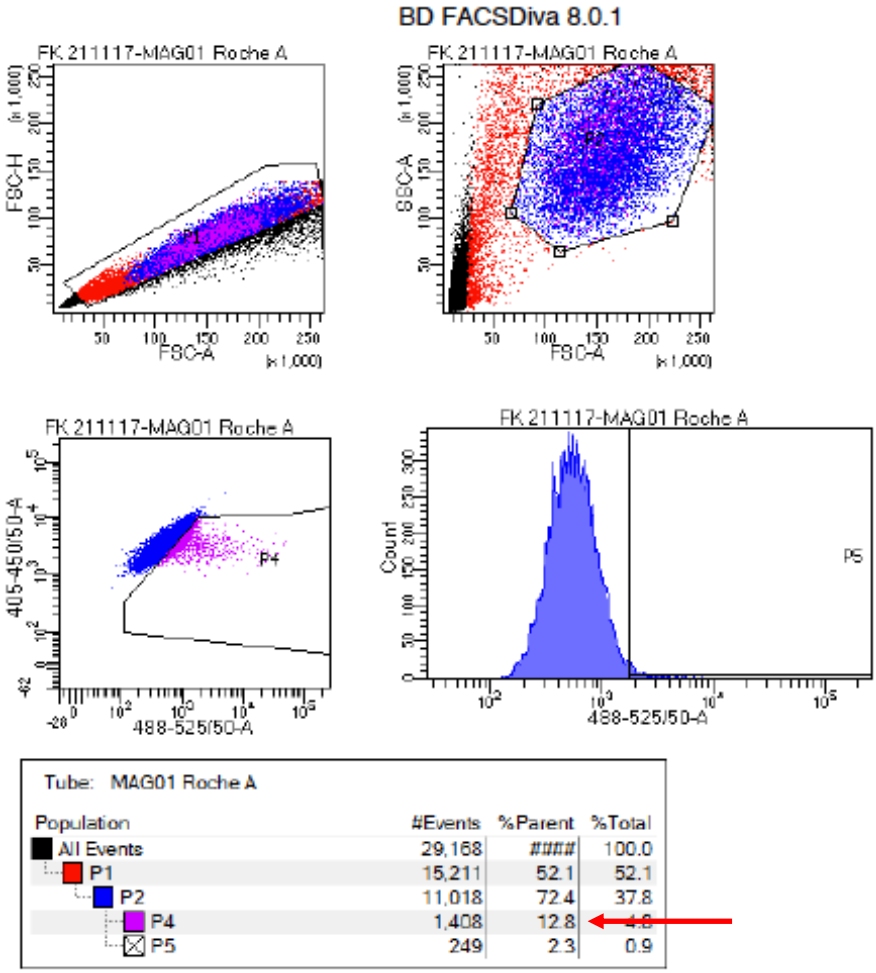

Figure 8-10: Representative image for Flow cytometry analysis of Mag01-transfected AD-MSC at 2 days after transfection using XtremeGENE HP. *P1 gate set for total cell population. P2 gate set for live cells. P4 gate set for GFP positive cells by using untransfected control cells to set the gate excluding GFP-negative population. Percentage of GFP-positive expression are indicated by the red arrow in the panel. The result shows 12.8% GFP-positive cells after transfection using XtremeGENE HP DNA transfection reagent.*

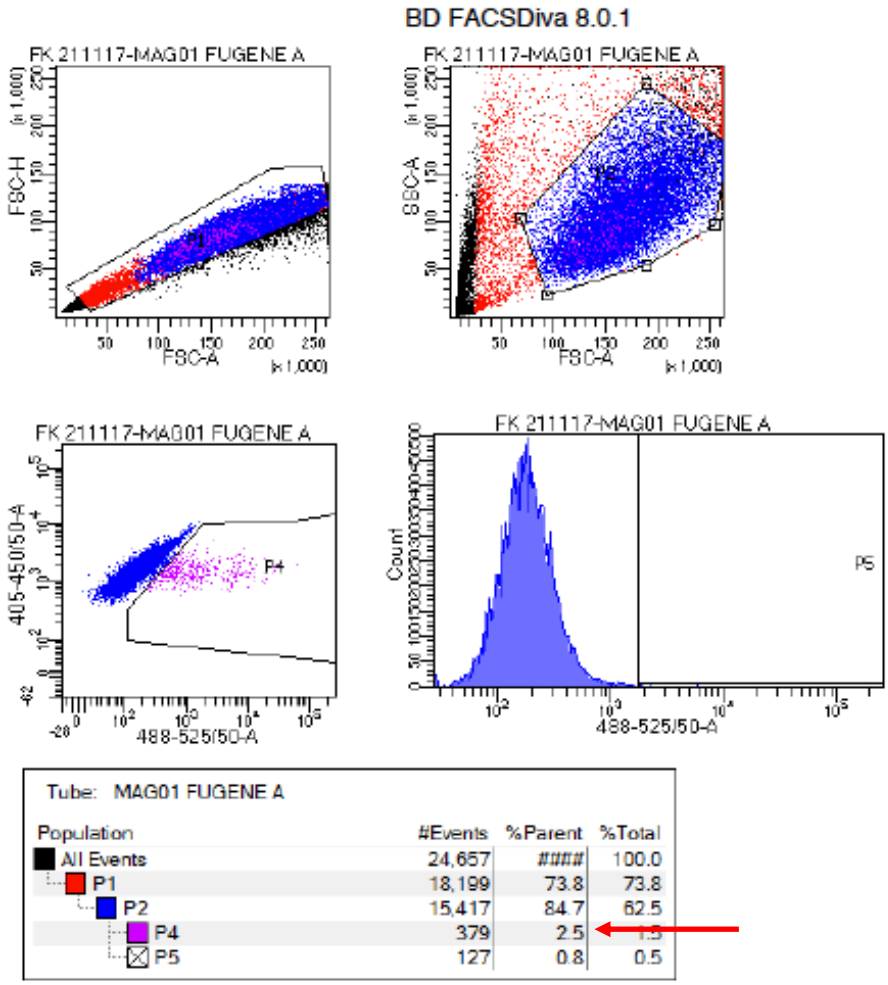

Figure 8-11: Representative image for Flow cytometry analysis of Mag01-transfected AD-MSC at 2 days after transfection using FugeneHD. *P1 gate set for total cell population. P2 gate set for live cells. P4 gate set for GFP positive cells by using untransfected control cells to set the gate excluding GFP-negative population. Percentage of GFP-positive expression are indicated by the red arrow in the panel. The result shows 58.2% GFP-positive cells after transfection using FugeneHD transfection reagent.*

8.6 magneTHerm V1.5 SYSTEM

8.6.1 magneTHerm V1.5 Setup

The physical principle that underlies the magneTherm system device function is that a current applied through a conductor determines the creation of a circular magnetic field around it, as described by Ampere's law:

$$B = \frac{\mu_0 \mathrm{I}}{2\pi r}$$

where B is the magnetic field, μ_0 the permeability of the free space, I is the current in the wire, and r the radius from the wire.

If the conductor is a coil (as for the magneTherm system), the magnetic field strength is enhanced, and a strong field is created at the centre of the coil, where all the magnetic field generated by each turn of the coil pass. The physical concept that drives the experiments is that MNPs subjected to an AC magnetic field:

1) lose energy as a consequence of their magnetisation reversal process, producing heat;
2) tend to vibrate, causing the cell membrane breaking

Figure 8-12 shows magneTherm system device for MNHT experiments.

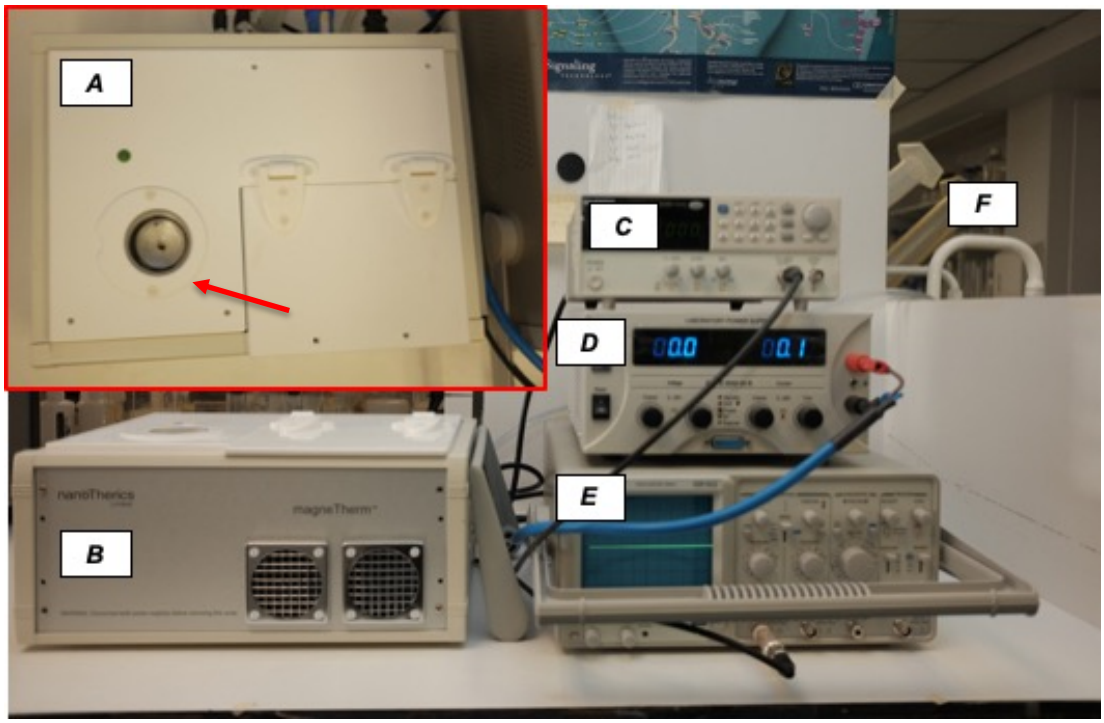

Figure 8-12: Nanotherics magneTherm system device used in the experiments.

Components of the system are: A) MagneTherm system (top down view). Red arrow shows water jacket and sample location B) MagneTherm system, C) Function generator, D) DC Power Suply E) Oscilloscope, F) Cooling water connecting tubes/Sink

8.6.2 magneTHerm V1.5 System Calculation Document

Three different capacitors used in the magneTherm™: a 200 nF capacitance; a 22 nF capitance; and a 6.2 nF capitance to achieve the desired frequency range for the 9-turn coil. The function generator was used to generate a square waveform at three different frequencies: 178.3 kHz (23.89 mT), 540 kHz (24.87 mT), and 1030 kHz (13.37 mT).

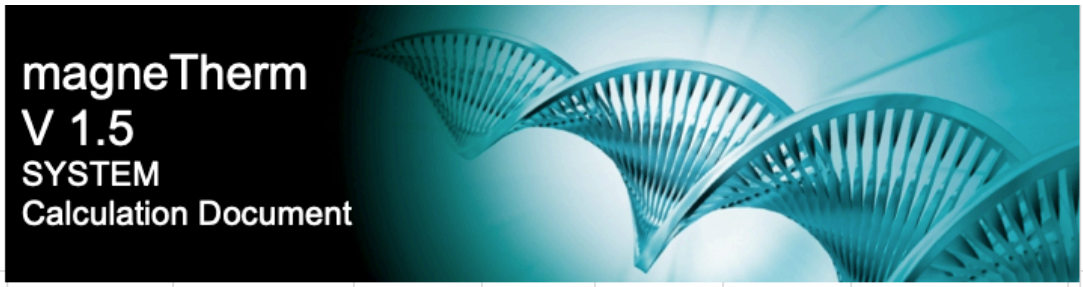

Calculations

nanoTherics limited

V =	800	Vp-p	N =	9	Turns
f =	178,300.0	(Hz)	I =	63.37328	A(rms)
C =	200	(nF)	ℓ =	0.03	m
I =	63.37328223	A(rms)	B =	23.89116	(mT)
V =	2500	Vp-p	N =	9	Turns
f =	540,000	(Hz)	I =	65.97681	A(rms)
C =	22	(nF)	ℓ =	0.03	m
I =	65.97681163	A(rms)	B =	24.87267	(mT)
V =	2500	Vp-p	N =	9	Turns
f =	1,030,000	(Hz)	I =	35.46531	A(rms)
C =	6.2	(nF)	ℓ =	0.03	m
I =	35.46531305	A(rms)	B =	13.37011	(mT)

V: volts
f: frequency
A: area, square meters
C: capitance
I: inductance
N: number of turns
B: magnetic field, Tesla (10000 gauss = 1 Tesla)

9 BIBLIOGRAPHY

Abraham Lee, J. L. (2006) *BioMEMS and Biomedical Nanotechnology: Volume I: Biological and Biomedical Nanotechnology*. doi: 10.1007/978-0-387-25842-3_6.

Ahmed, K., Tabuchi, Y. and Kondo, T. (2015) 'Hyperthermia: An effective strategy to induce apoptosis in cancer cells', *Apoptosis*. Springer US, 20(11), pp. 1411–1419. doi: 10.1007/s10495-015-1168-3.

Airenne, K. J., Hu, Y.-C., Kost, T. A., Smith, R. H., Kotin, R. M., Ono, C., Matsuura, Y., Wang, S. and Ylä-Herttuala, S. (2013) 'Baculovirus: an insect-derived vector for diverse gene transfer applications.', *Molecular therapy : the journal of the American Society of Gene Therapy*, 21(4), pp. 739–49. doi: 10.1038/mt.2012.286.

Akimoto, K., Kimura, K., Nagano, M., Takano, S., To'a Salazar, G., Yamashita, T. and Ohneda, O. (2013) 'Umbilical cord blood-derived mesenchymal stem cells inhibit, but adipose tissue-derived mesenchymal stem cells promote, glioblastoma multiforme proliferation.', *Stem cells and development*, 22(9), pp. 1370–86. doi: 10.1089/scd.2012.0486.

Alphandéry, E., Chebbi, I., Guyot, F. and Durand-Dubief, M. (2013) 'Use of bacterial magnetosomes in the magnetic hyperthermia treatment of tumours: A review'. doi: 10.3109/02656736.2013.821527.

Alphandéry, E., Faure, S., Seksek, O., Guyot, F. and Chebbi, I. (2011) 'Chains of Magnetosomes Extracted from AMB-1 Magnetotactic Bacteria for Application in Alternative Magnetic Field Cancer Therapy', 5(8), pp. 6279–6296. doi: 10.1021/nn201290k.

Alphandéry, E., Guyot, F. O. and Chebbi, I. (2012) 'Preparation of chains of magnetosomes, isolated from Magnetospirillum magneticum strain AMB-1 magnetotactic bacteria, yielding efficient treatment of tumors using magnetic hyperthermia', *International Journal of Pharmaceutics*, 434, pp. 444–452. doi: 10.1016/j.ijpharm.2012.06.015.

Alphandéry, E., Idbaih, A., Adam, C., Delattre, J. Y., Schmitt, C., Guyot, F. and Chebbi, I. (2017a) 'Chains of magnetosomes with controlled endotoxin release and partial tumor occupation induce full destruction of intracranial U87-Luc glioma in mice under the application of an alternating magnetic field', *Journal of Controlled Release*. Elsevier, 262(July), pp. 259–272. doi: 10.1016/j.jconrel.2017.07.020.

Alphandéry, E., Idbaih, A., Adam, C., Delattre, J. Y., Schmitt, C., Guyot, F. and Chebbi, I. (2017b) 'Development of non-pyrogenic magnetosome minerals coated with poly-l-lysine leading to full disappearance of intracranial U87-Luc glioblastoma in 100% of treated mice using magnetic hyperthermia',

Biomaterials. doi: 10.1016/j.biomaterials.2017.06.026.

Alphandéry, E., Lijeour, L., Lalatonne, Y. and Motte, L. (2010) 'Different signatures between chemically and biologically synthesized nanoparticles in a magnetic sensor: A new technology for multiparametric detection', *Sensors & Actuators: B. Chemical*, 147, pp. 786–790. doi: 10.1016/j.snb.2010.04.009.

Aluigi, M., Fogli, M., Curti, A., Isidori, A., Gruppioni, E., Chiodoni, C., Colombo, M. P., Versura, P., D'Errico-Grigioni, A., Ferri, E., *et al.* (2006) 'Nucleofection Is an Efficient Nonviral Transfection Technique for Human Bone Marrow-Derived Mesenchymal Stem Cells', *Stem Cells*. Wiley, 24(2), pp. 454–461. doi: 10.1634/stemcells.2005-0198.

Alvarez-Berríos, M. P., Castillo, A., Mendéz, J., Soto, O., Rinaldi, C. and Torres-Lugo, M. (2013) 'Hyperthermic potentiation of cisplatin by magnetic nanoparticle heaters is correlated with an increase in cell membrane fluidity', *International Journal of Nanomedicine*, 8, pp. 1003–1013. doi: 10.2147/IJN.S38842.

Amemiya, Y., Arakaki, A., Staniland, S. S., Tanaka, T. and Matsunaga, T. (2007) 'Controlled formation of magnetite crystal by partial oxidation of ferrous hydroxide in the presence of recombinant magnetotactic bacterial protein Mms6.', *Biomaterials*, 28(35), pp. 5381–9. doi: 10.1016/j.biomaterials.2007.07.051.

Andreas, K., Georgieva, R., Ladwig, M., Mueller, S., Notter, M., Sittinger, M. and Ringe, J. (2012) 'Highly efficient magnetic stem cell labeling with citrate-coated superparamagnetic iron oxide nanoparticles for MRI tracking', *Biomaterials*, 33, pp. 4515–4525. doi: 10.1016/j.biomaterials.2012.02.064.

Añez-Lingerfelt, M., Fox, G. E. and Willson, R. C. (2009) 'Reduction of DNA contamination in RNA samples for reverse transcription-polymerase chain reaction using selective precipitation by compaction agents', *Analytical Biochemistry*, 384(1), pp. 79–85. doi: 10.1016/j.ab.2008.09.009.

Arakaki, A., Masuda, F., Amemiya, Y., Tanaka, T. and Matsunaga, T. (2010) 'Control of the morphology and size of magnetite particles with peptides mimicking the Mms6 protein from magnetotactic bacteria', *Journal of Colloid and Interface Science*. Elsevier Inc., 343(1), pp. 65–70. doi: 10.1016/j.jcis.2009.11.043.

Arakaki, A., Nakazawa, H., Nemoto, M., Mori, T. and Matsunaga, T. (2008) 'Formation of magnetite by bacteria and its application', *Journal of the Royal Society Interface*, 5(26), pp. 977–999. doi: 10.1098/rsif.2008.0170.

Arakaki, A., Webb, J. and Matsunaga, T. (2003) 'A Novel Protein Tightly Bound to Bacterial Magnetic Particles in Magnetospirillum magneticum Strain AMB-1 *', 278(10), pp. 8745–8750. doi: 10.1074/jbc.M211729200.

Arakaki, A., Yamagishi, A., Fukuyo, A., Tanaka, M. and Matsunaga, T. (2014) 'Co-

ordinated functions of Mms proteins define the surface structure of cubo-octahedral magnetite crystals in magnetotactic bacteria', *Molecular Microbiology*, 93(3), pp. 554–567. doi: 10.1111/mmi.12683.

Araya, T., Kazuo, K., Nishikawa, S., Hadeharu, K., Sone, T., Nagae, H., Ikehata, Y., Nagano, I. and Fujimura, M. (2013) 'Antitumor effects of inductive hyperthermia using magnetic ferucarbotran nanoparticles on human lung cancer xenografts in nude mice', *OncoTargets and Therapy*, p. 237. doi: 10.2147/ott.s42815.

Armijo, L. M., Brandt, Y. I., Mathew, D., Yadav, S., Maestas, S., Rivera, A. C., Cook, N. C., Withers, N. J., Smolyakov, G. A., Adolphi, N. L., *et al.* (2012) 'Iron Oxide Nanocrystals for Magnetic Hyperthermia Applications', *Nanomaterials*, 2(2), pp. 134–146. doi: 10.3390/nano2020134.

Asín, L., Goya, G. F., Tres, a and Ibarra, M. R. (2013) 'Induced cell toxicity originates dendritic cell death following magnetic hyperthermia treatment.', *Cell death & disease*, 4, p. e596. doi: 10.1038/cddis.2013.121.

Asín, L., Ibarra, M. R., Tres, A. and Goya, G. F. (2012) 'Controlled cell death by magnetic hyperthermia: Effects of exposure time, field amplitude, and nanoparticle concentration', *Pharmaceutical Research*. doi: 10.1007/s11095-012-0710-z.

Aslan, H., Zilberman, Y., Arbeli, V., Sheyn, D., Matan, Y., Liebergall, M., Li, J. Z., Helm, G. A., Gazit, D. and Gazit, Z. (2006) 'Nucleofection-based ex vivo nonviral gene delivery to human stem cells as a platform for tissue regeneration.', *Tissue engineering*, 12(4), pp. 877–89. doi: 10.1089/ten.2006.12.877.

Atkinson, W. J., Brezovich, I. A. and Chakraborty, D. P. (1984) 'Usable Frequencies in Hyperthermia with Thermal Seeds', *IEEE Transactions on Biomedical Engineering*, BME-31(1), pp. 70–75. doi: 10.1109/TBME.1984.325372.

Au, P., Tam, J., Fukumura, D. and Jain, R. K. (2008) 'Bone marrow-derived mesenchymal stem cells facilitate engineering of long-lasting functional vasculature.', *Blood*, 111(9), pp. 4551–8. doi: 10.1182/blood-2007-10-118273.

Baba, D., Seiko, Y., Nakanishi, T., Zhang, H., Arakaki, A., Matsunaga, T. and Osaka, T. (2012) 'Effect of magnetite nanoparticles on living rate of MCF-7 human breast cancer cells', *Colloids and Surfaces B: Biointerfaces*. Elsevier B.V., 95, pp. 254–257. doi: 10.1016/j.colsurfb.2012.03.008.

Baek, K., Tu, C., Zoldan, J. and Suggs, L. J. (2016) 'Gene Transfection for Stem Cell Therapy', *Current Stem Cell Reports*, 2(1), pp. 52–61. doi: 10.1007/s40778-016-0029-5.

Balkwill, D. L., Maratea, D. and Blakemore, R. P. (1980) 'Ultrastructure of a

magnetotactic spirillum.', *Journal of bacteriology*. United States, 141(3), pp. 1399–1408.

Banasik, M. B. and McCray, P. B. (2010) 'Integrase-defective lentiviral vectors: Progress and applications', *Gene Therapy*, pp. 150–157. doi: 10.1038/gt.2009.135.

Bañobre-López, M., Teijeiro, A. and Rivas, J. (2013) 'Magnetic nanoparticle-based hyperthermia for cancer treatment', *Reports of Practical Oncology and Radiotherapy*, 18(6), pp. 397–400. doi: 10.1016/j.rpor.2013.09.011.

Bashir, J., Sherman, A., Lee, H., Kaplan, L. and Hare, J. M. (2014) 'Mesenchymal stem cell therapies in the treatment of musculoskeletal diseases.', *PM & R : the journal of injury, function, and rehabilitation*, 6(1), pp. 61–9. doi: 10.1016/j.pmrj.2013.05.007.

Bauer, J. S., Golovko, D., Henning, T. D., Sutton, E. J., Wendland, M. F., McDonald, D. M., Malek, F., Sennino, B. and Daldrup-Link, H. (2009) 'Relaxation effects of ferucarbotran-labeled mesenchymal stem cells at 1.5T and 3T: Discrimination of viable from lysed cells', *Magnetic Resonance in Medicine*, 62(2), pp. 325–332. doi: 10.1002/mrm.22011.

Bazylinski, D. A. and Frankel, R. B. (2004) 'Magnetosome formation in prokaryotes', *Nature Reviews Microbiology*. Nature Publishing Group, 2, p. 217. Available at: https://doi.org/10.1038/nrmicro842.

Bazylinski, D. A. and Williams, T. J. (2006) 'Ecophysiology of Magnetotactic Bacteria', in Schüler, D. (ed.) *Magnetoreception and Magnetosomes in Bacteria*, pp. 37–75.

De Becker, A. and Van Riet, I. (2015) 'Mesenchymal Stromal Cell Therapy in Hematology: From Laboratory to Clinic and Back Again.', *Stem cells and development*, 24(15), pp. 1713–29. doi: 10.1089/scd.2014.0564.

Bellizzi, G., Bucci, O. M. and Chirico, G. (2016) 'Numerical assessment of a criterion for the optimal choice of the operative conditions in magnetic nanoparticle hyperthermia on a realistic model of the human head', *International Journal of Hyperthermia*. Taylor and Francis Ltd, 32(6), pp. 688–703. doi: 10.3109/02656736.2016.1167258.

Benabdallah, B. F., Allard, E., Yao, S., Friedman, G., Gregory, P. D., Eliopoulos, N., Fradette, J., Spees, J. L., Haddad, E., Holmes, M. C., *et al.* (2010) 'Targeted gene addition to human mesenchymal stromal cells as a cell-based plasma-soluble protein delivery platform', *Cytotherapy*. Elsevier Inc., 12(3), pp. 394–399. doi: 10.3109/14653240903583803.

Bieback, K. and Kluter, H. (2008) 'Mesenchymal Stromal Cells from Umbilical Cord Blood', *Current Stem Cell Research & Therapy*. Bentham Science Publishers

Ltd., 2(4), pp. 310–323. doi: 10.2174/157488807782793763.

Bird, S. M., Rawlings, A. E., Galloway, J. M. and Staniland, S. S. (2016) 'Using a biomimetic membrane surface experiment to investigate the activity of the magnetite biomineralisation protein Mms6', *RSC Advances*. Royal Society of Chemistry, 6(9), pp. 7356–7363. doi: 10.1039/c5ra16469a.

Blakemore, R. (1975) 'Magnetotactic Bacteria', *Science*, 190(4212), pp. 377–379.

Blakemore, R. P., Short, K. A., Bazylinski, D. A., Rosenblatt, C. and Frankel, R. B. (1985) 'Microaerobic conditions are required for magnetite formation within aquaspirillum magnetotacticum', *Geomicrobiology Journal*, 4(1), pp. 53–71. doi: 10.1080/01490458509385920.

Le Blanc, K. and Ringdén, O. (2005) 'Immunobiology of human mesenchymal stem cells and future use in hematopoietic stem cell transplantation.', *Biology of blood and marrow transplantation : journal of the American Society for Blood and Marrow Transplantation*, 11(5), pp. 321–34. doi: 10.1016/j.bbmt.2005.01.005.

Blanco-Andujar, C., Ortega, D., Souther, P., Nesbitt, S. A., Thanh, N. T. K. and Pankhurst, Q. A. (2016) 'Real-time tracking of delayed-onset cellular apoptosis induced by intracellular magnetic hyperthermia', *Nanomedicine*, 11(2), pp. 121–136.

Bobis-Wozowicz, S., Miekus, K., Wybieralska, E., Jarocha, D., Zawisz, A., Madeja, Z. and Majka, M. (2011) 'Genetically modified adipose tissue-derived mesenchymal stem cells overexpressing CXCR4 display increased motility, invasiveness, and homing to bone marrow of NOD/SCID mice', *Experimental Hematology*. Elsevier Inc., 39(6). doi: 10.1016/j.exphem.2011.03.004.

Bonomi, A., Silini, A., Vertua, E., Signoroni, P. B., Coccè, V., Cavicchini, L., Sisto, F., Alessandri, G., Pessina, A. and Parolini, O. (2015) 'Human amniotic mesenchymal stromal cells (hAMSCs) as potential vehicles for drug delivery in cancer therapy: an in vitro study.', *Stem cell research & therapy*, 6, p. 155. doi: 10.1186/s13287-015-0140-z.

Bonzon, C., Bouchier-Hayes, L., Pagliari, L. J., G., D. R. and Newmeyer, D. D. (2006) 'Caspase-2–induced Apoptosis Requires Bid Cleavage: A Physiological Role for Bid in Heat Shock–induced Death', *Molecular Biology of the Cell*, 17, pp. 2150–2157. doi: 10.1091/mbc.E05.

Botzler, C., Schmidt, J., Luz, A., Jennen, L., Issels, R. and Multhoff, G. (1998) 'Differential Hsp70 plasma-membrane expression on primary human tumors and metastases in mice with severe combined immunodeficiency', *International Journal of Cancer*, 77(6), pp. 942–948. doi: 10.1002/(SICI)1097-0215(19980911)77:6<942::AID-IJC25>3.0.CO;2-1.

Bouchier-Hayes, L., Oberst, A., McStay, G. P., Connell, S., Tait, S. W. G., Dillon, C. P., Flanagan, J. M., Beere, H. M. and Green, D. R. (2009) 'Characterization of Cytoplasmic Caspase-2 Activation by Induced Proximity', *Molecular Cell*. Elsevier Ltd, 35(6), pp. 830–840. doi: 10.1016/j.molcel.2009.07.023.

Boutry, S., Brunin, S., Mahieu, I., Laurent, S., Vander Elst, L. and Muller, R. N. (2008) 'Magnetic labeling of non-phagocytic adherent cells with iron oxide nanoparticles: A comprehensive study', *Contrast Media and Molecular Imaging*, 3(6), pp. 223–232. doi: 10.1002/cmmi.256.

Boveris, A. and Chance, B. (1973) 'The mitochondrial generation of hydrogen peroxide. General properties and effect of hyperbaric oxygen', *Biochemical Journal*, 134(3), pp. 707–716. doi: 10.1042/bj1340707.

Butcher, E. C. and Picker, L. J. (1996) 'Lymphocyte Homing and Homeostasis', *Science*. American Association for the Advancement of Science (AAAS), 272(5258), pp. 60–67. doi: 10.1126/science.272.5258.60.

Calderwood, S. K. and Hahn, G. M. (1983) 'Thermal sensitivity and resistance of insulin-receptor binding in thermotolerant cells', *BBA - Biomembranes*, 734(1), pp. 76–82. doi: 10.1016/0005-2736(83)90077-9.

Caplan, A. I. and Dennis, J. E. (2006) 'Mesenchymal stem cells as trophic mediators.', *Journal of cellular biochemistry*, 98(5), pp. 1076–84. doi: 10.1002/jcb.20886.

Carrey, J., Mehdaoui, B. and Respaud, M. (2011) 'Simple models for dynamic hysteresis loop calculations: Application to hyperthermia optimization', *J. Appl. Phys.*, 109, p. 083921. doi: 10.1063/1.3551582.

de Carvalho, T. G., Pellenz, F. M., Laureano, A., da Rocha Silla, L. M., Giugliani, R., Baldo, G. and Matte, U. (2018) 'A simple protocol for transfecting human mesenchymal stem cells', *Biotechnology Letters*. Springer Netherlands, 40(3), pp. 617–622. doi: 10.1007/s10529-018-2505-8.

Castelli, C., Ciupitu, A. T., Rini, F., Rivoltini, L., Mazzocchi, A., Kiessling, R. and Parmiani, G. (2001) 'Human heat shock protein 70 peptide complexes specifically activate antimelanoma t cells', *Cancer Research*, 61(1), pp. 222–227.

Chapel, A., Bertho, J. M., Bensidhoum, M., Fouillard, L., Young, R. G., Frick, J., Demarquay, C., Cuvelier, F., Mathieu, E., Trompier, F., *et al.* (2003) 'Mesenchymal stem cells home to injured tissues when co-infused with hematopoietic cells to treat a radiation-induced multi-organ failure syndrome.', *The journal of gene medicine*, 5(12), pp. 1028–38. doi: 10.1002/jgm.452.

Chen, C., Ma, Q., Jiang, W. and Song, T. (2011) 'Phototaxis in the magnetotactic bacterium Magnetospirillum magneticum strain AMB-1 is independent of magnetic fields', *Applied Microbiology and Biotechnology*, 90(1), pp. 269–

275. doi: 10.1007/s00253-010-3017-1.

Chiriac, H., Petreus, T., Carasevici, E., Labusca, L., Herea, D.-D., Danceanu, C. and Lupu, N. (2015) 'In vitro cytotoxicity of Fe-Cr-Nb-B magnetic nanoparticles under high frequency electromagnetic field', *Journal of Magnetism and Magnetic Materials*, 380, pp. 13–19. doi: 10.1016/j.jmmm.2014.10.015.

Cho, J. A., Park, H., Lim, E. H. and Lee, K. W. (2012) 'Exosomes from breast cancer cells can convert adipose tissue-derived', *Int J Oncol*. doi: 10.3892/ijo.2011.1193.

Coccè, V., Farronato, D., Brini, A. T., Masia, C., Giannì, A. B., Piovani, G., Sisto, F., Alessandri, G., Angiero, F. and Pessina, A. (2017) 'Drug Loaded Gingival Mesenchymal Stromal Cells (GinPa-MSCs) Inhibit In Vitro Proliferation of Oral Squamous Cell Carcinoma', *Scientific Reports*. doi: 10.1038/s41598-017-09175-4.

Cole, A. J., Yang, V. C. and David, A. E. (2011) 'Cancer theranostics: The rise of targeted magnetic nanoparticles', *Trends in Biotechnology*. Elsevier Ltd, 29(7), pp. 323–332. doi: 10.1016/j.tibtech.2011.03.001.

Conde, J., Dias, J. T., GrazÃº, V., Moros, M., Baptista, P. V. and de la Fuente, J. M. (2014) 'Revisiting 30 years of biofunctionalization and surface chemistry of inorganic nanoparticles for nanomedicine', *Frontiers in Chemistry*, 2(July), pp. 1–27. doi: 10.3389/fchem.2014.00048.

Corchero, J. L. and Villaverde, A. (2009) 'Biomedical applications of distally controlled magnetic nanoparticles', *Trends in Biotechnology*. doi: 10.1016/j.tibtech.2009.04.003.

Cornejo, E., Subramanian, P., Li, Z., Jensen, G. J. and Komeili, A. (2016) 'Dynamic remodeling of the magnetosome membrane is triggered by the initiation of biomineralization', *mBio*, 7(1), pp. 1–9. doi: 10.1128/mBio.01898-15.

Corot, C., Robert, P., Idée, J. M. and Port, M. (2006) 'Recent advances in iron oxide nanocrystal technology for medical imaging', *Advanced Drug Delivery Reviews*, 58(14), pp. 1471–1504. doi: 10.1016/j.addr.2006.09.013.

Cousin, B., Ravet, E., Poglio, S., De Toni, F., Bertuzzi, M., Lulka, H., Touil, I., André, M., Grolleau, J. L., Péron, J. M., *et al.* (2009) 'Adult stromal cells derived from human adipose tissue provoke pancreatic cancer cell death both in vitro and in vivo', *PLoS ONE*. doi: 10.1371/journal.pone.0006278.

Csoboz, B., Balogh, G. E., Kusz, E., Gombos, I., Peter, M., Crul, T., Gungor, B., Haracska, L., Bogdanovics, G., Torok, Z., *et al.* (2013) 'Membrane fluidity matters: Hyperthermia from the aspects of lipids and membranes', *International Journal of Hyperthermia*, 29(5), pp. 491–499. doi: 10.3109/02656736.2013.808765.

Cuiffo, B. G. and Karnoub, A. E. (2012) 'Mesenchymal stem cells in tumor development: emerging roles and concepts.', *Cell adhesion & migration*, 6(3), pp. 220–30. doi: 10.4161/cam.20875.

Damdindorj, L., Karnan, S., Ota, A., Hossain, E., Konishi, Y., Hosokawa, Y. and Konishi, H. (2014) 'A Comparative Analysis of Constitutive Promoters Located in Adeno-Associated Viral Vectors', *PLoS ONE*. Edited by J. Pratap, 9(8), p. e106472. doi: 10.1371/journal.pone.0106472.

Damdindorj, L., Karnan, S., Ota, A., Takahashi, M., Konishi, Y., Hossain, E., Hosokawa, Y. and Konishi, H. (2012) 'Assessment of the long-term transcriptional activity of a 550-bp-long human β-actin promoter region', *Plasmid*, 68(3), pp. 195–200. doi: 10.1016/j.plasmid.2012.07.003.

Das, P., Colombo, M. and Prosperi, D. (2019) 'Recent advances in magnetic fluid hyperthermia for cancer therapy', *Colloids and Surfaces B: Biointerfaces*. doi: 10.1016/j.colsurfb.2018.10.051.

Deatsch, A. E. and Evans, B. A. (2014) 'Heating efficiency in magnetic nanoparticle hyperthermia', *Journal of Magnetism and Magnetic Materials*, 354, pp. 163–172. doi: 10.1016/j.jmmm.2013.11.006.

Ding, Y., Li, Jinhua, Liu, J., Yang, J., Jiang, W., Tian, J., Li, Y., Pan, Y. and Li, Jilun (2010) 'Deletion of the ftsZ-Like Gene Results in the Production of Superparamagnetic Magnetite Magnetosomes in Magnetospirillum gryphiswaldense † Downloaded from', *JOURNAL OF BACTERIOLOGY*, 192(4), pp. 1097–1105. doi: 10.1128/JB.01292-09.

Dominici, M., Le Blanc, K., Mueller, I., Slaper-Cortenbach, I., Marini, F., Krause, D., Deans, R., Keating, A., Prockop, D. and Horwitz, E. (2006) 'Minimal criteria for defining multipotent mesenchymal stromal cells. The International Society foDominici, M., Le Blanc, K., Mueller, I., Slaper-Cortenbach, I., Marini, F., Krause, D., … Horwitz, E. (2006). Minimal criteria for defining multipotent mesenc', *Cytotherapy*. doi: 10.1080/14653240600855905.

Duchi, S., Sotgiu, G., Lucarelli, E., Ballestri, M., Dozza, B., Santi, S., Guerrini, A., Dambruoso, P., Giannini, S., Donati, D., *et al.* (2013) 'Mesenchymal stem cells as delivery vehicle of porphyrin loaded nanoparticles: Effective photoinduced in vitro killing of osteosarcoma', *Journal of Controlled Release*. Elsevier B.V., 168(2), pp. 225–237. doi: 10.1016/j.jconrel.2013.03.012.

Ďuriniková, E., Kučerová, L. and Matúšková, M. (2014) 'Mesenchymal stromal cells retrovirally transduced with prodrug-converting genes are suitable vehicles for cancer gene therapy.', *Acta virologica*, pp. 1–13. doi: 10.4149/av_2014_01_3.

Dvorak, H. F. (1986) 'Dvorak HF : Tumors : Wounds that do not heal . Similarities between tumor stroma generation', *N Engl J Med*, 315, pp. 1650–1659. doi: 10.1056/NEJM198612253152606.

El-Orabi, N. F., Rogers, C. B., Gray Edwards, H. and Schwartz, D. D. (2011) 'Heat-induced inhibition of superoxide dismutase and accumulation of reactive oxygen species leads to HT-22 neuronal cell death', *Journal of Thermal Biology*. Elsevier, 36(1), pp. 49–56. doi: 10.1016/j.jtherbio.2010.11.002.

Elfick, A., Rischitor, G., Mouras, R., Azfer, A., Lungaro, L., Uhlarz, M., Herrmannsdörfer, T., Lucocq, J., Gamal, W., Bagnaninchi, P., *et al.* (2017) 'Biosynthesis of magnetic nanoparticles by human mesenchymal stem cells following transfection with the magnetotactic bacterial gene mms6', *Scientific Reports*. Nature Publishing Group, 7. doi: 10.1038/srep39755.

Faivre, D., Böttger, L. H., Matzanke, B. F. and Schüler, D. (2007) 'Intracellular magnetite biomineralization in bacteria proceeds by a distinct pathway involving membrane-bound ferritin and an iron(II) species', *Angewandte Chemie - International Edition*, 46(44), pp. 8495–8499. doi: 10.1002/anie.200700927.

Feng, S., Wang, L., Palo, P., Liu, X. and Mallapragada, S. K. (2013) 'Integrated Self-Assembly of the Mms6 Magnetosome Protein to Form an Iron-Responsive Structure', pp. 14594–14606. doi: 10.3390/ijms140714594.

Fouillard, L., Chapel, A., Bories, D., Bouchet, S., Costa, J. M., Rouard, H., Hervé, P., Gourmelon, P., Thierry, D., Lopez, M., *et al.* (2007) 'Infusion of allogeneic-related HLA mismatched mesenchymal stem cells for the treatment of incomplete engraftment following autologous haematopoietic stem cell transplantation [8]', *Leukemia*, 21(3), pp. 568–570. doi: 10.1038/sj.leu.2404550.

Frank, J. A., Anderson, S. A., Kalsih, H., Jordan, E. K., Lewis, B. K., Yocum, G. T. and Arbab, A. S. (2004) 'Methods for magnetically labeling stem and other cells for detection by in vivo magnetic resonance imaging', *Cytotherapy*. doi: 10.1080/14653240410005267-1.

Franke, K., Kettering, M., Lange, K., Kaiser, W. A. and Hilger, I. (2013) 'The exposure of cancer cells to hyperthermia, iron oxide nanoparticles, and mitomycin C influences membrane multidrug resistance protein expression levels', *International Journal of Nanomedicine*. doi: 10.2147/IJN.S37465.

Frankel, R. B., Bazylinski, D. A., Johnson, M. S. and Taylor, B. L. (1997) 'Magneto-aerotaxis in marine coccoid bacteria', *Biophysical Journal*, 73(2), pp. 994–1000. doi: 10.1016/S0006-3495(97)78132-3.

Friedenstein, A., Chailakhyan, R., Latsinik, N., Panasyuk, A. and Keiliss-Borok, I. (1974) 'Stromal cells responsible for transferring the microenvironment of the hemopoietic tissues. Cloning in vitro and retransplantation in vivo'. Transplantation, pp. 17: 331-340.

Fu, Q., Huang, T., Wang, X., Lu, C., Liu, F., Yang, G., Wang, Y. and Wang, B. (2017)

'Association of elevated reactive oxygen species and hyperthermia induced radiosensitivity in cancer stem-like cells', *Oncotarget*, 8(60), pp. 101560–101571. doi: 10.18632/oncotarget.21678.

Fukuda, Y., Okamura, Y., Takeyama, H. and Matsunaga, T. (2006) 'Dynamic analysis of a genomic island in Magnetospirillum sp. strain AMB-1 reveals how magnetosome synthesis developed', *FEBS Letters*, 580(3), pp. 801–812. doi: 10.1016/j.febslet.2006.01.003.

Fuller, K. J., Issels, R. D., Slosman, D. O., Guillet, J. G., Soussi, T. and Polla, B. S. (1994) 'Cancer and the heat shock response', *European Journal of Cancer*, 30(12), pp. 1884–1891. doi: 10.1016/0959-8049(94)00362-9.

Galloway, J. M., Arakaki, A., Masuda, F., Tanaka, T., Matsunaga, T. and Staniland, S. S. (2011) 'Magnetic bacterial protein Mms6 controls morphology, crystallinity and magnetism of cobalt-doped magnetite nanoparticles in vitro', *Journal of Materials Chemistry*, 21(39), pp. 15244–15254. doi: 10.1039/c1jm12003d.

Galloway, J. M., Bramble, J. P., Rawlings, A. E., Burnell, G., Evans, S. D. and Staniland, S. S. (2012) 'Biotemplated magnetic nanoparticle arrays', *Small*, 8(2), pp. 204–208. doi: 10.1002/smll.201101627.

Gao, C., Li, S., Zhao, T., Chen, J., Ren, H., Zhang, H., Wang, X., Lang, M., Liu, J., Gao, S., *et al.* (2015) 'SCF, regulated by HIF-1α, promotes pancreatic ductal adenocarcinoma cell progression', *PLoS ONE*. doi: 10.1371/journal.pone.0121338.

Gao, Z., Zhang, L., Hu, J. and Sun, Y. (2013) 'Mesenchymal stem cells: A potential targeted-delivery vehicle for anti-cancer drug, loaded nanoparticles', *Nanomedicine: Nanotechnology, Biology, and Medicine*. doi: 10.1016/j.nano.2012.06.003.

Ge, Y., Zhang, Y., Xia, J., Ma, M., He, S., Nie, F. and Gu, N. (2009) 'Effect of surface charge and agglomerate degree of magnetic iron oxide nanoparticles on KB cellular uptake in vitro', *Colloids and Surfaces B: Biointerfaces*, 73(2), pp. 294–301. doi: 10.1016/j.colsurfb.2009.05.031.

Gheisari, Y., Soleimani, M., Azadmanesh, K. and Zeinali, S. (2008) 'Multipotent mesenchymal stromal cells: optimization and comparison of five cationic polymer-based gene delivery methods.', *Cytotherapy*, 10(8), pp. 815–23. doi: 10.1080/14653240802474307.

Gilchrist, R. K., Medal, R., Shorey, W. D., Hanselman, R. C., Parrott, J. C. and Taylor, C. B. (1957) 'Selective inductive heating of lymph nodes', *Annals of surgery*, 146(4), pp. 596–606. doi: 10.1097/00000658-195710000-00007.

Glish, G. L. and Vachet, R. W. (2003) 'The basics of mass spectrometry in the twenty-

first century.', *Nature reviews. Drug discovery*, 2(2), pp. 140–50. doi: 10.1038/nrd1011.

Gnecchi, M. and Melo, L. G. (2009) 'Bone marrow-derived mesenchymal stem cells: Isolation, expansion, characterization, viral transduction, and production of conditioned medium', *Methods in Molecular Biology*, 482, pp. 281–294. doi: 10.1007/978-1-59745-060-7_18.

Gobbo, O. L., Sjaastad, K., Radomski, M. W., Volkov, Y. and Prina-Mello, A. (2015) 'Magnetic nanoparticles in cancer theranostics', *Theranostics*, 5(11), pp. 1249–1263. doi: 10.7150/thno.11544.

Goldhawk, D. E., Lemaire, C., McCreary, C. R., McGirr, R., Dhanvantari, S., Thompson, R. T., Figueredo, R., Koropatnick, J., Foster, P. and Prato, F. S. (2009) 'Magnetic resonance imaging of cells overexpressing maga, an endogenous contrast agent for live cell imaging', *Molecular Imaging*, 8(3), pp. 129–139. doi: 10.2310/7290.2009.00006.

Gorby, Y. A., Beveridge, T. J. and Blakemore, R. P. (1988) 'Characterization of the bacterial magnetosome membrane.', *Journal of bacteriology*, 170(2), pp. 834–841. doi: 10.1128/jb.170.2.834-841.1988.

Gordon, R. T., Hines, J. R. and Gordon, D. (1979) 'Intracellular hyperthermia a biophysical approach to cancer treatment via intracellular temperature and biophysical alterations', *Medical Hypotheses*, 5(1), pp. 83–102. doi: 10.1016/0306-9877(79)90063-X.

Gorojod, R. M., Alaimo, A., Porte Alcon, S., Saravia, F. and Kotler, M. L. (2017) 'Interplay between lysosomal, mitochondrial and death receptor pathways during manganese-induced apoptosis in glial cells.', *Archives of toxicology*, 91(9), pp. 3065–3078. doi: 10.1007/s00204-017-1936-7.

Gorshkov, V., Bubis, J. A., Solovyeva, E. M., Gorshkov, M. V. and Kjeldsen, F. (2019) 'Protein corona formed on silver nanoparticles in blood plasma is highly selective and resistant to physicochemical changes of the solution', *Environmental Science: Nano*. Royal Society of Chemistry, 6(4), pp. 1089–1098. doi: 10.1039/c8en01054d.

Goya, G. F., Asín, L. and Ibarra, M. R. (2013) 'Cell death induced by AC magnetic fields and magnetic nanoparticles: current state and perspectives', *International Journal of Hyperthermia*, 29(8), pp. 810–8. doi: 10.3109/02656736.2013.838646.

Grunberg, K., Muller, E., Otto, A., Reszka, R., Linder, D., Kube, M., Reinhardt, R. and Schuler, D. (2004) 'Biochemical and Proteomic Analysis of the Magnetosome Membrane in', *Appl. Environ. Microbiol.*, 70(2), pp. 1040–1050. doi: 10.1128/AEM.70.2.1040.

Gu, G., Qi, H., Jiang, T., Ma, B., Fang, Z., Xu, H. and Zhang, Q. (2017) 'Investigation of the cytotoxicity, apoptosis and pharmacokinetics of raddeanin A', *Oncology Letters*. Spandidos Publications, 13(3), pp. 1365–1369. doi: 10.3892/ol.2017.5588.

Hacein-Bey-Abina, S., Garrigue, A., Wang, G. P., Soulier, J., Lim, A., Morillon, E., Clappier, E., Caccavelli, L., Delabesse, E., Beldjord, K., *et al.* (2008) 'Insertional oncogenesis in 4 patients after retrovirus-mediated gene therapy of SCID-X1.', *The Journal of clinical investigation*, 118(9), pp. 3132–42. doi: 10.1172/JCI35700.

Haleem-Smith, H., Derfoul, A., Okafor, C., Tuli, R., Olsen, D., Hall, D. J. and Tuan, R. S. (2005) 'Optimization of high-efficiency transfection of adult human mesenchymal stem cells in vitro', *Mol Biotechnol*, 30(1), pp. 9–20. doi: 10.1385/MB:30:1:009.

Halim, N. S. S. A., Fakiruddin, K. S., Ali, S. A. and Yahaya, B. H. (2014) 'A comparative study of non-viral gene delivery techniques to human adipose-derived mesenchymal stem cell', *International Journal of Molecular Sciences*, 15(9), pp. 15044–15060. doi: 10.3390/ijms150915044.

Halpern, J. L., Kilbarger, A. and Lynch, C. C. (2011) 'Mesenchymal stem cells promote mammary cancer cell migration in vitro via the CXCR2 receptor.', *Cancer letters*, 308(1), pp. 91–9. doi: 10.1016/j.canlet.2011.04.018.

Hammer, K., Kazcorowski, A., Liu, L., Behr, M., Schemmer, P., Herr, I. and Nettelbeck, D. M. (2015) 'Engineered adenoviruses combine enhanced oncolysis with improved virus production by mesenchymal stromal carrier cells', *International Journal of Cancer*, 137(4), pp. 978–990. doi: 10.1002/ijc.29442.

Hanahan, D. and Coussens, L. M. (2012) 'Accessories to the crime: functions of cells recruited to the tumor microenvironment.', *Cancer cell*, 21(3), pp. 309–22. doi: 10.1016/j.ccr.2012.02.022.

He, S., Nakada, D. and Morrison, S. J. (2009) 'Mechanisms of Stem', *Annual Review of Cell and Developmental Biology*. doi: 10.1146/annurev.cellbio.042308.113248.

Hedayati, M., Thomas, O., Abubaker-Sharif, B., Zhou, H., Cornejo, C., Zhang, Y., Wabler, M., Mihalic, J., Gruettner, C., Westphal, F., *et al.* (2013) 'The effect of cell cluster size on intracellular nanoparticle-mediated hyperthermia: is it possible to treat microscopic tumors?', *Nanomedicine (London, England)*, 8(1), pp. 29–41. doi: 10.2217/nnm.12.98.

Hedayatnasab, Z., Abnisa, F. and Daud, W. M. A. W. (2017) 'Review on magnetic nanoparticles for magnetic nanofluid hyperthermia application', *Materials and Design*. Elsevier Ltd, 123, pp. 174–196. doi: 10.1016/j.matdes.2017.03.036.

Helledie, T., Nurcombe, V. and Cool, S. M. (2008) 'A simple and reliable electroporation method for human bone marrow mesenchymal stem cells.', *Stem cells and development*, 17(4), pp. 837–48. doi: 10.1089/scd.2007.0209.

Henning, T. D., Sutton, E. J., Kim, A., Golovko, D., Horvai, A., Ackerman, L., Sennino, B., McDonald, D., Lotz, J. and Daldrup-Linka, H. E. (2009) 'The influence of ferucarbotran on the chondrogenesis of human mesenchymal stem cells', *Contrast Media and Molecular Imaging*, 4(4), pp. 165–173. doi: 10.1002/cmmi.276.

Hermantara, R., Kerans, F. A., R, R., Herningtyas, E. H. and Lazuardi, L. (2016) 'Induced-Coagulated Plasma-Fibrin Gels as a Biological Scaffold for Cell Attachment and Proliferation of Umbilical Cord-Derived Mesenchymal Stem Cells (UC-MSC)', *Indonesian Journal of Biotechnology*. Universitas Gadjah Mada, 19(2), p. 159. doi: 10.22146/ijbiotech.9310.

Hervault, A. and Thanh, N. T. K. (2014) 'Magnetic nanoparticle-based therapeutic agents for thermo-chemotherapy treatment of cancer.', *Nanoscale*, 6(20), pp. 11553–11573. doi: 10.1039/c4nr03482a.

Heyen, U. and Schüler, D. (2003) 'Growth and magnetosome formation by microaerophilic Magnetospirillum strains in an oxygen-controlled fermentor', *Applied Microbiology and Biotechnology*. Springer Verlag, 61(5–6), pp. 536–544. doi: 10.1007/s00253-002-1219-x.

Hildebrandt, B., Wust, P., Ahlers, O., Dieing, A., Sreenivasa, G., Kerner, T., Felix, R. and Riess, H. (2002) 'The cellular and molecular basis of hyperthermia', *Critical Reviews in Oncology/Hematology*, 43(1), pp. 33–56. doi: 10.1016/S1040-8428(01)00179-2.

Ho, L. H., Read, S. H., Dorstyn, L., Lambrusco, L. and Kumar, S. (2008) 'Caspase-2 is required for cell death induced by cytoskeletal disruption', *Oncogene*, 27(24), pp. 3393–3404. doi: 10.1038/sj.onc.1211005.

Hou, C. H., Lin, F. L., Hou, S. M. and Liu, J. F. (2014) 'Hyperthermia induces apoptosis through endoplasmic reticulum and reactive oxygen species in human Osteosarcoma cells', *International Journal of Molecular Sciences*, 15(10), pp. 17380–17395. doi: 10.3390/ijms151017380.

Huang, D. M., Hsiao, J. K., Chen, Ying Chun, Chien, L. Y., Yao, M., Chen, Y. K., Ko, B. S., Hsu, S. C., Tai, L. A., Cheng, H. Y., *et al.* (2009) 'The promotion of human mesenchymal stem cell proliferation by superparamagnetic iron oxide nanoparticles', *Biomaterials*. Elsevier Ltd, 30(22), pp. 3645–3651. doi: 10.1016/j.biomaterials.2009.03.032.

Huang, G. T.-J., Gronthos, S. and Shi, S. (2009) 'Mesenchymal stem cells derived from dental tissues vs. those from other sources: their biology and role in regenerative medicine.', *Journal of dental research*, 88(9), pp. 792–806. doi:

10.1177/0022034509340867.

Huang, H. S. and Hainfeld, J. F. (2013) 'Intravenous magnetic nanoparticle cancer hyperthermia', *International Journal of Nanomedicine*. doi: 10.2147/IJN.S43770.

Huang, Y. W., Cambre, M. and Lee, H. J. (2017) 'The Toxicity of Nanoparticles Depends on Multiple Molecular and Physicochemical Mechanisms', *International journal of molecular sciences*, 18(12). doi: 10.3390/ijms18122702.

Ip, J. E., Wu, Y., Huang, J., Zhang, L., Pratt, R. E. and Dzau, V. J. (2007) 'Mesenchymal stem cells use integrin β1 not CXC chemokine receptor 4 for myocardial migration and engraftment', *Molecular Biology of the Cell*, 18(8), pp. 2873–2882. doi: 10.1091/mbc.E07-02-0166.

Ito, A., Nakahara, Y., Tanaka, K., Kuga, Y., Honda, H. and Kobayashi, T. (2003) 'Time Course of Biodistribution and Heat Generation of MagnetiteCationicLiposomes in Mouse Model', *Jpn. J. Hyperthermic Oncol*, 19(3), pp. 151–159.

Ito, A., Shinkai, M., Honda, H. and Kobayashi, T. (2005) 'Medical Application of Functionalized Magnetic Nanoparticles', 100(1), pp. 1–11. doi: 10.1263/jbb.100.1.

Ito, A., Shinkai, M., Honda, H., Wakabayashi, T., Yoshida, J. and Kobayashi, T. (2001) 'Augmentation of MHC class I antigen presentation via heat shock protein expression by hyperthermia', *Cancer Immunology, Immunotherapy*, 50(10), pp. 515–522. doi: 10.1007/s00262-001-0233-7.

Ito, A., Shinkai, M., Honda, H., Yoshikawa, K., Saga, S., Wakabayashi, T., Yoshida, J. and Kobayashi, T. (2003) 'Heat shock protein 70 expression induces antitumor immunity during intracellular hyperthermia using magnetite nanoparticles', *Cancer Immunology, Immunotherapy*, 52(2), pp. 80–88. doi: 10.1007/s00262-002-0335-x.

Jäättelä, M. (1999) 'Heat shock proteins as cellular lifeguards', *Annals of Medicine*, 31, pp. 261–271. doi: 10.3109/07853899908995889.

Jang, J. T., Lee, J., Seon, J., Ju, E., Kim, M., Kim, Y. Il, Kim, M. G., Takemura, Y., Arbab, A. S., Kang, K. W., *et al.* (2018) 'Giant Magnetic Heat Induction of Magnesium-Doped γ-Fe 2 O 3 Superparamagnetic Nanoparticles for Completely Killing Tumors', *Advanced Materials*. Wiley-VCH Verlag, 30(6). doi: 10.1002/adma.201704362.

Jemal, A., Bray, F., Center, M. M., Ferlay, J., Ward, E. and Forman, D. (2016) 'Global Cancer statistics', *CA: A Cancer Journal for Clinician*, 66(1), pp. 7–30. doi: 10.3322/caac.20107.Available.

Jeong, U., Teng, X., Wang, Y., Yang, H. and Xia, Y. (2007) 'Superparamagnetic colloids: Controlled synthesis and niche applications', in *Advanced Materials*, pp. 33–60. doi: 10.1002/adma.200600674.

Jogler, C. and Schuler, D. (2009) 'Genomics, Genetics, and Cell Biology of Magnetosome Formation', *Annual Review of Microbiology*, 63, pp. 501–521. doi: 10.1146/annurev.micro.62.081307.162908.

Johannsen, M., Gneveckow, U., Eckelt, L., Feussner, A., Waldöfner, N., Scholz, R., Deger, S., Wust, P., Loening, S. A. and Jordan, A. (2005) 'Clinical hyperthermia of prostate cancer using magnetic nanoparticles: presentation of a new interstitial technique.', *International journal of hyperthermia : the official journal of European Society for Hyperthermic Oncology, North American Hyperthermia Group*, 21(7), pp. 637–47. Available at: http://www.ncbi.nlm.nih.gov/pubmed/16304715 (Accessed: 22 August 2019).

Johannsen, M., Gneveckow, U., Thiesen, B., Taymoorian, K., Cho, C. H., Waldöfner, N., Scholz, R., Jordan, A., Loening, S. A. and Wust, P. (2007) 'Thermotherapy of Prostate Cancer Using Magnetic Nanoparticles: Feasibility, Imaging, and Three-Dimensional Temperature Distribution', *European Urology*, 52(6), pp. 1653–1662. doi: 10.1016/j.eururo.2006.11.023.

Johannsen, M., Thiesen, B., Wust, P. and Jordan, A. (2010) 'Magnetic nanoparticle hyperthermia for prostate cancer', *Int. J. Hyperthermia*, 26(8), pp. 790–795. doi: 10.3109/02656731003745740.

Jung, Y., Kim, J. K., Shiozawa, Y., Wang, Jingcheng, Mishra, A., Joseph, J., Berry, J. E., McGee, S., Lee, E., Sun, H., *et al.* (2013) 'Recruitment of mesenchymal stem cells into prostate tumours promotes metastasis.', *Nature communications*, 4, p. 1795. doi: 10.1038/ncomms2766.

Kaestner, L., Scholz, A. and Lipp, P. (2015) 'Conceptual and technical aspects of transfection and gene delivery', *Bioorganic and Medicinal Chemistry Letters*. Elsevier Ltd, 25(6), pp. 1171–1176. doi: 10.1016/j.bmcl.2015.01.018.

Kalber, T. L., Ordidge, K. L., Southern, P., Loebinger, M. R., Kyrtatos, P. G., Pankhurst, Q. A., Lythgoe, M. F. and Janes, S. M. (2016) 'hyperthermia treatment of tumors by mesenchymal stem cell-delivered superparamagnetic iron oxide nanoparticles', *International Journal of Nanomedicine*, 11, pp. 1973–1983. doi: 10.2147/IJN.S94255.

Kallumadil, M., Tada, M., Nakagawa, T., Abe, M., Southern, P. and Pankhurst, Q. A. (2009) 'Suitability of commercial colloids for magnetic hyperthermia', *Journal of Magnetism and Magnetic Materials*, 321(10), pp. 1509–1513. doi: 10.1016/j.jmmm.2009.02.075.

Kang, S., Bhang, S. H., Hwang, S., Yoon, J. K., Song, J., Jang, H. K., Kim, S. and Kim, B. S. (2015) 'Mesenchymal Stem Cells Aggregate and Deliver Gold

Nanoparticles to Tumors for Photothermal Therapy', *ACS Nano*. doi: 10.1021/acsnano.5b02207.

Kashyap, S., Woehl, T. J., Liu, X., Mallapragada, S. K. and Prozorov, T. (2014) 'Nucleation of Iron Oxide Nanoparticles Mediated by Mms6 Protein in Situ', (9), pp. 9097–9106. doi: 10.1021/nn502551y.

Kasten, A., Siegmund, B. J., Grüttner, C., Kühn, J. P. and Frerich, B. (2014) 'Tracking of adipose tissue-derived progenitor cells using two magnetic nanoparticle types', *Journal of Magnetism and Magnetic Materials*. Elsevier, 380, pp. 34–38. doi: 10.1016/j.jmmm.2014.08.044.

Katzmann, E., Scheffel, A., Gruska, M., Plitzko, J. M. and Schüler, D. (2010) 'Loss of the actin-like protein MamK has pleiotropic effects on magnetosome formation and chain assembly in Magnetospirillum gryphiswaldense', *Molecular Microbiology*, 77(1), pp. 208–224. doi: 10.1111/j.1365-2958.2010.07202.x.

Kaur, Jatinder, Kaur, Jasbir and Ralhan, R. (2000) 'Induction of apoptosis by abrogation of HSP70 expression in human oral cancer cells', *International Journal of Cancer*, 85(1), pp. 1–5. doi: 10.1002/(SICI)1097-0215(20000101)85:1<1::AID-IJC1>3.0.CO;2-O.

Kerans, F. F. A., Lungaro, L., Azfer, A. and Salter, D. M. (2018) 'The potential of intrinsically magnetic mesenchymal stem cells for tissue engineering', *International Journal of Molecular Sciences*, 19(10). doi: 10.3390/ijms19103159.

Khandhar, A. P., Ferguson, R. M., Simon, J. A. and Krishnan, K. M. (2012) 'Tailored magnetic nanoparticles for optimizing magnetic fluid hyperthermia', *Journal of Biomedical Materials Research - Part A*, 100 A(3), pp. 728–737. doi: 10.1002/jbm.a.34011.

Kim, H.-C., Kim, E., Jeong, S. W., Ha, T.-L., Park, S.-I., Lee, S. G., Lee, S. J. and Lee, S. W. (2015) 'Magnetic nanoparticle-conjugated polymeric micelles for combined hyperthermia and chemotherapy.', *Nanoscale*, 7(39), pp. 16470–80. doi: 10.1039/c5nr04130a.

Kim, T. K. and Eberwine, J. H. (2010) 'Mammalian cell transfection: The present and the future', *Analytical and Bioanalytical Chemistry*, 397(8), pp. 3173–3178. doi: 10.1007/s00216-010-3821-6.

Kim, Y. J., Ebara, M. and Aoyagi, T. (2013) 'A smart hyperthermia nanofiber with switchable drug release for inducing cancer apoptosis', *Advanced Functional Materials*, 23(46), pp. 5753–5761. doi: 10.1002/adfm.201300746.

Kobayashi, T. (2011) 'Cancer hyperthermia using magnetic nanoparticles', *Biotechnology Journal*, pp. 1342–1347. doi: 10.1002/biot.201100045.

Kobayashi, T., Kakimi, K., Nakayama, E. and Jimbow, K. (2014) 'Antitumor

immunity by magnetic hyperthermia', *Nanomedicine*, 9(11), pp. 1715–1726. doi: 10.2217/NNM.14.106.

Koike, N., Fukumura, D., Gralla, O., Au, P., Schechner, J. S. and Jain, R. K. (2004) 'Tissue engineering: creation of long-lasting blood vessels. Supplemental Information', *Nature*. doi: 10.1038/428138a.

Kolinko, I., Lohße, A., Borg, S., Raschdorf, O., Jogler, C., Tu, Q., Pósfai, M., Tompa, É., Plitzko, J. M., Brachmann, A., *et al.* (2014) 'Biosynthesis of magnetic nanostructures in a foreign organism by transfer of bacterial magnetosome gene clusters', *Nature Nanotechnology*, 9(3), pp. 193–197. doi: 10.1038/nnano.2014.13.

Komarova, S., Roth, J., Alvarez, R., Curiel, D. T. and Pereboeva, L. (2010) 'Targeting of mesenchymal stem cells to ovarian tumors via an artificial receptor', *Journal of Ovarian Research*, 3(1), pp. 1–14. doi: 10.1186/1757-2215-3-12 LK - http://sfx.library.uu.nl/utrecht?sid=EMBASE&issn=17572215&id=doi:10.1186%2F1757-2215-3-12&atitle=Targeting+of+mesenchymal+stem+cells+to+ovarian+tumors+via+an+artificial+receptor&stitle=J.+Ovarian+Res.&title=Journal+of+Ovarian+Research&volume=3&issue=1&spage=&epage=&aulast=Komarova&aufirst=Svetlana&auinit=S.&aufull=Komarova+S.&coden=&isbn=&pages=-&date=2010&auinit1=S&auinitm=.

Komeili, A. (2012) 'Molecular mechanisms of compartmentalization and biomineralization in magnetotactic bacteria', *FEMS Microbiology Reviews*, 36(1), pp. 232–255. doi: 10.1111/j.1574-6976.2011.00315.x.

Komeili, A., Li, Z., Newman, D. K. and Jensen, G. J. (2006) *Magnetosomes Are Cell Membrane Invaginations Organized by the Actin-Like Protein MamK Arash*, *Science*. doi: 10.1002/nme.1803.

Komeili, A., Vali, H., Beveridge, T. J. and Newman, D. K. (2004) 'Magnetosome vesicles are present before magnetite formation, and MamA is required for their activation', *Proc. Natl Acad. Sci. USA 101*, 101, pp. 3839–3844. doi: 10.1039/C39780000281.

Konings, A. W. T. and Ruifrok, A. C. C. (1985) 'Role of Membrane Lipids and Membrane Fluidity in Thermosensitivity and Thermotolerance of Mammalian Cells', *Radiation Research Society*, 102(1), pp. 86–98.

Kuhn, N. Z. and Tuan, R. S. (2010) 'Regulation of stemness and stem cell niche of mesenchymal stem cells: implications in tumorigenesis and metastasis.', *Journal of cellular physiology*, 222(2), pp. 268–77. doi: 10.1002/jcp.21940.

Kultima, J. R., Xu, C., Wojtkiewicz, G. R., Vemula, P. K., Miranda-Nieves, D., Matthiesen, M. E., Juneja, V., Phillips, J. A., Zhao, W., Ankrum, J. A., *et al.* (2012) 'Tracking Mesenchymal Stem Cells with Iron Oxide Nanoparticle

Loaded Poly(lactide-co-glycolide) Microparticles', *Nano Letters*, 12(8), pp. 4131–4139. doi: 10.1021/nl301658q.

Kumar, C. S. S. R. and Mohammad, F. (2011) 'Magnetic nanomaterials for hyperthermia-based therapy and controlled drug delivery', *Advanced Drug Delivery Reviews*, 63, pp. 789–808. doi: 10.1016/j.addr.2011.03.008.

van Landeghem, F. K. H., Maier-Hauff, K., Jordan, A., Hoffmann, K.-T., Gneveckow, U., Scholz, R., Thiesen, B., Brück, W. and von Deimling, A. (2009) 'Post-mortem studies in glioblastoma patients treated with thermotherapy using magnetic nanoparticles.', *Biomaterials*, 30(1), pp. 52–7. doi: 10.1016/j.biomaterials.2008.09.044.

Lefèvre, C. T., Abreu, F., Lins, U. and Bazylinski, D. A. (2011) 'A bacterial backbone: magnetosomes in magnetotactic bacteria', in Rai, M. and Duran, N. (eds) *Metal Nanoparticles in Microbiology*. Berlin: Springer-Verlag, pp. 75–102. doi: 10.1007/978-3-642-18312-6.

Lemine, O. M., Omri, K., Iglesias, M., Velasco, V., Crespo, P., De La Presa, P., El Mir, L., Bouzid, H., Yousif, A. and Al-Hajry, A. (2014) 'Fe2O3 by sol-gel with large nanoparticles size for magnetic hyperthermia application', *Journal of Alloys and Compounds*. Elsevier B.V., 607, pp. 125–131. doi: 10.1016/j.jallcom.2014.04.002.

Lepock, J. R. (2003) 'Cellular effects of hyperthermia: Relevance to the minimum dose for thermal damage', *International Journal of Hyperthermia*, 19(3), pp. 252–266. doi: 10.1080/0265673031000065042.

Lévy, M., Wilhelm, C., Siaugue, J.-M., Horner, O., Bacri, J.-C. and Gazeau, F. (2008) 'Magnetically induced hyperthermia: size-dependent heating power of γ-Fe(2)O(3) nanoparticles.', *Journal of physics. Condensed matter : an Institute of Physics journal*, 20(20), p. 204133. doi: 10.1088/0953-8984/20/20/204133.

Levy, O., Brennen, W. N., Han, E., Rosen, D. M., Musabeyezu, J., Safaee, H., Ranganath, S., Ngai, J., Heinelt, M., Milton, Y., *et al.* (2016) 'A prodrug-doped cellular Trojan Horse for the potential treatment of prostate cancer.', *Biomaterials*, 91, pp. 140–150. doi: 10.1016/j.biomaterials.2016.03.023.

Lian, Q., Zhang, Yuelin, Zhang, J., Hua, ;, Zhang, K., Wu, X., Zhang, Yang, Francis, M. ;, Lam, F.-Y., Kang, S., *et al.* (2010) 'Functional Mesenchymal Stem Cells Derived From Human Induced Pluripotent Stem Cells Attenuate Limb Ischemia in Mice', *Circulation*, 121, pp. 1113–1123. doi: 10.1161/CIRCULATIONAHA.109.898312.

Liao, S.-H., Liu, C.-H., Bastakoti, B. P., Suzuki, N., Chang, Y., Yamauchi, Y., Lin, F.-H. and Wu, K. C.-W. (2015) 'Functionalized magnetic iron oxide/alginate core-shell nanoparticles for targeting hyperthermia.', *International journal of nanomedicine*, 10, pp. 3315–27. doi: 10.2147/IJN.S68719.

Lima-Tenório, M. K., Gómez Pineda, E. A., Ahmad, N. M., Fessi, H. and Elaissari, A. (2015) 'Magnetic nanoparticles: In vivo cancer diagnosis and therapy', *International Journal of Pharmaceutics*. doi: 10.1016/j.ijpharm.2015.07.059.

Lima, J., Gonçalves, A. I., Rodrigues, M. T., Reis, R. L. and Gomes, M. E. (2015) 'The effect of magnetic stimulation on the osteogenic and chondrogenic differentiation of human stem cells derived from the adipose tissue (hASCs)', *Journal of Magnetism and Magnetic Materials*. Elsevier, 393, pp. 526–536. doi: 10.1016/j.jmmm.2015.05.087.

Liu, H.-L., Hua, M.-Y., Yang, H.-W., Huang, C.-Y., Chu, P.-C., Wu, J.-S., Tseng, I.-C., Wang, J.-J., Yen, T.-C., Chen, P.-Y., *et al.* (2010) 'Magnetic resonance monitoring of focused ultrasound/magnetic nanoparticle targeting delivery of therapeutic agents to the brain', *Proceedings of the National Academy of Sciences*, 107(34), pp. 15205–15210. doi: 10.1073/pnas.1003388107.

Liu, R.-T., Liu, J., Tong, J.-Q., Tang, T., Kong, W.-C., Wang, X.-W., Li, Y. and Tang, J.-T. (2012) 'Heating effect and biocompatibility of bacterial magnetosomes as potential materials used in magnetic fluid hyperthermia', *Progress in Natural Science: Materials International*, 22(1), pp. 31–39. doi: 10.1016/j.pnsc.2011.12.006.

Liu, R. T., Liu, J., Tong, J. Q., Tang, T., Kong, W. C., Wang, X. W., Li, Y. and Tang, J. T. (2012) 'Heating effect and biocompatibility of bacterial magnetosomes as potential materials used in magnetic fluid hyperthermia', *Progress in Natural Science: Materials International*. Elsevier B.V., 22(1), pp. 31–39. doi: 10.1016/j.pnsc.2011.12.006.

Liu, S., Ginestier, C., Ou, S. J., Clouthier, S. G., Patel, S. H., Monville, F., Korkaya, H., Heath, A., Dutcher, J., Kleer, C. G., *et al.* (2011) 'Breast cancer stem cells are regulated by mesenchymal stem cells through cytokine networks.', *Cancer research*, 71(2), pp. 614–24. doi: 10.1158/0008-5472.CAN-10-0538.

Liu, X. L., Yang, Y., Ng, C. T., Zhao, L. Y., Zhang, Y., Bay, B. H., Fan, H. M. and Ding, J. (2015) 'Magnetic vortex nanorings: a new class of hyperthermia agent for highly efficient in vivo regression of tumors.', *Advanced materials (Deerfield Beach, Fla.)*, 27(11), pp. 1939–44. doi: 10.1002/adma.201405036.

Lohße, A., Ullrich, S., Katzmann, E., Borg, S., Wanner, G., Richter, M., Voigt, B., Schweder, T. and Schüler, D. (2011) 'Functional analysis of the magnetosome Island in magnetospirillum gryphiswaldense: The mamAB operon is sufficient for magnetite biomineralization', *PLoS ONE*, 6(10). doi: 10.1371/journal.pone.0025561.

Lower, B. H. and Bazylinski, D. A. (2013) 'Magnetosomes in Magneto-Tactic Bacteria The Bacterial Magnetosome: A Unique Prokaryotic Organelle', *J Mol Microbiol Biotechnol*, 23, pp. 63–80. doi: 10.1159/000346543.

Lu, C.-H., Chiu, H.-Y., Chen, C.-Y., Hu, Y.-C., Lin, K.-J., Yen, T.-C., Chang, Y.-H. and Hwang, S.-M. (2012) 'Improved chondrogenesis and engineered cartilage formation from TGF-β3-expressing adipose-derived stem cells cultured in the rotating-shaft bioreactor', *Tissue Engineering - Part A*, 18(19–20), pp. 2114–2124. doi: 10.1089/ten.TEA.2012.0010.

Lu, T., Hu, P., Su, X., Li, C., Ma, Y. and Guan, W. (2014) 'Isolation and characterization of mesenchymal stem cells derived from fetal bovine liver.', *Cell and tissue banking*, 15(3), pp. 439–50. doi: 10.1007/s10561-013-9410-0.

Ludwig, R., Stapf, M., Dutz, S., Müller, R., Teichgräber, U. and Hilger, I. (2014a) 'Structural properties of magnetic nanoparticles determine their heating behavior - an estimation of the in vivo heating potential.', *Nanoscale research letters*, 9(1), p. 602. doi: 10.1186/1556-276X-9-602.

Ludwig, R., Stapf, M., Dutz, S., Müller, R., Teichgräber, U. and Hilger, I. (2014b) 'Structural properties of magnetic nanoparticles determine their heating behavior - an estimation of the in vivo heating potential', *Nanoscale Research Letters*, 9(1). doi: 10.1186/1556-276X-9-602.

Ludwig, R., Teran, F. J., Teichgraeber, U. and Hilger, I. (2017) 'Nanoparticle-based hyperthermia distinctly impacts production of ROS, expression of Ki-67, TOP2A, and TPX2, and induction of apoptosis in pancreatic cancer', *International Journal of Nanomedicine*, 12, pp. 1009–1018. doi: 10.2147/IJN.S108577.

Mahmoudi, M., Sant, S., Wang, B., Laurent, S. and Sen, T. (2011) 'Superparamagnetic iron oxide nanoparticles (SPIONs): Development, surface modification and applications in chemotherapy', *Advanced Drug Delivery Reviews*. Elsevier B.V., 63(1–2), pp. 24–46. doi: 10.1016/j.addr.2010.05.006.

Mahmoudi, M., Simchi, A., Imani, M., Shokrgozar, M. A., Milani, A. S., Häfeli, U. O. and Stroeve, P. (2010) 'A new approach for the in vitro identification of the cytotoxicity of superparamagnetic iron oxide nanoparticles', *Colloids and Surfaces B: Biointerfaces*, 75(1), pp. 300–309. doi: 10.1016/j.colsurfb.2009.08.044.

Maier-Hauff, K., Rothe, R., Scholz, R., Gneveckow, U., Wust, P., Thiesen, B., Feussner, A., von Deimling, A., Waldoefner, N., Felix, R., *et al.* (2007) 'Intracranial thermotherapy using magnetic nanoparticles combined with external beam radiotherapy: results of a feasibility study on patients with glioblastoma multiforme.', *Journal of neuro-oncology*, 81(1), pp. 53–60. doi: 10.1007/s11060-006-9195-0.

Mailänder, V., Lorenz, M. R., Holzapfel, V., Musyanovych, A., Fuchs, K., Wiesneth, M., Walther, P., Landfester, K. and Schrezenmeier, H. (2008) 'Carboxylated superparamagnetic iron oxide particles label cells intracellularly without transfection agents', *Molecular Imaging and Biology*, 10(3), pp. 138–146. doi:

10.1007/s11307-007-0130-3.

Majda, J. A., Gerner, E. W., Vanlandingham, B., Gehlsen, K. R. and Cress, A. E. (1994) 'Heat Shock-Induced Shedding of Cell Surface Integrins in A549 Human Tumor Cells in Culture', 210, pp. 46–51.

Majeed, J., Pradhan, L., Ningthoujam, R. S., Vatsa, R. K., Bahadur, D. and Tyagi, A. K. (2014) 'Enhanced specific absorption rate in silanol functionalized Fe3O4 core-shell nanoparticles: study of Fe leaching in Fe3O4 and hyperthermia in L929 and HeLa cells.', *Colloids and surfaces. B, Biointerfaces*, 122, pp. 396–403. doi: 10.1016/j.colsurfb.2014.07.019.

Makridis, A., Topouridou, K., Tziomaki, M., Sakellari, D., Simeonidis, K., Angelakeris, M., Yavropoulou, M. P., Yovos, J. G. and Kalogirou, O. (2014) 'In vitro application of Mn-ferrite nanoparticles as novel magnetic hyperthermia agents', *Journal of Materials Chemistry B*. Royal Society of Chemistry, 2(47), pp. 8390–8398. doi: 10.1039/c4tb01017e.

Mannucci, S., Ghin, L., Conti, G., Tambalo, S., Lascialfari, A., Orlando, T., Benati, D., Bernardi, P., Betterle, N., Bassi, R., *et al.* (2014) 'Magnetic nanoparticles from Magnetospirillum gryphiswaldense increase the efficacy of thermotherapy in a model of Colon Carcinoma', *PLoS ONE*. Public Library of Science, 9(10). doi: 10.1371/journal.pone.0108959.

Mannucci, S., Tambalo, S., Conti, G., Ghin, L., Milanese, A., Carboncino, A., Nicolato, E., Marinozzi, M. R., Benati, D., Bassi, R., *et al.* (2018) 'Magnetosomes Extracted from Magnetospirillum gryphiswaldense as Theranostic Agents in an Experimental Model of Glioblastoma', *Contrast Media and Molecular Imaging*. Hindawi Limited, 2018. doi: 10.1155/2018/2198703.

Markides, H., Rotherham, M. and El Haj, A. J. (2012) 'Biocompatibility and toxicity of magnetic nanoparticles in regenerative medicine', *Journal of Nanomaterials*. doi: 10.1155/2012/614094.

Matsumine, A., Kusuzaki, K., Matsubara, T., Shintani, K., Satonaka, H., Wakabayashi, T., Miyazaki, S., Morita, K., Takegami, K. and Uchida, A. (2007) 'Novel hyperthermia for metastatic bone tumors with magnetic materials by generating an alternating electromagnetic field.', *Clinical & experimental metastasis*, 24(3), pp. 191–200. doi: 10.1007/s10585-007-9068-8.

Mauro, V. P. and Chappell, S. A. (2014) 'A critical analysis of codon optimization in human therapeutics', *Trends in Molecular Medicine*. Elsevier Ltd, 20(11), pp. 604–613. doi: 10.1016/j.molmed.2014.09.003.

Mazur, J., Roy, K. and Kanwar, J. R. (2018) 'Recent advances in nanomedicine and survivin targeting in brain cancers', *Nanomedicine*, 13(1), pp. 105–137. doi:

10.2217/nnm-2017-0286.

Mirzaei, H., Salehi, H., Oskuee, R. K., Mohammadpour, A., Mirzaei, H. R., Sharifi, M. R., Salarinia, R., Darani, H. Y., Mokhtari, M., Masoudifar, A., *et al.* (2018) 'The therapeutic potential of human adipose-derived mesenchymal stem cells producing CXCL10 in a mouse melanoma lung metastasis model', *Cancer Letters*. doi: 10.1016/j.canlet.2018.01.029.

Mishra, Pravin J., Mishra, Prasun J., Humeniuk, R., Medina, D. J., Alexe, G., Mesirov, J. P., Ganesan, S., Glod, J. W. and Banerjee, D. (2008) 'Carcinoma-associated fibroblast-like differentiation of human mesenchymal stem cells', *Cancer Research*. doi: 10.1158/0008-5472.CAN-08-0943.

Mohammed, L., Gomaa, H. G., Ragab, D. and Zhu, J. (2017) 'Particuology Magnetic nanoparticles for environmental and biomedical applications : A review', *Particuology*. Chinese Society of Particuology, 30, pp. 1–14. doi: 10.1016/j.partic.2016.06.001.

Moll, G., Rasmusson-Duprez, I., von Bahr, L., Connolly-Andersen, A.-M., Elgue, G., Funke, L., Hamad, O. A., Lönnies, H., Magnusson, P. U., Sanchez, J., *et al.* (2012) 'Are therapeutic human mesenchymal stromal cells compatible with human blood?', *Stem cells (Dayton, Ohio)*, 30(7), pp. 1565–74. doi: 10.1002/stem.1111.

Mondal, S., Manivasagan, P., Bharathiraja, S., Santha Moorthy, M., Nguyen, V. T., Kim, H. H., Nam, S. Y., Lee, K. D. and Oh, J. (2017) 'Hydroxyapatite Coated Iron Oxide Nanoparticles: A Promising Nanomaterial for Magnetic Hyperthermia Cancer Treatment.', *Nanomaterials (Basel, Switzerland)*, 7(12). doi: 10.3390/nano7120426.

Mornet, S., Vasseur, S., Grasset, F. and Duguet, E. (2004) 'Magnetic nanoparticle design for medical diagnosis and therapy', *J. Mater. Chem.*, 14, pp. 2161–2175. doi: 10.1039/b402025a.

Moros, M., Ambrosone, A., Stepien, G., Fabozzi, F., Marchesano, V., Castaldi, A., Tino, A., M de la Fuente, J. and Tortiglione, C. (2015) 'Deciphering intracellular events triggered by mild magnetic hyperthermia in vitro and in vivo', *Nanomedicine*, 10(14), pp. 2167–2183. doi: DOI 10.2217/nnm.15.70.

Mosca, J. D., Hendricks, J. K., Buyaner, D., Davis-Sproul, J., Chuang, L. C., Majumdar, M. K., Chopra, R., Barry, F., Murphy, M., Thiede, M. A., *et al.* (2000) 'Mesenchymal stem cells as vehicles for gene delivery [In Process Citation]', *Clin Orthop*.

Moskowitz, B. M., Bazylinski, D. A., Egli, R., Frankel, R. B. and Edwards, K. J. (2008) 'Magnetic properties of marine magnetotactic bacteria in a seasonally stratified coastal pond (Salt Pond, MA, USA)', *Geophysical Journal International*, 174(1), pp. 75–92. doi: 10.1111/j.1365-246X.2008.03789.x.

Mouiseddine, M., François, S., Semont, A., Sache, A., Allenet, B., Mathieu, N., Frick, J., Thierry, D. and Chapel, A. (2007) 'Human mesenchymal stem cells home specifically to radiation-injured tissues in a non-obese diabetes/severe combined immunodeficiency mouse model', in *British Journal of Radiology*. doi: 10.1259/bjr/25927054.

Mukhopadhyay, S., Panda, P. K., Sinha, N., Das, D. N. and Bhutia, S. K. (2014) 'Autophagy and apoptosis: where do they meet?', *Apoptosis : an international journal on programmed cell death*, 19(4), pp. 555–66. doi: 10.1007/s10495-014-0967-2.

Müller, F. D., Raschdorf, O., Nudelman, H., Messerer, M., Katzmann, E., Plitzko, J. M., Zarivach, R. and Schüler, D. (2014) 'The FtsZ-like protein FtsZm of Magnetospirillum gryphiswaldense likely interacts with its generic homolog and is required for biomineralization under nitrate deprivation', *Journal of Bacteriology*, 196(3), pp. 650–659. doi: 10.1128/JB.00804-13.

Multhoff, G., Botzler, C., Jennen, L., Schmidt, J., Ellwart, J. and Issels, R. (1997) 'Heat shock protein 72 on tumor cells: a recognition structure for natural killer cells.', *Journal of Immunology*, 158(9), pp. 4341–4350. Available at: http://www.ncbi.nlm.nih.gov/pubmed/9126997.

Multhoff, G., Mizzen, L., Winchester, C. C., Milner, C. M., Wenk, S., Eissner, G., Kampinga, H. H., Laumbacher, B. and Johnson, J. (1999) 'Heat shock protein 70 (Hsp70) stimulates proliferation and cytolytic activity of natural killer cells', *Experimental Hematology*, 27(11), pp. 1627–1636. doi: 10.1016/S0301-472X(99)00104-6.

Mun, J. Y., Shin, K. K., Kwon, O., Lim, Y. T. and Oh, D. B. (2016) 'Minicircle microporation-based non-viral gene delivery improved the targeting of mesenchymal stem cells to an injury site', *Biomaterials*. Elsevier Ltd, 101, pp. 310–320. doi: 10.1016/j.biomaterials.2016.05.057.

Murat, D., Quinlan, A., Vali, H. and Komeili, A. (2010) 'Comprehensive genetic dissection of the magnetosome gene island reveals the step-wise assembly of a prokaryotic organelle', *Proceedings of the National Academy of Sciences*. National Academy of Sciences, 107(12), pp. 5593–5598. doi: 10.1073/PNAS.0914439107.

Nagasawa, T., Hirota, S., Tachibana, K., Takakura, N., Nishikawa, S., Kitamura, Y., Yoshida, N., Kikutani, H. and Kishimoto, T. (1996) 'Defects of B-cell lymphopoiesis and bone-marrow myelopoiesis in mice lacking the CXC chemokine PBSF/SDF-1.', *Nature*, 382(6592), pp. 635–8. doi: 10.1038/382635a0.

Narum, D. L., Kumar, S., Rogers, W. O., Fuhrmann, S. R., Liang, H., Oakley, M., Taye, A., Sim, B. K. L. and Hoffman, S. L. (2001) 'Codon optimization of gene fragments encoding Plasmodium falciparum merzoite proteins enhances DNA

vaccine protein expression and immunogenicity in mice', *Infection and Immunity*, 69(12), pp. 7250–7253. doi: 10.1128/IAI.69.12.7250-7253.2001.

Nayak, S. and Herzog, R. W. (2010) 'Progress and prospects: Immune responses to viral vectors', *Gene Therapy*, pp. 295–304. doi: 10.1038/gt.2009.148.

Niess, H., Thomas, M. N., Schiergens, T. S., Kleespies, A., Jauch, K.-W., Bruns, C., Werner, J., Nelson, P. J. and Angele, M. K. (2016) 'Genetic engineering of mesenchymal stromal cells for cancer therapy: turning partners in crime into Trojan horses', *Innovative Surgical Sciences*, 1(1), pp. 19–32. doi: 10.1515/iss-2016-0005.

Nixon, A. J., Watts, A. E. and Schnabel, L. V (2012) 'Cell- and gene-based approaches to tendon regeneration', *Journal of Shoulder and Elbow Surgery*, 21, pp. 278–294. doi: 10.1016/j.jse.2011.11.015.

Nolta, J. A., Hanley, M. B. and Kohn, D. B. (1994) *Sustained Human Hematopoiesis in Immunodeficient Mice by Cotransplantation of Marrow Stroma Expressing Human Interleukin-3: Analysis of Gene Transduction of Long-Lived Progenitors*, *Blood*. Available at: www.bloodjournal.org.

Norozi, F., Ahmadzadeh, A., Shahrabi, S., Vosoughi, T. and Saki, N. (2016) 'Mesenchymal stem cells as a double-edged sword in suppression or progression of solid tumor cells', *Tumor Biology*. Tumor Biology, 37(9), pp. 11679–11689. doi: 10.1007/s13277-016-5187-7.

Norrman, K., Fischer, Y., Bonnamy, B., Wolfhagen Sand, F., Ravassard, P. and Semb, H. (2010) 'Quantitative Comparison of Constitutive Promoters in Human ES cells', *PLoS ONE*. Edited by D. S. Milstone, 5(8), p. e12413. doi: 10.1371/journal.pone.0012413.

Nudelman, H. and Zarivach, R. (2014) 'Structure prediction of magnetosome-associated proteins', *Frontiers in Microbiology*, 5(JAN), pp. 1–17. doi: 10.3389/fmicb.2014.00009.

Otani, K., Yamahara, K., Ohnishi, S., Obata, H., Kitamura, S. and Nagaya, N. (2009) 'Nonviral delivery of siRNA into mesenchymal stem cells by a combination of ultrasound and microbubbles.', *Journal of controlled release : official journal of the Controlled Release Society*, 133(2), pp. 146–53. doi: 10.1016/j.jconrel.2008.09.088.

Pacioni, S., D'Alessandris, Q. G., Giannetti, S., Morgante, L., De Pascalis, I., Coccè, V., Bonomi, A., Pascucci, L., Alessandri, G., Pessina, A., *et al.* (2015) 'Mesenchymal stromal cells loaded with paclitaxel induce cytotoxic damage in glioblastoma brain xenografts.', *Stem cell research & therapy*, 6, p. 194. doi: 10.1186/s13287-015-0185-z.

Pardoe, H., Chua-anusorn, W., St. Pierre, T. G. and Dobson, J. (2001) 'Structural and

magnetic properties of nanoscale iron oxide particles synthesized in the presence of dextran or polyvinyl alcohol', *Journal of Magnetism and Magnetic Materials*, 225(1–2), pp. 41–46. doi: 10.1016/S0304-8853(00)01226-9.

Park, J. R., Kim, E., Yang, J., Lee, H., Hong, S. H., Woo, H. M., Park, S. M., Na, S. and Yang, S. R. (2015) 'Isolation of human dermis derived mesenchymal stem cells using explants culture method: expansion and phenotypical characterization', *Cell and Tissue Banking*. doi: 10.1007/s10561-014-9471-8.

Park, J. S., Suryaprakash, S., Lao, Y. H. and Leong, K. W. (2015) 'Engineering mesenchymal stem cells for regenerative medicine and drug delivery', *Methods*. Elsevier Inc., 84, pp. 3–16. doi: 10.1016/j.ymeth.2015.03.002.

Patsula, V., Moskvin, M., Dutz, S. and Horák, D. (2016) 'Size-dependent magnetic properties of iron oxide nanoparticles', *Journal of Physics and Chemistry of Solids*. Elsevier, 88, pp. 24–30. doi: 10.1016/j.jpcs.2015.09.008.

Patterson, S. S., Dionisi, H. M., Gupta, R. K. and Sayler, G. S. (2005) 'Codon optimization of bacterial luciferase (lux) for expression in mammalian cells', *Journal of Industrial Microbiology and Biotechnology*, 32(3), pp. 115–123. doi: 10.1007/s10295-005-0211-8.

Pawlik, A., Nowak, J. M., Grzanka, D., Gackowska, L., Michalkiewicz, J. and Grzanka, A. (2013) 'Hyperthermia induces cytoskeletal alterations and mitotic catastrophe in p53-deficient H1299 lung cancer cells', *Acta Histochemica*. Elsevier GmbH., 115(1), pp. 8–15. doi: 10.1016/j.acthis.2012.02.006.

Peng, L. H., Huang, Y. F., Zhang, C. Z., Niu, J., Chen, Y., Chu, Y., Jiang, Z. H., Gao, J. Q. and Mao, Z. W. (2016) 'Integration of antimicrobial peptides with gold nanoparticles as unique non-viral vectors for gene delivery to mesenchymal stem cells with antibacterial activity', *Biomaterials*. doi: 10.1016/j.biomaterials.2016.06.057.

Pessina, A., Coccè, V., Pascucci, L., Bonomi, A., Cavicchini, L., Sisto, F., Ferrari, M., Ciusani, E., Crovace, A., Falchetti, M. L., *et al.* (2013) 'Mesenchymal stromal cells primed with Paclitaxel attract and kill leukaemia cells, inhibit angiogenesis and improve survival of leukaemia-bearing mice.', *British journal of haematology*, 160(6), pp. 766–78. doi: 10.1111/bjh.12196.

Pieber, T. R., Absenger, M., Fröhlich, E., Samberger, C., Kueznik, T., Roblegg, E. and Zimmer, A. (2009) 'Cytotoxicity of nanoparticles independent from oxidative stress', *The Journal of Toxicological Sciences*, 34(4), pp. 363–375. doi: 10.2131/jts.34.363.

Plati, J., Bucur, O. and Khosravi-Far, R. (2011) 'Apoptotic cell signaling in cancer progression and therapy', *Integrative Biology*, 3(4), pp. 279–296. doi: 10.1039/c0ib00144a.

Prozorov, T., Mallapragada, S. K., Narasimhan, B., Wang, L., Williams, T. J., Palo, P., Bazylinski, D. A., Prozorov, R., Canfield, P. C. and Nilsen-Hamilton, M. (2007) 'Protein-Mediated Synthesis of Uniform Superparamagnetic Magnetite Nanocrystals', *Advanced Functional Materials*, 17(6), pp. 951–957. doi: 10.1002/adfm.200600448.

Qiao, B., Shui, W., Cai, L., Guo, S. and Jiang, D. (2015) 'Human mesenchymal stem cells as delivery of osteoprotegerin gene: Homing and therapeutic effect for osteosarcoma', *Drug Design, Development and Therapy*, 9, pp. 969–976. doi: 10.2147/DDDT.S77116.

Qiao, L., Xu, Z., Zhao, T., Zhao, Z., Shi, M., Zhao, R. C., Ye, L. and Zhang, X. (2008) 'Suppression of tumorigenesis by human mesenchymal stem cells in a hepatoma model.', *Cell research*, 18(4), pp. 500–7. doi: 10.1038/cr.2008.40.

Rabin, Y. (2002) 'Is intracellular hyperthermia superior to extracellular hyperthermia in the thermal sense?', *International journal of Hyperthermia*, 6736(January). doi: 10.1080/0265673011011671.

Ramachandra Kurup Sasikala, A., Thomas, R. G., Unnithan, A. R., Saravanakumar, B., Jeong, Y. Y., Park, C. H. and Kim, C. S. (2016) 'Multifunctional Nanocarpets for Cancer Theranostics: Remotely Controlled Graphene Nanoheaters for Thermo-Chemosensitisation and Magnetic Resonance Imaging', *Scientific Reports*. Nature Publishing Group, 6(February), pp. 1–14. doi: 10.1038/srep20543.

Ramasamy, R., Lam, E. W.-F., Soeiro, I., Tisato, V., Bonnet, D. and Dazzi, F. (2007) 'Mesenchymal stem cells inhibit proliferation and apoptosis of tumor cells: impact on in vivo tumor growth.', *Leukemia*, 21(2), pp. 304–10. doi: 10.1038/sj.leu.2404489.

Rana, S., Jadhav, N. V., Barick, K. C., Pandey, B. N. and Hassan, P. A. (2014) 'Polyaniline shell cross-linked Fe3O4 magnetic nanoparticles for heat activated killing of cancer cells', *Dalton Transactions*. Royal Society of Chemistry, 43(32), pp. 12263–12271. doi: 10.1039/c4dt00898g.

Rand, W., Snow, H. D., Elliott, D. G. and G.M., H. (1985) 'Induction heating method for use in causing necrosis of neoplasm', *US Patent Specification (1985), 4, 545, 368*, II(19), pp. 5–9.

Raschdorf, O., Forstner, Y., Kolinko, I., Uebe, R., Plitzko, J. M. and Schüler, D. (2016) 'Genetic and Ultrastructural Analysis Reveals the Key Players and Initial Steps of Bacterial Magnetosome Membrane Biogenesis', *PLoS Genetics*, 12(6), pp. 1–23. doi: 10.1371/journal.pgen.1006101.

Raschdorf, O., Müller, F. D., Pósfai, M., Plitzko, J. M. and Schüler, D. (2013) 'The magnetosome proteins MamX, MamZ and MamH are involved in redox control of magnetite biomineralization in Magnetospirillum gryphiswaldense',

Molecular Microbiology, 89(5), pp. 872–886. doi: 10.1111/mmi.12317.

Rast, L. and Harrison, J. G. (no date) *Computational Modeling of Electromagnetically Induced Heating of Magnetic Nanoparticle Materials for Hyperthermic Cancer Treatment*. Available at: www.nsti.org,.

Rawlings, A. E., Bramble, J. P., Hounslow, A. M., Williamson, M. P., Monnington, A. E., Cooke, D. J. and Staniland, S. S. (2016) 'Ferrous Iron Binding Key to Mms6 Magnetite Biomineralisation: A Mechanistic Study to Understand Magnetite Formation Using pH Titration and NMR Spectroscopy', *Chemistry - A European Journal*. doi: 10.1002/chem.201600322.

Reddy, L. H., Arias, J. L., Nicolas, J. and Couvreur, P. (2012) 'Magnetic nanoparticles: Design and characterization, toxicity and biocompatibility, pharmaceutical and biomedical applications', *Chemical Reviews*, 112(11), pp. 5818–5878. doi: 10.1021/cr300068p.

Reimer, P. and Balzer, T. (2003) 'Ferucarbotran (Resovist): a new clinically approved RES-specific contrast agent for contrast-enhanced MRI of the liver: properties, clinical development, and applications.', *European radiology*. Germany, 13(6), pp. 1266–1276. doi: 10.1007/s00330-002-1721-7.

Rhodes, L. V., Antoon, J. W., Muir, S. E., Elliott, S., Beckman, B. S. and Burow, M. E. (2010) 'Effects of human mesenchymal stem cells on ER-positive human breast carcinoma cells mediated through ER-SDF-1/CXCR4 crosstalk', *Molecular Cancer*. doi: 10.1186/1476-4598-9-295.

Richard B. Frankel, J.Williams, T. and A.Bazylinski, D. (2006) 'Magneto-Aerotaxis', in Schüler, D. (ed.) *Magnetoreception and Magnetosomes in Bacteria*, pp. 1–24. doi: 10.1007/7171.

Richter, M., Kube, M., Bazylinski, D. A., Lombardot, T., Glöckner, F. O., Reinhardt, R. and Schüler, D. (2007) 'Comparative Genome Analysis of Four Magnetotactic Bacteria Reveals a Complex Set of Group-Specific Genes Implicated in Magnetosome Biomineralization and Function † Downloaded from', *JOURNAL OF BACTERIOLOGY*, 189(13), pp. 4899–4910. doi: 10.1128/JB.00119-07.

Riegler, J., Liew, A., Hynes, S. O., Ortega, D., O'Brien, T., Day, R. M., Richards, T., Sharif, F., Pankhurst, Q. A. and Lythgoe, M. F. (2013) 'Superparamagnetic iron oxide nanoparticle targeting of MSCs in vascular injury', *Biomaterials*. Elsevier Ltd, 34(8), pp. 1987–1994. doi: 10.1016/j.biomaterials.2012.11.040.

Rizal, R., Kerans, F. F. A., Hermantara, R. and Herningtyas, E. H. (2018) 'Isolation, characterization, proliferation, differentiation, and freeze-thaw survival of human wharton's jelly mesenchymal stem cells from early and late passages', *Bioscience Research*, 15(1).

Rodgers, F., Blakemore, R., Blakemore, N., Frankel, R., Bazylinski, D., Maratea, D. and Rodgers, C. (1990) 'Intercellular structure in a many-celled magnetotactic prokaryote', *Archives of Microbiology*, 154(1). doi: 10.1007/BF00249172.

Rodríguez-Luccioni, H. L., Latorre-Esteves, M., Ménndez-Vega, J., Soto, O., Rodr??guez, A. R., Rinaldi, C. and Torres-Lugo, M. (2011) 'Enhanced reduction in cell viability by hyperthermia induced by magnetic nanoparticles.', *International journal of nanomedicine*. doi: 10.2147/IJN.S14613.

Roger, M., Clavreul, A., Venier-Julienne, M. C., Passirani, C., Sindji, L., Schiller, P., Montero-Menei, C. and Menei, P. (2010) 'Mesenchymal stem cells as cellular vehicles for delivery of nanoparticles to brain tumors', *Biomaterials*. Elsevier Ltd, 31(32), pp. 8393–8401. doi: 10.1016/j.biomaterials.2010.07.048.

Rong, C., Zhang, C., Zhang, Y., Qi, L., Yang, J., Guan, G., Li, Y. and Li, J. (2012) 'FeoB2 functions in magnetosome formation and oxidative stress protection in Magnetospirillum gryphiswaldense strain MSR-1', *Journal of Bacteriology*, 194(15), pp. 3972–3976. doi: 10.1128/JB.00382-12.

Rosensweig, R. E. (2002) 'Heating magnetic fluid with alternating magnetic field', *Journal of Magnetism and Magnetic Materials*. doi: 10.1016/S0304-8853(02)00706-0.

Rüster, B., Göttig, S., Ludwig, R. J., Bistrian, R., Müller, S., Seifried, E., Gille, J. and Henschler, R. (2006) 'Mesenchymal stem cells display coordinated rolling and adhesion behavior on endothelial cells.', *Blood*, 108(12), pp. 3938–44. doi: 10.1182/blood-2006-05-025098.

Sackstein, R. (2004) 'The Bone Marrow Is Akin to Skin: HCELL and the Biology of Hematopoietic Stem Cell Homing11Reprinted from J Invest Dermatol 122:1061-1069, 2004', *Journal of Investigative Dermatology Symposium Proceedings*. Elsevier BV, 9(3), pp. 215–223. doi: 10.1016/s0022-202x(15)53011-x.

Sackstein, R., Merzaban, J. S., Cain, D. W., Dagia, N. M., Spencer, J. A., Lin, C. P. and Wohlgemuth, R. (2008) 'Ex vivo glycan engineering of CD44 programs human multipotent mesenchymal stromal cell trafficking to bone.', *Nature medicine*, 14(2), pp. 181–7. doi: 10.1038/nm1703.

Sadhukha, T., Niu, L., Wiedmann, T. S. and Panyam, J. (2013) 'Effective elimination of cancer stem cells by magnetic hyperthermia', *Molecular Pharmaceutics*, 10(4), pp. 1432–1441. doi: 10.1021/mp400015b.

Sadhukha, T., O'Brien, T. D. and Prabha, S. (2014) 'Nano-engineered mesenchymal stem cells as targeted therapeutic carriers.', *Journal of controlled release : official journal of the Controlled Release Society*, 196, pp. 243–51. doi: 10.1016/j.jconrel.2014.10.015.

Sadhukha, T., Wiedmann, T. S. and Panyam, J. (2013) 'Inhalable magnetic nanoparticles for targeted hyperthermia in lung cancer therapy.', *Biomaterials*, 34(21), pp. 5163–71. doi: 10.1016/j.biomaterials.2013.03.061.

Santos, J. L., Pandita, D., Rodrigues, J., Pêgo, A. P., Granja, P. L. and Tomás, H. (2011) *Non-Viral Gene Delivery to Mesenchymal Stem Cells: Methods, Strategies and Application in Bone Tissue Engineering and Regeneration*.

Sato, I., Umemura, M., Mitsudo, K., Kioi, M., Nakashima, H., Iwai, T., Feng, X., Oda, K., Miyajima, A., Makino, A., *et al.* (2014) 'Hyperthermia generated with ferucarbotran (Resovist®) in an alternating magnetic field enhances cisplatin-induced apoptosis of cultured human oral cancer cells', *Journal of Physiological Sciences*, 64(3), pp. 177–183. doi: 10.1007/s12576-014-0309-8.

Scheffel, A., Gardes, A., Grunberg, K., Wanner, G. and Schüler, D. (2008) 'The major magnetosome proteins MamGFDC are not essential for magnetite biomineralization in Magnetospirillum gryphiswaldense but regulate the size of magnetosome crystals', *Journal of Bacteriology*, 190(1), pp. 377–386. doi: 10.1128/JB.01371-07.

Schüler, D. (2008) 'Genetics and cell biology of magnetosome formation in magnetotactic bacteria', *FEMS Microbiology Reviews*, 32(4), pp. 654–672. doi: 10.1111/j.1574-6976.2008.00116.x.

Schüler, D. and Baeuerlein, E. (1996) 'Iron-limited growth and kinetics of iron uptake in Magnetospirillum gryphiswaldense.', *Archives of microbiology*, 166(5), pp. 301–7. Available at: http://www.ncbi.nlm.nih.gov/pubmed/8929275 (Accessed: 19 August 2019).

Schüler, D. and Baeuerlein, E. (1998) 'Dynamics of iron uptake and Fe3O4 biomineralization during aerobic and microaerobic growth of Magnetospirillum gryphiswaldense.', *Journal of bacteriology*, 180(1), pp. 159–62. Available at: http://www.ncbi.nlm.nih.gov/pubmed/9422606 (Accessed: 19 August 2019).

Segers, V. F. M., Van Riet, I., Andries, L. J., Lemmens, K., Demolder, M. J., De Becker, A. J. M. L., Kockx, M. M. and De Keulenaer, G. W. (2006) 'Mesenchymal stem cell adhesion to cardiac microvascular endothelium: activators and mechanisms.', *American journal of physiology. Heart and circulatory physiology*, 290(4), pp. H1370-7. doi: 10.1152/ajpheart.00523.2005.

Sellins, K. S., Cohen, J. J., Sellins, K. S. and Cohen, J. J. (1991) 'Hyperthermia Induces Apoptosis in Thymocytes', 126(1), pp. 88–95.

Shevtsov, M. A., Yakovleva, L. Y., Nikolaev, B. P., Marchenko, Y. Y., Dobrodumov, A. V, Onokhin, K. V, Onokhina, Y. S., Selkov, S. A., Mikhrina, A. L., Guzhova, I. V, *et al.* (2014) 'Neuro-Oncology', 16(December 2013), pp. 38–

49. doi: 10.1093/neuonc/not141.

Shi, M., Li, J., Liao, L., Chen, B., Li, B., Chen, L., Jia, H. and Zhao, R. C. (2007) 'Regulation of CXCR4 expression in human mesenchymal stem cells by cytokine treatment: role in homing efficiency in NOD/SCID mice.', *Haematologica*, 92(7), pp. 897–904. doi: 10.3324/haematol.10669.

Shipunova, V. O., Kotelnikova, P. A., Aghayeva, U. F., Stremovskiy, O. A., Novikov, I. A., Schulga, A. A., Nikitin, M. P. and Deyev, S. M. (2019) 'Self-assembling nanoparticles biofunctionalized with magnetite-binding protein for the targeted delivery to HER2/neu overexpressing cancer cells', *Journal of Magnetism and Magnetic Materials*. Elsevier B.V., 469(August 2018), pp. 450–455. doi: 10.1016/j.jmmm.2018.09.015.

Shubayev, V. I., Pisanic, T. R. and Jin, S. (2009) 'Magnetic nanoparticles for theragnostics', *Advanced Drug Delivery Reviews*. Elsevier B.V., 61(6), pp. 467–477. doi: 10.1016/j.addr.2009.03.007.

Silva, A. C., Oliveira, T. R., Mamani, J. B., Malheiros, S. M. F., Malavolta, L., Pavon, L. F., Sibov, T. T., Amaro, E., Tannús, A., Vidoto, E. L. G., *et al.* (2011) 'Application of hyperthermia induced by superparamagnetic iron oxide nanoparticles in glioma treatment.', *International journal of nanomedicine*, 6, pp. 591–603. doi: 10.2147/IJN.S14737.

Silver, R. K., Lehr, H. B., Summers, A., Greene, A. E. and Coriell, L. L. (1964) 'Use of Dielectric Heating (Shortwave Diathermy) in Thawing Frozen Suspensions of Tissue Culture Cells.', *Proceedings of the Society for Experimental Biology and Medicine*. SAGE Publications, 115(2), pp. 453–455. doi: 10.3181/00379727-115-28939.

Simmons, S. L., Bazylinski, D. A. and Edwards, K. J. (2006) *South-Seeking Magnetotactic in the Northern Hemisphere*, *Science*.

Soetaert, F., Kandala, S. K., Bakuzis, A. and Ivkov, R. (2017) 'Experimental estimation and analysis of variance of the measured loss power of magnetic nanoparticles', *Scientific Reports*, 7(1), pp. 1–15. doi: 10.1038/s41598-017-07088-w.

Spaeth, E. L., Dembinski, J. L., Sasser, A. K., Watson, K., Klopp, A., Hall, B., Andreeff, M. and Marini, F. (2009) 'Mesenchymal stem cell transition to tumor-associated fibroblasts contributes to fibrovascular network expansion and tumor progression.', *PloS one*, 4(4), p. e4992. doi: 10.1371/journal.pone.0004992.

Spaldin, N. A. (2003) *MAGNETIC MATERIALS Fundamentals and device applications*. Cambridge University Press. Available at: http://www.cambridge.org.

Srivastava, P. K., Udono, H., Blachere, N. F. and Li, Z. (1994) 'Heat shock proteins transfer peptides during antigen processing and CTL priming.', *Immunogenetics*, 39, pp. 93–98.

Staniland, S. S. and Rawlings, A. E. (2016) 'Crystallizing the function of the magnetosome membrane mineralization protein Mms6', 0, pp. 883–890. doi: 10.1042/BST20160057.

Suriyanto, Ng, E. Y. K. and Kumar, S. D. (2017) 'Physical mechanism and modeling of heat generation and transfer in magnetic fluid hyperthermia through Néelian and Brownian relaxation: a review', *Biomedical engineering online*, 16(1), p. 36. doi: 10.1186/s12938-017-0327-x.

Suto, M., Hirota, Y., Mamiya, H., Fujita, A., Kasuya, R., Tohji, K. and Jeyadevan, B. (2009) 'Heat dissipation mechanism of magnetite nanoparticles in magnetic fluid hyperthermia', *Journal of Magnetism and Magnetic Materials*. doi: 10.1016/j.jmmm.2009.02.070.

Tanaka, M., Arakaki, A. and Matsunaga, T. (2010) 'Identification and functional characterization of liposome tubulation protein from magnetotactic bacteria', *Molecular Microbiology*, 76(2), pp. 480–488. doi: 10.1111/j.1365-2958.2010.07117.x.

Tanaka, M., Mazuyama, E., Arakaki, A. and Matsunaga, T. (2011) 'MMS6 Protein Regulates Crystal Morphology during Nano-sized Magnetite Biomineralization in-Vivo', *The Journal of Biological Chemistry*, 286(8), pp. 6386–6392.

Tietze, R., Zaloga, J., Unterweger, H., Lyer, S., Friedrich, R. P., Janko, C., Ottler, M. P. €, Dürr, S. and Alexiou, C. (2015) 'Magnetic nanoparticle-based drug delivery for cancer therapy', *Biochemical and Biophysical Research Communications*. doi: 10.1016/j.bbrc.2015.08.022.

Tlsty, T. D. and Coussens, L. M. (2006) 'TUMOR STROMA AND REGULATION OF CANCER DEVELOPMENT', *Annual Review of Pathology: Mechanisms of Disease*. doi: 10.1146/annurev.pathol.1.110304.100224.

Tran, S. E. F., Meinander, A., Holmström, T. H., Rivero-Müller, A., Heiskanen, K. M., Linnau, E. K., Courtney, M. J., Mosser, D. D., Sistonen, L. and Eriksson, J. E. (2003) 'Heat stress downregulates FLIP and sensitizes cells to Fas receptor-mediated apoptosis', *Cell Death and Differentiation*, 10(10), pp. 1137–1147. doi: 10.1038/sj.cdd.4401278.

Tsai, K.-S., Yang, S.-H., Lei, Y.-P., Tsai, C.-C., Chen, H.-W., Hsu, C.-Y., Chen, L.-L., Wang, H.-W., Miller, S. A., Chiou, S.-H., *et al.* (2011) 'Mesenchymal stem cells promote formation of colorectal tumors in mice.', *Gastroenterology*, 141(3), pp. 1046–56. doi: 10.1053/j.gastro.2011.05.045.

Tu, S., McStay, G. P., Boucher, L. M., Mak, T., Beere, H. M. and Green, D. R. (2006) 'In situ trapping of activated initiator caspases reveals a role for caspase-2 in heat shock-induced apoptosis', *Nature Cell Biology*, 8(1), pp. 72–77. doi: 10.1038/ncb1340.

Uchimura, E., Yamada, S., Uebersax, L., Fujita, S., Miyake, M. and Miyake, J. (2007) 'Method for reverse transfection using gold colloid as a nano-scaffold', *Journal of Bioscience and Bioengineering*. Elsevier BV, 103(1), pp. 101–103. doi: 10.1263/jbb.103.101.

Udono, H. and Srivastava, P. K. (1993) 'Heat shock protein70-associated peptides elicit specific cancer immunity', *J Exp Med*, 178(1391), p. 1396.

Uebe, R. and Schüler, D. (2016) 'Magnetosome biogenesis in magnetotactic bacteria', *Nature Reviews Microbiology*. Nature Publishing Group, 14(10), pp. 621–637. doi: 10.1038/nrmicro.2016.99.

Uebe, R., Voigt, B., Schweder, T., Albrecht, D., Katzmann, E., Lang, C., Böttger, L., Matzanke, B. and Schüler, D. (2010) 'Deletion of a fur-like gene affects iron homeostasis and magnetosome formation in Magnetospirillum gryphiswaldense', *Journal of Bacteriology*, 192(16), pp. 4192–4204. doi: 10.1128/JB.00319-10.

Ullrich, S., Ullrich, S., Kube, M., Kube, M., Schu, S., Schu, S., Reinhardt, R., Reinhardt, R., Schu, D. and Schu, D. (2005) 'A Hypervariable 130-Kilobase Genomic Region of', *Microbiology*, 187(21), pp. 7176–7184. doi: 10.1128/JB.187.21.7176.

Vanaja, D. K., Grossmann, M. E., Celis, E. and Young, C. Y. F. (2000) 'Tumor prevention and antitumor immunity with heat shock protein 70 induced by 15-deoxy-Δ12,14-prostaglandin J2in transgenic adenocarcinoma of mouse prostate cells', *Cancer Research*, 60(17), pp. 4714–4718.

Villanueva, A., De La Presa, P., Alonso, J. M., Rueda, T., Martínez, A., Crespo, P., Morales, M. P., Gonzalez-Fernandez, M. A., Valdés, J. and Rivero, G. (2010) 'Hyperthermia hela cell treatment with silica-coated manganese oxide nanoparticles', *Journal of Physical Chemistry C*, 114(5), pp. 1976–1981. doi: 10.1021/jp907046f.

Wang, L., Pan, J., Wang, T., Song, M. and Chen, W. (2013) 'Pathological cyclic strain-induced apoptosis in human periodontal ligament cells through the RhoGDIα/caspase-3/PARP pathway.', *PloS one*, 8(10), p. e75973. doi: 10.1371/journal.pone.0075973.

Wang, L., Prozorov, T., Palo, P. E., Liu, X., Vaknin, D., Prozorov, R., Mallapragada, S. and Nilsen-hamilton, M. (2012) 'Self-assembly and biphasic iron-binding characteristics of Mms6, a bacterial protein that promotes the formation of superparamagnetic magnetite nanoparticles of uniform size and shape',

Biomacromolecules, 13, pp. 98–105.

Wang, X., Gao, J., Ouyang, X., Wang, J., Sun, X. and Lv, Y. (2018) 'Mesenchymal stem cells loaded with paclitaxel– poly(Lactic-co-glycolic acid) nanoparticles for glioma-targeting therapy', *International Journal of Nanomedicine*. doi: 10.2147/IJN.S167142.

Wang, Y., Shang, S. and Li, C. (2015) 'Comparison of different kinds of nonviral vectors for gene delivery to human periodontal ligament stem cells', *Journal of Dental Sciences*. Elsevier Taiwan LLC, 10(4), pp. 414–422. doi: 10.1016/j.jds.2015.02.002.

Wiehe, J. M., Kaya, Z., Homann, J. M., Wöhrle, J., Vogt, K., Nguyen, T., Rottbauer, W., Torzewski, J., Fekete, N., Rojewski, M., *et al.* (2013) 'GMP-adapted overexpression of CXCR4 in human mesenchymal stem cells for cardiac repair.', *International journal of cardiology*, 167(5), pp. 2073–81. doi: 10.1016/j.ijcard.2012.05.065.

Wilhelm, C., Fortin, J.-P. and Gazeau, F. (2007) 'Tumour cell toxicity of intracellular hyperthermia mediated by magnetic nanoparticles', *Journal of nanoscience and nanotechnology*. American Scientific Publishers, 7(8), pp. 2933–2937.

Wu, C. and Dunbar, C. E. (2011) 'Stem cell gene therapy: The risks of insertional mutagenesis and approaches to minimize genotoxicity', *Frontiers of Medicine in China*, pp. 356–371. doi: 10.1007/s11684-011-0159-1.

Wu, H. H., Zhou, Y., Tabata, Y. and Gao, J. Q. (2019) 'Mesenchymal stem cell-based drug delivery strategy: from cells to biomimetic', *Journal of Controlled Release*. doi: 10.1016/j.jconrel.2018.12.019.

Wust, P., Gneveckow, U., Johannsen, M., Böhmer, D., Henkel, T., Kahmann, F., Sehouli, J., Felix, R., Ricke, J. and Jordan, A. (2006) 'Magnetic nanoparticles for interstitial thermotherapy - Feasibility, tolerance and achieved temperatures', *International Journal of Hyperthermia*, 22(8), pp. 673–685. doi: 10.1080/02656730601106037.

Wydra, R. J., Rychahou, P. G., Evers, B. M., Anderson, K. W., Dziubla, T. D. and Hilt, J. Z. (2015) 'The role of ROS generation from magnetic nanoparticles in an alternating magnetic field on cytotoxicity.', *Acta biomaterialia*, 25, pp. 284–90. doi: 10.1016/j.actbio.2015.06.037.

Yamagishi, A., Narumiya, K., Tanaka, M. and Matsunaga, T. (2016) 'Core Amino Acid Residues in the Morphology-Regulating Protein , Mms6 , for Intracellular Magnetite Biomineralization', *Nature Publishing Group*. Nature Publishing Group, (October), pp. 1–10. doi: 10.1038/srep35670.

Yan, X. L., Fu, C. J., Chen, L., Qin, J. H., Zeng, Q., Yuan, H. F., Nan, X., Chen, H. X., Zhou, J. N., Lin, Y. L., *et al.* (2012) 'Mesenchymal stem cells from primary

breast cancer tissue promote cancer proliferation and enhance mammosphere formation partially via EGF/EGFR/Akt pathway', *Breast Cancer Research and Treatment*. doi: 10.1007/s10549-011-1577-0.

Yang, C. T., Li, K. Y., Meng, F. Q., Lin, J. F., Young, I. C., Ivkov, R. and Lin, F. H. (2018) 'ROS-induced HepG2 cell death from hyperthermia using magnetic hydroxyapatite nanoparticles', *Nanotechnology*, 29(37), p. 375101. doi: 10.1088/1361-6528/aacda1.

Yang, C. Y., Tai, M. F., Chen, S. T., Wang, Y. T., Chen, Y. F., Hsiao, J. K., Wang, J. L. and Liu, H. M. (2009) 'Labeling of human mesenchymal stem cell: Comparison between paramagnetic and superparamagnetic agents', *Journal of Applied Physics*, 105(7), pp. 1–4. doi: 10.1063/1.3072821.

Yijun, H., Weijia, Z., Wei, J., Chengbo, R. and Ying, L. (2007) 'Disruption of a fur-like gene inhibits magnetosome formation in Magnetospirillum gryphiswaldense MSR-1.', *Biochemistry. Biokhimiia*, 72(11), pp. 1247–53. Available at: http://www.ncbi.nlm.nih.gov/pubmed/18205608 (Accessed: 19 August 2019).

Yin, P. T., Shah, S., Pasquale, N. J., Garbuzenko, O. B., Minko, T. and Lee, K. B. (2016) 'Stem cell-based gene therapy activated using magnetic hyperthermia to enhance the treatment of cancer', *Biomaterials*. Elsevier Ltd, 81, pp. 46–57. doi: 10.1016/j.biomaterials.2015.11.023.

Yoo, J. and Lee, Y. J. (2007) 'Effect of hyperthermia on TRAIL-induced apoptotic death in human colon cancer cells: Development of a novel strategy for regional therapy', *Journal of Cellular Biochemistry*, 101(3), pp. 619–630. doi: 10.1002/jcb.21203.

Zachari, M. A., Chondrou, P. S., Pouliliou, S. E., Mitrakas, A. G., Abatzoglou, I., Zois, C. E. and Koukourakis, M. I. (2014) 'Evaluation of the alamarblue assay for adherent cell irradiation experiments', *Dose-Response*. University of Massachusetts, 12(2), pp. 246–258. doi: 10.2203/dose-response.13-024.Koukourakis.

Zaragosi, L.-E., Billon, N., Ailhaud, G. and Dani, C. (2006) 'Nucleofection Is a Valuable Transfection Method for Transient and Stable Transgene Expression in Adipose Tissue-Derived Stem Cells', *STEM CELLS*. Wiley, 25(3), pp. 790–797. doi: 10.1634/stemcells.2006-0235.

van der Zee, J. (2002) 'Heating the patient: A promising approach?', *Annals of Oncology*, 13(8), pp. 1173–1184. doi: 10.1093/annonc/mdf280.

Zhang, H., Liu, X., Feng, S., Wang, W., Schmidt-rohr, K., Nilsen-hamilton, M., Vaknin, D. and Mallapragada, S. (2015) 'Morphological Transformations in the Magnetite Biomineralizing Protein Mms6 in Iron Solutions: A Small-Angle X - ray Scattering Study'. doi: 10.1021/la5044377.

Zhang, J., Wang, X., Cui, W., Wang, W., Zhang, H., Liu, L., Zhang, Z., Li, Z., Ying, G., Zhang, N., *et al.* (2013) 'Visualization of caspase-3-like activity in cells using a genetically encoded fluorescent biosensor activated by protein cleavage', *Nature Communications*, 4. doi: 10.1038/ncomms3157.

Zhang, X.-Y., Robledo, B. N., Harris, S. S. and Hu, X. P. (2014) 'A Bacterial Gene, mms6, as a New Reporter Gene for Magnetic Resonance Imaging of Mammalian Cells', *Molecular Imaging*, 13, pp. 1–12. doi: 10.2310/7290.2014.00046.

Zhao, Y., Tang, S., Guo, J., Alahdal, M., Cao, S., Yang, Z., Zhang, F., Shen, Y., Sun, M., Mo, R., *et al.* (2017) 'Targeted delivery of doxorubicin by nano-loaded mesenchymal stem cells for lung melanoma metastases therapy.', *Scientific reports*, 7, p. 44758. doi: 10.1038/srep44758.

Zou, Y. R., Kottmann, A. H., Kuroda, M., Taniuchi, I. and Littman, D. R. (1998) 'Function of the chemokine receptor CXCR4 in haematopoiesis and in cerebellar development.', *Nature*, 393(6685), pp. 595–9. doi: 10.1038/31269.

Zurkiya, O., Chan, A. W. S. and Hu, X. (2008) 'MagA is sufficient for producing magnetic nanoparticles in mammalian cells, making it an MRI reporter', *Magnetic Resonance in Medicine*, 59(6), pp. 1225–1231. doi: 10.1002/mrm.21606.

Zuvin, M., Koçak, M., Ünal, Ö., Akkoç, Y., Kutlu, Ö., Yağci Acar, H., Gözüaçik, D. and Koşar, A. (2019) 'Nanoparticle based induction heating at low magnitudes of magnetic field strengths for breast cancer therapy', *Journal of Magnetism and Magnetic Materials*. Elsevier B.V., 483, pp. 169–177. doi: 10.1016/j.jmmm.2019.03.117.